2018

Building performance enhancement using phase change materials and solar photovoltaic thermal systems

Wenye Lin
University of Wollongong

UNIVERSITY OF WOLLONGONG AUSTRALIA

Building performance enhancement using phase change materials and solar photovoltaic thermal systems

Wenye Lin

B.Eng, M.Sc.Eng

This thesis is presented as part of the requirements for the conferral of the degree:

Doctor of Philosophy

Faculty of Engineering and Information Sciences

Sustainable Buildings Research Centre

June 2018

Declaration

I, Wenye Lin, declare that this thesis submitted in partial fulfilment of the requirements for the conferral of the degree Doctor of Philosophy, from the University of Wollongong, is wholly my own work unless otherwise referenced or acknowledged. This document has not been submitted for qualifications at any other academic institution.

Wenye Lin

August 6, 2017

Abstract

Due to the significant and ever-growing energy demand of building heating, ventilation and air conditioning (HVAC) systems, energy consumption in the building sector is continuously increasing. The development and deployment of advanced energy technologies and the improvement in the energy efficiency of building HVAC systems are therefore essential to significantly reduce energy consumption and achieve sustainability in the built environment. Solar photovoltaic thermal (PVT) collectors and thermal energy storage (TES) using phase change materials (PCMs) are among the sustainable and environmentally friendly technologies. The integration of PVT collectors and PCMs into buildings and building HVAC systems could be an alternative solution to rationalise the utilisation of solar energy so as to improve building thermal performance and energy efficiency. Although different solar thermal systems with integrated PCMs have been studied over the last decades, only a few trials have been carried out to simultaneously integrate PVT collectors and PCMs with buildings and building HVAC systems. This thesis presents the development, modelling, experimental investigation, and design optimisation of building and building HVAC systems with PCMs and PVT collectors for improved building performance in terms of effective thermal management and enhanced energy efficiency. Three different approaches have been developed in this study to integrate PCMs and PVT collectors to develop energy efficient buildings and building HVAC systems. These systems are: i) buildings with envelopes enhanced by PCMs (called PCM enhanced buildings) and PVT collectors for space heating; ii) a centralised PCM thermal energy storage (TES) system with integrated PVT collectors for solar heat storage and; iii) an air source heat pump system with integrated PVT collectors and PCM layers laminated into building ceiling for space conditioning.

In PCM enhanced buildings with integrated PVT collectors, the heated air from the PVT collectors was used for space heating during the daytime, while the PCM layer laminated into the building envelopes was used to increase the local thermal mass and reduce the fluctuations in the indoor air temperature. A building envelope-integrated PCM model which considered the hysteresis phenomenon was developed, validated, and used to facilitate the system performance modelling. The thermal performance of a PCM enhanced house using PVT collectors for space heating was first evaluated

through a parametric study and then the influence of the design variables on the building thermal performance was examined further using the Taguchi method. To maximise the thermal benefit of this house, the Taguchi-Fibonacci search method was developed to optimise the system design with both discrete and continuous variables. It was found that the building thermal performance can be enhanced significantly using the PCMs and PVT collectors, and the wall insulation layer was critical to ensure high thermal performance. It also showed that the utilisation of PVT ventilation can improve the thermal performance of PCMs in building envelopes, while enhancing the building envelopes with PCMs is an effective solution to rationalise the thermal energy collected from PVT collectors for indoor space heating. In comparison to a baseline case without using the PVT ventilation and PCMs, the thermal performance of the PCM-enhanced house using the PVT ventilation can be raised to 72.2%. It demonstrated the substantial thermal benefits in terms of building thermal performance by simultaneously using PVT collectors and PCMs in buildings for space heating.

The performance of a centralised PCM TES system with integrated PVT collectors was evaluated based on a lab-scale test rig where the thermal charging and discharging processes were characterised through a series of experiments designed using the Taguchi method. This experimental analysis resulted in two correlations for the two key performance indicators (*i.e.* average heat transfer effectiveness and the effective PCM charging time), which were then used to formulate the design optimisation problems. Two bi-objective optimisation strategies, one using a controlled elitist genetic algorithm (GA) and a multi-criteria decision-making (MCDM) method, and the other using fuzzy clustering, were developed to search for the reasonably optimal solution to the optimisation problem. The optimal design identified using the bi-objective optimisation strategy using the controlled elitist GA - MCDM process can achieve an average heat transfer effectiveness and effective PCM charging time of 59.29% and 6.11 hours, respectively. This design outperformed the single-objective optimal design identified by the Taguchi method and the design without optimisation. The optimisation using the fuzzy clustering-based bi-objective algorithm which simplified the bi-objective optimisation process delivered an optimal solution close to the one using the controlled elitist GA – MCDM process. This study also provides

useful performance indicators and novel bi-objective optimisation strategies which can be used for the optimisation of similar PCM TES coupled with solar thermal systems.

In the heat pump system with integrated PVT collectors and PCM layers laminated into the building ceiling, a new concept of PCM utilisation was proposed by laminating two PCM layers with an air channel between them into the ceiling to enhance the local thermal mass, while at the same time, serve as a centralised TES to temporally store the low grade thermal energy generated from the PVT collectors. A mathematical model for the PCM TES unit which considered the hysteresis phenomenon was developed and validated to facilitate the system modelling. The proposed system could generate 156.5 kWh of electricity during a Melbourne winter week, and reduce the consumption of electricity from 72.0 kWh to 42.3 kWh, resulting in a net generation of 114.2 kWh of electricity, unlike where only the air source heat pump was used. A Taguchi-based study was carried out to examine the influence of various design variables on the system performance. To maximise the net generation of electricity, an optimisation using the hybrid Particle Swarm Optimization and Hooke-Jeeves pattern search (PSO-HJ) technique was implemented. By using the optimal design identified, the energy consumption of the air conditioning system can be reduced by 41.6% under the Melbourne winter weather conditions, in comparison to a baseline case without optimisation. The net generation of electricity can be further improved by 13.7% through optimisation, even though the electricity generated from the PVT collectors was reduced by 1.3%, compared to the baseline case without optimisation. The evaluation and design optimisation of the proposed system demonstrated the significant energetic benefits of the proposed system for space heating, and the substantial energy efficiency enhancement via design optimisation.

The findings obtained from this thesis showed that integrating PVT collectors and PCMs in buildings and building HVAC systems can greatly enhance building thermal management and energy efficiency. It also demonstrated that design optimisation is essential to maximise the benefits of using such systems.

Acknowledgement

First of all, I would like to express my deepest gratitude and thanks to my supervisors, Dr Zhenjun Ma and Dr Georgios Kokogiannakis. I would like to thank Zhenjun for his patient guidance and experienced supervision throughout my research. My sincere gratitude also goes to Georgios, for his helpful comments and advice to improve my research. This thesis could not be completed without their invaluable support.

I would like to devote my appreciation to Mr John Barron and Mr Craig McLauchlan, for their technical support to setup the experimental test rig. I would like to thank Mr Steven Beltrame for his help in experimental system commissioning.

I am also very grateful to Mr Stefan Gschwander from Fraunhofer Institute for Solar Energy Systems ISE, for sharing his knowledge on phase change materials and giving me his suggestions to enrich my research skills.

My appreciation also goes to Mr Haoshan Ren, for his help in the development of new optimisation strategies. The cooperation with him was a delighted experience and very important to my research.

I would like to sincerely thank all the staff and research students in the Sustainable Buildings Research Centre (SBRC) for their company and constant support throughout my Ph.D. study.

Finally, I would like to express my special appreciation to my family. I would like to thank my wife, Sherry, for her constant love, invaluable company and encouragement. I am grateful to my parents for their endless love and support.

Publications arising from this thesis

Journal papers published

- Lin W.Y., Ma Z.J., Cooper P., Sohel M.I. and Yang L.W. 2016. Thermal performance investigation and optimization of buildings with integrated phase change materials and solar photovoltaic thermal collectors. *Energy and Buildings*, vol.116, pp.562-573.

- Lin W.Y. and Ma Z.J. 2016. Using Taguchi-Fibonacci search method to optimize phase change materials enhanced buildings with integrated solar photovoltaic thermal collectors. *Energy*, vol.106, pp.23-37.

- Lin W.Y., Ma Z.J., Sohel M.I. and Cooper P. 2014. Development and evaluation of a ceiling ventilation system enhanced by solar photovoltaic thermal collectors and phase change materials. *Energy Conversion and Management*, vol.88, pp.218-230.

- Ma Z.J., Lin W.Y. and Sohel M.I. 2016: Nano-enhanced phase change materials for improved building performance. *Renewable and Sustainable Energy Reviews*, vol.5, pp.1256-1268.

Journal paper submitted for peer review

- Lin W.Y., Ma Z.J., Ren H.S., Gschwander S. and Wang S.G. 2017. Experimental investigation and bi-objective optimisation of a thermal energy storage system using phase change materials, Submitted to *Renewable Energy*.

Conference paper

- Ma Z.J., Lin W.Y. and Sohel M.I. 2016. Optimization of a ceiling ventilation system with integrated photovoltaic thermal collectors and phase change materials. *11th Conference on Advanced Building Skins*, Bern, Switzerland, October 2017.

- Ma Z.J., Lin W.Y. and Sohel M.I. 2015. Using Solar Photovoltaic Thermal Collectors in Phase Change Materials Enhanced Buildings for Thermal Performance Management. *7th International Conference on Compressors and Refrigeration*, Xi'an, China, October 2015

- Lin W.Y., Ma Z.J. and Cooper P. 2016. Thermal performance evaluation and optimal design of buildings with integrated air-based photovoltaic thermal collectors and phase change materials using the Hooke-Jeeves pattern search method. *12th REHVA World Conference*, Aalborg, Denmark, May 2016.

- Ren H.S., Lin W.Y., Ma Z.J., Cooper P. and Fan W.K. 2017. Thermal performance evaluation of an integrated photovoltaic thermal-phase change material system using Taguchi method. *Improving Residential Energy Efficiency International Conference*, February 2017.

Contents

List of Figures

List of Tables

Nomenclature

A	heat transfer area
ANOVA	analysis of variance
$a', a'', \ldots, a^{(z)}$	the first, second, … z^{th} positions in L_{com}-*metric* ranking list in Eq. (5.12)
a_0-a_3	coefficients in Eq. (5.3)
a_L, a_l	lower limits of the search ranges for the continuous factors
b_0-b_2	coefficients in Eq. (5.7)
b_U, b_u	upper limits of the search ranges for the continuous factors
c	coefficient in Eq. (2.5)
$\vec{c}_k$	centre of the k^{th} cluster
c_p	specific heat capacity, ((J/kg·K))
c_t	temperature modifier in Eq. (6.8)
COP	coefficient of performance
CTPE	coefficient of thermal performance enhancement
d_h	hydrate diameter, (m)
DOF	degree of freedom
E	electricity (kWh)
F	Fibonacci sequence
f	phase change fraction, (%)
F_{COP}	COP modifier of the heat pump according to the performance map
f_{ij}	j^{th} criterion for i^{th} alternative solution
GA	genetic algorithm
Gz	Graetz number
GRI	global ranking indicator
h	heat transfer coefficient, (W/(m^2·K))
H_{PCM}	volumetric enthalpy of PCMs, (J/m^3)
h_{PCM}	specific enthalpy of PCMs, (J/kg)
HP	heat pump
HJ	Hooke-Jeeves pattern search
HVAC	heating, ventilation and air conditioning
I	length of the search range, *i.e.* factor interval
I_t	l solar irradiation (W/m^2)

IMA	incident angle modifier
k	thermal conductivity, (W/(m·K))
KPI	key performance indicator
L	length, (m)
LRI	local ranking indicator
M	number of the PCM brick in the direction of the air flow
m	mass, (kg)
MCDM	multi-criteria decision-making
N	number of the air channels
n	number, or coefficient in Eq.(2.5)
Nu	Nusselt number
O	original set of objects
O'	augmented object set
P	population of the optimisation variables in Chapter 5, or power in Chapter 6, (W)
PCM	phase change material
PLF	part load factor
PLR	part load ratio
PSO	particle swarm optimisation
Pr	Prandtl number
PVT	photovoltaic thermal
Δp	pressure difference
Q	heat (J)
Q_i	scalar quantity L_{com}-*metric*,
$\dot{Q}$	rate of heat flow (W)
q	heat absorbed per area of the room surface, (J/m^2)
$\dot{q}$	heat flux, (W/m^2)
$\dot{Q}_m$	mass flow rate, (kg/s)
$\dot{Q}_v$	volume flow rate, (l/s)
R	thermal resistance, (m^{2}W/K)
r	membership exponent in Eq. (5.17)
Ra	Rayleigh number
Re	Reynold number

R_i	scalar quantity L_∞-*metric*
s	phase boundary position, (m)
s^2	variance of objective response
S_i	scalar quantity L_1-*metric*
S/N	signal-to-noise ratio
SS	sum of squares of factors
SS'	pure sum of squares
T	temperature, (^{o}C)
t	time, (s)
T_m	phase change temperature, (^{o}C)
Δt_{ch}	effective PCM charging time, (h)
TES	thermal energy storage
U	overall heat transfer coefficient, (W/(m^2·K))
u	velocity, (m/s)
u_{ik}	membership coefficient of the object $\vec{y}_i$ to cluster $\vec{c}_k$,
v	weight for L_1-*metric*
Var	Variance
W	width, (m)
w	weighting factor
x_i	i^{th} continuous factors in Eq. (4.1)
$\vec{x}$	optimisation variable vector
y	objective response or function
$\vec{y}$	object
z_j	j^{th} discrete factors in Eq. (4.1)
%C	percentage contribution, (%)

Greek letters

α	absorptivity
α_j, β_j,	values of the discrete factors in Eq. (4.1)
Γ	ideal object set
γ	latent PCM heat of fusion, (J/(kg·K))
δ	thickness (m)
ε	heat transfer effectiveness
ε_b	emissivity

$\bar{\varepsilon}_{ch}$	average heat transfer effectiveness for charging performance, (%)
η	efficiency
Λ	elite set
μ	rate of variance
ξ	friction factor
ρ	density, (kg/m^3)
ρ_{ref}	reflectance
σ	Stefan-Boltzmann constant
ς	mutation rate
τ	time parameter, (h)
φ	weighting factor related to the PCM thermodynamic state, (%)
ψ	energy storage percentage
ϕ	elite rate

Subscripts

air-b	heat transfer direction from the air to the bottom plate
alt	alternative solutions on Pareto front
amb	ambient
air-PCM$_2$	heat transfer direction from the air to the PCM layer 2
b	bottom plate of PVT collectors
b-rsp	heat transfer direction from the bottom plate to the roof space
c	criteria (*i.e.* objectives) in bi-objective optimisation
COMO	heat transfer towards the plasterboard of the building envelope
con	consumption
cond	conductive heat transfer
conv	convective heat transfer
cs	cross-section areas of fins
e	elite
eq	equivalent
f	friction
fs	factors with significant influence on the objective response
fin-air	heat transfer direction from the fins to the absorber plate
fin-b	heat transfer direction from the absorber plate to the bottom plate
g	glass cover

im	inverse mapping
ins	insulation
io	ideal object
ins	insulation
k	cluster
l	liquid phases of PCMs
M	maximal index in the Fibonacci sequence
mu	mutation
nc	natural convective heat transfer
P	population
p-air	heat transfer direction from the absorber plate to the air
p-fin	heat transfer direction from absorber plate to the fins
PCM_1-*air*	heat transfer direction from the PCM layer 1 to the air
PCM_1-PCM_2	heat transfer direction from the PCM layer 1 to the PCM layer 2
PV	photovoltaic
PV-air	heat transfer direction from the PV panel to the air
PV-b	heat transfer direction from the PV panel to the bottom plate
PV-g	heat transfer direction from the PV panel to the glass cover
rad	radiative heat transfer
rs	roof space
s	solid phases of PCMs
sky	sky radiative heat transfer
t	total sampling number during the charging period
tot	total
w	wind-driven force convective heat transfer
0	reference value
v	variables

Superscripts

g	g^{th} generation
k	k^{th} time step
*	minimal
-	maximal

Chapter 1 Introduction

1.1 Background and motivation

The increase in greenhouse gas emissions, the shortage of primary energy and the continuously growing demand for energy have become major public concerns over the previous decades (Chen X.J. *et al.* 2014). Buildings are among the major energy consumers and as such, account for almost 45% of global energy usage and emit a similar share of greenhouse gas emissions (Butler 2008). Most of the energy used in buildings is for heating, ventilation, and air conditioning (HVAC) (Perez-Lombard *et al.* 2008). Due to the expected increase in population, urbanisation, economic growth, and the growing demand for better indoor thermal comfort, the energy consumption of building HVAC systems is projected to increase by more than 70% from 2010 to 2050 (Diana *et al.* 2015). The development and deployment of advanced energy technologies and improvements in energy efficiency of building HVAC systems are therefore the essential requirements needed to reduce building energy consumption and achieve sustainability of the built environment (Wang *et al.* 2010; Zalba and Marin 2003; Saitoh *et al.* 2003).

Solar photovoltaic thermal (PVT) collectors are sustainable and environmentally friendly technologies which can help to offset the pressure applied by building energy consumption (Sohel *et al.* 2014). A PVT collector is a liquid or air-based module which uses solar energy to simultaneously produce electricity and low grade thermal energy (Zondag 2008). Liquid based PVT collectors tend to be more efficient, but the heated air in air-based PVT collectors can be directly used for space heating or as preheated air for HVAC systems (Kumar and Rosen 2011). Unlike separate solar technologies used to generate heat and electricity, PVT collectors are more cost effective (Rakesh and Marc 2011; Chow *et al.* 2007). However, since solar energy is intermittent, the PVT collectors can only be used during the daytime, and even then the performance of the PVT collectors can be affected by weather conditions. For these reasons, exploring alternative ways to improve the performance of such systems is important and the option of integrating thermal energy storage (TES) systems with PVT collectors could be a promising solution to better manage the thermal and energy requirements of buildings (Labat *et al.* 2014).

Thermal energy storage (TES) systems have been used to store and release thermal energy on a short-term, diurnal, or seasonal basis (Iten *et al.* 2016), depending on the thermal load requirements of buildings. The International Renewable Energy Agency (2011) estimated that 1.4 million GWh of energy and 400 million tonnes of CO_2 emissions per year could be saved from the building and industrial sectors in Europe through a more extensive use of heat and cold storage systems. Over the last two decades, TES systems with phase change materials (PCMs) have been receiving more attention because PCMs with high energy storage densities can store a large amount of thermal energy and release it for later use at relatively constant temperatures, so they are well suited for building applications (Soare *et al.* 2013; Parameshwaran *et al.* 2012; Pramod *et al.* 2012). PCMs can be integrated into building envelopes to increase the building thermal mass and improve indoor thermal comfort, or they can be integrated with building HVAC systems for load shifting and demand control.

To date, PCMs are mostly used in demonstration projects due to the lack of cost effective systems and solutions, which is why effective solutions with high performance are needed to promote the deployment of PCMs in buildings. The use of PCMs in building envelopes (*i.e.* passive utilisation) may have limited benefits because in many instances they fail to respond to rapid variations in the demand for indoor heating and cooling, and their storage capacity cannot be fully utilised due to small temperature variations between daytime and night time (Iten *et al.* 2014). The application of PCMs in building HVAC systems (*i.e.* active utilisation) often performs well for demand side management (Zhu N. *et al.* 2009; Zhai X.Q. *et al.* 2015; Vakilaltojjar and Saman 2001; Chen X.J. 2014) because the forced convection enhances the heat transfer. However, many PCMs, particularly organic PCMs, have a low thermal conductivity which may still impede their rapid response to load variation. Various measures have been proposed and used to solve the low thermal conductivity of PCMs, including but not limited to the insertion of high thermal conductivity materials or carbon fins/foams (Agyenim *et al.* 2010a), micro-encapsulation (Cabeza *et al.*, 2007), direct contact with heat transfer fluid (Farid *et al.* 2004), and adding the nanoparticles (Weinstein *et al.* 2008; Cui *et al.* 2011). These measures improved the thermal conductivity of PCMs, but they reduced the energy storage density, which offsets part of the benefits achieved through the increased thermal conductivity. Unlike enhancing the thermal properties of PCMs, the processes for proper design and

optimisation of PCM systems, as well as the effective integration of PCMs with thermal energy source systems and buildings, are generally more cost effective (Lazaro *et al.* 2009a; Dolado *et al.* 2011b), and therefore more practical and of interest to facilitate the use of PCMs in buildings.

A lot of effort has also gone into investigating how solar thermal systems perform with PCMs, and these systems with integrated PCMs offered more flexibility to maximise the system operation through effectively using solar energy, but only a few trials have been carried out to investigate the performance of buildings with integrated PVT collectors and PCMs. This means that the research in this area is far from sufficient. This is why high performance solutions and strategies to integrate both technologies into buildings and building HVAC systems are still needed. Furthermore, most existing research regarding the typically-called "design optimisation" of PVT and/or PCM systems relied on either parametric studies or empirical correlations to improve the system performance. The lack of the optimisation methodologies in this field indicated the necessity of introducing various design optimiation strategies into the optimisation of buildings with integrated PVT collectors and PCMs. In addition, most existing models for PCMs did not consider the hysteresis phenomenon (*i.e.* the solidification curve is not identical with the melting curve) which exists in a large number of commonly used PCMs. It is therefore a very important factor that needs to be considered to accurately present all stages of the actual phase change process in simulations.

There are several scientific challenges from different aspects to address the above research gaps:

- There is currently no systemetic approach investigating potential solutions to integrated PCMs with PVT collectors in buildings.
- Secondly, there are insufficient optimisation studies on buildings and HVAC systems with integrated PVT collectors and PCMs.
- Finally, the development of accurate but time-efficient PCM models is the prerequisite to achieve system simulation and optimisation.

1.2 Research aim and objectives

The aim of this project is to explore, evaluate and optimise effective solutions and strategies to integrate PCMs and PVT collectors in buildings and building HVAC systems to improve building thermal performance management and energy efficiency. The specific objectives are as follows:

a) To model and evaluate the thermal performance of buildings with integrated PVT collectors for space heating and with the envelopes enhanced by PCMs (named as PCM enhanced buildings);

b) To develop an optimisation strategy to optimise the thermal performance of the PCM enhanced buildings with integrated PVT collectors for space heating;

c) To perform an experimental investigation on the charging performance of a PCM TES system with integrated PVT collectors, and to develop multi-objective optimisation strategies to optimise the system; and

d) To model the performance and implement the optimisation of a heat pump system with integrated PVT collectors and PCM layers laminated into the building ceiling for space heating.

By addressing the above research objectives, the mensioned challenges can be overcome and several scientific contributions can be achieved accordingly.

- Different system integration strategies were investigated, and their performances were analysed to provide a systmetic investigation of integrating PCMs with PVT collectors in buildings;

- Different optimisation strategies were introduced and developed to optimise the performance of the buildings and building HVAC systems with using PCMs and PVT collectors;

- Several models for PCM components and PCM TES unit were developed and validated to satisfy different requirements in performance modelling and optimisation. These models can be used for future research in this field.

1.3 Research methodology

The overall research methodology used in this thesis is shown in Fig. 1.1. Three systems with integrated PCMs and PVT collectors in buildings and building HVAC systems were developed, evaluated and optimised, including i) buildings with envelopes enhanced by PCMs and PVT collectors for space heating; ii) a centralised PCM TES system with integrated PVT collectors for solar heat storage and iii) an air source heat pump system with integrated PVT collectors and PCM layers laminated into the building ceiling for space conditioning, as shown in Fig. 1.2.

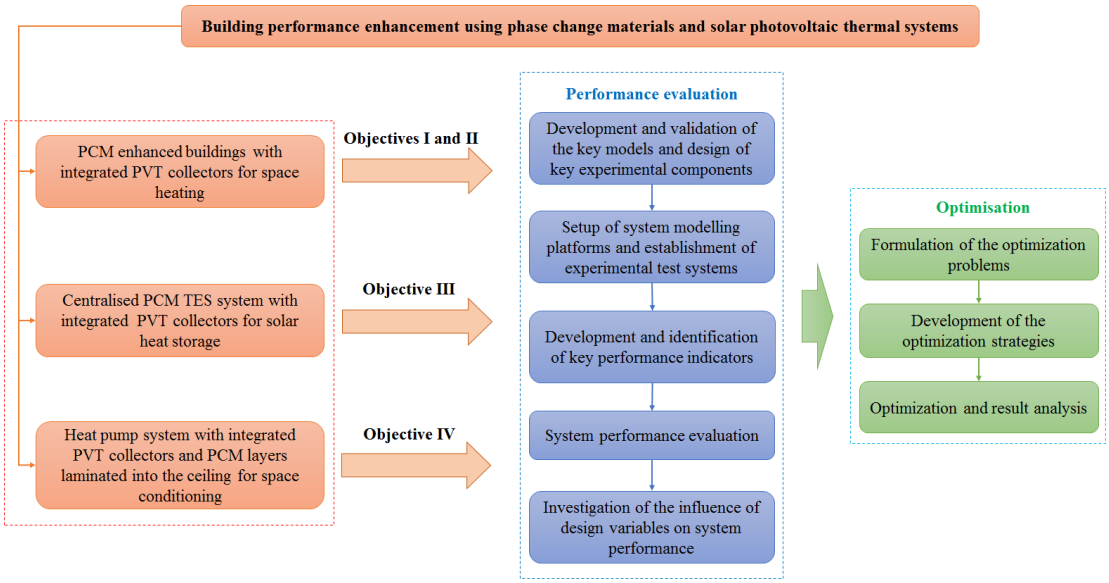

Fig. 1.1 Overall research methodology used in this thesis.

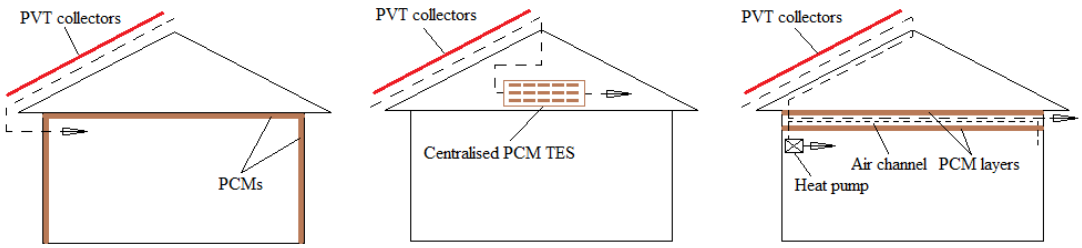

i) ii) iii)

Fig. 1.2 Sketch of the three systems with integrated PCMs and PVT collectors in buildings and building HVAC systems to be investigated.

To achieve Objective I, a building envelope-integrated PCM model which considered the hysteresis phenomenon of PCMs was first developed and validated to facilitate the setup of a modelling system. The thermal performance of the PCM enhanced buildings with integrated PVT collectors for space heating was then numerically evaluated based

on a key performance indicator (KPI) developed to quantify the likely benefits of using PVT collectors and PCMs. The influence of key design variables on the building thermal performance was also investigated.

In Objective II, a new optimisation method which can solve multi-dimensional optimisation problems with discrete and continuous optimisation variables was developed and used for the design optimisation of the PCM enhanced buildings with integrated PVT collectors for space heating. The key design variables identified based on the outcomes achieved through Objective I were optimised to maximise the thermal performance of the PCM enhanced buildings with integrated PVT collectors for space heating.

Objective III was achieved by first investigating the charging performance of a centralised PCM TES system with integrated PVT collectors in a lab-scale experimental setup. A number of PCM bricks were organised in arrays within a rectangular air duct to form the PCM TES unit in the system. Here, a series of experiments were designed using the Taguchi method and based on the results two correlations related to the KPIs were developed and used as the optimisation functions. In this study, two bi-objective optimisation strategies were developed to increase the confidence of the optimal solutions; one strategy was developed using the controlled elitist genetic algorithm (a variant of elitist non-dominated sorting genetic algorithm (Mathwork 2016)) and a multi-criteria decision-making (MCDM) process (Opricovic 1998), while the other was developed based on the fuzzy clustering method (Jajuga 1991).

A heat pump system with integrated PVT collectors and PCM layers laminated into the building ceiling was modelled and optimised to achieve Objective IV. Two PCM layers with an air channel between them were laminated into the ceiling to enhance the local thermal mass and also serve as a centralised TES unit for the heat pump system to provide a new solution for improving building thermal and energy efficiency performance. A PCM TES unit model which also considered the hysteresis phenomenon and the interaction with building envelopes was developed, validated, and then used to establish the modelling system. The performance of the proposed system and the influence of key design variables were investigated numerically. A design optimisation problem was also formulated and solved using the hybrid Particle

Swarm Optimisation and Hooke-Jeeves pattern search (PSO-HJ) algorithm to maximise the energy efficiency of the system.

1.4 Thesis outline

This chapter introduced the background and motivation of this research, and also outlined the research objectives and overall research methodology. The subsequent chapters are organised as follows.

Chapter 2 presents a literature review of recent developments on modelling, experiments, and optimisation of PCMs and PVT collectors for building thermal and demand side management. It also describes the modelling of heat transfer and phase change process of PCMs and reviews the optimisation strategies for the PCM systems.

Chapter 3 presents the numerical modelling and thermal performance evaluation of buildings with integrated PVT collectors for space heating and envelopes enhanced by PCMs. The thermal energy storage using PCMs can be enhanced by the heated air from the PVT collectors to facilitate the indoor space heating. A parametric study and a Taguchi-based analysis were carried out to investigate the enhanced building thermal performance using the PCMs and PVT collectors for space heating.

Chapter 4 presents the development of a new design optimisation strategy, named as Taguchi-Fibonacci search method, to optimise the thermal performance of the PCM enhanced buildings with integrated PVT collectors for space heating. The optimal solution was then compared with a baseline case that was not optimised.

Chapter 5 presents an experimental investigation and a bi-objective optimisation of a centralised PCM TES system with integrated PVT collectors. Two correlations regarding the performance of a PCM TES unit were established based on a series of experiments, and then used as the optimisation functions to formulate the optimisation problem. A bi-objective optimisation strategy using the controlled elitist genetic algorithm (Mathwork 2016) and multi-criteria decision-making process (Opricovic 1998) were used to determine an optimal Pareto front and the compromise optimal designs of the PCM TES unit. Another fuzzy clustering-based optimisation algorithm was then developed and used to solve the same optimisation problem as a comparison to increase the confidence in the optimal solution identified.

Chapter 6 presents the numerical modelling, evaluation and optimisation of a heat pump system with integrated PVT collectors and PCM layers laminated into the building ceiling. In the system, the heated air from PVT collectors was used to charge the PCM TES. Two PCM layers with an air channel between them were laminated in building ceiling to enhance the local thermal mass, at the same time, to serve as a centralised TES for indoor space heating directly, or to preheat the air for the indoor unit of the air source heat pump. The benefit of using the proposed system was evaluated by comparing it with a baseline case using the heat pump only. The influence of major design variables on the system performance was studied using the Taguchi method. A design optimisation using the hybrid Particle Swarm Optimisation and Hooke-Jeeves pattern search algorithm was then carried out to maximise the building energy efficiency.

Chapter 7 summarises the key findings from this thesis, and provides some recommendations for future work in this research area.

Chapter 2 Literature review

This thesis will investigate the strategies needed to integrate phase change materials (PCMs) with solar photovoltaic thermal (PVT) collectors in buildings to achieve better indoor thermal performance and promote energy efficiency. This chapter is a literature review of recent research work into the development, modelling, experiments, and optimisations carried out in this field to identify some gaps in the research to facilitate the optimal integration of phase change materials and solar photovoltaic thermal collectors into buildings to improve building performance.

This chapter is organised as follows: Section 2.1 introduces the classification and characteristics of PCMs, and the containment methods of PCMs for building applications; Section 2.2 summarises the modelling of PCM heat transfer and phase change processes, as well as the various assumptions and simplifications of the available PCM models; Sections 2.3 and 2.4 are the overviews of studies into the passive and active applications of PCMs in buildings, respectively. A brief review of the design and optimisation of PCM systems for building applications is presented in Section 2.5, while Section 2.6 briefly reviews the studies of building integrated PVT collector (BIPVT). The key findings from the literature review are summarised in Section 2.7.

2.1 PCMs for building applications

2.1.1 PCM classification and characteristics

PCMs are substances that can absorb, store, and release a large amount of thermal energy within a narrow temperature range through phase transitions (Kuznik *et al.* 2011). This phase transition can be solid-solid, gas-liquid, solid-liquid, and even solid-gas (Abhatlow 1983), of which solid-liquid PCMs with substantial alternatives and a small change in volume during the phase change process are well suited for thermal energy storage (TES) applications. This is why they have been widely considered in the building sector (Osterman *et al.* 2012). The PCMs discussed in this thesis refer to solid-liquid PCMs.

PCMs are mainly categorised as organic, inorganic and eutectic materials (Beatens *et al* 2010), each of which can be further subdivided as shown in Fig. 2.1. Organic PCMs

can be classified as paraffin and non-paraffin, such as fatty acids, sugar alcohols, esters and glycols (Hasnain 1998), which cover a phase change temperature range of 0-200ºC (Mehling and Cabeza 2008). Organic PCMs generally have undesirable properties such as flammability, low thermal conductivity, and low volumetric latent heat storage capacity. Inorganic PCMs mainly include salt hydrates and salts where the salt hydrates tend to have a phase change temperature range of 5-130ºC (Mehling and Cabeza 2008; Dieckman 2008). Unlike organic PCMs, inorganic PCMs have a relatively high volumetric latent heat storage capacity and thermal conductivity, and they are inflammable, with sharp phase transition and low costs (Kuznik *et al.* 2011). However, segregation and supercooling are the major issues which affect their durability and thermal performance (Tyagi and Buddhi *et al.* 2007).

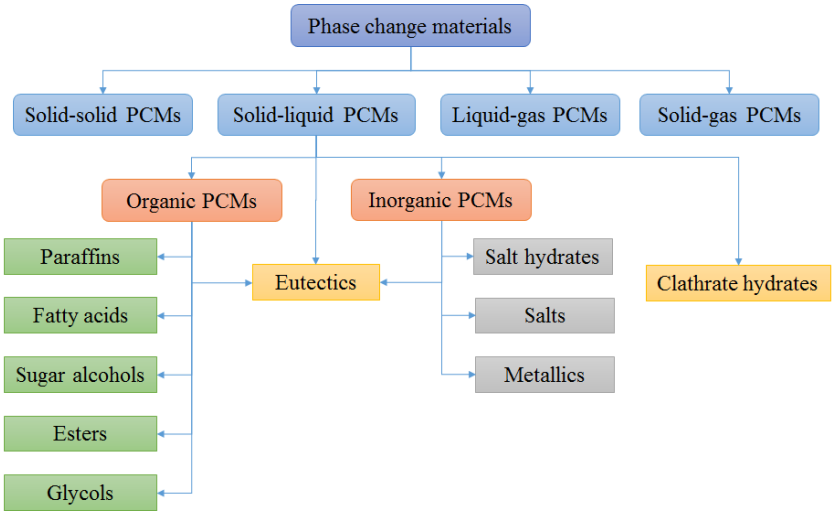

Fig. 2.1 PCM classifications.

Eutectics are isolated from organic and inorganic PCMs because they can be mixtures of organic materials, inorganic materials, or organic-inorganic eutectics (Sharma *et al.* 2009). Eutectics are minimum-melting compositions of multiple components in which different components are mixed in certain proportions to create congruent phase transition behaviour with definite melting and freezing points (Verma *et al.* 2008). As well as common PCM categories, clathrate hydrates, including gas hydrates, which can form at ambient pressure and have a high latent heat, look promising to be used as PCMs (Castellani *et al.* 2014). The phase change temperature and specific volume enthalpy of some of the PCM categories discussed above are summarised in Fig. 2.2.

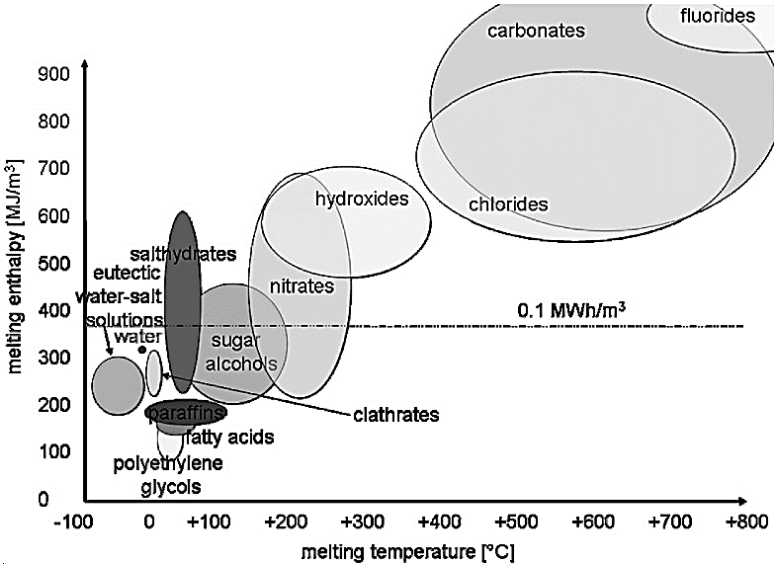

Fig. 2.2 Classes of PCMs and their typical phase change temperature and enthalpy ranges (Mehling and Cabeza 2008).

2.1.2 Selection criteria of PCMs for building applications

PCMs to be used in building applications share some general selection criteria in terms of the thermal, physical, chemical, and kinetic properties, as well as cost and availability, which have been summarised and recommended by a number of researchers (Sharma and Sagara 2005; Baetens *et al.* 2010). The main selection criteria are listed below:

- Desired thermal properties: favourable phase change temperature range based on climatic conditions and application modes, high latent heat of fusion for latent heat storage, high specific heat for additional sensible heat storage, and high thermal conductivity to facilitate fast charging and discharging of thermal energy;

- Desired physical properties: small volume changes during phase transition, small vapour pressure during operation, and a congruent phase change process;

- Desired kinetic properties: high nucleation rate to avoid supercooling, and sufficient crystallisation;

- Desired chemical properties: long-term chemical stability, no segregation, non-corrosiveness, non-toxicity, and no fire hazard; and

- Economics: low cost and large scale availability.

2.1.3 Integrating PCMs in buildings

PCMs can be used passively or actively in buildings, as shown in Fig. 2.3. PCMs can be incorporated into building envelopes to increase the thermal mass and reduce indoor temperature fluctuations, or reduce the heating and cooling loads. PCMs can also be integrated with building heating, ventilation, and air conditioning (HVAC) systems as centralised TES units to improve system efficiency, achieve peak load shifting or reduce the power consumption of HVAC systems. A number of PCMs used in building envelopes and HVAC systems are summarised in Table 2.1 and Table 2.2, respectively. These tables show that the phase change temperature of PCMs in most studies into heating and cooling applications was between 0-60^{o}C and many of them were close to the indoor thermal comfort temperature. The storage of solar thermal energy using PCMs to facilitate indoor space heating has been one of the hottest research topics and as such has attracted increasing attention as PCMs provide an efficient approach to overcoming the intermittency of solar energy. Although numerous PCMs are now available for building applications, it is practically difficult to find a perfect PCM with all the desired properties for various applications.

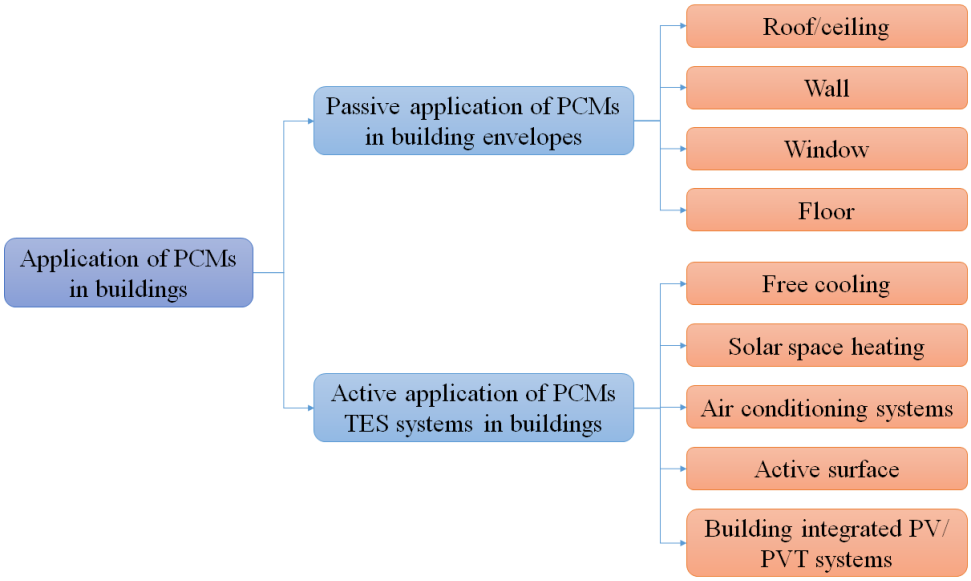

Fig. 2.3 PCMs in building applications.

Table 2.1 A number of reported PCMs used in building envelopes.

PCMs (or PCM composites)	Phase change temperature range (^oC)		Heat of fusion (melting/solidification) (kJ/kg)	Configuration	Application approach	Reference
	melting	solidification				
Naturally occurring fatty acids/glycerides	16.5-26.5		116.7	Rectangular	PCM-cellulose wall insulation	Biswa and Abhari 2014
BioPCM M182	22.65 (peak)*	19.78 (peak)	209.48/207.53	Rectangular	PCM roof layer	Jayalath *et al.* 2016a
$CaCl_2$+NaCl+KCl+H_2O	26-28		188	Rectangular	PCM roof layer	Pasupathy and Velraj 2008
ClimSel C 32	32		264			
RT27 (organic)	28	26	179	Rectangular	PCM wall layer	Castell *et al.* 2010
SP25 A8 (inorganic)	26	25	180			
Micronal PCM	26		110	Rectangular	PCM concrete wall	Cabeza *et al.* 2007
PCM gypsum	20.9 (peak)	20.4 (peak)	30.7	Rectangular	PCM wall board	Athienitis *et al.* 1997
RT25 (organic)	25±0.5		147±15	Rectangular	PCM facade panel for windows	Weinlader *et al.* 2005
S27 ($CaCl_2.6H_2O$ based)	27±0.5		190±19			
L30 ($LiNO_3.3H_2O$ based)	30±0.5		270±27			
-	26		110	Rectangular	PCM gypsum wallboard	Ascione *et al.* 2014
GR41 organic PCM and inorganic carrier matrix	43		63	Rectangular	PCM wall layer	Huang M.J. *et al.* 2006
GR27	28		72			
ENERGAIN	22.2 (peak), 13.6 (on-set)	17.8 (peak), 23.5 (on-set)	107.5/104.5	Rectangular	PCM wallboard	Kuznik *et al.* 2008a, 2008b, and 2010; Kuznik and Virgone 2009a and 2009b

(*Continue*)

PCMs (or PCM composites)	Phase change temperature range (^{o}C)		Heat of fusion (melting/solidification) (kJ/kg)	Configuration	Application approach	Reference
	melting	solidification				
Emerest 2326 (mixture of butyl stearate and butyl palmitate)	20.61 (peak), 16.92 (on-set)	18.22 (peak), 19.35 (on-set)	139.9/139.7	Rectangular	PCM gypsum wallboard	Scalat *et al.* 1996
Heptadecane	22		214	Rectangular	activated PCM ceiling panel	Koschenz and Lehmann 2004
RT27 (organic)	28	26	179	Rectangular	PCM cellulose insulation wall layer	Evers *et al.* 2010
TH29 (salt hydrate)	29	26	175			
Paraffin	around 20		120	Rectangular	PCM floor layer	Zhang Y.P. *et al.* 2006
GR25 (organic PCM and inorganic carrier matrix)	26		-	Rectangular	PCM gypsum wall board	Ahmad *et al.* 2006
polyethylene glycol (PEG600)	around 20-25		-	Rectangular		
n-Octadecane	27		243.5	Cylinder	PCM enhanced brick	Alawadhi 2008
n-Eicosane	37		241			
P116	47		225			
Paraffin	32.5 (peak)	25.9 (peak)	131	Cylinder	PCM wall component	Medina *et al.* 2008
mixture of capric acid and 1-dodecanol (eutectic)	28 (range of 2^{o}C)	25.1 (range of 1^{o}C)	103.5/119.8	Rectangular	PCM wallboard	Lu *et al.* 2014

* peak and on-set indicate the peak and on-set temperatures of the DSC curves, respectively.

Table 2.2 A number of reported PCMs used for building HVAC systems for air conditioning.

PCMs (or PCM composites)	Phase change temperature range (^oC)		Heat of fusion (melting/solidification) (kJ/kg)	Configuration	Application approach	Energy sources	Ref.
	melting	solidification					
DX-53 (paraffin based)	51-55		144.6	Rectangular	Liquid-based PCM TES unit	solar heat	Chen C. *et al.* 2014
Mixture of salt and paraffin	23		180	Rectangular	air-based PCM TES unit	solar heat	Waqas and Kumar 2013
RT20 (organic)	20-22		172 (over 11-26^oC)	Rectangular	air-based PCM TES unit	night time coolness	Butala and Stritih 2009
RT27 (organic)	25-28	28-25	179 (over 20-35^oC)	Rectangular	air-based PCM TES unit	night time coolness	Dolado *et al.* 2011b; Dolado *et al.* 2012a and 2012b; Lazaro *et al.* 2009a
$CaCl_2 \cdot 6H_2O$	29		-	Rectangular	air-based PCM TES unit	solar heat	Saman *et al.* 2005
Self-developed PCM (fatty acid)	22-26		190	Rectangular	air-based PCM TES unit	night time coolness	Kang *et al.* 2003
self-developed PCM	16.91	14.97	115.1	Sphere	water-based PCM TES unit	solar heat	Zhai *et al.* 2014
Paraffin	43-53		226	Rectangular	air-based PCM TES unit	solar heat	Summer *et al.* 2012
$CaCl_2 \cdot 6H_2O$	-		-	rectangular	water-based PCM TES unit	solar heat	Helm *et al.* 2009
RT20 (organic)	22 (peak)*	20 (peak)	160-180	Sphere	air-based PCM TES unit	electric power	Chaiyat 2015

(*Continue*)

PCMs (or PCM composites)		Phase change temperature range (^{o}C)		Heat of fusion (melting/solidification) (kJ/kg)	Configuration	Application approach	Energy sources	Ref.
S15 (salt hydrate based)		15		142	Cylinder	water-based PCM TES unit	solar heat	Chen X.J. *et al.* 2014
MT17	(mixture of paraffin and stearic acid)	17.5	18.5	77/86	-	air-based PCM TES unit	electric power	Yamaha and Misaki 2015
MT19		20.5	21.5	86/87				
MT21		20.5	21.5	87/85				
MT23		22	21.5	83/76				
Mixture of n-paraffin (C16-20)		-		-	Rectangular	air-based PCM TES unit and PCM ceiling board	electric power	Kondo and Ibamoto 2006
-		16-25		180	Rectangular	air-based PCM TES unit	night time coolness	Gowreesunker *et al.* 2013
S21 (salt hydrate based)		22		170	Rectangular	air-based PCM TES unit	electric power	Fiorentini *et al.* 2015
Paraffin and expanded perlite composite		28		210	Rectangular	water-based PCM TES unit	solar heat	Malvi *et al.* 2011
PCM40		42-44		168	Sphere	water-based PCM TES unit	-	Aldoss and Rahman 2014
PCM50		50-52		200				
PCM60		60-62		209				
Microtek 37D (paraffin)		25-35	33-22	222	Rectangular	air-based PCM TES unit	electric power	Labat *et al.* 2014

(*Continue*)

PCMs (or PCM composites)	Phase change temperature range (^{o}C)		Heat of fusion (melting/solidification) (kJ/kg)	Configuration	Application approach	Energy sources	Ref.
-	38 or 36 (optimal)		150	Rectangular	activated PCM floor layers	electric power	Jin and Zhang 2011
-	18 or 16 (optimal)		150				
Self-develop PCM (paraffin)	around 60		150	Rectangular	activated PCM floor layer	electric power	Zhang Y.P. *et al.* 2006
RT42 (organic)	38-43	43-37	174	Rectangular	air-based PCM TES unit	solar heat	RT42 (organic)
Emerst 2326	20.45 (peak), 17.15 (on-set)	18.65 (peak), 19.45 (on-set)	138.6/135.9	-	air-based PCM TES unit	internal load	Lee *et al.* 2000
Unicere 55 (paraffin)	53.68 (peak), 47.19 (on-set)	52.54 (peak), 53.71 (on-set)	189.4/182.3				
ENERGAIN	22.2 (peak), 13.6 (on-set)	17.8 (peak), 23.5 (on-set)	107.5/104.5	Rectangular	air-based PCM TES unit	night time coolness and internal load	Lopez *et al.* 2013
RT5HC (organic)	5.5		240	Cylinder	water-based direct contact PCM TES unit	electric power	De Falco *et al.* 2016
water	0		around 334	Cylinder	liquid-based PCM TES unit	electric power	Tay *et al.* 2012a and 2012b

(*Continue*)

PCMs (or PCM composites)	Phase change temperature range (^{o}C)	Heat of fusion (melting/solidification) (kJ/kg)	Configuration	Application approach	Energy sources	Ref.
capric and lauric acid	16.91	115.1	Cylinder	water-based PCM TES unit	electric power	Zhai *et al.* 2015
$CaCl_2 \cdot 6H_2O$	27.9-29.85	187.45	Cylinder	water-based PCM TES unit	solar heat	Esen *et al.* 1998
Paraffin	32-32.1	251				
$Na_2SO_4 \cdot 10H_2O$	39-39.15	180				
Paraffin-wax	46.7-46.85	209				

* peak and on-set indicate the peak and on-set temperatures of the DSC curves, respectively.

2.1.4 Containment of PCMs for building applications

PCMs must be contained in building applications to prevent the loss of PCMs in the liquid phase, or isolate from the surroundings. Various methods of containment have been used to prepare PCM building components or develop TES units for building applications.

2.1.4.1 Impregnation

Impregnation allows for a direct and economical incorporation or immersion of PCMs into conventional construction materials (Soares *et al.* 2013). The building materials used to support the PCMs should be porous materials, whose porosity is small enough to provide a surface tension strong enough to prevent the PCMs from leaking in the liquid phase. However, this impregnation may affect the mechanical strength of the building materials and run the risk of bleeding during the PCM melting process. Building materials such as gypsum (Feldman and Banu 1991), concrete (Hadjieva *et al.* 2000), cement (Li H. *et al.* 2010), cellulose (Evers *et al.* 2010), vermiculite (Li X.Q. *et al.* 2016), and ceramic (Novais *et al.* 2015) can be impregnated with PCMs, and other porous materials such as SiO_2 matrix (Wang W.L. *et al.* 2009) and porous-graphite-matrix (Py *et al.* 2001) can also be used as supporting material to enhance thermal conductivity. The shape of PCMs can be stabilised using copolymer as a special impregnation whose PCM fraction can be as much as 80% in weight (Zhang Y.P. *et al.* 2006). The advantages of such shape-stabilised PCMs have been demonstrated in a number of studies (Xiao *et al.* 2001 and 2002; Zhou D. *et al.* 2012; Soares *et al.* 2013), including the large heat of fusion, the ability to retain the shape during phase change, and good long-term performance), all of which.

2.1.4.2 Macro-encapsulation

Macro-encapsulation has been used as a containment method for the last several decades; it refers to enclosing bulk PCMs with containers larger than 1 mm (Salunkhe and Shembekar 2012). Macro-encapsulation can be cylindrical, rectangular and spherical in shape, *etc*. Unlike impregnating PCMs, macro-encapsulating bulk PCMs ensures there is a large heat storage capacity. It has been reported that rectangular and cylindrical containers are the most intensely analysed configurations for macro-encapsulating PCMs (Agyenim *et al.* 2010).

A shell-and-tube system is one of the most popular cylindrical macro-encapsulation because the thermal charge and discharge processes are achieved by heat transfer between the PCMs and heat transfer fluids. PCMs can be filled in on the shell side or tube side, and then the heat transfer fluid flows through the tube(s) or shell. This heat transfer process will be enhanced due to heat convection when PCMs are encapsulated in the shell side (Hendra *et al.* 2005). For instance, the thermal performance of two different scenarios where the PCM filled in the tube and the shell side respectively was compared theoretically by Esen *et al.* (1998), and the filling the PCM in the shell side was recommended because it would reduce the melting time. Hendra *et al.* (2005) studied the heat transfer characteristics of a staggered tubes heat storage system numerically when PCMs was filled into the shell side; they found that the convection heat transfer in the melted PCM in shell side was the dominant heat transfer mechanism compared with the thermal conduction.

Rectangular macro-encapsulation of PCMs has been widely applied in building applications due to its easy installation. It is usually used as a form of thin PCM layers or PCM slabs that can be integrated into building envelopes. For example, PCMs were placed inside hollow glass bricks that were used as building components for indoor thermal management (Bontempsa *et al.* 2011). Compact storage modules (CSM) containing different PCMs were used by Castell *et al.* (2010) to smooth the fluctuations of daily indoor air temperatures. Ahmad *et al.* (2006) compared the thermal behaviour of three PCM enhanced wallboards where the macro-encapsulation of polyethylene glycol PEG 600 inside PVC panels had the best thermal performance due to its higher thermal capacity, conductivity and durability. The layers or slabs of PCM can also be used to develop PCM TES units which can then be integrated into HVAC systems for effective thermal management. For example, a PCM cold storage unit consisting of PCM plates enhanced by fins was studied by Butala and Stritih (2009) when being used to free cool buildings. The thermal performance of a PCM TES unit with a matrix of CSM panels (Rubitherm 2016) was studied numerically by Dolado *et al.* (2012b). The charging and discharging processes of an air-based PCM TES unit for solar air systems was simulated and experimentally validated by Charvat *et al.* (2014).

Since spherical macro-encapsulated PCMs have good bed porosity and a relatively large thermal area (Ismail *et al.* 2003; Cho and Choi 2000) when packed in storage

tanks, they have also been widely studied (De Gracia and Cabeza 2016). For instance, Ismail and Henriquez (2000) and Ismail *et al.* (2003) numerically studied the influence that the sphere size, initial temperature, and external temperature has on the solidification of PCMs inside the spherical capsules.

2.2.3 Micro-encapsulation and nano-encapsulation

Micro-encapsulation of PCMs is a term used when PCMs are encapsulated in particles smaller than 1 mm in diameter, while nano-encapsulated is a term that refers to the micro-encapsulated PCMs whose size is less than 1000 nm (Salunkhe and Shembekar 2012). The inherent characteristic of a large surface-to-volume ratio means that micro-encapsulation can enhance heat transfer with the surrounding material (Cabeza *et al.* 2011), but it may aggravate the problem of super-cooling (Al-Shannaq *et al.* 2015). The preparation of micro-encapsulated PCM relies on either chemical or physical methods. The chemical method was most commonly used (Zhang X.X. *et al.* 2005; Sukhorukov *et al.* 2005) because it can fabricate micro-encapsulated PCMs smaller than 100 um (Zhao and Zhang 2011). Micro-encapsulated PCMs are more likely to be mixed with conventional building construction materials such as plaster (Laia *et al.* 2010; Toppi and Mazzarella 2013) and concrete (Jayalath *et al.* 2016b), to prepare different PCM enhanced construction materials for building applications.

This review has presented the characteristics of different PCM containment methods. To maximise the capacity of thermal energy storage, macro-encapsulation tends to outperform other PCM containment methods because bulk PCMs can be encapsulated rather than being dispersed into building construction materials. Macro-encapsulated PCMs can also be used as components to develop centralised TES units, which allow heat exchange between PCMs and heat transfer fluids.

2.2 Modelling of PCM heat transfer and phase change process

Numerical modelling of the PCM phase change process is an effective way of facilitating the design and optimisation of PCM systems for building applications. This section outlines the common problems during PCM modelling, and presents the corresponding solutions towards these problems.

2.2.1 Stefan problem

The phase transition of a material is described by a particular kind of boundary value problems for partial differential equations where the phase boundary can move with time (Dutil *et al.* 2011). They are often difficult to solve because of the inherent non-linear nature at the moving solid-liquid interface which is controlled by the release and absorption of heat. This kind of problem is known as the Stefan problem (Stefan 1889) which was first generalised by Joseph Stefan as the energy equation at the boundary (see Eq. (2.1)).

$$\gamma\rho_{PCM}\left(\frac{ds(t)}{dt}\right)=k_s\left(\frac{\delta T_s}{\delta t}\right)-k_l\left(\frac{\delta T_l}{\delta t}\right) \tag{2.1}$$

where γ is the latent PCM heat of fusion, ρ is the density, $s(t)$ is the boundary position, k is thermal conductivity, t is the time, T is the temperature, and the subscripts s and l indicate the solid and liquid phases of PCMs, respectively.

Since the position and velocity of the phase boundaries are not known a priori, simulating the phase transition is complicated (Dutil *et al.* 2011). There are two main numerical approaches for solving the Stefan problem, *i.e.* the enthalpy method based on a fixed grid and an interface immobilisation technique based on the adaptive mesh (Ismail and De Jesus 1999). In the interface immobilisation technique, the grid covering the solid-liquid interfaces must be densified so that details of the physical processes can be captured and reasonably represented. In contrast, the enthalpy method enables the phase change problem to be simplified by identifying the governing equations for two phases so that the interface conditions are automatically achieved, and by creating a mushy zone which avoids sharp discontinuities between the two phases (Sharma *et al.* 2009). The enthalpy method was introduced by Voller (1990) and the energy control function is expressed in Eq. (2.2).

$$\frac{\partial H}{\partial t}=\nabla\cdot\left(k\nabla T\right) \tag{2.2}$$

where H is the total volumetric enthalpy, depending on the temperature.

For pure PCMs with an isothermal phase change temperature (see Fig. 2.4a)), the enthalpy of PCMs can be expressed as Eq. (2.3). For impure PCMs with a mushy phase change process (see Fig. 2.4b)), the enthalpy can be written as Eq. (2.4) (Nedjar 2002).

$$H_{PCM}(T)=\int_{T_m}^{T}\rho c_p dT+\rho f(T)\gamma \tag{2.3}$$

$$H_{PCM}(T)=\begin{cases}\int_{T_0}^{T}\rho_s c_{p,s}dT, \text{for}\, T<T_s\\ \int_{T_0}^{T_s}\rho_s c_{p,s}dT+\int_{T_s}^{T}\dfrac{\rho\gamma}{T_l-T_s}dT, \text{for}\, T_s\le T\le T_l\\ \int_{T_0}^{T_s}\rho_s c_{p,s}dT+\rho\gamma+\int_{T_l}^{T}\rho_l c_{p,l}dT, \text{for}\, T>T_l\end{cases} \tag{2.4}$$

where c_p is the specific heat capacity, f is the local liquid phase fraction, H_{PCM} is the volumetric enthalpy and T_0 is the reference temperature for enthalpy calculation. The discretisation of the energy control equation has been detailed in Voller (1990) and Nedjar (2002). A variant of the enthalpy method is the effective heat capacity method where the enthalpy partial differential item $\frac{\partial H_{PCM}}{\partial t}$ is replaced as $c_p(T)\frac{\partial T}{\partial t}$ to achieve a non-linear equation with a single variable T (Faghri *et al.* 2010).

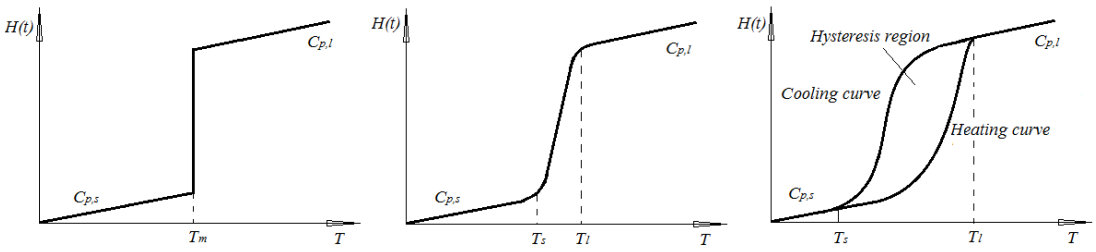

a) b) c)

Fig. 2.4 Typical enthalpy-temperature relationships: a) isothermal phase change; b) mushy phase change; c) phase change with hysteresis.

The enthalpy method has been widely considered in applications where there is no alteration to the numerical scheme at the interface (Hunter 1989). It is also better suited to model PCMs with a range of fusion temperatures (Furzerland 1980), and it is more convenient to deal with complex geometries (Iten and Liu 2014), than other methods.

2.2.2 Hysteresis phenomenon and heat transfer problems within PCMs

1) Hysteresis phenomenon

The traditional enthalpy method used a simplified isothermal or a single *h*-*T* relationship that does not capture the detailed physical phenomenon of hysteresis. However, some studies have shown that the consideration of hysteresis phenomenon

(see Fig. 2.4c)) is necessary to avoid the obvious deviation between the simulation and real conditions. For instance, Chandrasekharan *et al.* (2013) developed an enhanced simulation model for PCM building walls by using separate heating and cooling *h*-*T* curves and then comparing its performance with using the single *h*-*T* curve. The results showed that hysteresis had an obvious influence on the surface of the wall surface and the indoor temperature. Bony and Citherlet (2007) validated a numerical model of a PCM enhanced hot water tank. In the numerical model, the phase change process in the lower and upper parts of the hysteresis region was assumed to follow linear transition lines with slopes that are identical to the slopes of *h*-*T* relationships in the solid and liquid phases; they found the necessity of considering the hysteresis phenomenon based on the experimental validation. Dolado *et al.* (2011a) developed an empirical model for a PCM-to-air heat exchanger by adopting the separate heating and cooling *h*-*T* curves. Delcroix *et al.* (2015) studied the phase change behaviour of a building wall component incorporated with bulk PCMs by mapping the *h*-*T* curves according to the experimental results. They found a quick transition within the hysteresis region existed when the heating process was interrupted and the direction of the heat flux was reversed. These studies showed that the hysteresis phenomenon needs to be considered when developing appropriate models for PCMs.

2) Heat convection and heat conduction within PCMs

The natural heat convection that occurs as PCMs melt plays an important role in some macro-encapsulated PCMs (Bathelt *et al.* 1979; Sparrow *et al.* 1978). Bony and Citherlet (2007) validated a numerical model for a cylindrical bulk PCM module using experimental data and found that the modelling results deviated from the experimental data if the heat convection inside the PCM container was not considered. To simplify modelling the influence of natural heat convection in liquid bulk PCMs, an effective thermal conductivity was introduced and utilised (Farid and Husian 1990; Hirata and Nishida 1989), as described in Eq. (2.5).

$$\frac{k_{eq}}{k_l} = cRa^n \tag{2.5}$$

where R_a is the Rayleigh number, c and n are the correlation constants, and the subscript *eq* indicates the equivalent.

In some situations, however, it is better to omit natural heat convection because it can simplify modelling complexity. For instance, heat convection can be ignored for thin PCM layers in a horizontal direction because the convection heat transfer induced by gravity is linked to the difference in density between the liquid and solid phases (Iten and Liu 2014). A fin-enhanced PCM store with internal fins was modelled using a simplified analytical model and a two-dimensional numerical model with heat conduction only by Lamberg (2004), respectively; it was found that the numerical results of both models were consistent with the experimental data. A general model for analysing the thermal characteristics of PCM TES systems with various configurations was developed and validated by Kang *et al.* (1999); the model showed that even though the heat convection and the sensible heat capacity of PCMs were omitted, reasonable agreements between the modelling results and experimental results can be still achieved. A validation of a numerical model for a PCM-to-air heat exchanger was presented by Lopez *et al.* (2013); here the heat transfer in the PCMs encapsulated in Aluminium plates in the PCM-to-air heat exchanger was assumed to be two-dimensional heat conduction; a good agreement with the experimental data was observed. A lumped assumption by Hed and Bellander (2006) was used to model the thermal behaviour of PCM layers in a PCM-to-air heat exchanger, and despite its simplicity, there was a small error of 0.1-0.3^{o}C for the outlet air temperature and of 0.4^{o}C for the PCM temperature compared to the experimental data. Four numerical models for a PCM TES unit, including a semi-analytical model, a one-dimensional finite difference model, a two-dimension finite difference model, and a fluid dynamic model, were developed and compared by Dolado *et al.* (2006). The results showed that the one-dimensional and two-dimensional finite difference models were consistent with the experimental data, while the computational cost of the one-dimensional finite difference model was much lower than the two-dimensional finite difference model.

To model PCMs in the building envelopes, the assumption that one-dimensional heat conduction dominates the heat transfer within the PCMs was widely accepted. Because PCMs are either contained in micro-encapsulations and supporting materials, or encapsulated in macro-encapsulation whose thickness is far less than their height. The movement of PCMs in the former micro-encapsulated containments was limited whereas in the latter case (*i.e.* thin macro-encapsulated containments), the high aspect ratio of the PCM containers in a vertical direction impedes the development of natural

heat convection when heated from the side. Many researchers have shown the validity of assuming dominant one-dimensional heat conduction. For instance, Lu *et al.* (2014) developed and validated a one-dimensional PCM wall TRNSYS model which excluded the influence of natural heat convection; the validation based on experiments in a full-size room showed there was a consistent match degree ranging from 90.1% to 98.8% between the numerical modelling and experimental validation. Zhang Y. *et al.* (2014) carried out an experiment using a temperature-change hot chamber method to validate two heat transfer models for PCMs encapsulated in copper plates. The two models were developed based on the enthalpy method and the equivalent heat capacity method in which natural heat convection was not considered; the simulation data matched well with the experimental data, with errors in the PCM temperature of less than 1.0°C. Kuznik and Virgone (2009a) validated the performance of a one-dimensional PCM wallboard model and the results showed that the maximum and average differences of the inside air temperature between the modelling and experimental results were 1.1°C and 0.2°C, respectively.

2.2.3 Heat transfer between PCMs and heat transfer fluids within PCM TES units

Numerous heat transfer correlations have been presented by many studies to calculate the heat transfer coefficients between PCMs and heat transfer fluids. The using of appropriate heat transfer correlations in accordance with specific situations is a key to accurately model the heat transfer within PCM TES units. Under turbulent flow, the Dittus-Boelter equation (Bergman *et al.* 2011), as described in Eq. (2.6), has been used to calculate the heat transfer between the heat transfer fluids in channels and PCMs (Waqas and Kumar 2013, and Borderon *et al.* 2015).

$$Nu = \begin{cases} 0.023 Re^{0.8} Pr^{0.4}, \text{if the heat transfer fluid is heated;} \\ 0.023 Re^{0.8} Pr^{0.3}, \text{if the heat transfer fluid is cooled.} \end{cases} \quad (2.6)$$

where Nu is the Nusselt number, Re is the Reynold number, and Pr is the Prandtl number.

Correlations similar to Eq. (2.6) were also reported for the heat transfer calculation within PCM TES units. For instance, Edwards and Jensen (1994) and Zhang and Faghri (1996) used Eq.(2.7) to calculate the heat transfer between heat transfer fluids flowing in longitudinally finned tubes and PCMs encapsulated in the cylinder side.

$$Nu = \frac{0.023\left(L/d_h\right)^{0.2}}{\left(1.35-0.35L/d_h\right)} Re^{0.8} Pr^{0.4} \tag{2.7}$$

Liu M. *et al.* (2011) and Chen C. *et al.* (2014) used Eq. (2.8) to calculate the convective heat transfer within a TES unit with PCM plates.

$$Nu = \begin{cases} 1.233\left(\dfrac{L}{d_h \cdot Re \cdot Pr}\right)^{-1/3} + 0.4, \text{for} \dfrac{L}{d_h \cdot Re \cdot Pr} \le 0.001 \\ 7.541 + 6.874\left(\dfrac{10^3 L}{d_h \cdot Re \cdot Pr}\right)^{-0.488} e^{\frac{-245L}{d_h \cdot Re \cdot Pr}}, \text{for} \dfrac{L}{d_h \cdot Re \cdot Pr} > 0.001 \end{cases} \tag{2.8}$$

Esen *et al.* (1998) used Eq. (2.9) to calculate the Nusselt number of the heat transfer fluids flowing through the cylinder side of a PCM TES unit.

$$Nu_{cylinder} = Nu_{pipe} \cdot \left[1.08 - 0.794 e^{-1.62 d_h / Re_{cylinder}}\right], \text{for } Re_{cylinder} > 2200 \tag{2.9}$$

where Nu_{pipe} is the Nusselt number on the pipe side, as calculated by Eq. (2.6).

Gnielinski equation (Gnielinski 1976), as shown in Eq. (2.10), is another equation commonly used to calculate the convective heat transfer under turbulent flow in PCM TES units (Hamada *et al.* 2003).

$$Nu = \frac{\left(\xi/8\right)\left(Re-1000\right)Pr}{1+12.7\sqrt{\xi/8}\left(Pr^{2/3}-1\right)}\left[1+\left(\frac{d_h}{L}\right)^{2/3}\right]c_t, \text{for } Re = 2300 \sim 10^6, Pr = 0.6 \sim 10^5 \tag{2.10}$$

where ξ is the friction factor, d_h is the hydraulic diameter, L is the length of the air channel, and c_t is the temperature modifier.

Some other empirical correlations were also reported and used to calculate the heat transfer under some complicated conditions. For instance, Reynolds-Colburn analogy (Holman 1997), as described in Eq. (2.11), was used to calculate the heat transfer coefficient within an air channel with rough PCM surfaces (Hed and Bellander (2006)).

$$h_{conv} = \frac{\xi \rho c_p u}{2Pr^{2/3}} \tag{2.11}$$

where u is the flow rate of heat transfer fluids.

Under laminar flow, the Nusselt number is commonly set as a constant according to the aspect ratio of the channel (Bergman *et al.* 2011). Some equations were also

reported for the calculation of Nusselt number under laminar flow in order to considering additional influences. For instance, Borderon *et al.* (2015) used the Graetz–Nusselt relationship (Shah and London 1978) to calculate laminar heat transfer within the air gaps between the PCM layers, while considering the thermal entrance region, as shown in Eq. (2.12).

$$Nu = 7.541 + \frac{0.0253 RePrd_h}{L} \tag{2.12}$$

Rohsenow *et al.* (1985) presented an empirical correlation to calculate heat transfer in the shell side under laminar flow in a shell-to-tube PCM TES unit, as shown in Eq. (2.13).

$$Nu_{cylinder} = 3.36 + 4.12\left[\left(d_{h.} / Re_{cylinder}\right) - 0.205\right]^{0.569}, \text{ for } Re_{cylinder} \le 2200 \tag{2.13}$$

Heat transfer correlation based on Graetz (*Gz*) number under laminar flow, as shown in Eq. (2.14), was used to calculate heat transfer in the tube side of a PCM shell-and-tube exchanger (Saxena *et al.* 1982).

$$Nu = 2Gz^{1/3} \tag{2.14}$$

To calculate heat transfer of the PCM ball bed, the correlations proposed by Beek (1962) were used (Ismail and Stuginsky 1999), as shown in Eqs. (2.15) and (2.16), for the random arrangement and the cubic arrangement of PCM balls.

$$Nu = 3.22Re^{1/3}Pr^{1/3} + 0.117Re^{0.8}Pr^{0.4}, \text{for } Re > 40 \tag{2.15}$$

$$Nu = 2.42Re^{1/3}Pr^{1/3} + 0.129Re^{0.8}Pr^{0.4} + 1.4Re^{0.4}, \text{for } Re > 40 \tag{2.16}$$

2.3 Passive application of PCMs in building envelopes

Passive application of PCMs in building envelopes is a simple and straightforward approach to using PCMs in buildings. Building envelopes offer large areas which can facilitate heat transfer between the PCMs and indoor space. PCMs can be integrated passively into various building envelopes such as roofs or ceilings, walls, windows, and floors, to improve the local thermal mass for building thermal and load management (Parameshwaran *et al.* 2012), as shown in Fig. 2.3. In these applications, PCMs can store or release thermal energy when the indoor temperature rises or falls beyond the phase change temperature range, so that fluctuations in indoor temperature

can be smoothed, or for air-conditioned buildings, the energy consumption of the air conditioning systems can be reduced by load shifting and reduction.

A layer of PCM and a layer of insulation were incorporated between two outer layers of steel as the PCM enhanced roof structure of a residential building (Jayalath *et al.* 2016a). It was found that the PCM enhanced roof can provide better thermal comfort by smoothing the fluctuations of indoor temperature whilst reducing the demand for heating and cooling.

A roof structure enhanced by two PCM layers with different phase change temperatures was investigated by Pasupathy and Velraj (2008). This experimental and theoretical analysis showed that a double layer PCM roof structure could maintain a stable and comfortable temperature over a day under various weather conditions.

A PCM enhanced roof panel with PCMs in the conical holes in the concrete slab (see Fig. 2.5) was studied by Alawadhi and Alqallaf (2011) through simulations. The results showed that the heat flux towards the indoor environment can be reduced by up to 39% when the configuration of the holes was the cone frustum. Similar results using PCM enhanced bricks for reducing the indoor heat gain in a hot climate were also reported by Alawadhi (2008).

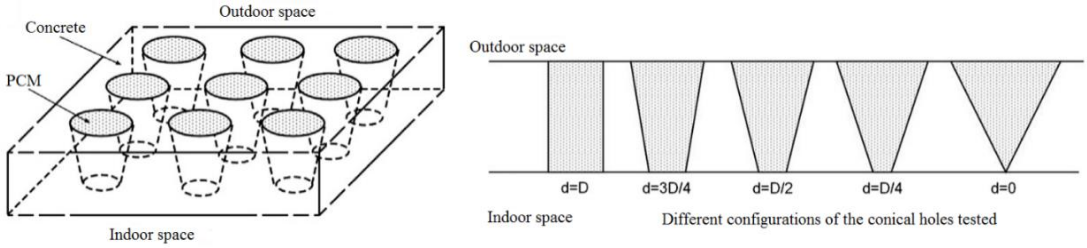

Fig. 2.5 PCM enhanced roof panel with different configurations of conical holes (Alawadhi and Alqallaf 2011).

The performance of PCMs and structural insulated panels (SIPs) as a united PCMSIPs technology for building thermal management (see Fig. 2.6) was studied by Medina *et al.* (2008). The experimental results showed that the peak heat flux can be reduced by 62% when PCMSIPs with a PCM concentration of 20% were applied.

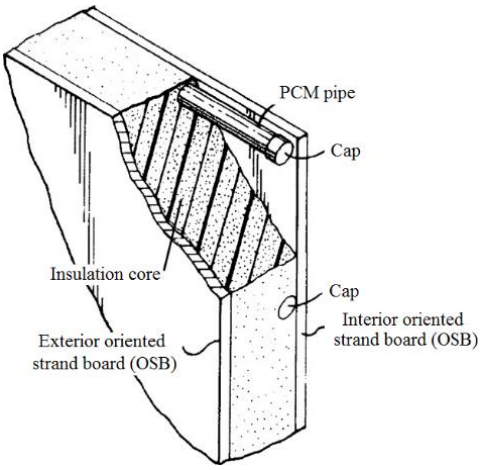

Fig. 2.6 The PCM SIPs (Medina *et al.* 2008).

A full-scale test on the thermal performance of a PCM copolymer composite wallboard (see Fig. 2.7) was carried out by Kuznik and Virgone (2009b), in which night time ventilation and solar radiation were used to regenerate the PCM enhanced wallboard under emulated summer and winter days, respectively. The results showed that fluctuations in the indoor temperature were smoothed and the indoor thermal stratification was eliminated due to enhanced natural convection.

The thermal performance of a PCM wallboard partition wall for lightweight buildings was investigated in a full-scale test room (Kuznik *et al.* 2008b). It was found that the fluctuations in temperature were smoothed, especially when overheating occurred. Further energetic modelling showed that 5 mm thick PCM wallboard can double the amount of thermal energy stored.

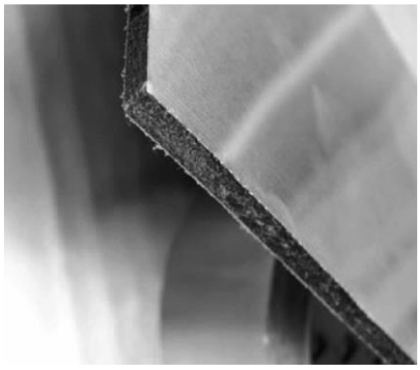

Fig. 2.7 The PCM wallboard (Kuznik and Virgone 2009b).

A cavity wall structure incorporated with a PCM layer was studied numerically under the weather conditions of Southeast England (Huang M.J. *et al.* 2006). The study

revealed that a cavity wall augmented with 20 mm of PCM GR27 and a 20 mm air space can help satisfy the thermal comfort requirements and also prevent condensation from developing in the cavity.

The thermal performance of concrete enhanced by micro-encapsulated PCMs was evaluated by Cabeza *et al.* (2007) through comparative experiments based on two real size concrete cubicles. It was found that concrete enhanced with PCMs improved thermal inertia of the cubicles which smoothed the fluctuations in indoor air temperature, but the discharging time during the night had to be enough to make this scenario effective.

The effectiveness of encapsulated PCMs installed into building walls for peak air-conditioning load shifting was evaluated numerically by Halford and Boehm (2007). It was found that a load shift from 19% to 57% can be achieved by using PCMs, however, the melting fraction of PCMs was very low.

The thermal benefit of using gypsum boards impregnated with butyl stearate (an organic PCM) in a passive solar building was examined by Athienitis *et al.* (1997), who found that gypsum board enhance with the PCM reduced the heating load during the night.

The thermal performance and energy performance of a refurbished building with additional PCM plaster inside the exterior envelope under Mediterranean climates was investigated numerically by Asicone *et al.* (2014). It was showed that the comfort hours can be improved substantially if PCMs with an appropriate phase change temperature were used in the naturally ventilated passive house, however, the cooling energy only decreased by 7.2% in the same house with indoor air conditioning.

The energy saving potential of using micro-encapsulated PCMs mixed with cellulose insulation in cavity walls was investigated by Biswas and Abhari (2014) in a hot and humid climate. It was found that having PCM inside the wall cavity saved the same amount of cooling energy as adding PCM to the entire cavity, but the energy savings were directly related to the orientation of PCM enhanced walls.

A daylight element combining double glazing with PCMs was developed by Weinlader *et al.* (2005), as shown in Fig. 2.8. It was found that the PCMs were not

used efficiently due to constant indoor thermostat settings, even though the PCM enhanced glazing did reduce the heat loss of the house.

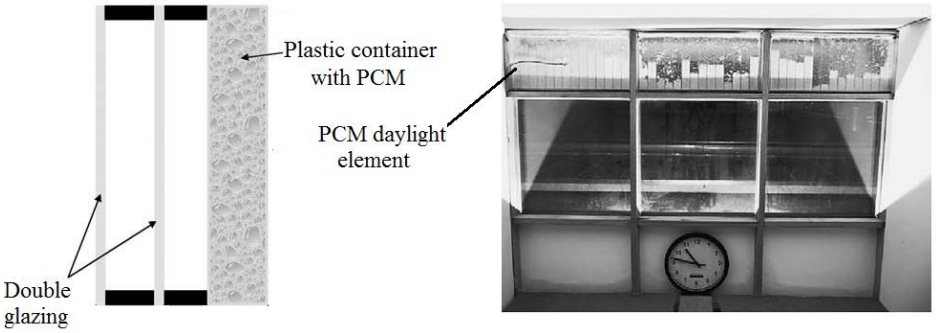

Fig. 2.8 The PCM daylight element (Weinlader *et al.* 2005).

A PCM enhanced internal window shutter was used by Silva *et al.* (2016), who then found that the maximal and minimal indoor temperatures decreased and increased up to 8.7% and 16.7%, respectively, if the PCM enhanced internal window shutter was used. At the same time, the maximum and minimum temperature peaks were delayed for 1 h and 30 minutes respectively.

A PCM enhanced prototype tile was designed to form a passive floor heating system for a solar house (Cerona *et al.* 2011), as shown in Fig. 2.9. This tile stabilised the room temperature and reduced the demand for heating during the night but the effectiveness of the PCM enhanced tiles was limited to floor that can receive direct solar radiation.

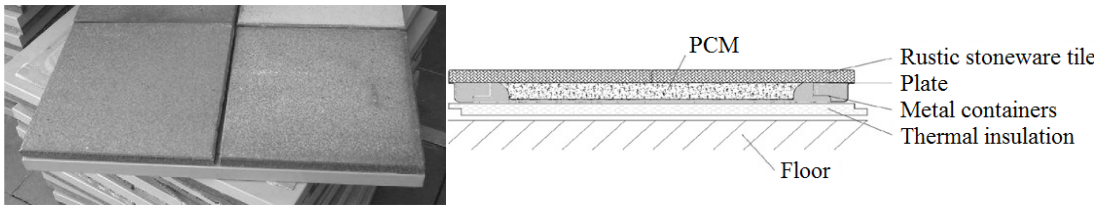

Fig. 2.9 The prototype of the PCM enhanced tile (Cerona *et al.* 2011).

This review indicates that the use of PCMs in building envelopes can enhance the indoor thermal comfort by reducing temperature fluctuations, and has the potential to reduce the energy consumption of air conditioning by shifting or decreasing the heating and cooling loads. The walls and roofs (or ceilings) seem to be the most popular positions for installing PCMs. But the thermal benefits of the PCMs are limited due to the low natural convection heat transfer between indoor environment and PCM

enhanced building envelopes (Kang *et al.* 2003), variations in weather conditions (Ascione *et al.* 2014), the low efficiency of PCMs utilisation (Weinlader *et al.* 2005; Halford and Boehm 2007), and small temperature variations between daytime and night time (Iten *et al.* 2014).

2.4 Active application of PCM TES systems in buildings

Unlike the passive application of PCMs in building envelopes, the active application of PCM TES systems in buildings can enable the active storage and release of thermal energy (Borderon *et al.* 2015). PCM TES systems can be integrated with HVAC systems to shift the thermal load from an on-peak period to an off-peak period, or conserve the overall primary energy used for heating and cooling by rationalising the utilisation of renewable and non-renewable energy.

2.4.1 PCM TES units integrated with solar space heating and free cooling systems

PCM TES systems can be integrated with solar space heating to rationalise energy utilisation and improve its overall performance. For instance, Chen C. *et al.* (2014) designed and tested a vertical phase change TES device as part of a solar-PCM fresh air heating system for office buildings. The results showed that this system can achieve a thermal energy discharging efficiency of 93%.

Waqas and Kumar (2013) presented a parametric study of a PCM-based solar air heating system, as shown in Fig. 2.10, for space heating during the winter season. It was found that the performance of the PCM TES system can be maximised when the melting temperature of PCM was close to the indoor comfort temperature during the winter months.

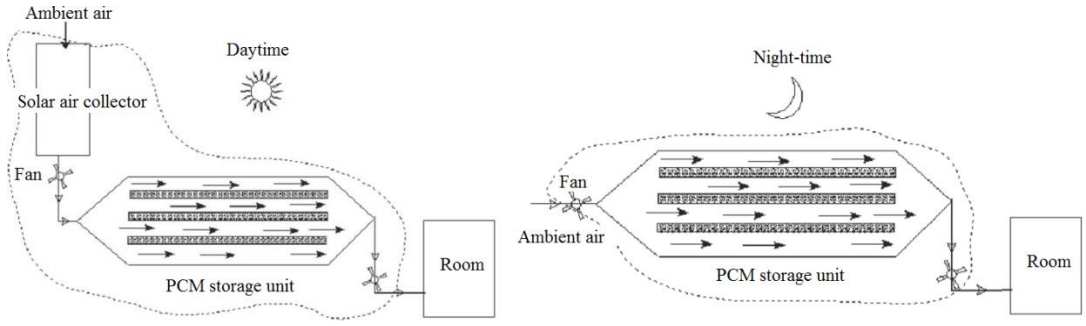

Fig. 2.10 The PCM-based solar air heating system (Waqas and Kumar 2013).

Saman *et al.* (2005) numerically investigated a PCM TES unit as a component of a roof integrated solar heating system. The dynamic performance of this unit using two PCM configurations, including a normal flat plate and a conical capsule, were compared. It was concluded that the air flow rate must be determined carefully to maximise system performance.

PCM TES systems were also integrated into free cooling systems using ambient coolness to maintain acceptable indoor thermal comfort. Here the ambient coolness can be stored in the PCM TES system through natural or mechanical ventilation during the night and then released during the daytime via circulating the room air between the PCM TES systems and indoor environment to condition the indoor space.

Borderon *et al.* (2015) analysed the performance of a PCM TES unit coupled with a ventilation system to maintain the summer comfort in a residential building. PCM TES units with various configurations were compared numerically under different weather conditions. It was found that that the thermal comfort in the house was improved significantly when the PCM system was used, but only a fraction of the PCM solidified during the night, thus indicating that the system was not well designed.

Kang *et al.* (2003) investigated a night ventilation system with a PCM packed bed storage, as shown in Fig. 2.11. They found that the night ventilation system with the PCM TES had better thermal performance than ordinary night ventilation technology with only using building fabric for storing coolness. The overall COP of the experiment installation reached 80, which indicates it has enormous potential in the field of energy efficiency building.

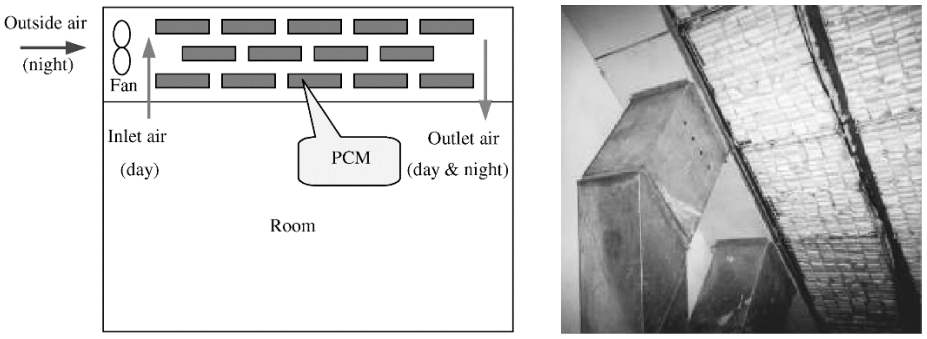

Fig. 2.11 The night ventilation system (Kang *et al.* 2003).

2.4.2 PCM TES units integrated with air conditioning systems

A lot of efforts has gone into integrating PCM TES units with building air conditioning systems to enhance system efficiency or provide functional purposes.

An air distribution system in an office building with a storage device using PCMs in the air ducts for peak load shaving was proposed and numerically studied by Yamaha and Misaki (2011). It was shown that this system can achieve full peak load shifting during the period of concern while maintaining a relatively constant room temperature.

The performance of a displacement ventilation (DV) system in an airport departure hall whose diffusers were retrofitted with a PCM heat exchanger, as shown in Fig. 2.12, was evaluated by Gowreesunker *et al.* (2013) under various discharging strategies. The simulation results showed that the PCM enhanced DV system reduced 34% and 22% of the demand for air conditioning respectively, under the control strategies of 'no night ventilation' and 'limiting control ventilation' during summer days.

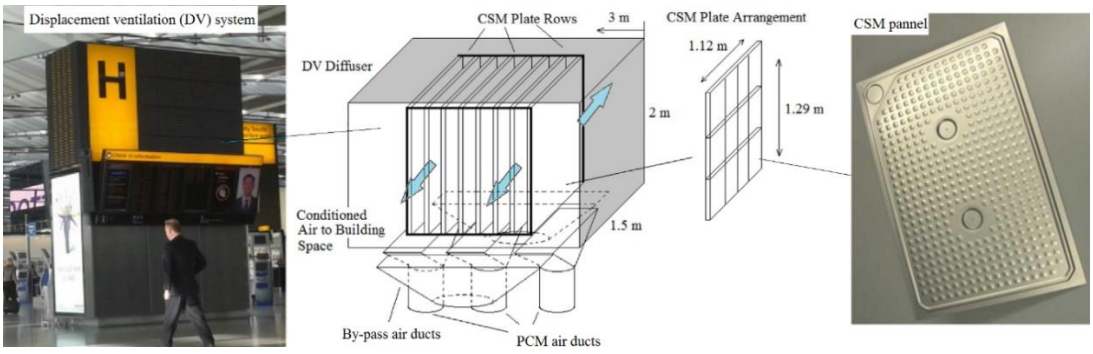

Fig. 2.12 The displacement ventilation system with a retrofitted PCM heat exchanger in the diffuser (Gowreesunker *et al.* 2013).

The benefit of integrating a packed PCM ball bed with a domestic air conditioner was evaluated by Chaiyat (2015). It was found that almost 9.1% of electrical power can be saved with a payback period of around 4.15 years, compared to using a conventional system.

An air conditioning system enhanced by PCM ceiling wallboard which was installed in an office building to pre-cool the return air, as shown in Fig. 2.13, was investigated by Kondo and Ibamoto (2006). It was found that the peak load can be shifted by charging the PCM ceiling board overnight, while the indoor air was pre-cooled before being returned to the air handling unit during the peak shaving period. Compared to

conventional rock wool ceiling board, an operational cost reduction of 3.4% can be achieved and the maximum thermal load can be cut by 9.4%.

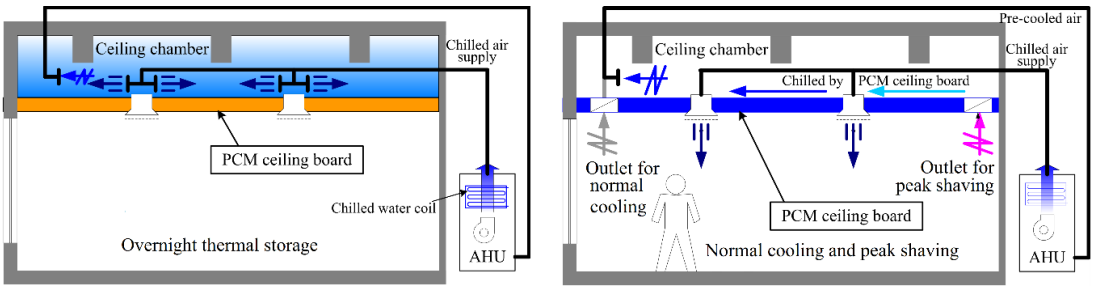

Fig. 2.13 The air conditioning system enhanced by PCM ceiling wallboard (Kondo and Ibamoto 2006).

A cylindrical PCM cold storage unit with a finned tube inside was coupled with an ejector cooling system to store the excess cooling capacity of the system, while providing cooling energy when the ejector was turned off (Chen X.J. *et al.* 2014). The medium temperature source from solar collectors or industrial waste at around 120°C can be used to drive the ejector cooling system. It was also found that the PCM TES unit could maintain a more stable COP of the ejector cooling system.

A compact PCM TES unit with capillary tubes was developed to facilitate the heat rejection and thermal balance of a heating and cooling system with a solar absorption chiller (Helm *et al.* 2009), as shown in Fig. 2.14. The pilot running of this system showed that by using the PCM TES unit, 50% of the daily rejected heat load can be covered by the latent heat storage and shifted to off-peak hours under cooling operation mode; this resulted in a corresponding thermal COP of 0.72 and a corresponding electrical COP of 7-10, respectively. Under heating mode, the PCM TES allowed an efficient operation of the solar thermal system with a low operation temperature.

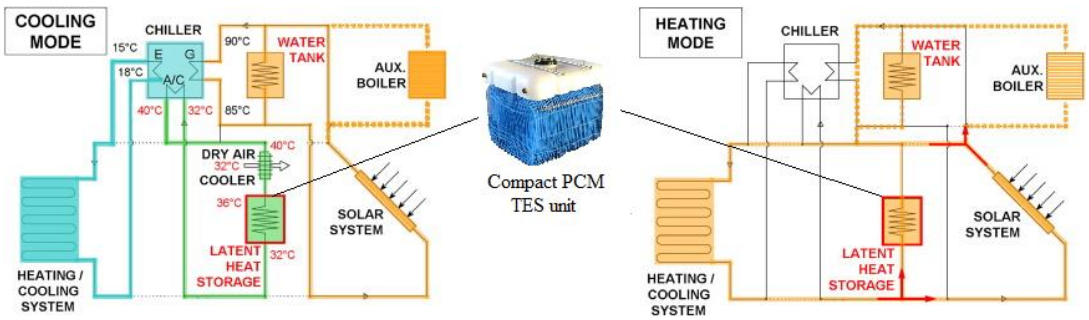

Fig. 2.14 The heating/cooling system with a solar absorption chiller PCM TES (Helm *et al.* 2009).

A solar thermal energy powered adsorption air conditioning system integrated with a PCM cold storage system was proposed by Zhai *et al.* (2014). The tests showed that total charging and discharging capacities of 1016 kJ and 943 kJ were achieved within 300 minutes and 120 minutes, respectively.

2.4.3 PCM TES units integrated with heating/cooling surface in building envelopes

Another active application of a PCM TES system is integrating PCMs with heating/cooling surfaces in buildings where PCMs serve as on-site TES units. For instance, an under floor electric heating system enhanced by a PCM layer between the heating surface and floor tiles was proposed and studied numerically by Farid and Chen (1999). It was found that the heat stored in the 30 mm thick PCM with a melting temperature of around 40^{o}C was enough to cover the heating load for one day and also provide a reasonably uniform heating temperature throughout the day.

A thermally activated ceiling panel enhanced by a micro-encapsulated PCM for retrofitting in lightweight buildings was proposed and tested in an office building (KosChenz and Lehmann 2004) (see Fig. 2.15). This panel consists of an integrated water capillary tube with a micro-encapsulated PCM and gypsum, and when this thermally activated ceiling system was used, the room temperature remained within a comfortable range.

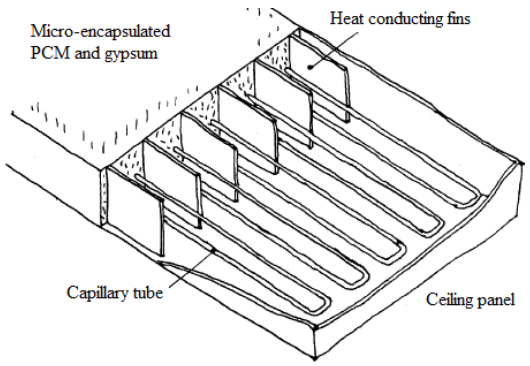

Fig. 2.15 The thermally activated ceiling panel enhanced by micro-encapsulated PCM (KosChenz and Lehmann 2004).

A new kind of under floor electric heating system integrated with shape-stabilised PCM plates, as shown in Fig. 2.16, was developed and investigated by Lin *et al.* (2005). It was found that the up surface temperature of the PCM plates stabilised at the phase

transition temperature during the whole testing day while more than half of the electric heat was shifted from the peak period to the off-peak period.

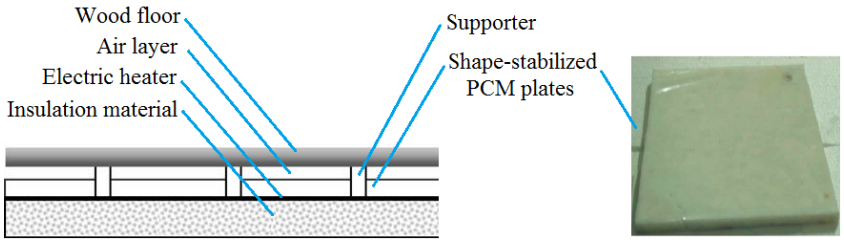

Fig. 2.16 The under floor electric heating system integrated with shape-stabilised PCM plates (Lin *et al.* 2005).

The thermal performance of a solar hot water driven low-temperature radiant floor heating system consisting of PCMs and a capillary mat was evaluated by Zhou and He (2015). It was found that the solar hot water radiant floor heating system with a PCM-capillary mat released heat about 2 times longer than using sand and polyethylene coils, and also provided a more uniform temperature.

A solar water heating floor with capillary plaits and a macro-packaged PCM layer was proposed and investigated by Huang K.L. *et al.* (2014). It was found that the PCM floor covered 47.7% of the heat supplied by solar water for 16 h during the pump-off period in a room with a floor area of 11.02 m^2.

As reviewed above, the PCM TES units with various configurations were studied to achieve building peak load shifting, enhance the indoor thermal comfort, and conserve air conditioning energy, *etc*. Typically, the force convection between the heat transfer fluids and PCMs within the PCM TES unit is the key to enable the systems to respond rapidly. However, the thermal resistance to heat transfer between the heat transfer fluids and the PCM is still a major consideration (Belusko and Bruno 2008), due to the low thermal conductivity of PCMs. Moreover, the compactness of the PCM TES units reported in the public domain varied over a wide range from 50% (Tay *et al.* 2012b; Hasnain 1998) to 90% (Helm *et al.* 2009), indicating there is still a huge potential for improving the density of energy storage.

2.5 Design and optimisation of PCM TES systems

Even though the use of PCMs in buildings has been studied extensively over the last two decades, a number of problems and concerns have apparently hindered the wide deployment of PCMs in buildings, such as the low efficiency of PCMs utilisation (Weinlader *et al.* 2005), the weather-dependent performance(Borderon *et al.* 2015; Asicone *et al.* 2014), poor heat transfer performance of PCM TES units (Dolado *et al.* 2011b), and low compactness (*i.e.* volume of the PCMs to the volume of the PCM TES units) of PCM TES units (Hasnain 1998). One cause of these problems is the low thermal conductivity particularly organic PCMs, which results in low thermal charge and discharge rates. Unlike the costly solutions to enhance the thermal properties of PCMs, design optimisation for PCM TES systems is generally more cost effective and therefore more practical and of greater interest (Lazaro *et al.* 2009a; Dolado *et al.* 2011b). Therefore, the design optimisation of PCM TES systems is important to enhance the system performance and is a prerequisite to facilitate the wide deployment of high-performance PCM TES systems.

2.5.1 Performance indicators for PCM applications in buildings

The performance of PCM systems in buildings can be evaluated from the unit level and the building level. The former focuses on the performance of single PCM building component or PCM TES unit, while the latter focuses on enhancing building performance due to the using of PCM systems.

2.5.1.1 Unit level

According to the different applications, the performance indicators for PCM building components and PCM TES units could differ. The key aspects summarised below are those commonly used to assess the performance of PCM building components and PCM enhanced active surfaces.

- Thermal energy storage versus time: reflects the storage of the required amount of thermal energy in a pre-determined time period (*e.g.* Bastani *et al.* (2014));
- Surface temperature management: reflects the ability of a PCM building component to maintain a desired and stable surface temperature (*e.g.* Drake 1987);

- Surface heat flux management: reflects the effects of reducing the external heat flux towards the indoor environment of passive PCM building components (*e.g.* Peippo *et al.* 1991; Alawadhi 2012; Kissock and Limas 2006), or smooth the surface heat flux fluctuation of a PCM enhanced active surface (*e.g.* Jin and Zhang 2011).

The performance indicators for PCM TES units tend to be more complex due to the heat transfer between PCMs and heat transfer fluids. Obviously, excellent heat transfer and efficient heat charge/discharge are the important indexes for evaluating the thermal performance of PCM TES units (Chen C. *et al.* 2014). Mehling and Cabeza (2008) recommended the energy storage density and the effectiveness of the heat transfer as the performance indicator of PCM TES systems. The thermal charging/discharging time is another vital performance indicator for PCM TES systems, which has been widely studied by several researchers (Zhai *et al.* 2015; Esen *et al.* 1998; Labat *et al.* 2014; Dolado *et al.* 2011b). Other performance indicators reported for PCM TES units include the utilisation percentage of PCMs (Dolado *et al.* 2012a), the charging/discharging power (Kuznik *et al.* 2015), the desired and stable outlet fluid temperature **(**Lazaro *et al.* 2009a; Summers *et al.* 2012), and the functional indicators to facilitate other systems (*e.g.* electric efficiency of the PCM enhanced PVT collectors reported by Malvi *et al.* (2011)).

2.2.1.2 Building level

The ultimate aim of using PCM building components or PCM TES systems is to improve indoor thermal and energy performance of buildings. The performance indicators for PCMs used at the building level includes the thermal, energy, economic, and sustainable benefits, and could be summarised as follows:

- Thermal indicators: indoor temperature and temperature fluctuations (*e.g.* Peippo *et al.* 1991; Padovan and Manzan 2014);

- Energy indicator: primary energy or power savings (*e.g.* Peippo *et al.* 1991)

- Economic indicators: peak load shifting (*e.g.* Jin and Zhang 2011), investment and operation cost (*e.g.* Evins 2015);

- Sustainable indicator: carbon emissions (*e.g.* Evins 2015).

The performance indicators in the unit level and building level tend to be used in different circumstances. Specifically, the unit level performance indicators can be used in the optimal design of individual PCM thermal energy storage (TES) components or units. The building level performance indicators can be used in the optimisation of buildings and building HVAC systems with integrated PCM TES components (or units) with a focus on the overall system performance.

In general, when the performance indicators from both unit and building levels need to be considered in optimisations, the performance indicators in the unit level can be first optimised to achieve a range of near optimal designs for PCM TES components (or units), based on which the system optimisation in terms of the building level can be carried out to search for the optimal coupling parameters and further identify the global optimal designs. A multi-objective optimisation problem can also be formulated to optimise these indicators simultaneously, especially when the interaction between the performance indicators in the unit level and building level is significant.

2.5.2 Design and design optimisation of PCM building components

Early work on the design of PCM building components mainly focused on using analytical methods to identify approximate parameters of PCM building components for engineering design. However, ideal conditions with simplified assumptions must be used to obtain these analytical designs which therefore tend to deviate from the actual conditions of application. Recently, empirical correlations and parametric studies based on either experiments or numerical modelling have been used for the optimal design of PCM building components to consider the dynamics in practical conditions.

Drake (1987) developed an analytical design rule for passive PCM solar heating walls in buildings. This rule provided two simplified equations to identify the optimal phase change temperature and PCM wallboard thickness, as described in Eqs. (2.17) and (2.18). Here the optimal transition temperature of a PCM wallboard component depends on the amount of solar heat flux absorbed and the heat losses.

$$T_{m,opt} = \frac{h_{conv}}{h_{conv} + U_{amb}} \overline{T}_{room} + \frac{h_{conv}}{h_{conv} + U_{amb}} \overline{T}_{amb} + \frac{I_t}{\tau_{diurnal}\left(h_{conv} + U_{amb}\right)} \tag{2.17}$$

$$\delta_{opt} = \frac{1}{\rho_{PCM}\gamma}\left[I_t - t_{day} h_{conv}\left(T_{m,opt} - T_{room,day}\right) - t_{day} U_{amb}\left(\overline{T}_{amb,day} - T_{m,opt}\right)\right] \tag{2.18}$$

where h_{conv} is the convective heat transfer coefficient between the wall surface and indoor air, U_{amb} is the overall heat transfer coefficient for the wall construction, I_t is the solar irradiation, $\tau_{diurnal}$ is the diurnal storage cycle (*i.e.* 24 h), and the subscript *amb* indicates ambient.

Peippo *et al.* (1991) proposed a three-step design methodology for a PCM enhanced passive solar heating wall. In the first step, the two equations shown in Eqs. (2.19) and (2.20) are used to determine the optimal phase transition temperature and the optimal thickness of the PCM layer, respectively.

$$T_{m,opt} = \overline{T}_{room} + \frac{q}{\overline{h}_{conv}\tau_{diurnal}} \tag{2.19}$$

$$\delta_{opt} = \frac{t_{night}\overline{h}_{conv}}{\rho_{PCM}\gamma}\left(T_{m,opt} - T_{night}\right) \tag{2.20}$$

where q is the heat absorbed per area of the room surface, $\overline{h}_{conv}$ is the average heat transfer coefficient between the wall surface and surroundings. In the second step, the simulations over the heating season were carried out to verify the optimal values of the phase change temperature and thickness of the PCM layer. Eventually, the heating energy consumption and the indoor temperature in a building with using the optimally designed PCM are evaluated.

Bastani *et al.* (2014) presented a design tool for the use of PCM wallboards in buildings; here the thermal dynamics of a PCM wallboard were identified by analysing variations in the surface temperature and liquid fraction based on numerically modelling. Two correlations relating to the Fourier number (*Fo*), the Biot number (*Bi*), and the Stefan number (*Ste*) were established under a steady state and a complete PCM liquefaction condition, respectively. These correlations were then used to identify the optimal thickness of a PCM wallboard.

Kuznik *et al.* (2008a) optimised the thermal behaviour of a lightweight internal partition wall using a PCM enhanced wallboard. They found that an optimal thickness

of around 10 mm for the PCM enhanced wallboard can maximise the thermal energy storage capacity due to the thermal resistance and thermal penetration of the PCM layer.

Alawadhi (2012) used an external window shutter filled with PCMs to reduce the solar heat gain and optimise its performance through simulations. The melting temperature and quantity of PCMs were varied to determine its thermal benefits parametrically. The results showed that heat gain through optimally designed windows can be reduced by 23.29%.

Kissock and Limas (2006) proposed a model-based design strategy for optimal placement of PCM layers within building components to minimise the thermal load transmitted from the building envelopes. The location of PCM was investigated parametrically based on a PCM enhanced wall model, and it was found that the maximal thermal load reduction can be achieved when PCM was located where the temperature was equal to the melting/freezing temperature of PCM.

These studies on the design and optimisation of PCM building components aimed to identify the optimal types, installation position, and thickness of PCMs. It can be concluded that optimising the design of PCM building components can maximise their thermal energy storage capacity, minimise the temperature fluctuations on building surfaces, or minimise the thermal load of building spaces.

2.5.3 Design and design optimisation of PCM TES units

The predominant design optimisation of PCM TES units focused on examining how the design variables affected their thermal performance. For instance, Zhai *et al.* (2015) carried out a series of simulations to analyse the charging performance of a fin tube PCM TES unit for high-temperature cooling by varying the structural parameters, including the annular fin pitch, the number of rectangular fins, the height of the rectangular fins, and the fin thickness. Based on the numerical parametric study, the optimal structural parameters identified could reduce PCM charging time by 26.3%.

Malvi *et al.* (2011) proposed and evaluated an integrated PV-solar thermal-PCM system (as shown in Fig. 2.17) through a parametric study to analyse how the thickness of PCM layer, PCM melting temperature, PCM thermal conductivity, water flow rate

and control strategy affected the performance of the system. They found that by including an appropriate PCM in the optimised system, the PV output can be increased by typically 9% with an average rise in water temperature of 20°C.

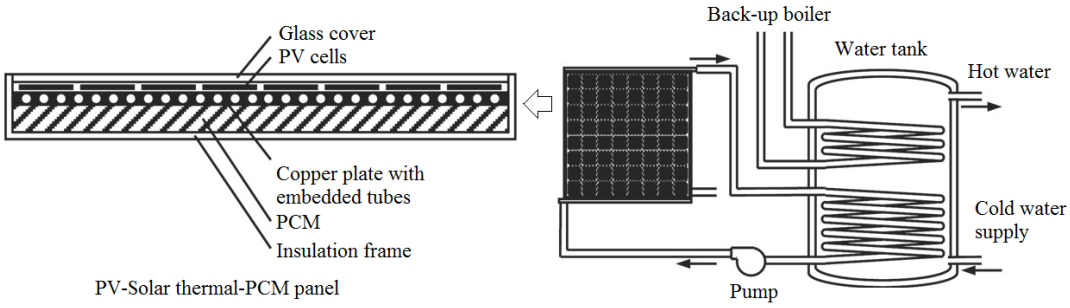

Fig. 2.17 The PV-solar thermal-PCM system (Malvi *et al.* 2011).

Summers *et al.* (2012) designed and optimised a built-in high-temperature solar air heater with PCMs beneath to maintain a consistent air outlet temperature and heat output throughout the daytime and night time. They concluded that a more stable outlet air temperature can be achieved by increasing the surface roughness, enhancing the PCM thermal conductivity through a metal mesh, and reducing the air flow rate.

Jin and Zhang (2011) carried out a parametric study of a double layer PCMs heating and cooling floor system for peak load shifting. Here the melting temperature, heat of fusion of the PCMs and location of the PCM layers were optimised based on an analysis of their influence on the heat flux fluctuation of the floor surface. The results showed that the optimal melting temperature of the PCMs for heating and cooling were 38°C and 18°C respectively when the PCM layer with lower phase change temperature was above the PCM layer with higher phase change temperature, while the optimal values changed to 33°C and 16°C when the locations of the two PCM layers were swapped.

Dolado *et al.* (2011b) characterised the thermal performance of the PCM-air heat exchanger shown in Fig. 2.18 which was developed using a matrix of PCM slabs with air channels between them. A number of design parameters were studied parametrically to investigate their influence on the heat transfer and flow within the PCM TES unit, including the air flow rate, the PCM properties, the air gap between the PCM slabs, the thickness of the PCM slab, the length of the PCM system, and the thermal conductivity and roughness of encapsulation surface. The results showed that

the hysteresis phenomenon during the phase change process, the enthalpy-temperature relationship, the encapsulation rugosity, and the length of the PCM system, have significant influence on how the PCM TES unit performs.

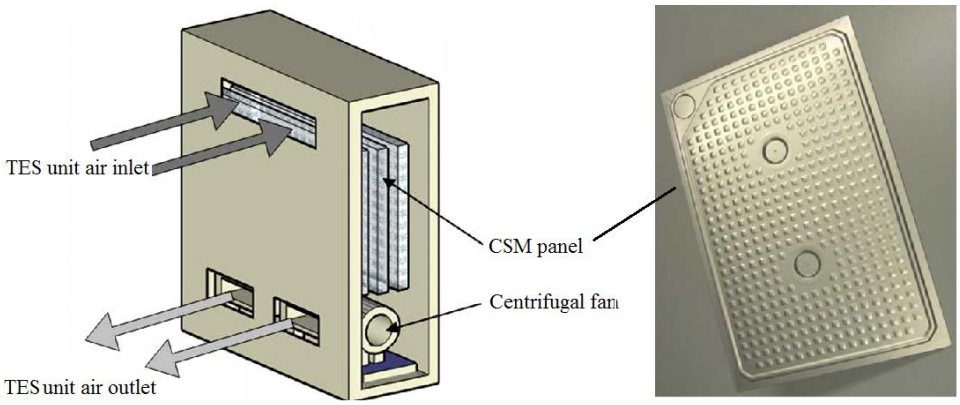

Fig. 2.18 The PCM-to-air heat exchanger and PCM slab used (Dolado *et al.* 2011b).

Wen *et al.* (2014) developed an algorithm to optimise the design of a PCM TES unit with PCMs filled in hexagonal modules and heat transfer fluid flowing along tubes in each PCM module. The PCM thermal conductivity, the latent heat, and the heat transfer fluid flow velocity were varied parametrically during this optimisation to identify the number of PCM modules needed to fulfil a given design power output target.

Esen *et al.* (1998) carried out a design optimisation for a solar-aided latent heat storage unit to optimise the PCM melting time. To identify the optimal geometric design, the influence of PCM type, cylinder radius, pipe radius, total PCM volume, and mass flow rate and inlet air temperature of the heat transfer fluid on the overall PCM melting time was parametrically modelled. Here, the PCM melting time was an essential criterion for an optimal design of the PCM TES unit because it must be compatible within the total sunny period in the daytime.

Amin *et al.* (2009 and 2012) carried out a design optimisation of a rectangular PCM TES unit to maximise the energy storage effectiveness. The optimal design was determined based on a series of parametric studies on the width of the gap between the PCM slabs, the mass flow rate of heat transfer fluid, and the thickness of the PCM slab.

Since the optimal design of PCM TES systems based on parametric studies is time consuming, a number of researchers have proposed some alternative design

methodologies to simplify the design of PCM TES systems based on empirical models. For example, Tay *et al.* (2010 and 2012a) proposed a practical design methodology based on the effectiveness-number of transfer unit (ε-NTU) method to design PCM TES units; here the average heat transfer effectiveness of the PCM TES unit is correlated with the NTU, as shown in Eqs. (2.21) and (2.22).

$$\bar{\varepsilon} = \int \varepsilon d\varphi = \int 1 - e^{-NTU} d\varphi \tag{2.21}$$

$$NTU = \frac{UA}{\dot{Q}_m c_p} = \frac{1}{R_{tot} \dot{Q}_m c_p} \tag{2.22}$$

where $\bar{\varepsilon}$ is the average heat transfer effectiveness, ε is the heat transfer effectiveness, φ is the phase change fraction, U is the overall heat transfer coefficient, A is the heat transfer area, $\dot{Q}_m$ is the mass flow rate of the heat transfer fluid, and R_{tot} is the total thermal resistance between the heat transfer fluid and PCM, which can be determined theoretically based on the configuration of the PCM TES unit.

Lazaro *et al.* (2009b) designed a PCM-air heat exchanger for free cooling in buildings. An empirical model correlating the outlet air temperature, the charging power, the average phase change temperature, and the number of PCM modules used was established based on an experimental study. With this model, the PCM TES unit can be configured and the desired phase change temperature can easily be determined.

Kuznik *et al.* (2015) developed a two-step dimensionless optimal design methodology for PCM TES units under specified applications. Here the influence of a set of dimensionless numbers derived from physical equations on the thermal behaviour of the TES unit was investigated based on parametric and sensitivity studies. It was concluded that the dimensionless numbers Bi/St and *Ste* were related to the selection of PCMs, while $1/BiFo$ was related to the optimal design of the system configuration. Accordingly, the influence of Bi/St versus *Ste* was mapped for a number of PCM candidates to develop a database, and then a two-step optimal design methodology can be implemented by selecting the best PCM to meet a design discharging power. If the desired discharging power cannot be achieved, the optimisation of system configuration presented by $1/BiFo$ was further carried out through the parametric study.

Labat *et al.* (2014) recommended using the global thermal behaviour of a PCM TES unit for design and optimisation, where the thermal performance of an air-based PCM TES unit was tested to achieve a dimensionless correlation between *Fo* and *St*. The correlation presented the relationship between the discharging time of the PCM TES unit and the air flow rate under a corresponding percentage of the total energy released. Accordingly, the size of the PCM TES unit or the discharging time can be achieved based on this dimensionless correlation.

Padovan and Manzan (2014) carried out a multi-objective design optimisation for a solar absorption chiller-PCM system to minimise the primary energy consumed by the boiler and the gross volume of the hot water tank, using the elitist non-dominated sorting multi-objective genetic algorithm (NSGA-II). The design variables considered were the height of water tank, the thickness of the tank insulation, the height and diameter of PCM modules, the number of PCM modules, the position height of PCM modules, and the phase change temperature of the PCM. This optimisation obtained a Pareto front which showed the trade-off between the two optimisation objectives, but it seems that the benefit improvement of these optimal designs is minor compared to the design achieved without using PCM in this particular case.

Dolado *et al.* (2012a) proposed a design optimisation strategy based on the response surface design methodology. This strategy consists of four steps: 1) modular design based on an empirical model; 2) improving the design through numerical simulations based on design of experiment (DOE); 3) design optimisation using response surface design methodology; and 4) confirmation test by checking the similarity of characteristic parameters between experimental and numerical results. A case study was then carried out to design a PCM-air heat exchanger for free cooling application in buildings. The optimal design compared to a non-optimal design showed that with the optimal design, the time to reach maximum air temperature in the room increased 19.7%, the initial investment decreased by 11%, and the PCM melting ratio improved by 23.2%, while the volume occupied by the unit increased around 3 times.

This review indicates that the performance of PCM TES systems can be enhanced through proper design and design optimisation. Thus, much more benefits can be achieved for an HVAC system with integrated with an optimally designed PCM TES unit. However, most existing studies rely on parametric studies and empirical

correlations to achieve ‘optimal’ designs for the PCM TES systems, and they often require excessive numerical/experimental tests or expert knowledge of the systems of concern.

2.6 Research on building integrated PVT (BIPVT) collectors

Photovoltaic thermal collectors are renewable energy technologies that can cogenerate thermal and electric energy (Charalambous *et al.* 2007), and also form a cohesive design, construction, and energy solution for the built environment (Bazilian *et al.* 2001). PVT collectors allow the enhancement of electrical efficiency by removing thermal energy and subsequently decreasing the operating temperature of the cells (Aste *et al.* 2008). Instead of using separate solar technologies to generate heat and electricity, PVT collectors are often considered to be more cost effective because electrical and thermal energy is generated from the same collector surface (Zondag *et al.* 2002; Kumar and Rosen 2011). Building facades provide an ideal area for installing PVT collectors (Chow 2010). It is also attractive for integrated PVT systems in buildings due to the potential utilisation of thermal energy generated from the building integrated PVT (BIPVT) systems for indoor air conditioning. BIPVT collectors can be liquid-based or air-based, as shown in Fig. 2.19. Significant effort has been made to experimental test, numerically investigate, and develop prototype BIPVT collectors.

Saitoh *et al* (2003) field tested a brine-based PVT collector and then analysed its total energy and exergy efficiency. They found that the total exergy efficiency outperformed a solar thermal collector and a PV collector, even though the thermal efficiency of the PVT collector was lower than the solar thermal collectors. The PVT system also reduced the area needed to install the panels by approximately 27%, compared to installing PV collectors and solar thermal collectors separately.

Nualboonrueng *et al.* (2012) investigated the performance of PVT systems (as shown in Fig. 2.19a) using commercial amorphous and multi-crystalline silicon PV panels as solar absorbers. It was found that the multi-crystalline silicon PVT generated 1.2 times as much electricity as amorphous silicon PVT, whilst also generating almost the same amount of thermal energy.

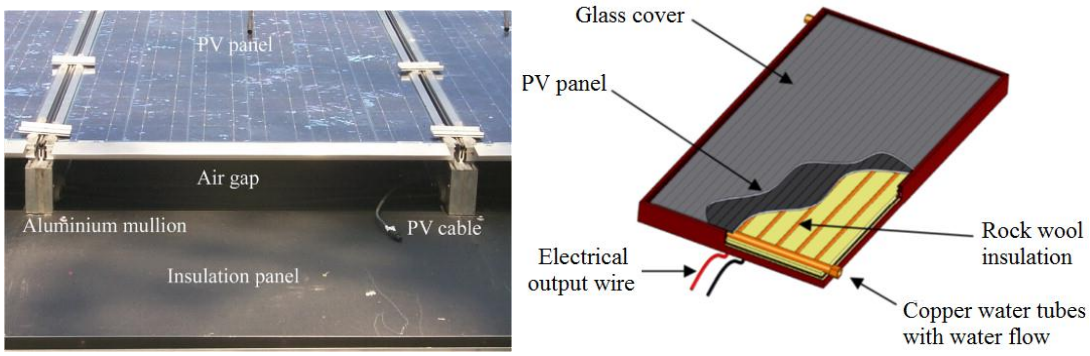

a) air-based PVT collector (Nualboonrueng *et al.* 2012)

b) water-based PVT collector (Aste *et al.* 2008)

Fig. 2.19 Examples of air-based and water-based PVT collectors.

Bambrook and Sproul (2012) investigated the performance of an air-based PVT collector. They then found that the electric benefit can be achieved in an air flow rate from 0.03 to 0.05 kg/s·m^2 with considering the electricity consumption of fans.

Tonui and Tripanagnostopoulos (2007) numerically investigated the performance of air-based PVT collectors enhanced by sheet metal suspended at the middle of the air channel and by the finned back wall. The electrical and thermal benefits when using the two low-cost performance enhancing approaches were studied parametrically. It was concluded that a finned back wall in the PVT collectors can provide enough heated air with a high total efficiency.

Ji *et al.* (2006) studied the influence of solar packing factor and water mass flow rate on the thermal and electrical performance of a wall-mounted water-based PVT collector. The simulation showed that an optimal water mass flow rate existed and the high packing factor improved system performance.

Shahsavar and Ameri (2010) numerically studied an air-based PVT collector with aluminium sheets in the air channel to increase the heat transfer area, as shown in Fig. 2.20. The performance of the PVT collector with and without using a glass cover, and with different number of fans was analysed and compared. It was found that an optimal number of fans existed for maximal electric efficiency and the glass cover can improve thermal efficiency while reducing the electric efficiency of the PVT collector.

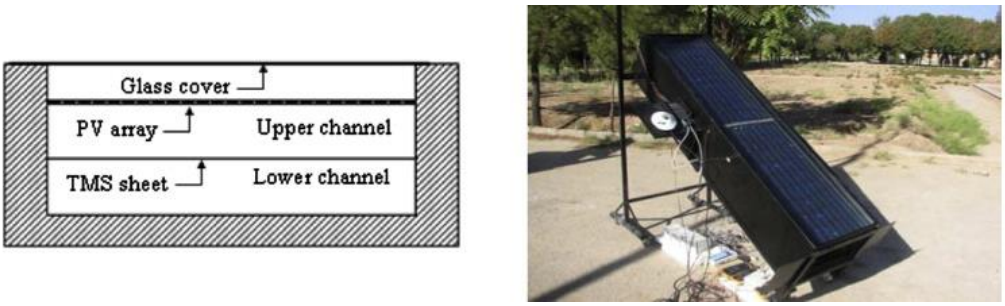

Fig. 2.20 An air-based PVT collector enhanced by aluminium sheets in the air channel (Shahsavar and Ameri 2010).

As well as experimental and numerical investigations, a number of BIPVT prototypes have been designed, developed and tested. For instance, Aste *et al.* (2008) developed and numerically studied an integrated solar PVT roof (as shown in Fig. 2.19b). A numerical model of the air-based PVT collector was developed and validated by measurements based on the developed prototype, which was then used to predict the thermal and electrical performance of the PVT collector.

Assoa *et al.* (2007) proposed and developed a novel hybrid PVT collector which enabled a simultaneous generation of preheated air and domestic hot water. This hybrid PVT collector was then examined experimentally based on the prototype test rig and it was found that the prototype can reach almost 80% thermal efficiency and also have a satisfactory cooling effect on the PV cells.

Shahsavar *et al.* (2011) numerically studied a BIPVT system which used the exhaust air from buildings during summer to cool PV panels, and also preheat the ventilation air for the air handling unit of air conditioning system for space heating during winter, as shown in Fig. 2.21. It was found that the production of electricity can be increased 7.5% and 10% by using the ventilation air and exhaust air for PV panels cooling, respectively. Thus an annual amount of 178.2 kWh of electrical and 3400.4 kWh of thermal energy can be saved.

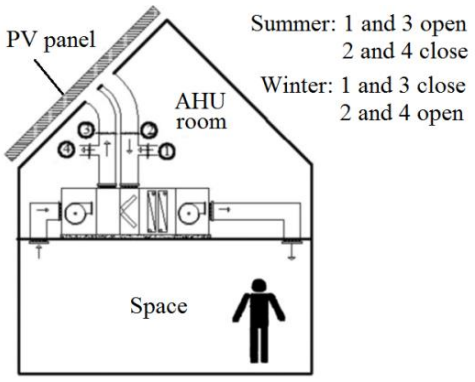

Fig. 2.21 The BIPVT system proposed (Shahsavar *et al.* 2011).

The PVT prototype that was measured based on a net zero energy building by Eicker and Dalibard (2011), as shown in Fig. 2.22. It was found that the PVT collectors could provide a cooling power of 60-65 W/m^2 during the night time when used to cool a warm storage tank, and a high energy efficiency ratio from 17 to 30 was achieved by using the PVT collectors.

Fig. 2.22 The PVT prototype tested on a Solar Decathlon house (Eicker and Dalibard 2011).Calise *et al.* (2016) proposed and simulated a novel poly-generation system which combined PVT collectors, a heat pump and an adsorption chiller to supply electricity, domestic hot water, and indoor space heating and cooling. This system could use 49% of the total solar energy with a yearly COP over 4 for cooling and 5.5 for heating, respectively. The thermos-economic optimisation for the system can reduce the simple pay-back period from over 16 years to around 14.5 years.

It has been shown that attaching PCMs with PV panels will maintain a low PV temperature (Ho *et al.* 2012; Huang M.J. 2011; Hasan *et al.* 2010 and 2014), and therefore avoid the degradation of PV power output (Browne *et al.* 2015). Moreover, this integration of PCMs with PVT collectors can also overcome the intermittency of solar energy with regards to thermal energy, and thus rationalise the utilisation of solar

thermal energy. A number of studies reported on the use of TES system to facilitate the cogeneration of PVT systems by enhancing the thermal and electrical efficiencies of the integrated systems. For instance, Al-Imam *et al.* (2016) examined the thermal and electrical performance of a PCM enhanced PVT collector system. This PVT-PCM system consisted of a compound parabolic concentrator (CPC) mounted water-based PVT collector and a PCM layer underneath. The results showed that a higher PVT thermal efficiency between 40-50% was achieved in winter, compared to without using the PCM of around 35%. The overall efficiency, including thermal and electrical efficiencies reached 55%-63% on a clear day. It was also found that the PCM layer can maintain a steady plate temperature after 3 m from the water entrance.

The integration of BIPVT collectors with building TES systems has also been reported. For instance, Chen Y.X. *et al.* (2010) proposed and studied a BIPVT-TES system using BIPVT collectors to generate electrical and thermal energy and using a ventilated concrete slab (VCS) in a solar house as TES. The simulations and experimental measurements showed that 9-12 kWh of thermal energy from BIPVT collectors can be stored in the VCS TES and then used passively to improve the building thermal performance. It has also been suggested to consider the accumulation of the thermal energy over consecutive sunny days in system design.

Fiorentini *et al.* (2015a) reported the development and implementation of an innovative air conditioning system integrated with an air-based PVT collector and a PCM TES. The thermal energy collected from the PVT collector was temporarily stored in the PCM storage and was used later for space heating or pre-heating the return/fresh air during winter. Based on the system above, a hybrid model predictive control strategy which consists of a high-level controller for operation mode determination and multiple low-level controller for operation parameters optimisation, was developed and experimentally investigated by the same authors (Fiorentini *et al.* 2015b and 2017). The results demonstrated that the air conditioning system integrated with the air-based PVT collector and the PCM TES was able to keep the indoor temperature within a comfort range with a higher COP compared with the reference standard air conditioner.

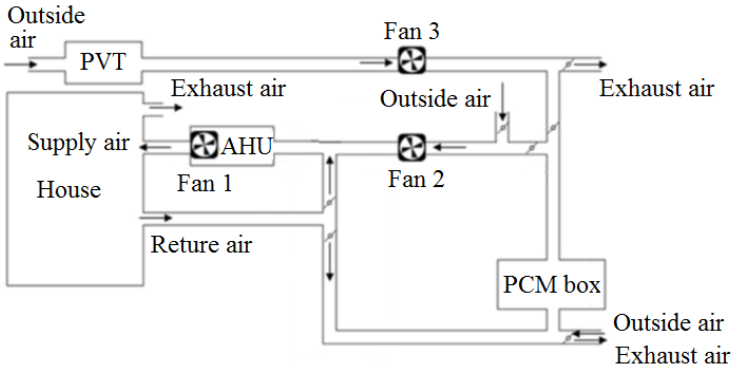

Fig. 2.23 The air conditioning system integrated with an air-based PVT collector and a PCM TES (Fiorentini *et al.* 2015).

This review shows that PVT collectors can cogenerate electricity and low grade thermal energy with a high overall efficiency. The BIPVT system provided a cost-effective on-site solution for energy generating and utilising solar energy. The extensive amount of research into PVT collectors has led to the development of PVT collector prototypes which are promising to be widely deployed. However, few studies focused on integrating PVT technology and TES technology, especially PCM TES, and this really needs further study.

2.7 Summary

A literature review of the development, modelling, experiments, and optimisations of PCMs and PVT systems in buildings to achieve better indoor thermal performance and promote energy efficiency is provided, from which some conclusions are summarised as follows:

1) The characteristics of PCMs could significantly influence the performance of PCM applications in buildings and therefore PCMs for building applications should be selected carefully. Of the various PCM containments with different configurations, micro-encapsulation and macro-encapsulation in a rectangular configuration are preferred in many studies, in which the macro-encapsulation is popular due to its large thermal energy storage capacity and ease installation in building envelopes and TES units.

2) Numerical modelling is an essential tool to facilitate the design and optimal application of PCM systems in buildings. The hysteresis phenomenon during

phase transition should be considered to achieve accurate simulation results, whilst the heat transfer between PCMs and heat transfer fluids could be determined by adopting appropriate heat transfer correlations.

3) Building envelopes can offer a large heat transfer area for the application of PCMs. The walls and roofs (or ceilings) are among the most popular positions for installing PCMs. The problems which limit the thermal benefits of passive PCM applications, such as the poor natural convection heat transfer between the indoor environment and PCM enhanced building envelopes, weather-dependent performance, and low efficiency of PCMs utilisation, should be further investigated and could be mitigated through optimal design.

4) PCM TES units can be directly used for solar space heating and free cooling to improve indoor thermal comfort by rationalising the utilisation of renewable energy. PCM TES units can also be integrated with various air conditioning systems to achieve peak load shifting, to conserve air conditioning energy, or to achieve other functional purposes. Design optimisation can be conducted to fulfil the requirements of small heat transfer resistance and high energy storage density of PCM TES units.

5) Design optimisation is a cost-effective and practical approach to effectively enhancing the performance of PCM systems in building applications. As the predominant studies relied mainly on simplified analytical evaluations, empirical correlations, and parametric studies, design optimisation using optimisation algorithms are therefore worth further investigation.

6) PVT collectors which could deliver more useful energy than the separate PV and solar thermal systems per unit collector area are renewable solutions to make full use of solar energy. To overcome the intermittency of solar energy so as to rationalise the utilisation of solar thermal energy generated from BIPVT collectors, the integration with PCMs with the BIPVT systems is an attractive solution.

Chapter 3 Thermal Performance Investigation of PCM enhanced Buildings with Integrated PVT Collectors

The literature review in Chapter 2 demonstrated the potential benefits of integrating phase change materials into building envelopes (*i.e.* PCM enhanced buildings) and the likely benefits of using air-based solar photovoltaic thermal (PVT) collectors in buildings. As the passively integrated PCMs in building envelopes cannot be fully utilised in many instances due to small temperature variations between daytime and night time (Iten *et al.* 2014), the utilisation of heated air from PVT collectors could increase the benefits of using PCMs in building envelopes for better indoor temperature regulation. However, the potential benefits of using PVT collectors in PCM enhanced buildings have not been reported. This chapter presents the thermal performance investigation of PCM enhanced passive buildings by using the heated air derived from PVT collectors for space heating (named as PVT ventilation hereafter). The passive buildings here refer to the buildings without using air-conditioning systems or other conventional heating devices. The thermal performance investigation of PCM enhanced buildings with the PVT ventilation was carried out using the TRNSYS simulation program (Beckman 2001).

This chapter is organised as follows. Section 3.1 briefly introduces the PCM enhanced building with the PVT ventilation. The setup of the modelling system for the PCM enhanced buildings with the PVT ventilation is described in Section 3.2. The research methodology used in this chapter is presented in Section 3.3. Section 3.4 presents the thermal performance evaluation results and the key findings of this chapter are summarised in Section 3.5.

3.1 Description of PCM enhanced buildings with the PVT ventilation

Fig 3.1 presents a PCM enhanced building integrated with PVT collectors. The PVT collectors were assumed to be installed on the north side of the roof under Australian climate conditions. A PCM layer was laminated into all external walls and the ceiling of the building. In this PCM enhanced building with integrated PVT collectors and without using an air-conditioning system, the functions of PVT collectors and PCMs in the building envelopes are coupled indirectly via indoor environment. During the winter daytime, the heated air generated from the PVT collectors can be directed into

the building for space heating if the temperature of the air from the PVT collectors is higher than the indoor air temperature. In this scenario, part of the thermal energy can be stored in the PCM layers laminated into the building envelopes, as the indoor air temperature is improved using the PVT ventilation. During the night time, the thermal energy stored in the PCM layers could be released into the indoor environment to increase the indoor air temperature. As the main benefit of using the low grade heat derived from air-based PVT collectors is for space heating, in this study, the thermal performance analysis of the PCM enhanced building with the PVT ventilation therefore focused on winter heating conditions, although night time radiative cooling effect of PVT collectors in summer can also improve the thermal performance of PCM enhanced buildings.

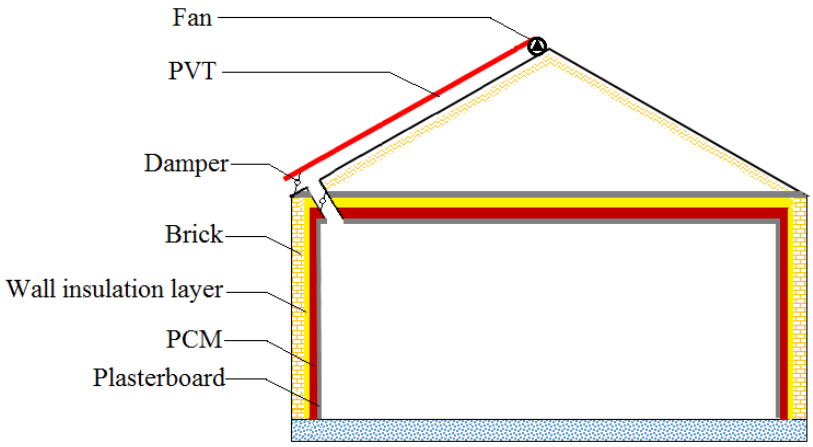

Fig. 3.1 Schematic illustration of the PCM enhanced building integrated with PVT collectors.

3.2 System modelling

3.2.1 Building modell

A house with a total floor area of 200 m^2 with two thermally separated zones (*i.e.* roof space and room space) was modelled using Google SketchUp and then imported into the TRNSYS Type 56 Multi-zone building component model. The area of the PVT collectors installed was 110 m^2, with a roof angle of 22.5^o (see Fig. 3.1). The major specifications of the house envelopes are summarised in Table 3.1.

Table 3.1 Major specifications of the house envelopes.

Building envelope	Materials used (from interior to exterior)
Wall	12 mm plasterboard
	Wall insulation layer with an *R*-value of 1.0 m^2K/W
	110 mm brick
Ceiling	12 mm plasterboard
	Ceiling insulation layer with an *R*-value of 3.0 m^2K/W
	12 mm plasterboard

3.2.2 PVT model

The PVT numerical model used was a dynamic model from Sohel *et al.* (2014), as shown in Fig. 3.2. The key governing equations used are presented in Eqs. (3.1) - (3.3). By using this PVT model, the outlet air temperature, the PV panel temperature and PVT back insulation temperature, electrical power generation and thermal energy collected can be determined.

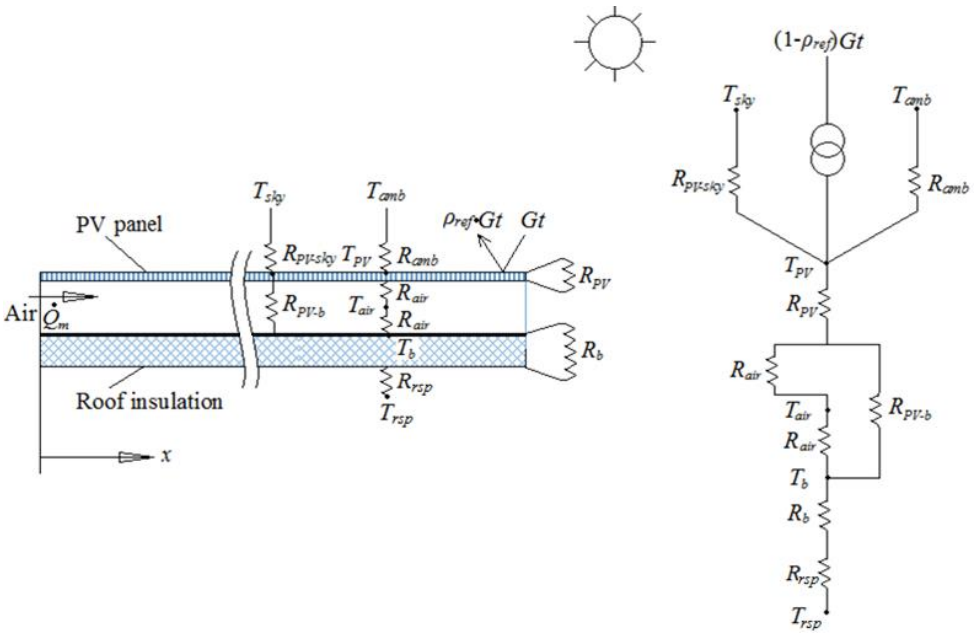

Fig. 3.2 PVT model used in this study (Sohel *et al.* 2014).

$$\dot{Q}_m c_{p,air} \frac{dT_{air}}{dx} = W_{PV}\left(\dot{q}_{PV-air} - \dot{q}_{air-b}\right) \tag{3.1}$$

$$m_{PV} c_{p,PV} \frac{dT_{PV}}{dt} = \left(1-\rho_{ref}\right)\cdot IAM \cdot \left(1-\eta_{PV}\right)\cdot A \cdot I_t - \dot{Q}_{loss} - \dot{Q}_{PV-air} - \dot{Q}_{PV-b} \tag{3.2}$$

$$m_b c_{p,b} \frac{dT_b}{dt} = \dot{Q}_{PV-b} + \dot{Q}_{air-b} - \dot{Q}_{b-rsp} \tag{3.3}$$

where $\dot{Q}_m$ is the air mass flow rate, T is the temperature, c_p is the specific heat capacity, m is the mass, A is the heat transfer area, ρ_{ref} is the reflectance of the PV panel, IAM is the incident angle modifier, I_t is the total solar irradiation on the PV panel, η_{PV} is the electrical efficiency, W is the width of the PVT collector, $\dot{q}$ is the heat flux rate, $\dot{Q}$ is the rate of heat flow, t is the time, R is the heat transfer resistance, subscripts *air, PV, b, loss and rsp* indicate the air, PV panel, bottom plate, heat loss to the ambient and roof space respectively, and *PV-air*, *PV-b*, *air-b*, *b-rsp* indicate the heat transfer directions from the PV panel to the air, from the PV panel to the back plate, from the working fluid to the back plate, from the back plate to the roof space, respectively.

3.2.3 Envelope-integrated PCM model

In order to integrate the PCM model within the house model, the corresponding envelopes in the house model were reduced to a single layer of the plasterboard, while the brick (or the external plasterboard layer of the ceiling) and wall insulation layer of the original house model were transplanted to the PCM model, as illustrated in Fig. 3.3. The PCM layer integrated with the transplanted brick layer (or the extra plasterboard of the ceiling) and the wall insulation layer is named as envelope-integrated PCM model hereafter. The envelope-integrated PCM model was developed using the finite difference method based on an enhanced enthalpy method, in which the heat transfer from outdoor and the heat flux through the building plasterboard layer were used as the exterior and interior boundary conditions, respectively. The governing equations of the energy balance for the PCM layer is shown in Eqs. (3.4), based on the assumptions employed below.

- The dominant heat transfer within the envelopes is one-dimensional thermal conduction;
- The shrinkage cavity caused due to the density change during the phase change process is considered to be evenly distributed within each PCM element (Shamsundar and Sparrow 1976);
- The wall insulation layer is simplified as a massless layer with pure thermal resistance;

- The PCM hysteresis phenomenon was simulated based on the method presented by Bony and Citherlet (2007) with separated heating and cooling curves to represent the enthalpy-temperature (*h*-*T*) relationship. However, the equivalent specific heat capacity ($c_{p,eq}$) within the hysteresis region is considered to vary with the PCM thermal dynamic state, as shown in Fig. 3.4;

- The liquid and solid specific heat capacities of the PCM beyond the phase change region are assumed to be constant.

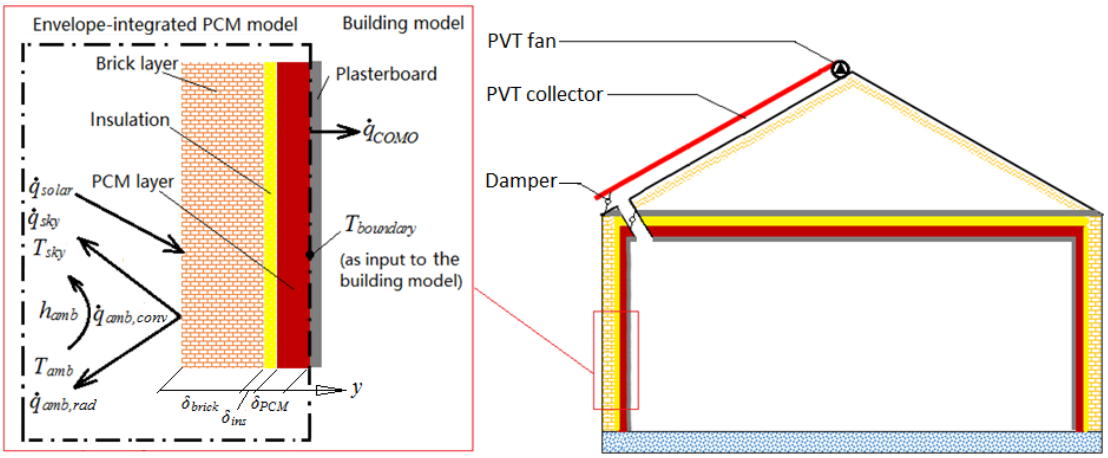

Fig. 3.3 Envelope-integrated PCM model.

The governing equations of the energy balance for the brick layer is shown in Eq. (3.5), and the boundary conditions for the PCM layer and the brick layer are summarised in Eq. (3.6).

$$\rho_{PCM}\frac{\partial h_{PCM}}{\partial t}=k_{PCM}\frac{\partial^2 T_{PCM}}{\partial y^2} \tag{3.4}$$

$$\rho_{brick}c_{p,brick}\frac{\partial T_{brick}}{\partial t}=k_{brick}\frac{\partial^2 T_{brick}}{\partial y^2} \tag{3.5}$$

$$\begin{cases} k_{PCM}\left.\dfrac{\partial T_{PCM}}{\partial y}\right|_{y=\delta_{PCM}+\delta_{ins}+\delta_{brick}} = -\dot{q}_{COMO} \\ k_{PCM}\left.\dfrac{\partial T_{PCM}}{\partial y}\right|_{y=\delta_{brick}+\delta_{ins}} = k_{brick}\left.\dfrac{\partial T_{brick}}{\partial y}\right|_{y=\delta_{brick}} = \dfrac{T_{brick}\big|_{y=\delta_{brick}} - T_{PCM}\big|_{y=\delta_{brick}+\delta_{ins}}}{R_{ins}} \\ k_{brick}\left.\dfrac{\partial T_{brick}}{\partial y}\right|_{y=0} = \dot{q}_{solar}-\dot{q}_{sky}-\dot{q}_{amb,rad}-\dot{q}_{amb,conv} \end{cases} \tag{3.6}$$

where ρ is the density, h_{PCM} is the specific enthalpy of the PCM used, h is the heat transfer coefficient, $\dot{q}$ is the heat flux, k is the thermal conductivity, δ is the thickness, y indicates the coordinate along the direction of PCM layer thickness, subscripts *rad*, *conv* and *COMO* indicate the radiative heat flux, convective heat transfer and heat transfer towards the plasterboard of the building envelope, subscripts *amb* and *ins* indicate the ambient and the wall insulation layer.

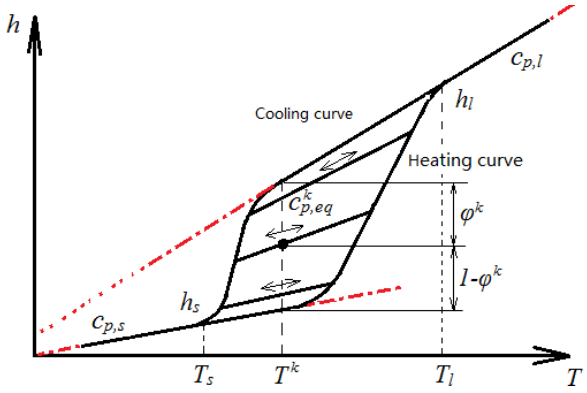

Fig. 3.4 Enthalpy-temperature relationship.

The governing equation of the PCM layer can be easily discretised and the relationship between the enthalpy and temperature of the PCM at the time step k+1 then can be determined by Eq. (3.7), while the enthalpy of the PCM at the time step k+1 can be determined based on the energy balance using the PCM thermodynamic state at the time step k.

$$h_{PCM}^{k+1}=\begin{cases} h_{heating}\left(T^{k+1}\right), & \begin{cases}\text{if } h_{PCM}^{k}=h_{heating}\left(T^{k}\right),\quad T^{k+1}\geq T^{k},\quad T_s<T^{k}<T_l\\ \text{or}\quad \text{if}\quad T^{k}\geq T_l\end{cases}\\ c_{p,eq}^{k}\left(T^{k+1}-T^{k}\right)+h_{PCM}^{k}, & \begin{cases}\text{if } h_{PCM}^{k}=h_{heating}\left(T^{k}\right),\quad T^{k+1}<T^{k},\quad T_s<T^{k}<T_l\\ \text{or}\quad \text{if}\quad h_{heating}(T^{k})<h_{PCM}^{k}<h_{cooling}(T^{k}),\quad T_s<T^{k}<T_l\\ \text{or}\quad \text{if}\quad h_{PCM}^{k}=h_{cooling}\left(T^{k}\right),\quad T^{k+1}>T^{k},\quad T_s<T^{k}<T_l\end{cases}\\ h_{cooling}\left(T^{k+1}\right), & \begin{cases}\text{if } h_{PCM}^{k}=h_{cooling}\left(T^{k}\right),\quad T^{k+1}\leq T^{k},\quad T_s<T^{k}<T_l\\ \text{or}\quad \text{if}\quad T^{k}\leq T_s\end{cases}\end{cases} \tag{3.7}$$

where $h_{heating}$ and $h_{cooling}$ represent the heating curve and cooling curve respectively, $c_{p,eq}$ is the equivalent specific heat capacity within the hysteresis region, T_s and T_l are the lower and upper temperature limits of the hysteresis region respectively, superscript k represents the time step k, and subscripts s and l indicate the solid and liquid states, respectively.

The equivalent specific heat capacity is calculated by Eq. (3.8), in which the weighting factor (*i.e.* φ) is related to the PCM thermodynamic state and can be determined by Eq. (3.9).

$$c_{p,eq}^{k} = \varphi^{k} \cdot c_{p,s} + \left(1-\varphi^{k}\right)\cdot c_{p,l}\,, \quad if\ h_{heating}(T^{k}) < h_{PCM}^{k} < h_{cooling}(T^{k}), \quad T_s < T^{k} < T_l \tag{3.8}$$

$$\varphi^{k} = \left[c_{p,l}T^{k} + \left(h_l - c_{p,l}T_l\right) - h_{PCM}^{k}\right] / \left[c_{p,l}T^{k} + \left(h_l - c_{p,l}T_l\right) - c_{p,s}T^{k}\right] \tag{3.9}$$

For a given PCM, its heating and cooling *h*-*T* relationships can be obtained from Differential Scanning Calorimetry (DSC) test data, or from the data sheets provided by manufacturers. This modelling method is also valid for PCM composites providing the *h*-*T* relationships with similar hysteresis regions.

3.3 Method for thermal performance investigation

3.3.1 Outline of the method

The research method employed to evaluate the thermal performance of the PCM enhanced buildings with the PVT ventilation is illustrated in Fig. 3.5. The performance evaluation consists of two main parts: parametric study and Taguchi-based analysis, based on the setup of the modelling system. In terms of the parametric study, a range of the test cases with different types of PCMs and various thicknesses of the PCM layers, as well as using or without using the PVT ventilation were designed. The thermal performance of the house with each case was then simulated and compared with that of the *Baseline* case without using the PVT ventilation and PCMs. According to the test results, further performance evaluation using Taguchi method was conducted to analyse the influence of each design variables (*i.e.* known as control factors in Taguchi method) on the thermal benefits by using the PVT ventilation and PCMs in building envelopes. The best combination of the factor levels (*i.e.* the best combination of the values of design variables) can be identified through the Taguchi-based analysis. Finally, the confirmation test of using the identified combination of the factor values was conducted. The design of the test cases, the development of the key performance indicator (KPI) and Taguchi-based sensitivity study are briefly presented in Sections 3.3.2, 3.3.3 and 3.3.4, respectively.

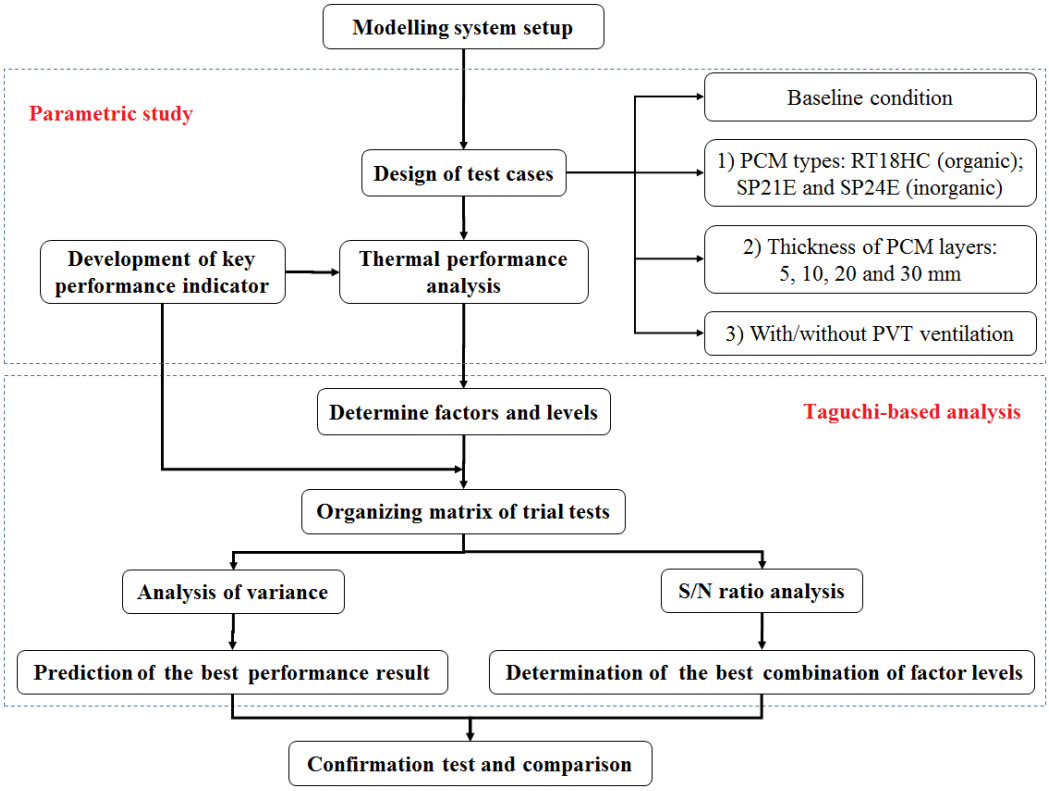

Fig. 3.5 Outline of the research methodology employed to evaluate the thermal performance of the PCM enhanced house with the PVT ventilation.

3.3.2 Design of the test cases

A range of test cases, as summarised in Table 3.2, were first designed and tested to evaluate and compare the thermal performance of the house with or without PCMs in the building envelopes, and with or without using the PVT ventilation. In these test cases, three different types of PCMs and four different thicknesses of the PCM layers were used. The PCMs considered were commercial PCMs from Rubitherm (2014), including the organic PCM of RT18HC, and the inorganic PCMs of SP24E and SP21E. The phase change temperature ranges of these three selected PCMs are close to the indoor thermal comfort temperature range. SP24E represents the PCMs whose phase change temperature range is close to the upper limit of the thermostat setting temperature, and RT18HC has a phase change temperature range close to the lower limit of the thermostat setting temperature. The phase change temperature range of SP21E is close to the mean value of the upper and lower limits of the thermostat setting temperature. The details of the heating and cooling specific enthalpy distribution over the temperature range of these PCMs obtained from the datasheet (Rubitherm 2014).

Table 3.2 Summary of the test cases studied.

Conditions	Test cases	PVT ventilation used	PCM layer thickness (mm)		
			RT18HC	SP21E	SP24E
Without using PVT ventilation and PCMs	*Test case* 1	No	0	0	0
Using PCMs only	*Test case* 2	No	5	5	5
	Test case 3		10	10	10
	Test case 4		20	20	20
	Test case 5		30	30	30
Using PVT ventilation only	*Test case* 6	Yes	0	0	0
Using PVT collectors and PCMs simultaneously	*Test case* 7	Yes	5	5	5
	Test case 8		10	10	10
	Test case 9		20	20	20
	Test case 10		30	30	30

The thermo-physical properties of the three types of PCMs used are presented in Table 3.3. The thicknesses of the PCM layers tested were 5, 10, 20 and 30 mm, respectively. In these test cases, the air mass flow rate of the PVT collectors used was 2000 kg/h. It is noteworthy that this study was mainly focused on the thermal performance enhancement of the house in terms of the indoor temperature variation. The effect of the air velocity on human thermal comfort was not considered.

Table 3.3 Thermo-physical properties of the PCMs used (Rubitherm 2014).

PCMs	Density at liquid/solid (kg/m^3)	Melting temperature range (^oC)	Solidification temperature range (^oC)	Specific heat capacity [kJ/(kg·K)]	Thermal conductivity [W/(m·K]
SP24E	1400/1500	24-25	23-21	2.0	0.6
SP21E	1400/1500	22-23	21-19	2.0	0.6
RT18HC	770/880	17-19	19-17	2.0	0.2

3.3.3 Development of the key performance indicator

In order to quantify the thermal performance enhancement of the PCM enhanced buildings with the PVT ventilation as compared with the house without using the PVT ventilation and PCMs, a performance indicator, Coefficient of Thermal Performance Enhancement (CTPE), as shown in Eq. (3.10), was developed to facilitate the performance evaluation. CTPE was defined as the decreasing percentage of the integral area below the lower thermostat but above the indoor air temperature (*i.e.* the

shadow area in Fig. 3.6) due to the use of the PCMs and the PVT ventilation, compared with the *Baseline* case (*i.e.* without using the PVT ventilation and PCMs). The shadow area indicated the time of the indoor air temperature below the lower thermostat limit (*i.e.* $T_{setting,low}$) weighted by the temperature difference, as shown in Fig. 3.6. The thermal performance of the house without PCMs integrated into the building envelopes and without using the PVT ventilation was used as the baseline condition, and its CTPE was set as zero correspondingly. It is worthwhile to note that only the lower limit of the indoor thermal comfort setting was used for winter space heating conditions. However, the use of PVT ventilation may cause overheating of the house during the daytime in winter, which was not considered in this study. It is also worthwhile to note that this study mainly focuses on the building thermal management due to the use of PCMs and PVT ventilation and the improvement in the electrical efficiency of the PVT collectors was not focused on in the thermal performance analysis.

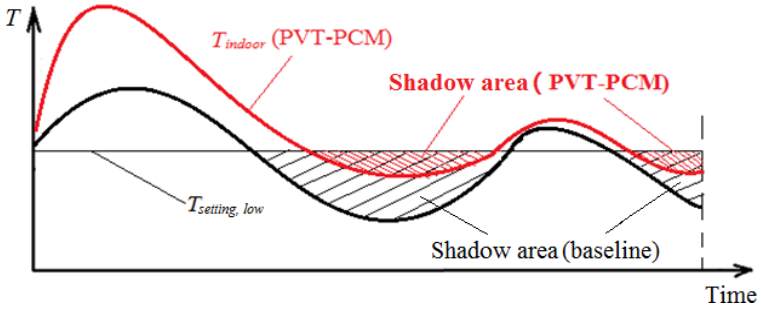

Fig. 3.6 Illustration of the working principle expressed in Eq. (3.10).

$$CTPE = 1 - \frac{\int_0^{tot} \left\{ -\min\left[0, (T_{indoor} - T_{setting,low})\right]\right\} dt}{\int_0^{tot} \left\{ -\min\left[0, (T_{indoor} - T_{setting,low})\right]\right\} dt \Big|_{baseline}} \tag{3.10}$$

where T_{indoor} is the indoor air temperature of the house with PCMs integrated in the building envelopes only, or with using PVT ventilation only, or with using both PCMs in the building envelopes and PVT ventilation simultaneously, and *tot* is the total time of concern.

3.3.4 Taguchi method

Taguchi method is used to design the matrix of experiments for robust design of a system or process. Analysis of variance (ANOVA) and signal-to-noise (*S/N*) ratio are used for data analysis (Taguchi 2004). ANOVA is commonly applied to investigate

the response significance of individual factors and identify the percentage contribution of each factor to the objective response. Based on the factors with high percentage contribution, the performance of the system or process using the best combination of the factor levels can be predicted by Eq.(3.11) (Milos and Miroslav 2013). The degree of freedom (*DOF*), the sum of squares of factors (*SS*), the pure sum of squares of factors (*SS'*), the variance of factors (*Var*) and the percentage contribution (%C) of factors are the key statistic parameters used in ANOVA. The details on how to calculate these parameters can be found in Roy (2010).

$$\hat{y}_{predict} = \bar{y} + \sum_{i=1}^{n_{fs}} \left(\bar{y}_{best,i} - \bar{y} \right) \tag{3.11}$$

where $\hat{y}_{predict}$ is the predicted response of the objective, n_{fs} is the number of the factors which significantly affect the objective response, $\bar{y}$ is the mean value of the objective responses of all experiments, $\bar{y}_{best,i}$ is the mean value of the objective responses when the i^{th} factor is set at its best level. The importance of the factors can be ranked by the percentage contribution.

In Taguchi method, *S/N* ratio, a statistic for performance measurement combining the information of mean and variance (Velibor and Milos 2011), is often used to identify the best combination of the levels of individual factors. The combination of the factor levels can be regarded as a better design for the system or process of concern, according to which, the better system or process performance can be achieved. Different *S/N* ratios can be chosen depending on the criterion for the quality characteristic selected (Taguchi 2004 and Roy 2010), as presented from Eq. (3.12) to Eq. (3.14). In this chapter, the CTPE is used as the quality characteristic; it is considered as the higher-the-better, and Eq. (3.12) is selected to calculate the *S/N* ratio of CTPE.

$$S/N = -10\log\left(\frac{1}{n} \sum_{j=1}^{n} \frac{1}{y_j^2} \right) \text{for the-higher-the-better} \tag{3.12}$$

$$S/N = -10\log\left(\frac{1}{n} \sum_{j=1}^{n} y_j^2 \right) \text{for the-lower-the-better} \tag{3.13}$$

$$S/N = 10\log\left(\frac{\bar{y}^2}{s^2} \right) \text{for the-nominal-the-better} \tag{3.14}$$

where y is the objective response, n is the number of the observations in a trial test, and subscript j is the j^{th} observed value of the objective response, s^2 is the variance. The importance of the factors can be ranked by the difference between maximal and minimal *S/N* ratios of different factor levels; a higher difference leads to a higher rank which indicates that this factor has more significant influence on the objective response than other factors.

3.4 Performance evaluation and optimisation

3.4.1 Validation of the building envelope-integrated PCM model

The experimental data reported by Kuznik and Virgone (2009) was used to validate the effectiveness of the envelope-integrated PCM model. In their experiments, a cubical enclosure with a PCM layer integrated into its three vertical walls was placed into a climate chamber. The PCM used is a commercial PCM composite product, ENERGAIN, from Dupont de Nemours Society. The density and thermal conductivity of the PCM composite were around 900 kg/m^3 and around 0.2 W/(m·K), and the specific heat of the PCM composite was shown in Fig. 3.7. The climate chamber was used to control the exterior temperature of the cubical enclosure by providing various external temperature conditions such as heating step, cooling step and sine temperature evolutions. The responses of the inside temperature of the enclosure under different external temperature conditions were measured using a Pt-100 sensor with a calculated resolution of ±0.25°C located at the centre of the enclosure.

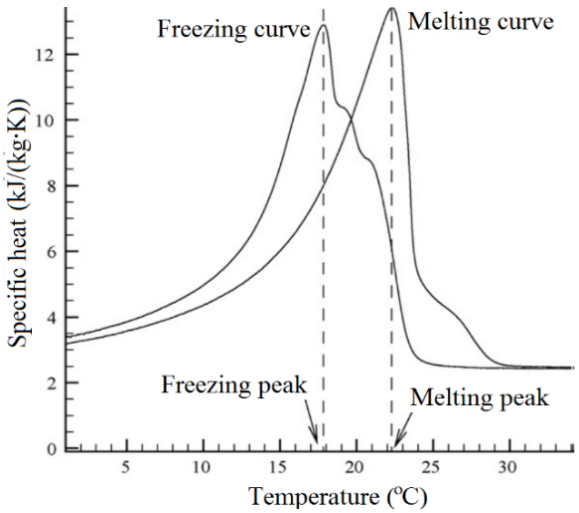

Fig. 3.7 The specific heat of the PCM composite used in Kuznik and Virgone (2009).

For model validation purposes, a cubical enclosure model comprising of the PCM layer in the three walls corresponding to the experimental cubical enclosure was established using the envelope-integrated PCM model developed. The long wave radiation heat exchanges among the interior surfaces of the enclosure, and between the exterior surface of the enclosure and the internal walls of the climatic chamber, were considered as the extra heat flux on the boundaries of the envelope-integrated PCM model. Fig. 3.8 illustrates the validation results. It can be seen that the simulation data agreed well with the experimental data reported in Kuznik and Virgone (2009) with relatively smaller deviations when compared to the results using a single *h*-*T* relationship for both heating and cooling processes as presented in Kuznik *et al.* (2010). The root mean square of the deviation between the model-predicted temperature and the experimental data reported in Kuznik and Virgone (2009) was around 0.3°C when the sinusoidal temperature setting was applied in the climatic chamber. The validation results indicated that this envelope-integrated PCM model can simulate the phase change process of PCMs with acceptable accuracy.

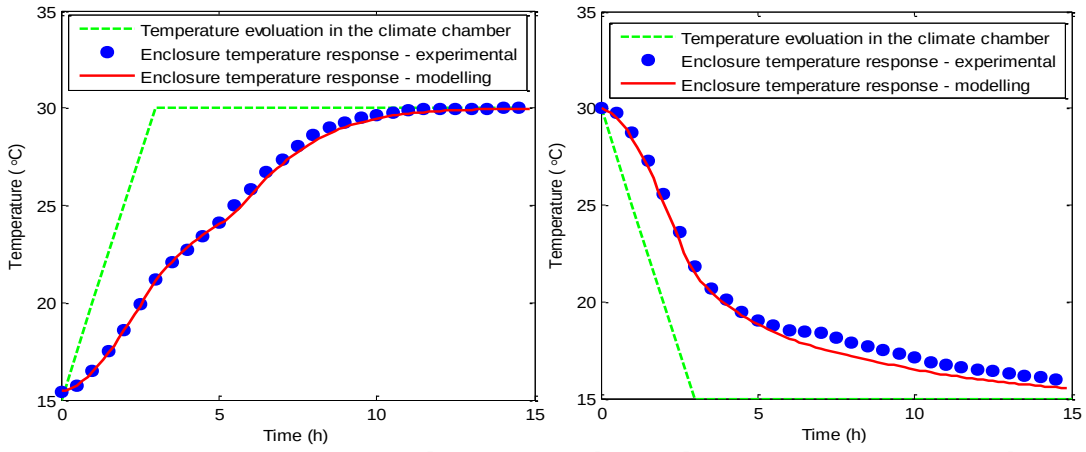

a) Heating step temperature evolution b) Cooling step temperature evolution

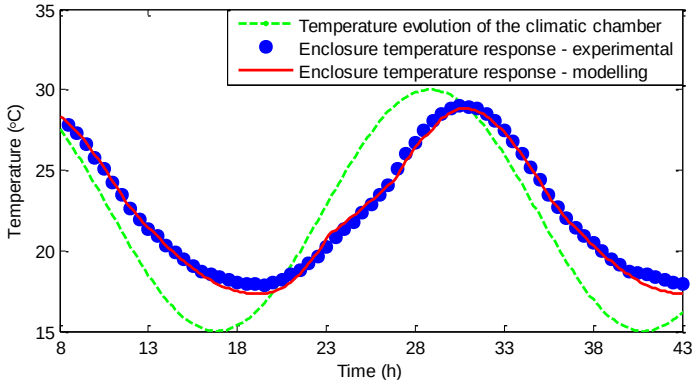

c) Sine temperature evolution

Fig. 3.8 Validation results of the envelope-integrated PCM model.

3.4.2 Setup of the test

As the living and sleeping spaces of the house were combined into one single air-node (*i.e.* the room space) in the house model, the higher value of the lower limit of the thermostat settings for the living space and sleeping space defined in Australian National House Energy Rating Scheme (2014) in winter conditions was used as the lower temperature requirement to maintain the thermal comfort of the house, as shown in Fig. 3.9.

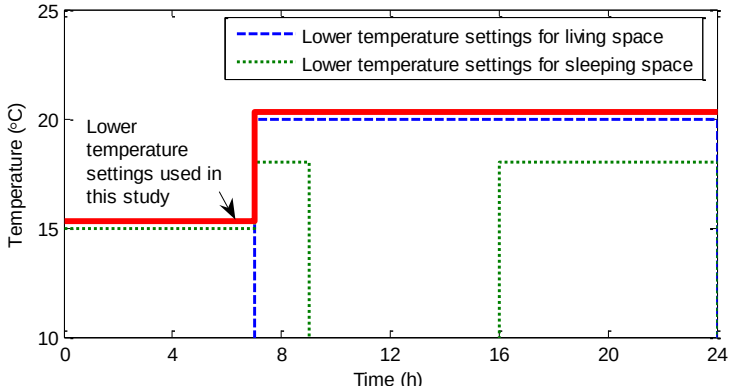

Fig. 3.9 Indoor temperature settings used in winter conditions.

The test results from the whole winter period (*i.e.* from June to August) under Sydney weather conditions were used to analyse the CTPE of the house while the test results from seven consecutive winter days were selected to illustrate the indoor temperature variations of the house due to the use of PCMs and the PVT ventilation for space heating. The solar irradiations, ambient air temperatures and outdoor humidity ratios in these seven selected test days are illustrated in Fig. 3.10.

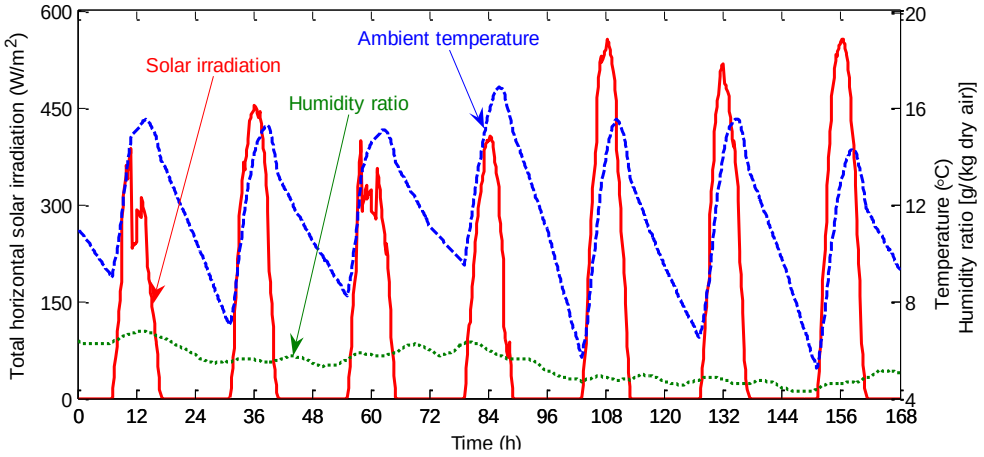

Fig. 3.10 Solar irradiations, ambient air temperatures and outdoor air humidity ratios during the seven selected test days.

3.4.3 Thermal performance of the house using the PCMs only

The CTPEs of the house by only using the different types of PCMs with different thicknesses (*i.e. Test cases* 2-5) were compared with that of the house without using the PVT ventilation and PCMs (*i.e. Test case* 1 (*Baseline* case)) and the results are summarised in Table 3.4. The CTPEs of the house by using RT18HC were -8.6%, -13.6%, -9.1% and -5.3% when the thicknesses of the PCM layer were 5, 10, 20 and 30 mm, respectively. The negative values of the CTPE indicated a decrease in indoor thermal performance of the house when using the PCMs only as compared to that of the *Baseline* case. This is mainly due to the non-existence of air-conditioning systems and/or other heating devices in the house. Consequently, the indoor temperature of the house during some more daytime periods and night time periods was close to or lower than that of the thermal comfort temperature setting, and the average temperature increase during the night time was less than the average temperature decrease during the daytime due to the use of PCMs.

The CTPEs of the house by using SP21E were -0.6%, 0.7%, 2.6% and 4.7% when the thicknesses of the PCM layer were 5, 10, 20 and 30 mm, respectively. Similar values can also be observed when SP24E was applied. Compared to RT18HC, the indoor thermal performance was slightly improved. The above results indicated that using PCMs alone cannot improve the indoor thermal performance of the house under Sydney winter heating conditions, which coincided with the conclusion achieved by Guichard *et al.* (2015).

Table 3.4 Coefficients of Thermal Performance Enhancement of the house by using PCMs with different thicknesses.

Test cases	PCM layer thickness (mm)	CTPE		
		RT18HC	SP21E	SP24E
Test case 1 (Baseline case)	0	0	0	0
Test case 2	5	-8.6%	-0.6%	-2.1%
Test case 3	10	-13.6%	0.7%	-1.1%
Test case 4	20	-9.1%	2.6%	0.2%
Test case 5	30	-5.3%	4.7%	1.8%

The indoor temperatures of the house by using the PCMs only and that of the *Baseline* case (*i.e. Test case* 1) under the seven selected consecutive winter days are shown in

Fig. 3.11. A sample of the results for the thicknesses of the PCM layer of 5 and 30 mm (*i.e. Test case* 2 and *Test case* 5) are presented in this chapter. Compared to the *Baseline* case (*i.e. Test case* 1), the indoor temperature fluctuations decreased due to the use of the PCMs in the building walls and ceiling. However, there was no clear difference in the indoor temperature during the night time when the three different types of PCMs with a thickness of 5 mm were used.

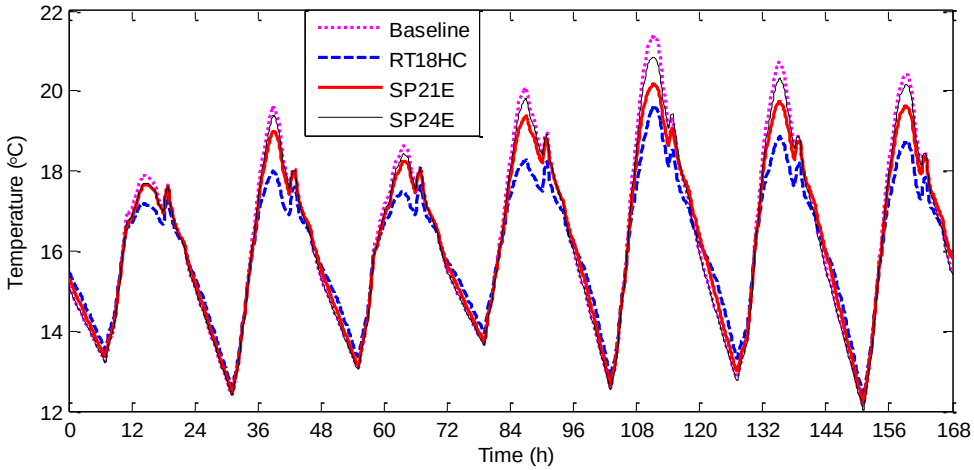

a) PCM layer thickness of 5 mm

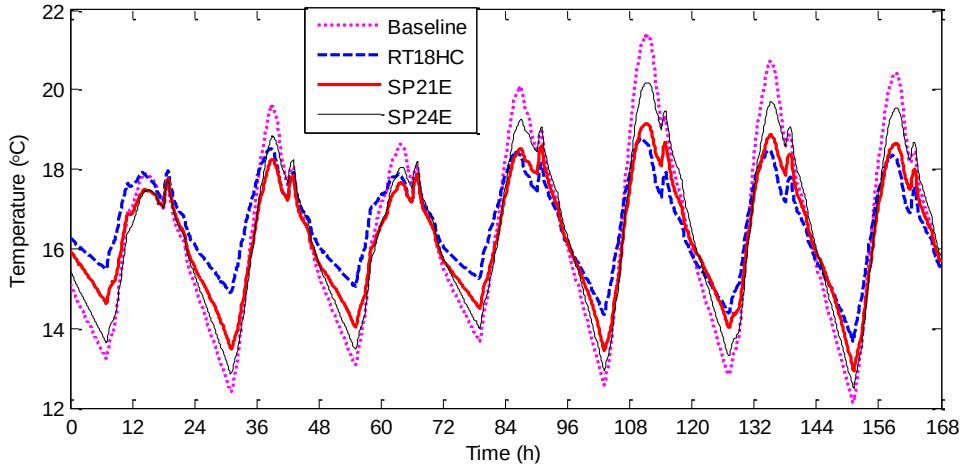

b) PCM layer thickness of 30 mm

Fig. 3.11 Indoor air temperatures of the house by using and without using the PCMs.

The difference among the indoor temperatures by using SP24E, SP21E and RT18HC can be observed when the thickness of the PCM layer increased to 30 mm. A clear discharging process during the night time can be observed when RT18HC was used as the indoor temperature obviously increased when compared to that of the *Baseline* case. However, it seems that the thermal energy stored in PCM SP24E was very limited due to its higher phase change temperature, as the indoor air temperature at night time was

just slightly increased. It is worthwhile to mention that as the phase change temperature of RT18HC was lower than the thermal comfort temperature setting specified for the daytime, the contribution of RT18HC for indoor thermal performance enhancement was therefore mainly from the night time.

3.4.4 Thermal performance of the PCM enhanced house with the PVT ventilation

Table 3.5 summarises the CTPEs of the house by using the PVT ventilation and PCMs with different thicknesses (*i.e. Test cases* 7-10), by using the PVT ventilation only (*i.e. Test case* 6), and that of the *Baseline* case (*i.e. Test case* 1). The CTPE of the house increased up to 38.1% when the PVT ventilation was used. Compared to the use of RT18HC and SP24E, higher CTPEs of the house were achieved when SP21E was used. The resulted CTPEs of the house were 43.3%, 46.3%, 48.8% and 53.1% when the thicknesses of SP21E were 5, 10, 20 and 30 mm, respectively. The use of RT18HC showed a better performance in terms of the CTPE (*i.e.* 52.1%) than that of using SP24E (*i.e.* 48.4%) when using the PVT ventilation and the thickness of the PCM layer was 30 mm, while with a thinner PCM layer, the CTPEs of the house that used RT18HC and the PVT ventilation were slightly lower than the CTPEs using SP24E and the PVT ventilation.

Table 3.5 Coefficients of Thermal Performance Enhancement of the house by using the PVT ventilation and PCMs.

Test cases	PCM layer thickness (mm)	CTPE		
		RT18HC	SP21E	SP24E
Test case 1	0	0	0	0
Test case 6	0	38.1%	38.1%	38.1%
Test case 7	5	40.0%	43.3%	40.3%
Test case 8	10	40.1%	46.3%	42.8%
Test case 9	20	43.4%	48.8%	46.2%
Test case 10	30	52.1%	53.1%	48.4%

It can be concluded that the use of the PVT ventilation and PCMs simultaneously can greatly improve the indoor thermal performance, when compared with the house by using the PCMs only and the *Baseline* case without using the PVT ventilation and the PCMs (see Table 3.4). Compared with the house by using the PVT ventilation only, the integration of PCMs in the building envelopes resulted in a further increase of the CTPE by more than 10%, when certain PCMs and thicknesses of the PCM layer were

used (see Table 3.5). The above results indicated that the PVT ventilation can effectively enhance the PCM performance of thermal energy storage through charging more thermal energy into the PCMs during the daytime and release it later during the night time for space heating in winter. The comparison of the indoor temperatures of the house by using the PVT ventilation only (*i.e. Test case* 6), with the cases where the PVT ventilation and the PCMs were used simultaneously, and with that of the *Baseline* case (*i.e. Test case* 1) under the same seven winter test days is presented in Fig. 3.12, where a sample of the results for the thicknesses of the PCM layer of 5 and 30 mm (*i.e. Test case* 7 and *Test case* 10) are presented.

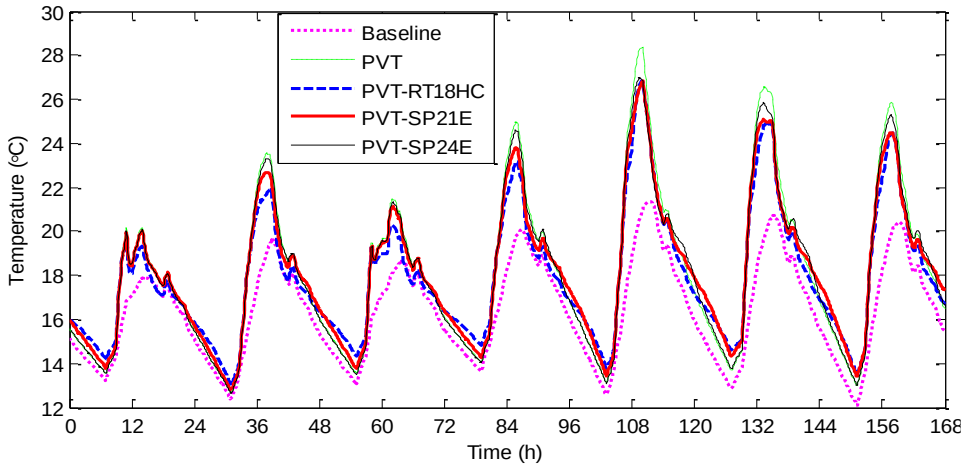

a) PCMs thickness of 5 mm

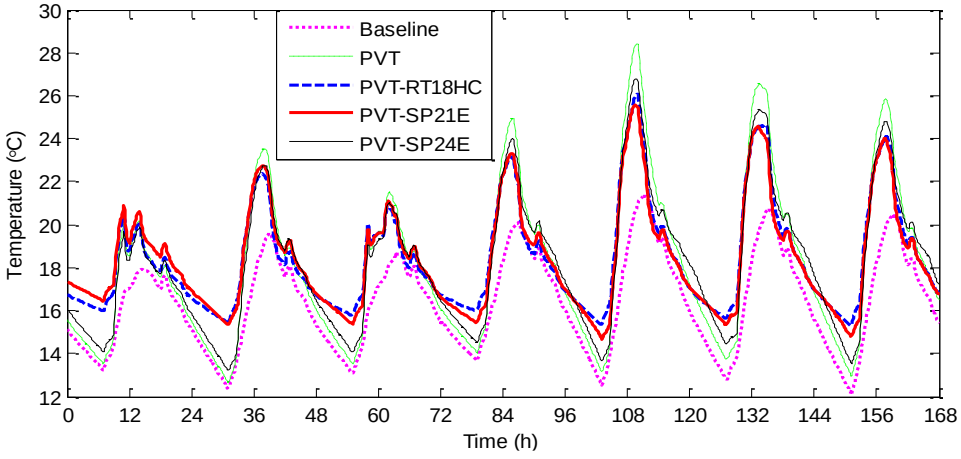

b) PCMs thickness of 30 mm

Fig. 3.12 Indoor air temperatures of the house by using the PVT ventilation and PCMs simultaneously, by using the PVT ventilation only and that of the *Baseline* case without using the PVT ventilation and PCMs.

Compared to the results presented in Fig. 3.11 by using the PCMs only, the indoor air temperature of the house increased significantly during the daytime when the heated

air from the PVT collectors was supplied to the house. However, during the night time, the indoor temperature was only slightly higher than that of using the PCMs only when the thickness of the PCM layer was 5 mm, due to the limited storage capacity of the PCMs used. When the PCM thickness increased to 30 mm, an obvious increase in the indoor temperature can be observed during the night time as compared to that of using the PCMs only. However, it seems that the amount of thermal energy stored in SP24E was small during the daytime even with the PVT ventilation and its thermal benefit to improve the indoor temperature during night time was therefore limited.

It seems important to select appropriate PCMs positioned at the building envelopes with different orientations. To understand this influence on the indoor air temperature, the thermodynamic state of the PCMs in terms of the boundary temperatures of the PCM layer close to the indoor of the PCM enhanced house with the PVT ventilation are presented, as shown in Fig. 3.13. The results for the north wall, south wall and ceiling with the PCM thickness of 20 mm are provided, as the north wall and south wall represent the sunny side and shady side of the building envelopes respectively, and the ceiling of the house was well insulated in comparison to the walls of the house (see Table 3.1). It can be seen that a higher boundary temperature of the PCM layer can be found in the ceiling when RT18HC was used. In the wall, the temperature fluctuation was relatively small when RT18HC was used, as compared to that using SP21E and SP24E. This is because that a large amount of heat was charged in and discharged from RT18HC at around its phase change temperature of 18^{o}C, which is lower than the phase change temperatures of SP21E and SP24E. Smaller boundary temperature fluctuations of the PCM layer in the ceiling were resulted when SP21E and SP24E were used, as compared to that in the north wall and south wall, due to the better insulation of the ceiling. More obvious PCM charging and discharging processes can also be found in the north wall when SP21E and SP24E were used, as compared to that of the south wall. This is due to the fact that the north wall exposed to strong solar radiation during the daytime and more heat was therefore charged into the PCM layers which reduced the temperature fluctuations. The above results illustrate that the insulation of the building envelopes plays an important role in ensuring the effectiveness of the PCMs used.

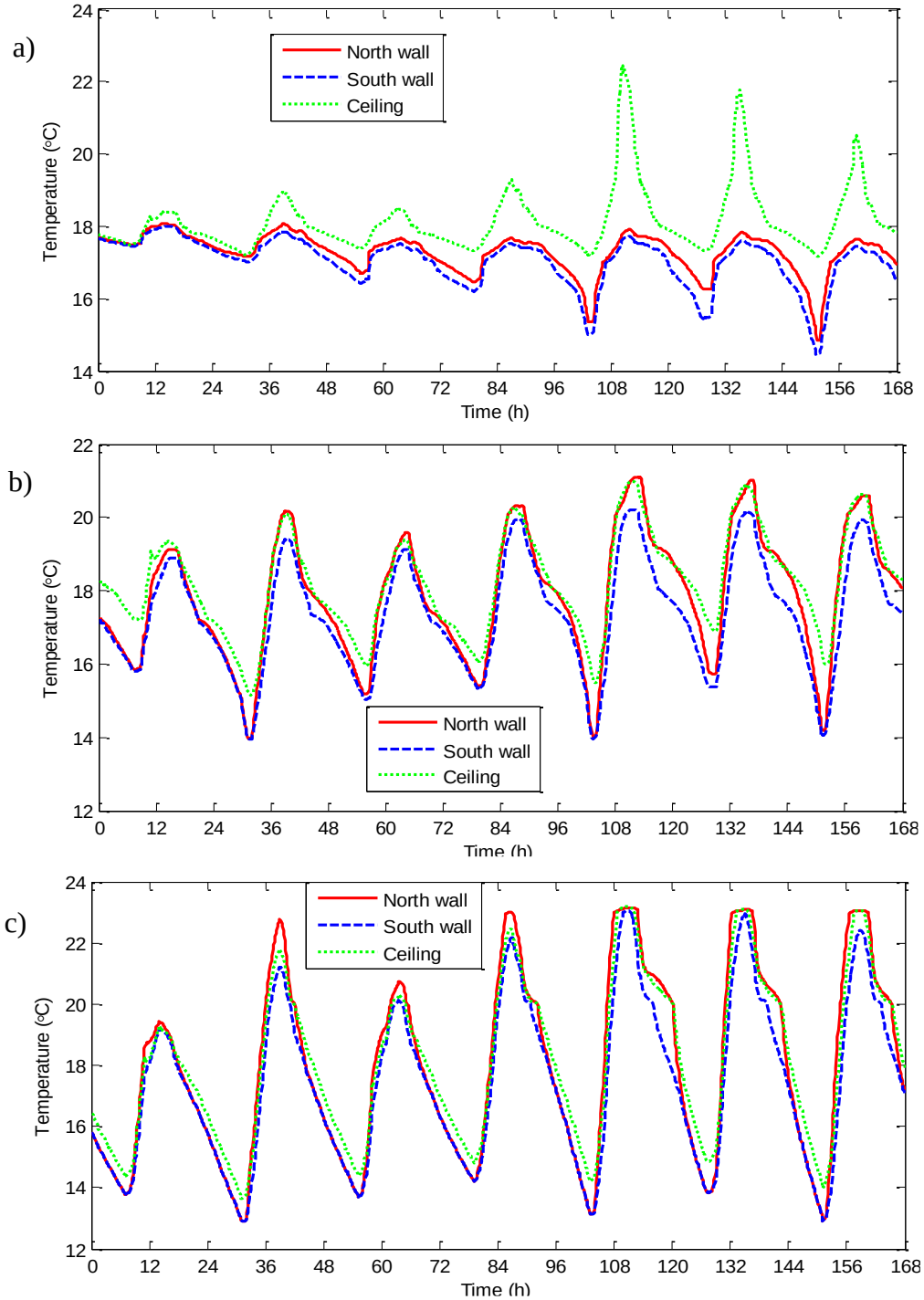

Fig. 3.13 Boundary temperatures of the PCM layers close to the plasterboard of the house model: a) RT18HC; b) SP21E; c) SP24E.

Based on the performance evaluation above, it is shown that using the PVT ventilation can improve the CTPE of PCM enhanced buildings under Sydney winter heating conditions. The thickness of the PCM layer and PCM types should be selected carefully to make full use of the PCM thermal storage capacity and to maximise the CTPE of the PCM enhanced house with the PVT ventilation. The thermal resistance

of the wall insulation layer of the house could also affect the performance of PCMs enhanced buildings.

3.4.5 Taguchi-based analysis

Based on the thermal performance investigation results from the parametric study of the system, further analysis based on the Taguchi method was conducted in order to achieve a better design, based on which, higher CTPE of the PCM enhanced house with the PVT ventilation can be achieved. The air flow rate of the PVT ventilation ($\dot{Q}_m$), the thickness of the PCM layer (δ_{PCM}), the PCM types and the thermal resistance of the wall insulation layer (R_{ins}) were considered as the control factors in the Taguchi-based analysis, as shown in Table 3.6. Three levels were considered for individual factors. The air flow rates of the PVT collectors used were 1000, 2000 and 3000 kg/h and the thicknesses of the PCM layer were 10, 20 and 30 mm, respectively. The three PCMs that were considered were RT18HC, SP21E and SP24E. The levels of the thermal resistance of the wall insulation layer were 1.0, 2.0 and 3.0 m^2·K/W, respectively. As there are four control factors and three factor levels, Standard $L_9(3^4)$ Orthogonal Array was selected to design the matrix of experiments, as shown in Table 3.7. The resulted CTPEs and *S/N* ratios of each trial test are also provided in Table 3.7.

Table 3.6 Control factors and corresponding levels in Taguchi design.

Factor / Level	Air flow rate of PVT collectors, (kg/h)	Thickness of PCM layer (mm)	PCM type	Thermal resistance of the wall insulation layer (m^2·K/W)
1	1000	10	RT18HC	1.0
2	2000	20	SP21E	2.0
3	3000	30	SP24E	3.0

The mean *S/N* ratios for each level of the control factors are summarised in Table 3.8. The best combination of the control factor levels can be identified by selecting the levels with highest *S/N* ratios. The identified best combination of the factor levels is the air flow rate of the PVT ventilation of 3000 kg/h, the thickness of the PCM layer of 30 mm, the PCM type of SP21E and the thermal resistance of the wall insulation layer of 3.0 m^2·K/W, respectively. To further investigate the significance of each control factor to the objective response, the ANOVA was conducted and the results are presented in Table 3.9. It can be seen that the thermal resistance of the wall

insulation layer of the house and the thickness of the PCM layer were the key factors which significantly influence the indoor thermal performance of the PCM enhanced buildings. The percentage contributions of the thermal resistance of the wall insulation layer and the thickness of the PCM layer were 56.6% and 18.4%, respectively.

Table 3.7 Taguchi $L_9(3^4)$ test plan.

Trial test No.	Air flow rate of PVT collectors (kg/h)	Thickness of PCM layer (mm)	PCM type	Thermal resistance of the wall insulation layer (m^2·K/W)	CTPE	*S/N* ratio
1	1000	10	SP21E	1	37.0%	-8.643
2	1000	20	RT18HC	2	56.4%	-4.979
3	1000	30	SP24E	3	58.6%	-4.637
4	2000	10	RT18HC	3	57.3%	-4.836
5	2000	20	SP24E	1	46.2%	-6.701
6	2000	30	SP21E	2	61.2%	-4.262
7	3000	10	SP24E	2	52.0%	-5.656
8	3000	20	SP21E	3	62.2%	-4.122
9	3000	30	RT18HC	1	53.4%	-5.455

Table 3.8 Response table of the CTPE.

Level	Air flow rate of PVT collectors (kg/h)		Thickness of PCM layer (mm)		PCM types		Thermal resistance of the wall insulation layer (m^2·K/W)	
	CTPE	*S/N*	CTPE	*S/N*	CTPE	*S/N*	CTPE	*S/N*
1	50.7%	-6.086	48.8%	-6.385	53.5%	-5.676	45.5%	-6.933
2	54.9%	-5.267	54.9%	-5.267	55.7%	-5.090	56.5%	-4.972
3	55.9%	-5.084	57.7%	-4.785	52.3%	-5.671	59.4%	-4.532
Optimal	Level 3		Level 3		Level 2		Level 3	
S/N_{max}-S/N_{min}	1.002		1.600		0.586		2.401	
Rank	3		2		4		1	

The predicted objective response using Eq. (3.11) was 63.3%, when only considering the significant factors of the thermal resistance of the wall insulation layer and the thickness of the PCM layer. A confirmation test was then conducted by using the best combination of the factor levels identified through *S/N* ratio analysis. The resulted CTPE of the house was 70.2%, which was higher than the predicted value, since it

considered all factors rather than only considering the significant factors. The CTPE of the case using the best combination of the factor levels was also much higher than the highest CTPE presented in Table 3.5 (*i.e.* 53.1% in *Test case* 10 with SP21E PCM), indicating the higher thermal performance of the PCM enhanced house with the PVT ventilation can be achieved through using the best combination of the factor levels as design parameters.

Table 3.9 Analysis of variance table.

Source	*DOF*	*SS*	*Var*	Variance ratio	*SS'*	%C
Air flow rate of PVT collectors	(2)	0.0046	Pooled	-	-	-
Thickness of PCM layer	2	0.0126	0.0063	3.9375	0.0094	18.4%
PCM type	(2)	0.0018	Pooled	-	-	-
Thermal resistance of the wall insulation layer	2	0.0322	0.0161	10.0625	0.0290	56.6%
Error	4	0.0064	0.0016	1.0	0.0128	25.0%
Total	8	0.0512	-	-	-	100.0 %

The above analysis showed that using Taguchi method can identify the best combination of the factor levels to improve the CTPE of the house. Taguchi method is easy to use and can solve multi-dimensional optimisation problems with less computational cost, compared to other commonly used search methods. However, it is worthwhile to mention that the optimal combination of the factor levels identified by using Taguchi method tends to be only "near optimal", due to its inherent limitation of using an orthogonal array in which the factor levels are discrete and need to be determined manually.

3.5 Summary

This chapter investigated the thermal performance of buildings with integrated air-based solar photovoltaic thermal collectors and phase change materials. The thermal energy derived from the PVT collectors was used for space heating in winter conditions while PCMs were laminated into the building envelopes to increase local thermal mass. The thermal performances of a house with three different types of PCMs

(*i.e.* organic PCM of RT18HC, and the inorganic PCMs of SP24E and SP21E) combined with the PVT ventilation were simulated and were compared with that of a house using the PVT ventilation only, using the PCMs only, and without using the PVT ventilation and the PCMs.

The results showed that using the PCMs in building envelopes can reduce the indoor temperature fluctuations. However, using the PCMs alone showed limited or no improvements in the indoor thermal conditions under Sydney winter heating conditions. It is noteworthy mentioning that the reducing indoor air temperature fluctuations did not mean the improvement in the indoor thermal performance, especially when there was no other air-conditioning systems or other heating devices in the house under cold weather conditions. In this case, the air temperature during some daytime periods may be reduced to values below the lower indoor temperature settings due to the use of PCMs, while the average air temperature increase during the night time was not enough to compensate the average temperature decrease during the daytime. The use of the heated air from the PVT collectors for space heating can significantly increase the indoor air temperature of the house during the winter daytime. The use of the PVT ventilation and PCMs can substantially increase the indoor thermal performance of the house. The Coefficients of Thermal Performance Enhancement (CTPEs) of the house during winter heating season increased to 43.4%, 48.8%, and 46.2% when the PVT ventilation with an air flow rate of 2000 kg/h and the PCMs of RT18HC, SP21E and SP24E with a thickness of 20 mm were used, respectively.

The CTPE of the house was further improved through using the Taguchi method which identified the best combination of the factor levels (*i.e.* the best combination of the design variable values). The CTPE of the house over the winter heating season reached 70.2% when the PVT air flow rate was 3000 kg/h, the PCM thickness was 30 mm, the PCM type was SP21E and the thermal resistance of the wall insulation layer was 3.0 $m^2 \cdot K/W$, respectively. The thermal resistance of the wall insulation layer of the house was a critical factor affecting the thermal performance of the PCM enhanced buildings with the PVT ventilation. Although both the thermal resistance of the wall insulation layer and PCM layers can improve the building thermal performance, the thermal resistance of the wall insulation layer cannot replace the PCM layers as PCMs can

store a large amount of thermal energy and use it later and can therefore greatly reduce the indoor temperature fluctuations.

Chapter 4 Thermal Performance Optimisation of PCM enhanced Buildings with Integrated PVT Collectors Using Taguchi-Fibonacci Search Method

The thermal performance investigation of PCM enhanced buildings with integrated air-based solar PVT collectors in Chapter 3 demonstrated that using the PVT ventilation and PCMs in building envelopes simutanuously can significantly improve building thermal performance. It was also shown that appropriate design of the proposed system can result in a better indoor thermal performance. However, as mentioned, due to the fact that Taguchi method can only provide "near optimal" solutions, it is worthwhile to promote the methodology for better system optimisation. This chapter presents the development and utilisation of a new optimisation method that suits the needs for optimising the thermal performance of PCM enhanced buildings with using air-based solar PVT collectors for winter space heating. The new method is named as Taguchi-Fibonacci search method, and can solve multi-dimensional optimisation problems with both discrete and continuous variables.

This chapter is organised as follows. Section 4.1 presents the development of the Taguchi-Fibonacci search method. The formulation of the optimisation problem is presented in Section 4.2. Section 4.3 provides the optimisation results and discussions. The key findings of this chapter are summarised in Section 4.4.

4.1 Development of Taguchi-Fibonacci search method

Taguchi method (Taguchi *et al.* 2004) used in Chapter 3 can solve multi-dimensional optimisation problems. However, the factor levels are limited to discrete values. In contrast, Fibonacci search method (Antonion and Lu 2007) can optimise continuous variables and identify the optimal solutions of one-dimensional optimisation problems. The combination of both methods can overcome the disadvantages of the limited discrete factor levels in Taguchi method and one-dimensional optimisation in Fibonacci search method. In the integrated Taguchi-Fibonacci search method, Fibonacci search method is used to drive the optimisation process through iterations while Taguchi method is used to design the matrix of trial tests in each iteration. As a

consequence, the search range of each factor can be continuously narrowed until the optimal values are identified.

By integrating Fibonacci search method with Taguchi method, Taguchi-Fibonacci search method can solve multi-dimensional optimisation problems with both continuous and discrete variables. For a design optimisation, the objective function can be generally described as below.

$$y = f(x_i, z_j), \quad \text{for} \quad x_i \in [a_i, b_i], \quad z_j = \{\alpha_j, \beta_j, \gamma_j, \cdots\}, \quad i = 1,2,\cdots i_{\max}, j = 1,2\cdots j_{\max} \quad (4.1)$$

where y is the objective function, x_i and z_j indicate the continuous and discrete factors respectively, a_i and b_i are the lower and upper limits of the search ranges of the continuous factors individually, and α_j, β_j, γ_j, … represent the values of the discrete factors.

4.1.1 Procedure of Taguchi-Fibonacci search method

The general procedures for implementation of Taguchi-Fibonacci search method are presented in Fig. 4.1, in which the key steps are briefly described below.

a) Determine the factor levels for continuous variables based on the factor search ranges defined using the Fibonacci search method (the details will be demonstrated in Section 4.1.2), while the values of the discrete factors are directly used as the factor levels;

b) Select a suitable orthogonal array (OA), design the matrix of experiments and conduct the trial tests. The OA containing four factor levels needs to be selected as Fibonacci search method can only generate four factor levels at each iteration;

c) Carry out the data analysis using ANOVA to identify the percentage contribution of each factor and errors. The details of ANOVA calculation can be found in Roy (2011);

d) Perform the *S/N* ratio analysis to identify the optimal levels for individual factors;

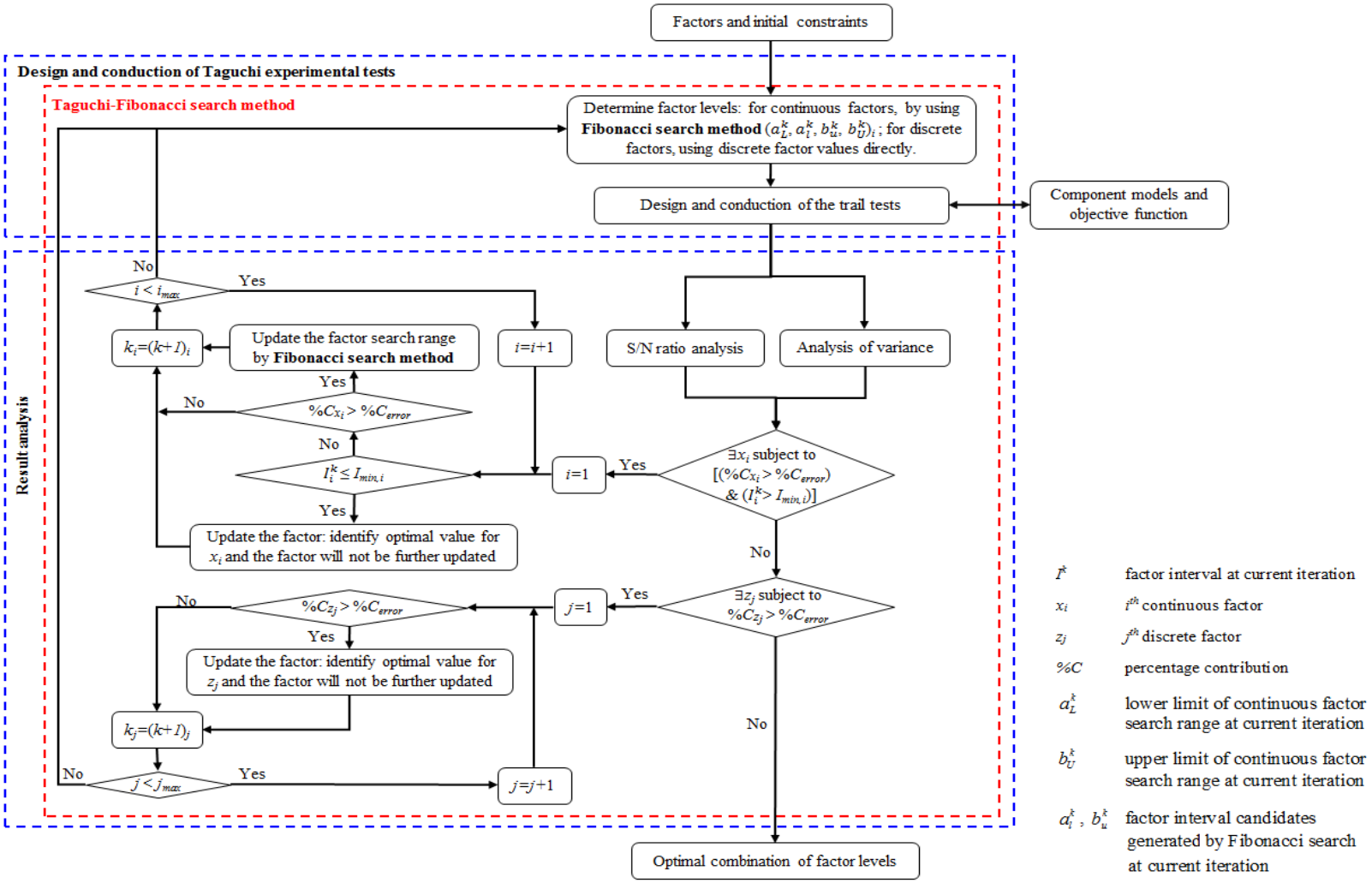

Fig. 4.1 Flowchart of Taguchi-Fibonacci search optimisation method.

e) Check the termination criteria of iteration. If the termination *Criterion I* is satisfied, go to *Step f)*. If the termination *Criterion II* is satisfied, go to *Step g)*. Otherwise, go to *Step h)*.

- *Criterion I*: $\exists\, x_i$ subject to $\%C_{x_i} > \%C_{error}$ and $I_i^k > I_{\min,i}$
- *Criterion II*: $\forall\, x_i$ subject to $\%C_{x_i} \le \%C_{error}$ or $I_i^k \le I_{\min,i}$ and

$$\exists\, z_j \text{ subject to } \%C_{z_j} > \%C_{error}$$

f) Update the continuous factors and their search ranges for next iteration. If there is only one factor left, then Fibonacci search method will be directly used to identify the optimal value for this factor and then go to *Step i)*. Otherwise, the rules described in Section 4.1.3 will be used to update each continuous factor and their search ranges, and then go to *Step a)*.

g) Update the discrete factors for next iteration. If there are only discrete factors left, the optimal values of these discrete factors can be directly identified by comparing the *S/N* ratios corresponding to their factor levels, and then go to *Step i)*. Otherwise, the rules described in Section 4.1.4 will be used to update each discrete factor, and then go to *Step a)*.

h) Select the optimal factor levels according to the corresponding highest *S/N* ratios;

i) Conduct the confirmation experiment and performance assessment.

4.1.2 Determination of the factor levels for continuous factors

The factor levels of continuous factors in each iteration are determined by the Fibonacci search method. For a continuous factor x_i, its lower and upper limits (*i.e.* $a_{L,i}^k$, and $b_{U,i}^k$,) of the search range at the current iteration are used as the two factor levels, while the other two middle factor levels ($a_{l,i}^k$ and $b_{u,i}^k$) are determined by Eqs. (4.2) - (4.5).

$$\begin{cases} a_{l,i}^k = b_{U,i}^k - I_i^{k+1} \\ b_{u,i}^k = a_{L,i}^k + I_i^{k+1} \end{cases} \tag{4.2}$$

$$I_i^{k+1} = \frac{F_{M-k}}{F_{M-k+1}} I_i^k, \quad \text{for} \quad k = 1,2\cdots, M-1 \tag{4.3}$$

$$I_i^k = b_{U,i}^k - a_{L,i}^k \tag{4.4}$$

$$\begin{cases} F_0 = F_1 = 1 \\ F_k = F_{k-1} + F_{k-2}, \quad \text{for} \quad k > 2 \end{cases} \tag{4.5}$$

where I_i^{k+1} is the factor interval (*i.e.* the length of the search range) of the next iteration as shown in Fig. 4.2, which can be determined by Fibonacci sequence, based on the factor interval at the current iteration; I_i^k is the factor interval at the current iteration, F_k is the Fibonacci value corresponding to the index k in the Fibonacci sequence, which reflects the narrowing rate of the factor search range at each iteration, subscript M represents the maximal index in the Fibonacci sequence. Fibonacci sequence corresponding to the maximal index should satisfy Eq. (4.6), in which the minimum factor interval ($I_{min,i}$) for each continuous factor is a user defined parameter.

$$\frac{I_i^1}{I_{\min,i}} \leq F_M \tag{4.6}$$

4.1.3 Update the continuous factors and their search ranges

For a given continuous factor x_i, if *Criterion III* is satisfied, this factor will be updated for next iteration by replacing all its levels with its optimal level with the highest *S/N* ratio at the current iteration. This factor will then not be further optimised. If *Criteria IV* is satisfied, the interval of this factor will be updated by using Eq. (4.3) for the next iteration. Otherwise, its factor search range in the current iteration will be directly used for the next iteration and no update is required (*i.e.* $I_i^{k+1} = I_i^k$).

- *Criterion III*: $I_i^k \leq I_{\min,i}$
- *Criterion IV*: $I_i^k > I_{\min,i}$ and $\%C_{x_i} > \%C_{error}$

The factor search range $[a_{L,i}^k, b_{u,i}^k]$ with the maximal *S/N* ratio (or $[a_{l,i}^k, b_{U,i}^k]$, if the maximal *S/N* ratio lays within $[a_{l,i}^k, b_{U,i}^k]$), as shown in Fig. 4.2, will be selected as the factor search range for next iteration. As a result, the following relationship in Eq. (4.7) can be easily derived.

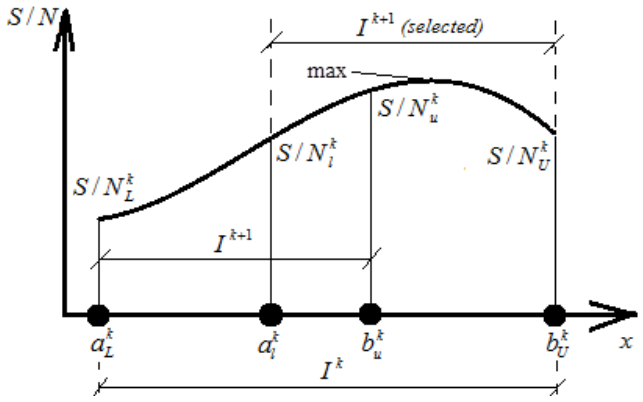

Fig. 4.2 An example of updating the search range of the continuous factors.

$$\begin{cases} a_{l,i}^{k+1} = b_{u,i}^{k}, \quad \text{for } I_i^{k+1} = b_{U,i}^{k} - a_{l,i}^{k}, \text{if } S/N_{\max} \text{ lies in } \left[a_{l,i}^{k}, b_{U,i}^{k}\right] \\ b_{u,i}^{k+1} = a_{l,i}^{k}, \quad \text{for } I_i^{k+1} = b_{u,i}^{k} - a_{L,i}^{k}, \text{if } S/N_{\max} \text{ lies in } \left[a_{L,i}^{k}, b_{u,i}^{k}\right] \end{cases} \tag{4.7}$$

Therefore, only one factor level needs to be generated in the factor search range for the next iteration while the other three can be derived from the current iteration. This illustrates that not all the trial tests in the next iteration need to be conducted and the search efficiency for the optimisation problem can therefore be improved.

4.1.4 Update the discrete factors

For a given discrete factor z_j, if *Criteria V* is satisfied, this factor will be updated for next iteration by replacing all its levels with its optimal level with the highest *S/N* ratio at the current iteration and this factor will then not be further considered in the later optimisation. Otherwise, the levels of this factor in the current iteration will be directly used in the next iteration and no update is required.

- *Criterion V*: $\%C_{z_j} > \%C_{error}$

4.2 Formulation of the optimisation problem

4.2.1 Optimisation methodology

The overall methodology used to optimise the thermal performance of the PCM enhanced house with the PVT ventilation is illustrated in Fig. 4.3. The optimisation variables (*i.e.* control factors) and the initial constraints (*i.e.* search ranges) of each variable are first determined. The levels of each factor can then be determined by the Fibonacci search method based on the search ranges defined. A matrix of trial tests is

arranged using Taguchi method. Each trial test is then carried out through simulations and the response of each trial test is calculated according to the optimisation objective defined. Based on the data analysis using ANOVA and *S/N* ratios, the termination criteria are then applied to determine whether the optimisation process should terminate or not. If the termination criteria are not satisfied, the factors or the search ranges of the corresponding factors to be further optimised are updated for next iteration. Otherwise, the optimal values identified will be used in the confirmation test and performance assessment.

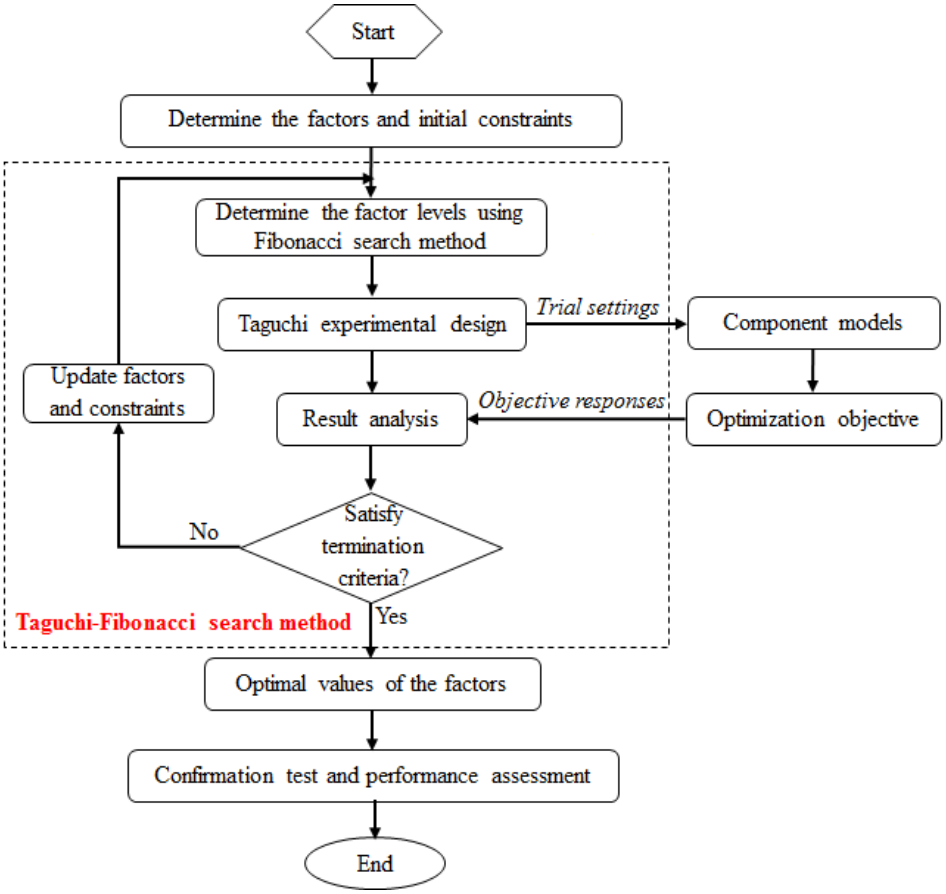

Fig. 4.3 Outline of the optimisation methodology.

4.2.2 Definition of the objective function

The indoor thermal performance enhancement of the house due to the use of the PVT ventilation and PCMs, in comparison with the original house without using the PVT ventilation and PCMs, was used as the optimisation objective. Therefore, the *S/N* ratio of Coefficient of Thermal Performance Enhancement (*i.e.* CTPE described by Eq.

(3.10) in Chapter 3) was used as the objective function. The *S/N* ratio of the CTPE was expected to be the-higher-the-better (described in Eq. (3.12) in Chapter 3).

4.2.3 Optimisation variables and constraints

The flow rate of solar air heaters, the PCM characteristics, and the PCM layer thickness have been reported as the critical variables for integrating PVT collectors with PCMs (Summers *et al.* 2012). The wall insulation layer was also important for the thermal performance of the PCM enhanced house with the PVT ventilation, as discovered in Chapter 3. The air flow rate of the PVT collectors ($\dot{Q}_m$), thermal resistance of the wall insulation layer (R_{ins}), PCM type and thickness of the PCM layer (δ_{PCM}) were therefore considered as the optimisation variables (*i.e.* control factor) in the optimisation problem.

The control factor of the PCM type is a discrete variable. Eight different types of PCM candidates from Rubitherm (2014) were used in the optimisation. The PCMs used and their thermo-physical properties are summarised in Table 4.1. The heating and cooling specific enthalpy distributions over the temperature range for these PCMs can be obtained from the datasheet provided in Rubitherm (2014). The control factors of the PVT air flow rate, the thermal resistance of the wall insulation layer, and the PCM layer thickness are the continuous variables. A relatively large search range varied from 250 to 8000 kg/h was used for the PVT air flow rate to demonstrate whether the proposed method can identify a reasonably optimal value, while, the effect of the air velocity on human thermal comfort was not considered in this study. The wall insulation layer in the original house had a thermal resistance of 1.0 m^2·K/W and an insulation thermal resistance of 3.0 m^2·k/W was considered to be sufficient. The search range for the thermal resistance of the wall insulation layer was therefore defined in the range of thermal resistances of 1.0 - 3.0 m^2·K/W. As organic and inorganic PCMs have different densities, the thicknesses of the organic and inorganic PCMs used in the optimisation varied between 5 and 50 mm, and between 5 and 30 mm, respectively. The minimal interval (*i.e.* $I_{min,i}$) used for the PVT air flow rate, the thermal resistance of the wall insulation layer, and the PCM layer thickness were 250 kg/h, 0.25 m^2·K/W and 2 mm, respectively.

Table 4.1 Thermo-physical properties of the PCMs considered (Rubitherm 2014).

PCMs		Density at liquid/solid (kg/m^3)	Melting temperature range (^{o}C)	Solidification temperature range (^{o}C)	Specific heat capacity [kJ/(kg·K)]	Thermal conductivity [W/(m·K]
Organic	RT18HC	770/880	17-19	19-17	2	0.2
	RT21HC		20-23	21-19		
	RT25HC		22-26	26-22		
	RT22HC	700/760	20-23	23-20		
Inorganic	SP21E	1400/1500	22-23	21-19	2	0.6
	SP24E		24-25	23-21		
	SP25E2		24-26	24-23		
	SP26E		25-27	25-24		

4.3 Optimisation results and discussions

The optimisation of the PCM enhanced house with the PVT ventilation was conducted over a total of 14 consecutive winter days under Sydney weather conditions, as shown in Fig. 4.4. It is expected that the methodology developed in this study can be easily adapted and used to other climates. Two scenarios named as *Scenario* 1 and *Scenario* 2 for organic and inorganic PCMs respectively, were designed and presented.

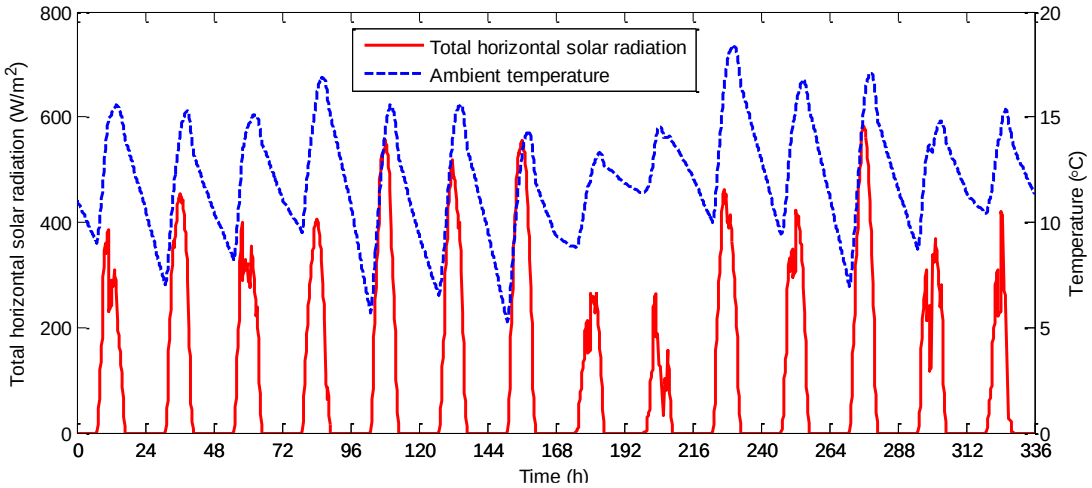

Fig. 4.4 Solar radiation and ambient air temperature during the 14 winter test days.

4.3.1 *Scenario 1*: Design optimisation using organic PCMs

In this test scenario, the optimisation of the thermal performance of organic PCM enhanced house with the PVT ventilation by using the proposed Taguchi-Fibonacci search method was carried out and the results are presented. Table 4.2 shows the matrix of the experiments designed by Taguchi method and the corresponding CTPE and *S/N* ratio of each trial test in the first iteration by using Taguchi-Fibonacci search method. In this iteration, the initial constraints were used by the Fibonacci search method to determine the factor levels. The lower and upper limits of the search range defined for continuous factors were used as *Level 1* and *Level 4* for each factor while the other two factor levels were determined using Eq. (4.2). For instance, the four levels determined for the PVT air flow rate were 250 (*Level 1*), 3213.2 (*Level 2*), 5036.8 (*Level 3*) and 8000 kg/h (*Level 4*), respectively. Based on Table 4.2, the average CTPEs and average *S/N* ratios of each level for individual factors at *Iteration* 1 of the optimisation can be determined and the results are presented in Table 4.3. The percentage contribution of each factor to the CTPE in each iteration by using ANOVA is summarised in Table

4.4 and the optimisation process of each iteration is demonstrated in Table 4.5 (for PCM type) and Fig. 4.5 - Fig. 4.7 (for continuous variables).

Table 4.2 Experiment layout designed by Taguchi method and corresponding responses and S/N ratios in *Iteration* 1 - *Scenario* 1.

Trial test No.	Experimental plan				CTPE and *S/N* ratio	
	$\dot{Q}_m$ (kg/h)	R_{ins} (m^2·K/W)	PCM type	δ_{PCM} (mm)	CTPE	*S/N*
1	250.0	1.00	RT25HC	5.0	15.2%	-16.348
2	250.0	1.75	RT18HC	22.2	32.5%	-9.760
3	250.0	2.25	RT21HC	32.8	31.4%	-10.066
4	250.0	3.00	RT22HC	50.0	32.8%	-9.675
5	3213.2	1.00	RT18HC	50.0	54.2%	-5.325
6	3213.2	1.75	RT25HC	32.8	49.9%	-6.036
7	3213.2	2.25	RT22HC	22.2	53.8%	-5.386
8	3213.2	3.00	RT21HC	5.0	51.7%	-5.723
9	5036.8	1.00	RT21HC	22.2	41.5%	-7.646
10	5036.8	1.75	RT22HC	5.0	41.7%	-7.598
11	5036.8	2.25	RT25HC	50.0	51.7%	-5.732
12	5036.8	3.00	RT18HC	32.8	58.3%	-4.689
13	8000.0	1.00	RT22HC	32.8	34.6%	-9.219
14	8000.0	1.75	RT21HC	50.0	44.8%	-6.983
15	8000.0	2.25	RT18HC	5.0	32.3%	-9.827
16	8000.0	3.00	RT25HC	22.2	41.6%	-7.621

Table 4.3 Response table of *Iteration* 1 - *Scenario* 1.

Factor	$\dot{Q}_m$			R_{ins}		
	Level	CTPE	*S/N*	Level	CTPE	*S/N*
Level 1	250.0	28.0%	-11.462	1	36.4%	-9.635
Level 2	3213.2	52.4%	-5.617	1.75	42.2%	-7.594
Level 3	5036.8	48.3%	-6.416	2.25	42.3%	-7.753
Level 4	8000.0	38.3%	-8.412	3	46.1%	-6.927

(*Continue*)

Factor	PCM type			δ_{PCM}		
	Level	CTPE	*S/N*	Level	CTPE	*S/N*
Level 1	RT25HC	39.6%	-8.934	5.0	35.2%	-9.874
Level 2	RT18HC	44.3%	-7.400	22.2	42.3%	-7.603
Level 3	RT21HC	42.3%	-7.604	32.8	43.5%	-7.502
Level 4	RT22HC	40.7%	-7.969	50.0	45.9%	-6.929

Fig. 4.5 shows the search process for the PVT air flow rate. The corresponding *S/N* ratios for *Levels 1-4* at *Iteration 1* were -11.462, -5.617, -6.416 and -8.412, respectively.

The results from ANOVA showed that the percentage contribution of the PVT air flow rate to the CTPE was 70.87% which was higher than the percentage contribution of the error (*i.e.* 9.70%). Therefore, a new search range of 250 - 5036.8 kg/h was generated for *Iteration 2*, due to the fact that the maximal *S/N* ratio (*i.e.* -5.617) was found at the factor level of 3213.2 kg/h (*i.e. Level 2*) at *Iteration 1*. Similarly, the search range generated for *Iteration* 3 was from 2073.5 to 5036.8 kg/h as the maximal *S/N* ratio (*i.e*. -5.319) was at the factor level of 3213.2 kg/h (*i.e. Level 3*) at *Iteration 2*. The same procedure was repeated at *Iteration 4*.

Table 4.4 Summary of percentage contribution in ANOVA - *Scenario* 1.

Source	*DOF*	*Iteration 1*	*Iteration 2*	*Iteration 3*	*Iteration 4*
$\dot{Q}_m$	3	70.87%	80.57%	20.16%	3.34%
R_{ins}	3	7.94%	12.17%	25.50%	5.15%
PCM type	3	0.61%	5.58%	41.42%	67.00%
δ_{PCM}	3	10.88%	0.65%	3.37%	6.57%
Error	3	9.70%	1.02%	9.55%	17.94%
Total	15	100.00%	100.00%	100.00%	100.00%

(*Continue*)

Source	*DOF*	*Iteration 5*	*Iteration 6*	*DOF*	*Iteration 7*	*Iteration 8*
$\dot{Q}_m$	3	27.83%	27.93%	3	43.14%	32.49%
R_{ins}	3	37.78%	50.36%	(3)	-	-
PCM type	(3)	-	-	(3)	-	-
δ_{PCM}	3	31.89%	20.19%	3	51.40%	48.14%
Error	6	2.49%	1.53%	9	5.46%	19.36%
Total	15	100.00%	100.00%	15	100.00%	100.00%

* *Iterations 9* and *10* were not listed as Taguchi-Fibonacci search method degraded to Fibonacci search method

However, the results from ANOVA for *Iteration 4* showed that the percentage contribution of the PVT air flow rate was 3.34%, which was lower than the percentage contribution of the error (*i.e.* 17.94%). Consequently, the same search range of the PVT air flow for *Iteration 4* was used for *Iteration 5*. As the percentage contributions of all the three continuous factors were lower than the percentage contribution of the error at *Iteration 4*, while the percentage contribution of the discrete factor (*i.e.* PCM type) was dominant and higher than the performance contribution of the error (see Table 4.4), the optimal value for the discrete factor was therefore determined and this factor was not further optimised in later iterations. As a result, the percentage contributions of the continuous factors were higher than the percentage contribution of the error in *Iteration 5* as the discrete factor was not considered in *Iteration 5*.

Consequently, the search range for the PVT air flow rate was further updated for *Iteration* 6 (see Fig. 4.5). The same process was continued from *Iteration 6* till to *Iteration 8* and the optimal value searched for of the PVT air flow rate (*i.e.* 2073.5 kg/h) was identified at *Iteration 8* as further updating of the search range of this factor would result in a factor interval less than the minimal factor interval defined (*i.e.* 250 kg/h).

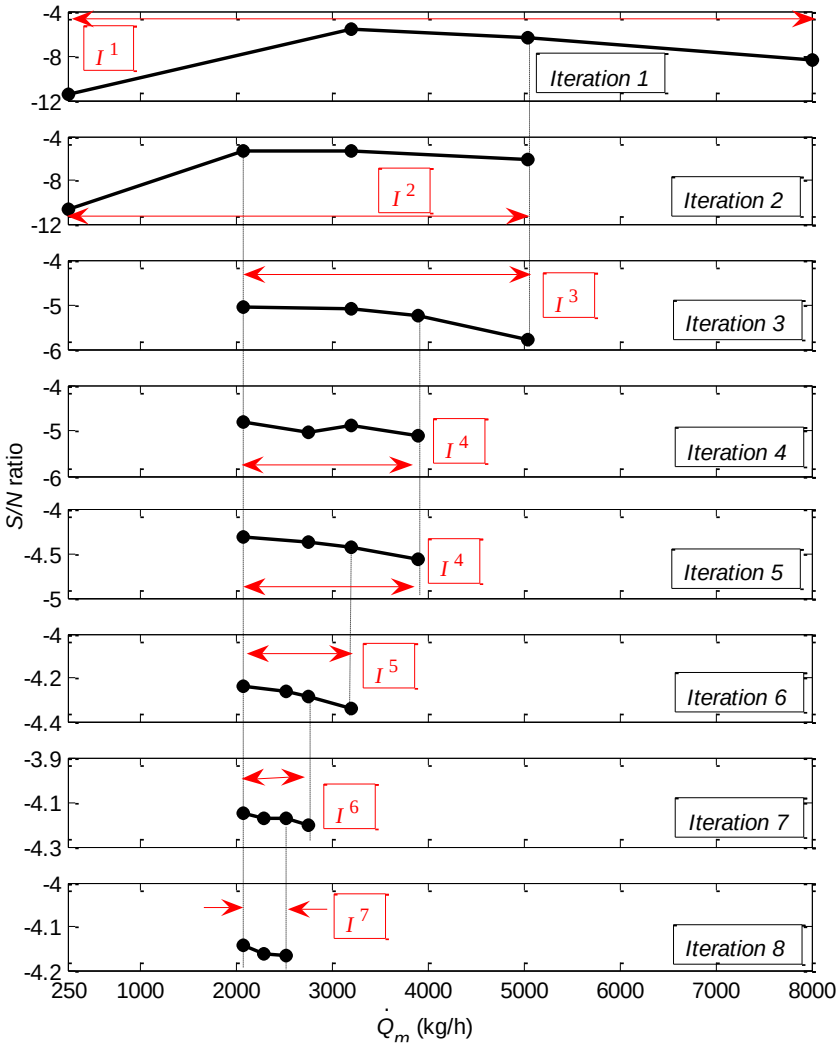

Fig. 4.5 Optimisation process of the PVT air flow rate by using Taguchi-Fibonacci search method in *Scenario* 1.

The search processes for the optimal PCM layer thickness and thermal resistance of the wall insulation layer are illustrated in Fig. 4.6 and Fig. 4.7, respectively. From Fig. 4.6, it can be seen that the search range of the PCM layer thickness was updated for *Iterations 2*, *6*, *7* and *8* as the percentage contributions of this factor in the previous iterations were higher than the percentage contribution of the error. After *Iteration 8*,

the optimal values for the other three factors have been identified. Taguchi-Fibonacci search optimisation therefore degraded to Fibonacci search optimisation since *Iteration 9*, due to the fact that there was only one factor left. The optimal value for the PCM layer thickness was identified as 50 mm at *Iteration 10*.

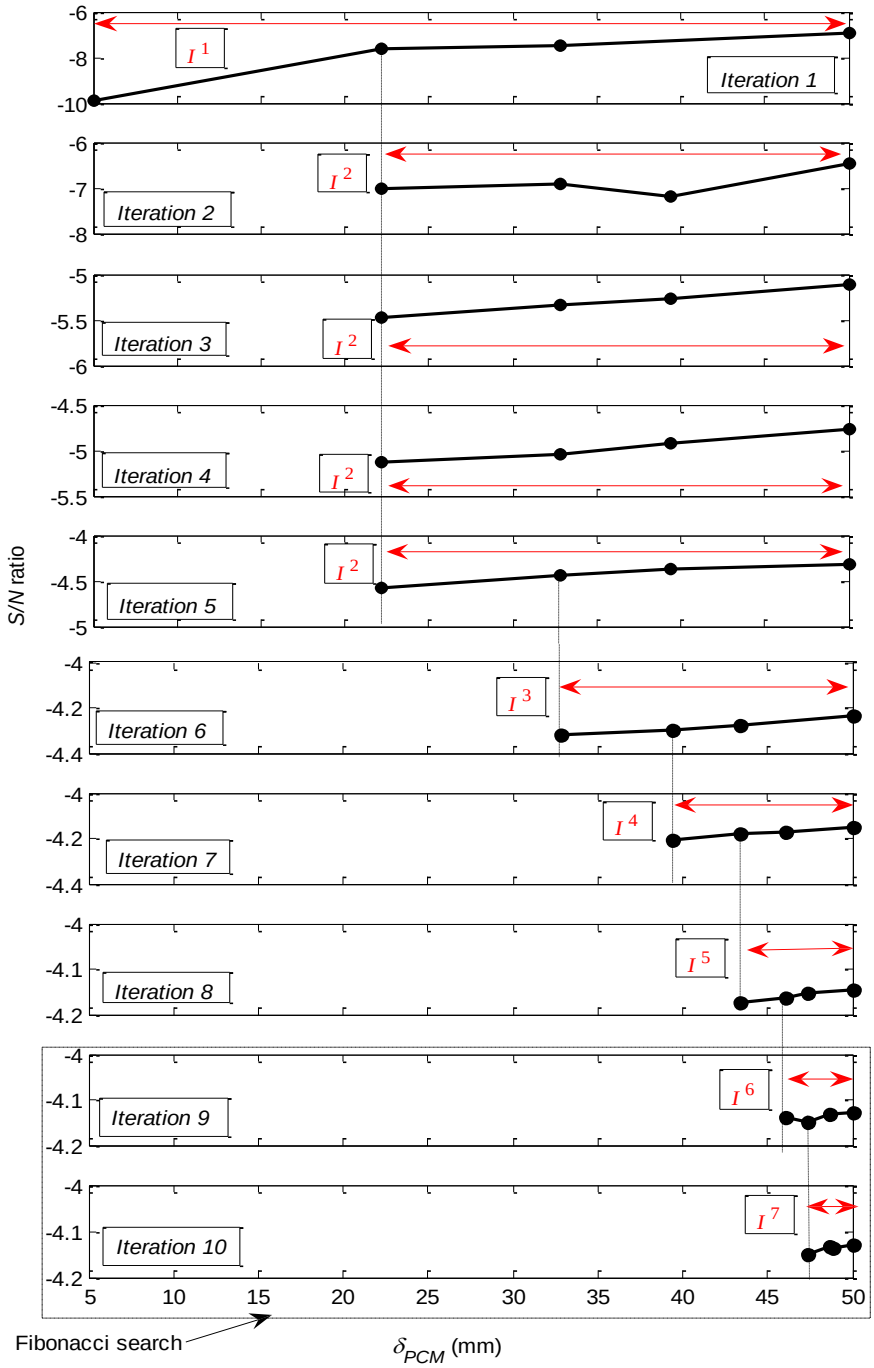

Fig. 4.6 Optimisation process of PCM layer thickness by using Taguchi-Fibonacci search method in *Scenario* 1.

It is worthwhile to mention that as the PCM cost was not considered in the objective function of the optimisation problem, the initial upper limit of 50 mm was identified as the optimal value for the PCM layer thickness. The results might be different if the PCM cost is considered in the objective function. However, the methodology developed can be adapted to the optimisation problems considering the PCM cost.

For the thermal resistance of the wall insulation layer, the search range was updated for *Iterations 3*, *4* and *6*, and the optimal value was identified as 3 m^2·K/W at *Iteration 6*.

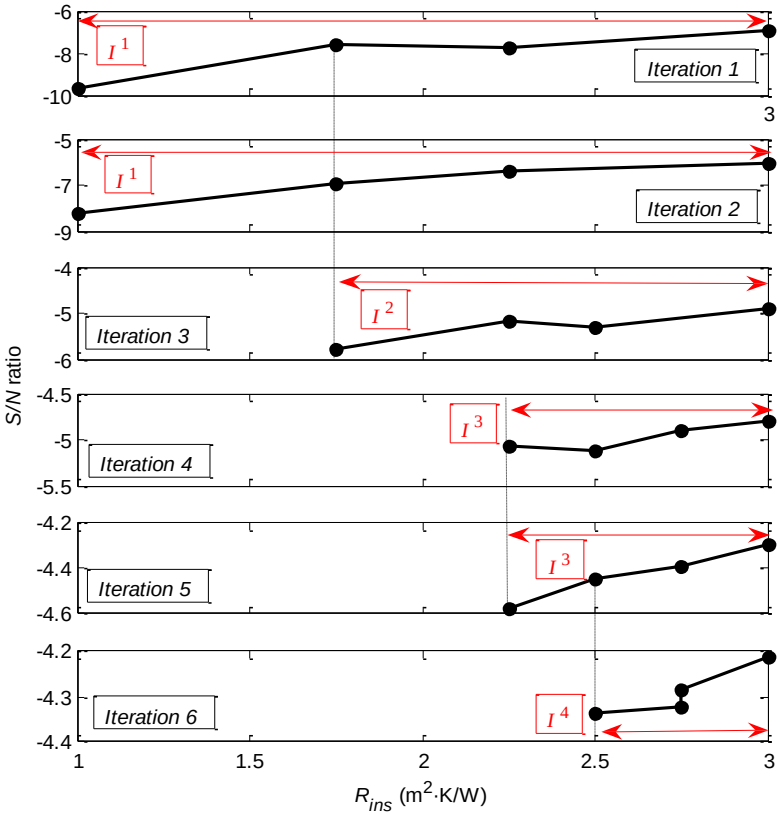

Fig. 4.7 Optimisation process of the thermal resistance of the wall insulation layer by using Taguchi-Fibonacci search method in *Scenario* 1.

For the discrete factor of the PCM type, the same factor levels were used at *Iterations 1-4* as Taguchi-Fibonacci search method in these four iterations were focused on the optimisation of the continuous variables. As mentioned earlier, as the percentage contribution of the discrete factor was dominant at *Iteration 4*, the optimal level of the PCM type was therefore identified at *Iteration 4*. This optimal level was then used in later iterations in order to allow the optimisation process to focus on the continuous

variables. The optimal PCM type identified was RT18HC, and the average *S/N* ratios for each level of the PCM type at *Iterations 1-4* are presented in Table 4.5.

Table 4.5 Average *S/N* ratios for each level of the PCM type - *Scenario* 1.

Iteration	*Iteration 1*		*Iteration 2*	
	Level	*S/N*	level	*S/N*
PCM type level and *S/N* ratio	RT25HC	-8.934	RT25HC	-7.533
	RT18HC	-7.400	RT18HC	-6.048
	RT21HC	-7.604	RT21HC	-6.854
	RT22HC	-7.969	RT22HC	-7.127
(*Continue*)				
Iteration	*Iteration 3*		*Iteration 4*	
	Level	*S/N*	level	*S/N*
PCM type level and *S/N* ratio	RT25HC	-5.610	RT25HC	-5.326
	RT18HC	-4.683	RT18HC	-4.434
	RT21HC	-5.229	RT21HC	-4.810
	RT22HC	-5.642	RT22HC	-5.309

Once the optimal values for all discrete and continuous factors were identified, the confirmation test was then conducted and the CTPE of the PCM enhanced house with the PVT ventilation using these optimal factor values was found to be 62.2%.

4.3.2 *Scenario 2*: Design optimisation using inorganic PCMs

Two optimisation cases were designed in *Scenario* 2. In the first case (*i.e. Optimisation test case* 1), the design optimisation was carried out under the factor search ranges defined in Section 4.1. In the second case (*i.e. Optimisation test case* 2), the search ranges of the factors were adjusted and redefined based on the optimisation results obtained in *Optimisation test case* 1, to increase the confidence in the optimal solution identified.

4.3.2.1 *Optimisation test case* 1

The same optimisation process used in *Scenario* 1 was applied for the inorganic PCM enhanced house with the PVT ventilation. The optimisation process was presented in Table 4.6 and Fig. 4.8 - Fig. 4.10. The percentage contributions of each factor using ANOVA are summarised in Table 4.7.

Table 4.6 Average *S/N* ratios for each level of the PCM type - *Optimisation test case* 1, *Scenario* 2.

Iteration	*Iteration 1*		*Iteration 2*		*Iteration 3*	
	Level	*S/N*	Level	*S/N*	Level	*S/N*
PCM type level and S/N ratio	SP25E2	-8.706	SP25E2	-6.531	SP25E2	-6.229
	SP26E	-8.587	SP26E	-7.135	SP26E	-6.370
	SP21E	-6.836	SP21E	-5.273	SP21E	-4.464
	SP24E	-8.538	SP24E	-7.057	SP24E	-6.509

(*Continue*)

Iteration	*Iteration 4*		*Iteration 5*	
	Level	*S/N*	Level	*S/N*
PCM type level and S/N ratio	SP25E2	-6.263	SP25E2	-5.002
	SP26E	-6.384	SP26E	-5.190
	SP21E	-4.373	SP21E	-3.328
	SP24E	-6.506	SP24E	-5.347

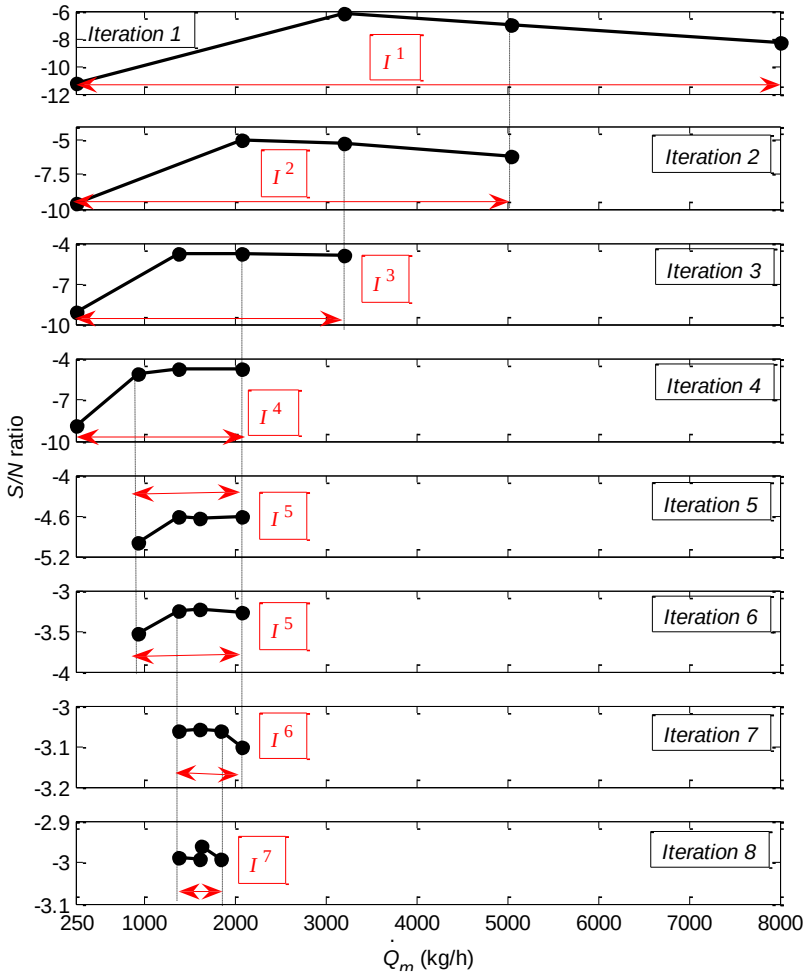

Fig. 4.8 Optimisation process of the PVT air flow rate by using Taguchi-Fibonacci search method in *Optimisation test case* 1, *Scenario* 2.

The optimal values for the PVT air flow rate, the thermal resistance of the wall insulation layer, and the PCM layer thickness were identified as 1640.4 kg/h, 3.0 m^2·K/W and 30 mm, respectively. The optimal level for the discrete factor of the PCM type was SP21E. The resulted CTPE of the PCM enhanced house with the PVT ventilation by using the combination of the optimal factor values identified was 72.2%. Similar to the results obtained in *Scenario* 1, the upper limit of the search range for the PCM layer thickness was identified as the optimal value, indicating that the search range defined might not be large enough. In the meanwhile, the optimal PVT air flow rate identified was much smaller than the upper limit of the search range defined, indicating that the large search range for the PVT air flow rate might be not necessary.

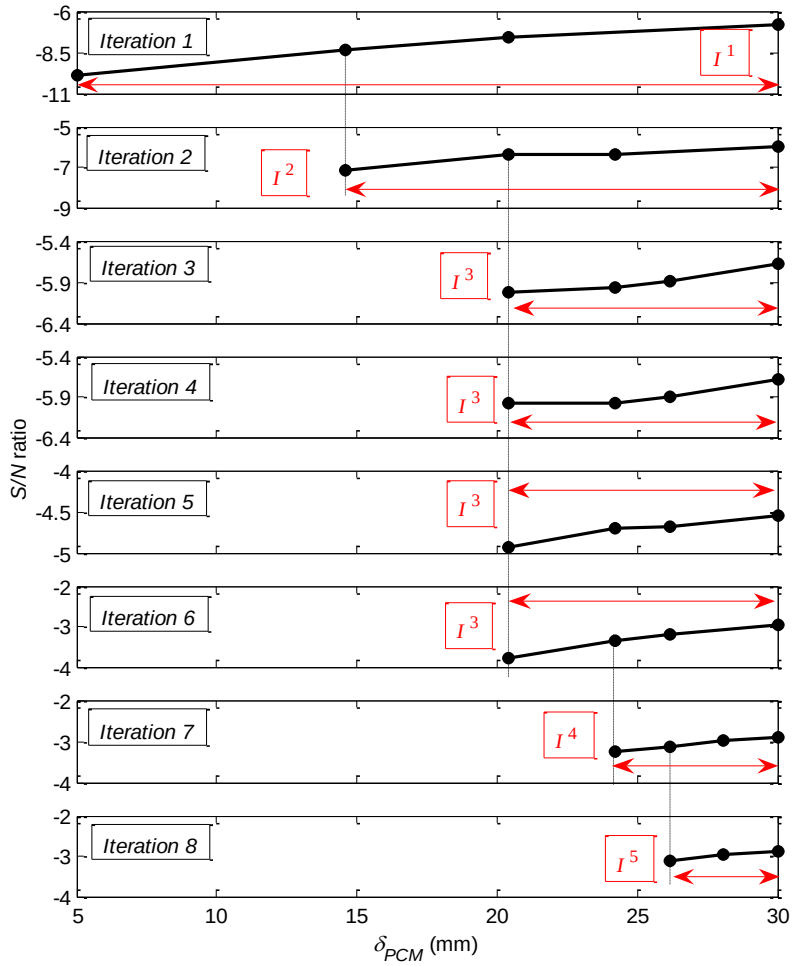

Fig. 4.9 Optimisation process of the PCM layer thickness by using Taguchi-Fibonacci search method in *Optimisation test case* 1, *Scenario* 2.

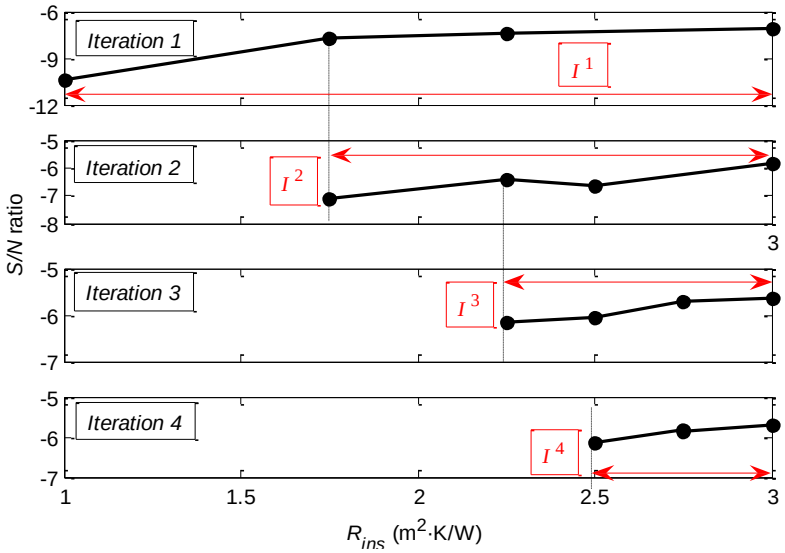

Fig. 4.10 Optimisation process of the thermal resistance of the wall insulation layer by using Taguchi-Fibonacci search method in *Optimisation test case* 1, *Scenario* 2.

Table 4.7 Summary of the percentage contribution in ANOVA - *Optimisation test case* 1, *Scenario* 2.

Source	*DOF*	*Iteration 1*	*Iteration 2*	*Iteration 3*	*Iteration 4*
$\dot{Q}_m$	3	50.46%	74.76%	72.98%	72.03%
R_{ins}	3	21.38%	4.36%	1.87%	0.57%
PCM type	3	8.37%	15.75%	22.68%	25.46%
δ_{PCM}	3	15.12%	3.37%	0.66%	0.76%
Error	3	4.67%	1.76%	1.81%	1.19%
Total	15	100.00%	100.00%	100.00%	100.00%

(*Continue*)

Source	*DOF*	*Iteration 5*	*DOF*	*Iteration 6*	*Iteration 7*	*Iteration 8*
$\dot{Q}_m$	3	2.78%	3	13.98%	1.31%	0.75%
R_{ins}	(3)	-	(3)	-	-	-
PCM type	3	91.66%	(3)	-	-	-
δ_{PCM}	3	1.79%	3	84.85%	97.98%	92.20%
Error	6	3.77%	6	1.16%	0.71%	7.04%
Total	15	100.00%	15	100.00%	100.00%	100.00%

4.3.2.2 *Optimisation test case* 2

Based on the optimal values identified in *Optimisation test case* 1, in *Optimisation test case* 2, the search range of the PVT air flow rate was decreased from 250-8000 kg/h to 250-3000 kg/h, while that of the PCM layer thickness was extended from 5-30 mm to 5-50 mm to confirm the optimal design. The optimisation process was presented in Table 4.8 and Fig. 4.11-Fig. 4.13.

Table 4.8 Average *S/N* ratios for each level of the PCM type - *Optimisation test case* 2, *Scenario* 2.

Iteration	*Iteration 1*		*Iteration 2*		*Iteration 3*	
	Level	*S/N*	Level	*S/N*	Level	*S/N*
PCM type level and *S/N* ratio	SP25E2	-7.991	SP25E2	-6.088	SP25E2	-5.263
	SP26E	-7.393	SP26E	-6.090	SP26E	-5.356
	SP21E	-5.097	SP21E	-4.530	SP21E	-3.090
	SP24E	-7.252	SP24E	-6.216	SP24E	-5.400

(*Continue*)

Iteration	*Iteration 4*		*Iteration 5*	
	Level	*S/N*	Level	*S/N*
PCM type level and *S/N* ratio	SP25E2	-5.089	SP25E2	-5.017
	SP26E	-5.088	SP26E	-5.017
	SP21E	-2.746	SP21E	-2.672
	SP24E	-5.037	SP24E	-4.965

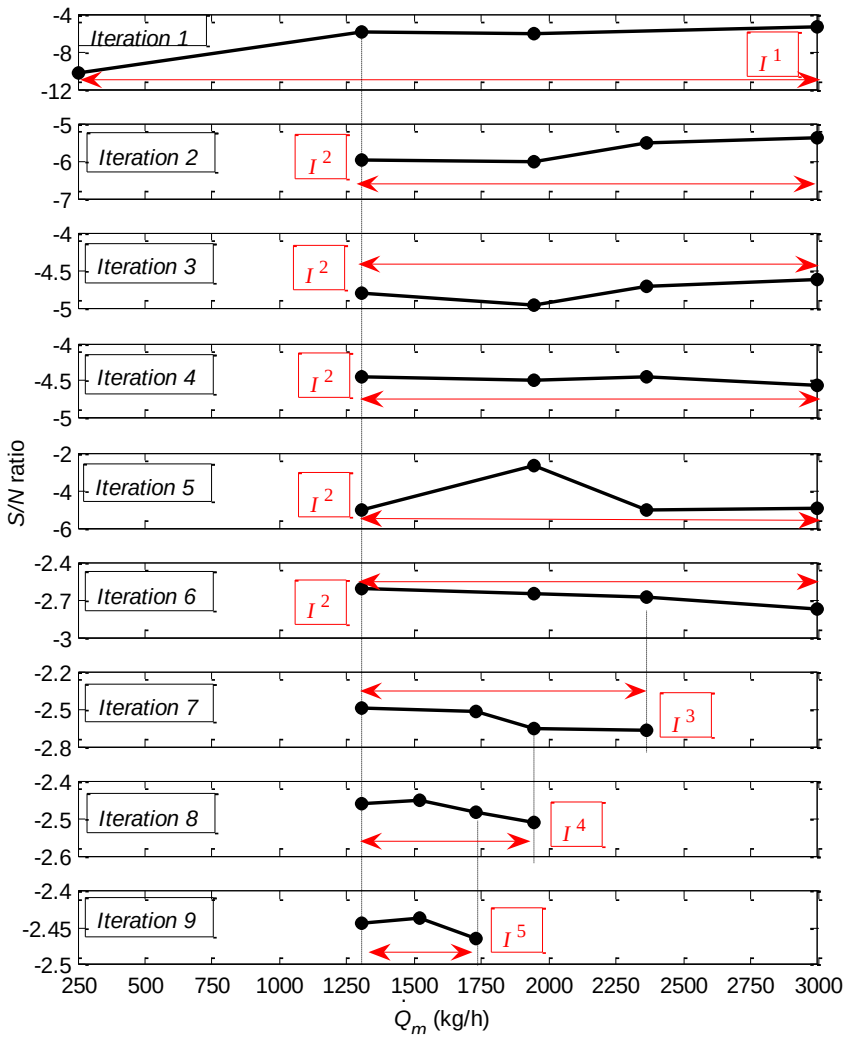

Fig. 4.11 Optimisation process of the PVT air flow rate by using Taguchi-Fibonacci search method in *Optimisation test case* 2, *Scenario* 2.

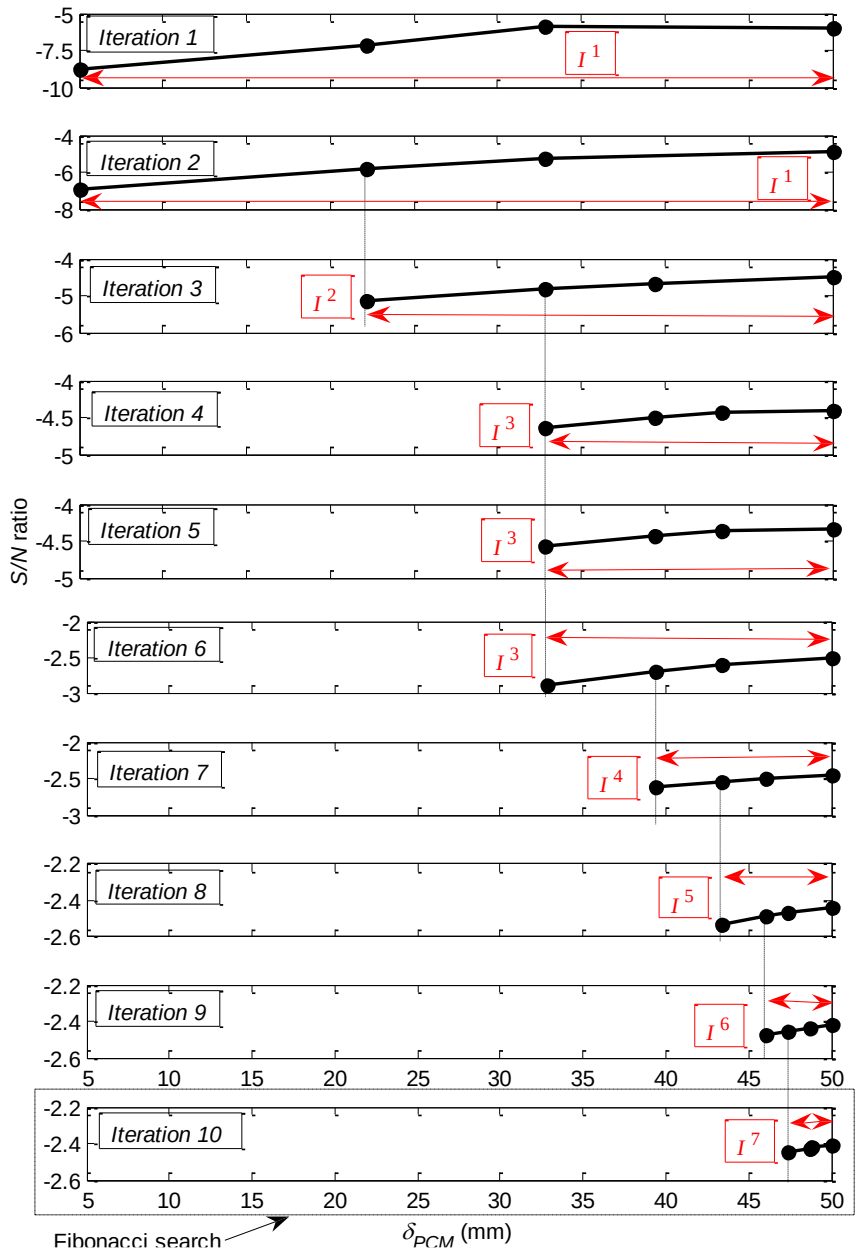

Fig. 4.12 Optimisation process of the PCM layer thickness by using Taguchi-Fibonacci search method in *Optimisation test case* 2, *Scenario* 2.

The percentage contributions of each factor using ANOVA are summarised in Table 4.9. The optimal values identified for the PVT air flow rate, the thermal resistance of the wall insulation layer and the PCM type were 1519.2 kg/h, 3.0 m^2·K/W, SP21E, respectively. The resulted CTPE of the house by using the optimal combination of the factor levels identified was 75.8%. The upper limit of 50 mm was identified as the optimal PCM layer thickness. As mentioned, this is because the PCM cost was not considered in the objective function.

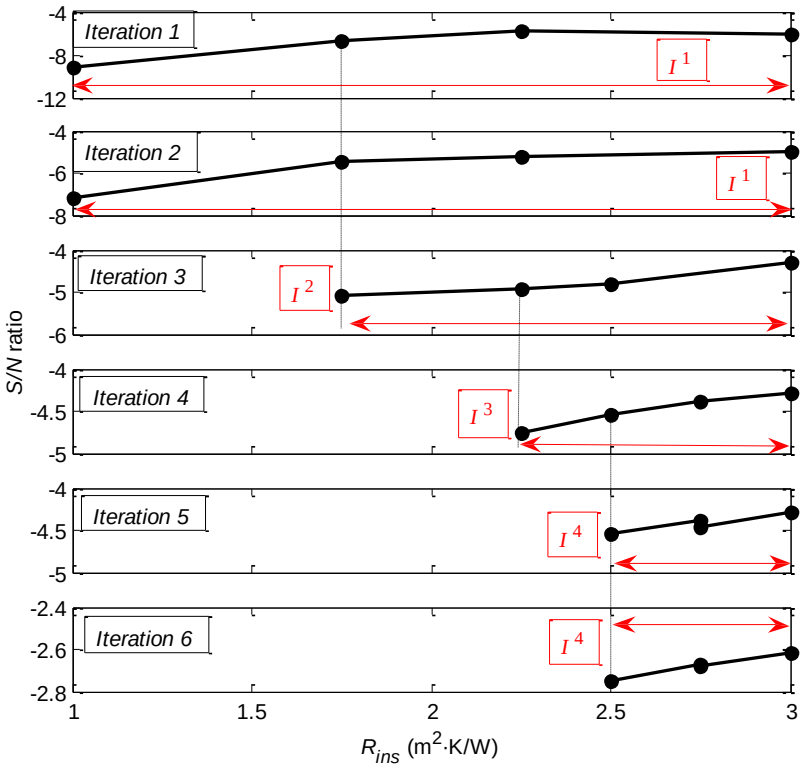

Fig. 4.13 Optimisation process of the thermal resistance of the wall insulation layer by using Taguchi-Fibonacci search method in *Optimisation test case* 2, *Scenario* 2.

Table 4.9 Summary of the percentage contribution in ANOVA - *Optimisation test case* 2, *Scenario* 2.

Source	*DOF*	*Iteration 1*	*Iteration 2*	*Iteration 3*	*Iteration 4*	*Iteration 5*
$\dot{Q}_m$	3	40.94%	1.50%	1.05%	-0.32%	-0.23%
R_{ins}	3	15.27%	29.82%	6.94%	2.31%	0.40%
PCM type	3	15.13%	23.97%	86.10%	95.46%	97.67%
δ_{PCM}	3	12.70%	24.44%	4.43%	0.35%	0.29%
Error	3	15.96%	20.27%	1.48%	2.20%	1.88%
Total	15	100.00%	100.00%	100.00%	100.00%	100.00%

(*Continue*)

Source	*DOF*	*Iteration 6*	*DOF*	*Iteration 7*	*Iteration 8*	*Iteration 9*
$\dot{Q}_m$	3	13.58%	3	11.02%	30.65%	23.97%
R_{ins}	3	8.45%	(3)	-	-	-
PCM type	(3)	-	(3)	-	-	-
δ_{PCM}	3	77.08%	3	88.12%	69.14%	75.67%
Error	6	0.89%	9	0.86%	0.21%	0.35%
Total	15	100.00%	15	100.00%	100.00%	100.00%

* *Iteration* 10 was not listed as Taguchi-Fibonacci search degraded to Fibonacci search.

From Fig. 4.14, it can be seen that the increase of the CTPEs of the house was significant when increasing the PCM layer thickness from 0 to 30 mm. However, the increase became very small when the PCM layer thickness was further increased.

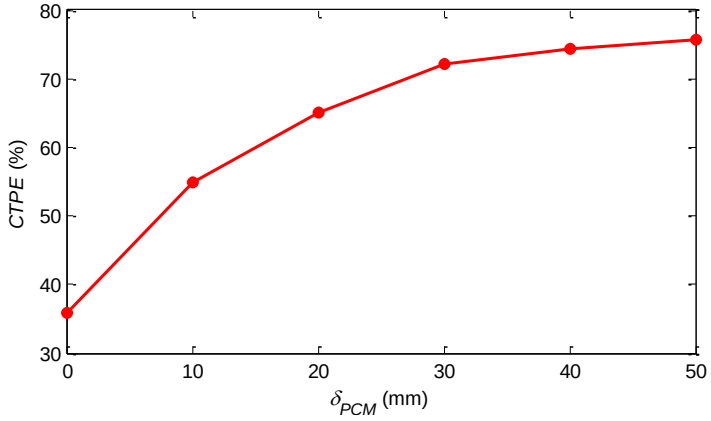

Fig. 4.14 CTPE of the PCM-PVT enhanced house with different PCM layer thicknesses (under the PVT air flow rate of 1640.4 kg/h, thermal resistance of the wall insulation layer of 3 $m^2 \cdot K/W$ and PCM type of SP21E).

From the above results, it can be seen that Taguchi-Fibonacci search method can identify an optimal solution for the PCM enhanced house with the PVT ventilation with a controlled number of iterations. The results from both scenarios showed that the optimal PCM types identified among the PCMs considered were RT18HC from organic PCMs and SP21E from inorganic PCMs due to their appropriate phase change temperature ranges and heat storage capacities, which facilitated that more heat was stored in and released from the PCM layers during the daytime and night time, respectively.

Based on the above optimization results of *Scenario* 1 and *Scenario* 2 (*Optimisation test case* 1), the optimal PCM type identified for the PCM enhanced house with the PVT ventilation was the inorganic PCM SP21E, as a higher CTPE of 72.2% can be achieved in comparison to that of 62.2% when using organic PCM RT18HC. In addition, the optimal layer thickness of the inorganic PCM (*i.e.* SP21E) can be smaller than that of the organic PCM (*i.e.* RT18HC). The optimisation result of *Scenario* 2 (*Optimisation test case* 1) was therefore considered as the final optimal result in this chapter.

4.4 Comparison between the optimal result and the cases without optimisation

To demonstrate the benefits of the optimisation, the CTPE of the PCM enhanced house with the PVT ventilation using the optimal design values was compared with that of the two cases where the non-optimised PCMs and the PVT ventilation were used (named as *Non-optimal* cases hereafter). The results of the comparison are presented in Table 4.10.

In Table 4.10, the *Non-optimal* cases selected were the PCM layer thickness of 20 mm, the thermal resistance of the wall insulation layer of 1 $m^2 \cdot K/W$, and the PVT air flow rate of 2000 kg/h, while the PCMs RT18HC and SP21E were used for the cases with using organic and inorganic PCMs, respectively. Note that the CTPEs were evaluated over 14 consecutive days under Sydney winter weather conditions. For the organic PCM enhanced house (*i.e.* using RT18HC) with the PVT ventilation, the CTPEs of the house were 37.3% and 62.2% for the *Non-optimal* case and the optimisation case using Taguchi-Fibonacci search method, respectively. Compared to the *Non-optimal* case, the CTPE of the house improved 24.85%. For the inorganic PCM enhanced house (*i.e*. SP21E) with the PVT ventilation, the CEPT of the house with optimisation was improved from 45.5 % to 72.2%, in comparison with the *Non-optimal* case.

Table 4.10 Comparison between the baseline design without optimisation and the optimised designs.

Group	Case	$\dot{Q}_m$ (kg/h)	R_{wall} (m^2·K/W)	PCM type	δ_{PCM} (mm)	CTPE	Difference
Organic PCMs	*Non-optimal* case using RT18HC	2000	1.00	RT18HC	20	37.3%	-
	Optimisation by using Taguchi-Fibonacci search method	2073.5	3.00	RT18HC	50	62.2%	24.85%
Inorganic PCMs	*Non-optimal* case using SP21E	2000	1.00	SP21E	20	45.5%	-
	Optimisation by using Taguchi-Fibonacci search method (*Optimisation test case* 1)	1640.4	3.00	SP21E	30	72.2%	26.68%

4.5 Summary

This chapter presented the performance optimisation of the PCM enhanced buildings with PVT collectors by using Taguchi-Fibonacci search method. The factors optimised are the PVT air flow rate, the PCM layer thickness, the PCM type and the thermal resistance of the wall insulation layer. In Taguchi-Fibonacci search method, Fibonacci search method was used to drive the optimisation process through iterations while Taguchi method was used to design the matrix of trial tests in each iteration. Signal-to-noise (*S/N*) ratio and analysis of variance (ANOVA) were used to determine the optimal levels of the individual factors and investigate the response significance of each factor, respectively.

The performance optimisation was carried out based on the house with integrated organic or inorganic PCMs and with the PVT ventilation presented in Chapter 3. It was shown that Taguchi-Fibonacci search method can identify an optimal solution for the PCM enhanced house with the PVT ventilation with a limited number of iterations. Compared to the cases of the organic and inorganic PCM enhanced house with the PVT ventilation but without optimisation, the Coefficients of Thermal Performance Enhancement (CTPEs) of the house using the values optimised by Taguchi-Fibonacci search method were improved from 37.3 and 45.5% to 62.2 and 72.2%, respectively.

Chapter 5 Experimental Investigation and Multi-objective Optimisation of the Charging Performance of a Centralised PCM TES System

Solar air heating systems are an alternative energy system for indoor air conditioning, but since solar energy is intermittent, integrating solar air systems with thermal energy storage (TES) systems would help to rationalise the potential use of solar energy (Labat *et al.* 2014). As shown in the literature review in Chapter 2, over the last two decades PCMs have been investigated as an option to store the thermal energy from solar air heating systems, and compared to the passive integration of PCMs into building envelopes, the active utilisation of PCM TES can rapidly respond to the fast variation of heat source and building load. When PCMs are coupled with a solar air system, the charging performance of PCM TES becomes critical, because within the limited daytime period, high efficient solar heat storage in the PCM TES is required.

Previous studies in the literature indicated that there has not been any work on the multi-objective optimisation of PCM TES systems with integrated PVT collectors for thermal energy storage based on experiments, so this chapter presents an experimental investigation and a bi-objective optimisation study to characterise and enhance the charging performance of a PCM TES system. The following two indicators were used to evaluate the performance of the PCM TES system and formulate the optimisation problem, which are the average heat transfer effectiveness and the effective PCM charging time. A range of experiments was designed using the Taguchi method and then carried out using a lab-scale test rig. Two bi-objective optimisation strategies, one using a controlled elitist genetic algorithm (GA) - multi-criteria decision-making (MCDM) process, and the other using fuzzy clustering, were then developed to determine the optimal solutions of the optimisation problem. The results from these bi-objective optimisation strategies were compared to each other in order to increase confidence in the optimal solutions identified; these results can then be used to facilitate the optimal design of PCM TES systems.

This chapter is organised as follows. The experimental system is described in Section 5.1. The research methodology, including the design of experimental plan and the bi-objective optimisation strategies, is described in Section 5.2. Section 5.3 presents the

characterisation and evaluation of the PCM TES system. The design optimisation for the PCM TES system is presented in Sections 5.4 and 5.5. Lastly, Section 5.6 summarises the key findings from this chapter.

5.1 Description of the experimental system

5.1.1 Experimental setup

The experiments in this study were carried out using a lab-scale test rig of a PVT-PCM system, as shown in Fig. 5.1. This test rig consists of a chiller, a PVT emulator, a PCM TES unit, a PCM fan, a custom-made heat exchanger, and several dampers. The PVT emulator utilises an electric heater and a variable speed fan (named as PVT fan) to mimic a PVT system, and the outlet air from the PVT emulator is used to charge the PCM TES unit. The air flow rate through the PVT emulator is controlled by varying the operating speed of the PVT fan, while the temperature of the outlet air from the PVT emulator is controlled by regulating the heat output of the electric heater. The rated air flow rate of the PVT fan was 300 l/s at a pressure difference of 200 Pa. The custom-made heat exchanger, chiller, and PCM fan are used to discharge the heat from the PCM TES unit; the PCM fan is the same as the PVT fan. A number of dampers are used to switch the system between the charging mode and discharging mode.

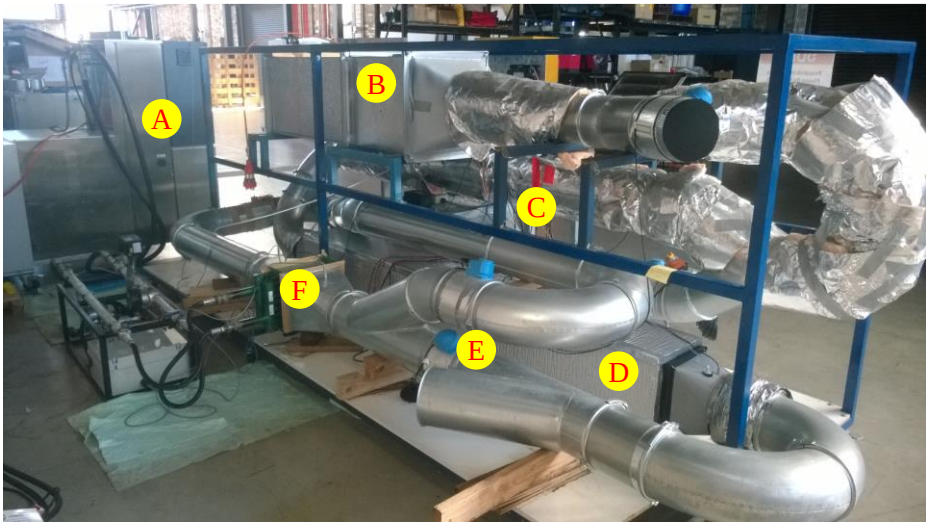

A - Chiller; B - PVT emulator; C - PCM fan; D - TES; E - Damper; F – Heat exchanger

Fig. 5.1 The lab-scale test rig of the PVT-PCM system.

The PCM TES unit is a rectangular duct made of wood, which was thermally insulated with polyolefin materials. The internal dimensions of the PCM TES duct were

approximately 2500 mm (length), 215 mm (width) and 250 mm (height), respectively. The PCM bricks can be place inside this PCM TES unit in arrays to create a number of air channels, as shown in Fig. 5.2. The PCM tested was a commercial salt hydrate of S21 supplied from PlusICE (2016), which was encapsulated in plastic containers as the PCM bricks shown in Fig. 5.3. The thermo-physical properties of this PCM S21 are summarised in Table 5.1. The PCM bricks are 500 mm long by 32 mm wide by 250 mm high. Five PCM bricks (in maximum) can be placed inside the rectangular TES duct in the direction of air flow. The number of PCM bricks across the direction of air flow depends on the size of the air channels selected.

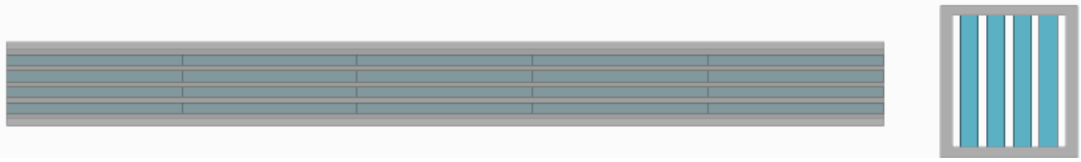

Fig. 5.2 Installation of a PCM TES unit.

Fig. 5.3 PCM bricks tested (PlusICE 2016).

Table 5.1 Thermo-physical properties of PCM S21 (PlusICE 2016).

Properties	Value
Nominal phase change temperature (^{o}C)	22
Density (kg/m^{3})	1530
Nominal latent heat capacity (kJ/kg)	170
Thermal conductivity (W/(m·K))	0.54
Specific heat capacity (kJ/(kg·K))	2.2

In this test rig the heated air from the PVT emulator can be directed into the PCM TES unit for heat charging and then exhausted to ambient by opening the dampers D2 and D3, as shown in Fig. 5.4. In the discharging mode, the system can operate either by using the circulating air by opening the dampers D4, D5 and D6 (*Option A)* or by using ambient air via opening the dampers D7, D5, D4, D2 and D1 (*Option B)*, either option

depends on the temperature of ambient air (see Fig. 5.4). Note that during the experiments the air flow between the charging mode and discharging mode were in opposite directions so that the desired heat transfer performance could be achieved while the PCM TES unit was under discharging process.

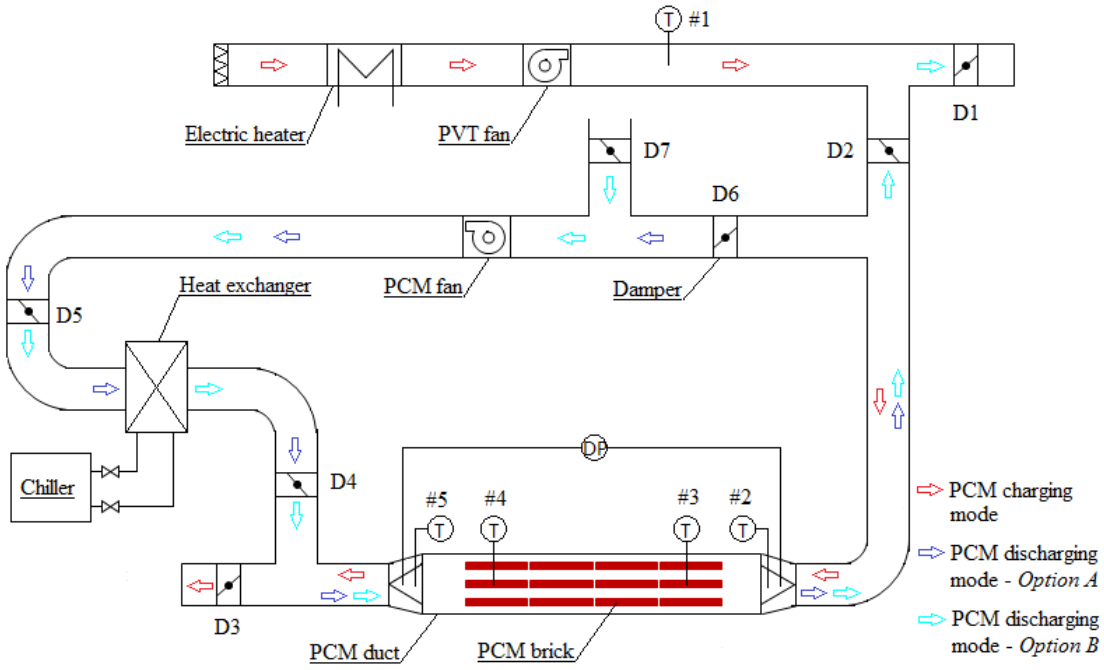

Fig. 5.4 Simplified schematic of the experimental system.

5.1.2 Measurement instruments

Five temperature sensors were used to measure the temperature of the outlet air from the PVT emulator (*i.e.* temperature sensor #1 in Fig. 5.4), the air temperature at both ends of the PCM TES unit (*i.e.* temperature sensors #2 and #5), as well as the PCM temperature of the two PCM bricks at each end of the PCM TES unit (see Fig. 5.4). A stainless steel tube bracketed on the outside of the PCM brick was inserted into the PCM brick to prevent the movement of the tube from moving inside the brick and the temperature sensor from being corroded by the PCM, as shown in Fig. 5.5. The inside of the steel tube was partially filled with thermal paste before inserting the temperature sensor. An air velocity sensor was used to measure the air velocity inside the air duct to calculate the volumetric air flow rate.

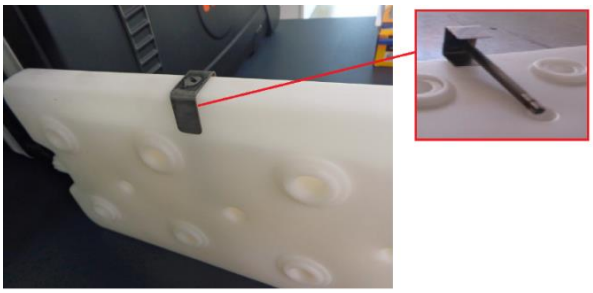

Fig. 5.5 Installing a temperature sensor into the PCM brick.

A CLIPSAL C-Bus residential controller is used to control the fan speed and record the measured data based on PICED software and CLIPSAL (Schneider Electric 2016). The sampling rate used in the experimental tests was 30 seconds. The measurement uncertainties of the key instruments used are summarised in Table 5.2.

Table 5.2 Major measurement instruments used and the claimed uncertainties.

Instrument	Function	Location	Measurement range	Accuracy
C-Bus digital temperature sensors	Temperature measurement	Two ends of the PCM TES duct; PVT emulator outlet; Inside of the PCM bricks	-10-80^{o}C	±0.5^{o}C
SIMENS QVM62.1	Air velocity measurement	Inlet of the PCM duct at the charging mode	0-10 m/s	±0.2 m/s+3% of the measured value

5.2 Research methodology

5.2.1 Outline of the methodology

The research methodology used here is outlined in Fig. 5.6; it consists of two major steps. The first step was the experimental investigation of the charging and discharging characteristics of the PCM TES unit with a primary focus on the charging performance of PCM because the temperature and the flow rate of heated air from the PVT emulator outlet can be controlled quite well within a relatively wide range. A matrix of experiments was designed using the Taguchi method and then carried out based on the lab-scale test rig introduced in Section 5.1. The signal-to-noise (*S/N*) ratio is used to analyse the performance of the PCM TES unit based on the two key performance indicators (KPIs) of the average heat transfer effectiveness and the effective charging

time. These two indicators are introduced in Section 5.2.3. According to the experimental results, the charging characteristics of the PCM TES unit and the best combination of the factor levels (*i.e.* values of design variables) corresponding to each KPI can be identified, and the significance of the control factors to each KPI can also be ranked. The Taguchi-based analysis can be regarded as a single-objective optimisation process for the design of the centralised PCM TES system.

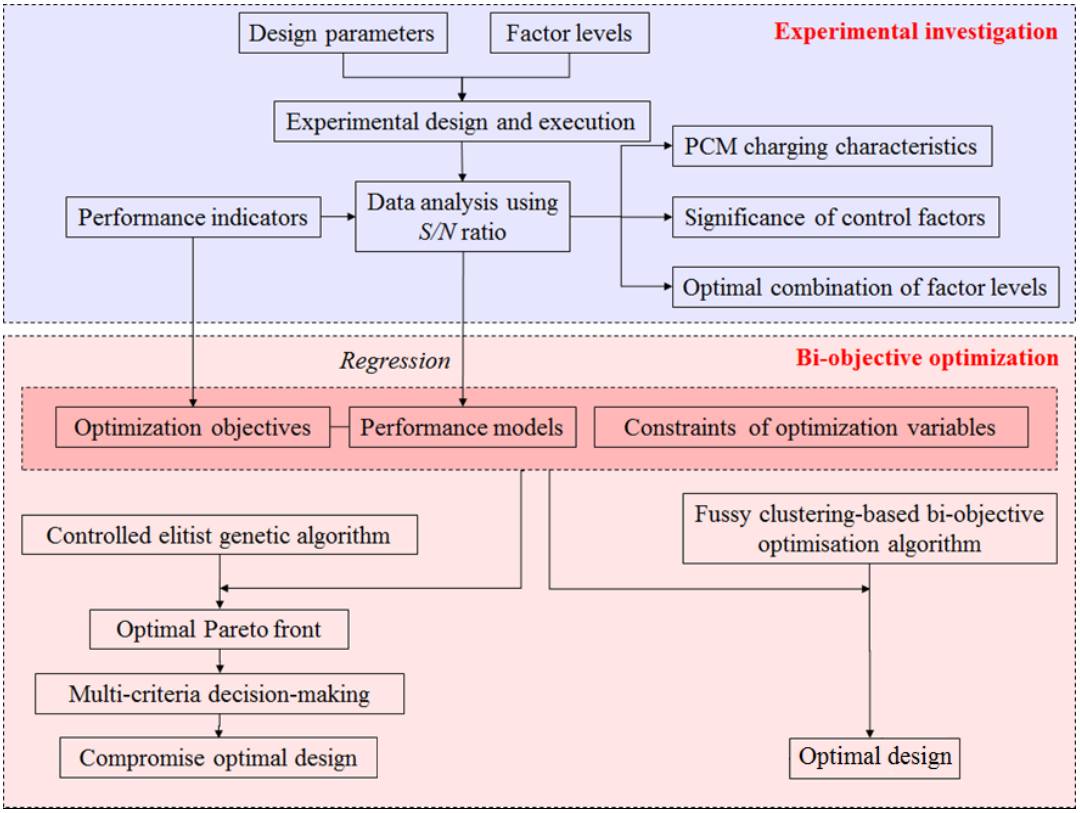

Fig. 5.6 Outline of the research methodology.

The second step is the multi-objective optimisation of the PCM TES system. Since the discrete factor levels were used in the experimental design, and the best combination of the factor levels identified through *S/N* ratio analysis are only 'near optimal' for each individual KPI, two bi-objective optimisation strategies were used to further identify the 'globally' optimal values of the key variables of the PCM TES unit. Two performance models were used to relate each KPI to the variables through regressions based on the experimental results and then used to predict the system performance in the bi-objective optimisation problem. In terms of optimisation strategies, the first bi-objective optimisation strategy consists of a controlled elitist GA optimisation and a MCDM process. The controlled elitist GA is used as the optimisation technique to identify an optimal Pareto front based on the constraints defined. In the Pareto front,

each combination of optimisation objectives could be considered as optimal, so the multi-criteria decision-making process was used to determine the 'globally' optimal solutions of the optimisation problem. This bi-objective optimisation strategy is introduced in Section 5.2.5. A second bi-objective optimisation strategy was developed using fuzzy clustering to provide an innovative bi-objective optimisation strategy that would directly identify optimal designs; it was then used to solve the same optimisation problem and also increase confidence in the optimal solutions identified by the first bi-objective optimisation strategy. Unlike the bi-objective optimisation strategy with the controlled elitist GA – MCDM process which first identifies the optimal Pareto front and then determines the compromise optimal solutions, the fuzzy clustering-based bi-objective optimisation strategy can directly identify the optimal solution. The fuzzy clustering-based optimisation strategy is introduced in Section 5.2.6.

5.2.2 Experimental design using Taguchi method

The Taguchi method (Taguchi 2004) was used to design and plan the experiment so that the multiple control factors of concern and certain levels of the control factors can be arranged orthogonally, and thus reduce the number of trial tests. Here, the following four key variables were considered to be the control factors: the inlet air temperature of the PCM TES unit, the air flow rate, the number of the PCM bricks along the direction of air flow, and the number of air channels in the PCM TES unit. The number of PCM bricks along the direction of air flow was used to represent the length of the PCM TES unit; this was considered to be a discrete variable in this study.

Three levels were considered for each factor; the three levels for the inlet air temperature of the PCM TES unit used in the charging mode were 42^{o}C, 37^{o}C and 32^{o}C, and they were determined based on the 20 ^{o}C, 15 ^{o}C, and 10^{o}C differences in temperature between the inlet air in the TES unit and the nominal PCM phase change temperature (*i.e.* 22^{o}C), respectively. The three levels for the air flow rate used during the charging mode were 150, 100, and 50 l/s, respectively. The levels of the number of the PCM bricks along the direction of air flow of the TES system considered were 3, 4, and 5 and the number of air channels was 3, 4, and 5, respectively. The air flow rate, the number of PCM bricks along the PCM TES unit, and the number of air channels were determined based on the capacity of the PVT fan, the size of the PCM

duct, and the dimensions of the PCM brick tested. The L_9 (3^4) orthogonal array was used to form a matrix of the trial tests and the resulting experimental design is presented in Table 5.3. As mentioned before, this study focused on PCM charging performance. While during PCM discharging, the maximum air flow from the PCM fan was used and cooled below 14^{o}C by the heat exchanger and the chiller in order to reduce the discharging time.

Table 5.3 Taguchi experimental plan and factor levels.

Trail test	Control factors			
	Inlet air temperature of the TES unit (^{o}C)	Charging air flow rate (l/s)	Number of PCM bricks along the TES unit	Number of air channels
1	42.0 (level 1)	100.0 (level 1)	4 (level 1)	4 (level 1)
2	42.0	50.0 (level 2)	5 (level 2)	5 (level 2)
3	42.0	150.0 (level 3)	3 (level 3)	3 (level 3)
4	37.0 (level 2)	100.0	5	3
5	37.0	50.0	3	4
6	37.0	150.0	4	5
7	32.0 (level 3)	100.0	3	5
8	32.0	50.0	4	3
9	32.0	150.0	5	4

In *S/N* ratio analysis, the factors are ranked according to the maximal *S/N* ratio difference among the different levels of each factor. The *S/N* ratio is also used to identify the optimal combination of the levels of each individual factor; here, two *S/N* ratios of the-lower-the-better and the-higher-the-better were used (Taguchi 2004).

5.2.3 Key performance indicators

Two key performance indicators, the average heat transfer effectiveness and the effective PCM charging time, were defined and used as objective responses to evaluate the charging performance of the PCM TES unit.

5.2.3.1 Average heat transfer effectiveness

Heat transfer effectiveness has been used in several studies to examine the performance of TES systems (Tay *et al.* 2012a and 2012b; Amin *et al.* 2012; Bergman *et al.* 2011). So, in this study, the average heat transfer effectiveness of the PCM TES over the PCM charging period was used as a KPI, which is the average ratio of the

actual heat charged into the TES system to the theoretical maximum heat that can be charged during PCM charging; it was determined by Eq. (5.1).

$$\bar{\varepsilon}_{ch} = \frac{1}{\Delta t_{ch}} \int_{t_{start}}^{t_{end}} \varepsilon_{ch} dt = \frac{1}{\Delta t_{ch}} \int_{t_{start}}^{t_{end}} \frac{T_{air,in} - T_{air,out}}{T_{air,in} - T_m} dt \approx \frac{1}{n_t} \sum_{i=1}^{n_t} \frac{(T_{air,in,i} - T_{air,out,i})}{(T_{air,in,i} - T_m)} \quad (5.1)$$

where $\bar{\varepsilon}_{ch}$ is the average heat transfer effectiveness, ε_{ch} is the heat transfer effectiveness, n_t is the total sampling number during the charging period, t_{start} and t_{end} represent the start time and completion time defined for the effective PCM charging period (measure in hours in this chapter), and the subscripts *air*, *in* and *out* indicate air inlet and outlet, respectively.

5.2.3.2 Effective PCM charging time

Many conventional, and especially organic PCMs, suffer from low thermal conductivity which makes it hard for them to address rapid changes in load during thermal charging and discharging processes. This is why an effective PCM charging time was developed and used as another KPI to evaluate the charging performance of the PCM TES unit. Here, the effective PCM charging time is considered as the difference in time when the temperature gradient of the first PCM brick close to the inlet of the TES unit suddenly decreases (after which the first PCM brick experiences a relatively small change in temperature gradient for certain period during the charging process), and when the temperature gradient of the last PCM brick close to the outlet of the TES unit suddenly increases (before which the last PCM brick experiences a relatively small change in temperature gradient for certain period during the charging process).

Both of the KPIs used may not be perfect but they could provide an indication of the performance of the PCM TES unit under different working conditions. The average heat transfer effectiveness aimed to be the-higher-the-better, while the objective for the effective PCM charging time was the-lower-the-better. Note also that although the PCM TES unit was well insulated, heat loss still existed, and since the amount is difficult to quantify, the heat loss was omitted. Moreover, to ensure that the two KPIs developed were valid, the initial PCM temperature in each experiment was held well below the low limit of the PCM phase change temperature range, while the inlet air temperature used to charge the PCMs was much higher than the upper limit of the PCM phase change temperature.

5.2.4 Formulation of the bi-objective optimisation problem

5.2.4.1 Optimisation objectives, and optimisation variables and constraints

In the bi-objective optimisation problem, the average heat transfer effectiveness and effective PCM charging time were used as the two contradictory optimisation objectives, and the four factors used in the Taguchi experimental design were considered as the optimisation variables. The constraints of these optimisation variables were determined based on the factor levels considered in the Taguchi experimental design and are defined as follows:

Continuous variables: $\begin{cases} T_{air,in} \in [32.0, 42.0]\,^{\circ}\mathrm{C} \\ \dot{Q}_v \in [50, 150]\,\mathrm{l/s} \end{cases}$;

Discrete variables: $\begin{cases} M \in \{3, 4, 5\} \\ N \in \{3, 4, 5\} \end{cases}$.

where $\dot{Q}_v$ is the air volume flow rate (measured in l/s in this chapter), M is the number of PCM bricks in the direction of air flow and N is the number of air channels.

5.2.4.2 Development of the performance models

Two performance models which related the optimisation objectives to the optimisation variables were developed and used to determine how the system would respond under different trail settings.

The performance model of the average heat transfer effectiveness was based on the PCM nominal melting temperature. The heat transfer effectiveness between the PCM bricks and the air flowing through the PCM TES unit was determined by Eq. (5.2); here, the overall heat transfer coefficient (U) is assumed to follow a third-order polynomial of the convective heat transfer coefficient (h_{conv}) as it can provide a decent regression based on the trials; it is described in Eq. (5.3). The convective heat transfer coefficient was determined using Eq. (5.4), and the Nusselt number (Nu) was calculated using Eq. (5.5).

$$\bar{\varepsilon}_{ch} = \varepsilon_{ch} = 1 - e^{-NTU} = 1 - e^{-\frac{1000 \cdot A \cdot U}{\rho_{air} \cdot c_{p,air} \cdot \dot{Q}_v}} \tag{5.2}$$

$$U = a_3 h_{conv}^3 + a_2 h_{conv}^2 + a_1 h_{conv} + a_0 \tag{5.3}$$

$$h_{conv} = \frac{Nu \cdot k_{air}}{d_h} \tag{5.4}$$

$$Nu = 0.023 Re^{0.8} Pr^{0.3} \tag{5.5}$$

where *NTU* is the Number of Transfer Units, *A* is the heat transfer area, and a_0-a_3 are the coefficients which were regressed based on the results of the Taguchi experiments.

The effective PCM charging time was determined based on the total thermal energy (Q_{tot}) stored in the PCM TES unit and the average heat transfer rate, and is defined in Eq. (5.6). The average heat transfer rate ($\dot{Q}$) and the latent heat (Q_{lat}) stored in the PCM TES unit were determined using Eqs. (5.7) and (5.8), respectively. The ratio of sensible heat (Q_{sen}) to the average heat transfer rate was calculated using Eq. (5.9), which was determined through the stepwise regression.

$$\Delta t_{ch} = \frac{Q_{tot}}{\dot{Q}} = \frac{Q_{lat}}{\dot{Q}} + \frac{Q_{sen}}{\dot{Q}} \tag{5.6}$$

$$\dot{Q} = 3.6 \times \rho_{air} c_{p,air} \dot{Q}_v \left(T_{air,in} - T_{air,out}\right) = 3.6 \times \rho_{air} c_{p,air} \dot{Q}_v \bar{\varepsilon}_{ch} \left(T_{air,in} - T_m\right) \tag{5.7}$$

$$Q_{lat} = m_{PCM} M (N-1) \gamma \tag{5.8}$$

$$\frac{Q_{sen}}{\dot{Q}} = b_3 T_{air,in} \dot{Q}_v + b_2 N^2 + b_1 N + b_0 \tag{5.9}$$

where $\bar{\varepsilon}_{ch}$ is the average heat transfer effectiveness calculated by Eq. (5.2), γ is the PCM latent heat of fusion, m_{PCM} is the mass of each PCM brick, b_0-b_3 are the coefficients regressed based on the results of the Taguchi experiments, and the subscripts *tot*, *lat* and *sen* represent total, latent and sensible, respectively.

5.2.5 Multi-objective optimisation strategy using the controlled elitist GA - MCDM

5.2.5.1 Multi-objective genetic algorithm optimisation technique

The elitist non-dominated sorting Genetic Algorithm (NSGA-II) as an optimisation technique has been used in a number of studies to solve multi-objective optimisation problems (Ko *et al.* 2015; Wong *et al.* 2016; Deb *et al.* 2000). Here, a variant of elitist NSGA-II implemented in Matlab, the controlled elitist GA (*i.e.* function 'gamultiobj'), was used to solve the bi-objective optimisation problem. The 'gamultiobj' function

employs two options, the 'ParetoFraction' and the 'DistanceFcn' to maintain diversity by controlling the number of individuals on the Pareto front and by favouring individuals that are some distance away on the Pareto front, respectively (Mathworks 2016).

5.2.5.2 Multi-criteria decision-making using the compromise ranking method

The compromise ranking method VIKOR, introduced by Opricovic (Opricovic 1998), is used to determine the globally optimal solution(s) in the Pareto front identified. This method identifies the compromise design(s) among a set of alternatives in the presence of the conflicting criteria by ranking them based on their distance from the ideal solution (Opricovic and Tzeng 2004). This distance is measured by three scalar quantities (*i.e.* S_i, R_i and Q_i, known as L_1-*metric*, L_∞-*metric* and L_{com}-*metric*, respectively; they are quantified with Eqs. (5.10) to (5.12)) and calculated for each alternative design (Caterino 2009).

$$S_i = \sum_{j=1}^{n_c} w_j \left(f_j^* - f_{ij}\right) / \left(f_j^* - f_j^-\right) \tag{5.10}$$

$$R_i = \max_j \left[w_j \left(f_j^* - f_{ij}\right) / \left(f_j^* - f_j^-\right)\right] \tag{5.11}$$

$$Q_i = v\left(S_i - S^*\right) / \left(S^- - S^*\right) + \left(1 - v\right)\left(R_i - R^*\right) / \left(R^- - R^*\right) \tag{5.12}$$

where f_{ij} is the j^{th} criterion for i^{th} alternative, m is the total number of criteria, w_i is the weight for individual criterion, f_j^* and f_j^- are the best and worst values of all criterion functions, S^*, S^-, $R^*$and R^- are the minimal and maximal values of S_i and R_i, respectively, n_c is the number of criteria, v is the weight of the strategy of 'the majority of criteria' ranging from 0 to 1 (Opricovic and Tzeng 2004). If the weight (v) is less than 0.5, then more weight is given to the magnitude of the worst performances exhibited by the alternatives in respect to each single criterion, and more weight is given to the global performance of the alternatives with respect to the whole of the criteria when the weight (v) is higher than 0.5.

Based on the three scalar quantities, three ranking lists can be generated in a decreasing order and the compromise designs can be identified based on the ranking lists. Accordingly, a compromise design (a') or designs ($a', a'', \ldots, a^{(z)}$) can be identified by following the rules described in Eq. (5.13) (Opricovic and Tzeng 2004).

$$\begin{cases} a', \text{if } Q_i(a'') - Q_i(a') \geq \dfrac{1}{n_{alt} - 1}, \text{ and } a' \text{ is best ranked by } S_i \text{ and } R_i; \\ a' \text{ and } a'', \text{if } Q_i(a'') - Q_i(a') \geq \dfrac{1}{n_{alt} - 1}, \text{ but } a' \text{ is not best ranked by } S_i \text{ or } R_i; \\ a', a'' \ldots a^{(z)}, \text{if } Q_i(a^{(z)}) - Q_i(a') < \dfrac{1}{n_{alt} - 1}, z \geq 2 \end{cases} \quad (5.13)$$

where a' is the alternative which is the best ranked in the ranking list by the scale quantity L_{com}-*metric*, $a'', a''', \ldots, a^{(z)}$ are the alternatives with the second, third … z^{th} positions in the ranking list by the scale quantity L_{com}-*metric*, and n_{alt} is the number of the alternatives in Pareto front. Details of this method can be found in Opricovic and Tzeng (2004).

5.2.6 The bi-objective optimisation strategy using the fuzzy clustering

The bi-objective optimisation strategy based on fuzzy clustering was used to optimise the objective functions $f_1(\vec{x})$ and $f_2(\vec{x})$ in a bi-objective optimisation problem, in which $\vec{x}$ is the optimisation variable vector (*i.e.* $(x_1, x_2, \ldots, x_{n_v})$, and n_v is the number of the optimisation variables). The introduction of the fuzzy clustering algorithm provides a method to evaluate and identify the potential optimal solutions in a bi-objective optimisation problem, based on which the optimal designs can be approached iteratively. It can also maintain the diversity of the optimal solutions during the optimisation progress, which enables the optimisation progress to converge from different groups (*i.e.* clusters) of objective responses.

An outline of the fuzzy clustering-based bi-objective optimisation strategy is shown in Fig. 5.7. Here the strategy begins by generating a number of random points (*i.e.* a number of random optimisation variable vectors, known as individuals in the population) within the optimisation variable constraints to create an initial population (P) using the function 'rand()' in Matlab, as shown in Eq. (5.14). The objective responses corresponding to individuals in the population can then be calculated using the objective functions, and then normalised using Eq. (5.15).

$$P = \{\vec{x}_i | \vec{x}_i = (x_{i,1}, x_{i,2}, \ldots, x_{i,n_v}), i = 1,2, \ldots, n_P\} \quad (5.14)$$

where n_P is the number of individuals in the population.

$$y_{i,j} = \begin{cases} \dfrac{f_j(\vec{x}_i) - \min\left(f_j(\vec{x}_i)\right)}{\max\left(f_j(\vec{x}_i)\right) - \min\left(f_j(\vec{x}_i)\right)}, \text{if } f_j(\vec{x}_i) \text{ need to be minimised;} \\ 1 - \dfrac{f_j(\vec{x}_i) - \min\left(f_j(\vec{x}_i)\right)}{\max\left(f_j(\vec{x}_i)\right) - \min\left(f_j(\vec{x}_i)\right)}, \text{if } f_j(\vec{x}_i) \text{ need to be maximised.} \end{cases} \quad (5.15)$$

where $y_{i,j}$ is the j^{th} normalised objective response of the i^{th} individual in the current population (in bi-objective optimisation problems, j equals to 1 or 2), and the subscripts *min* and *max* indicate the minimal and maximal values of the objective responses in the generation. According to Eq. (5.15), the bi-objective optimisation problem is to minimise y_1 and y_2.

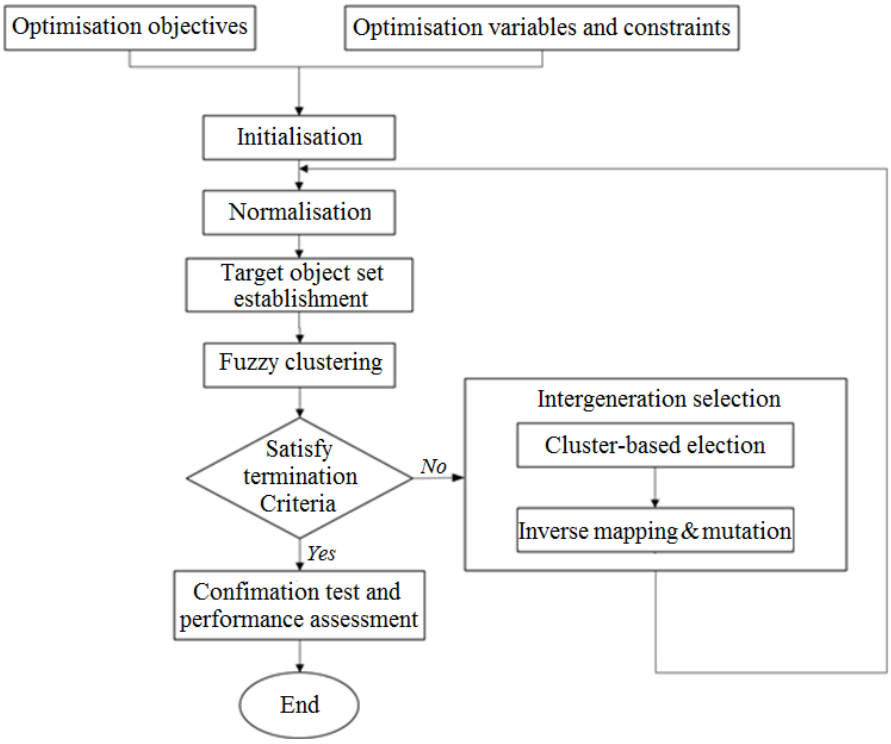

Fig. 5.7 Outline of the fuzzy clustering-based optimisation strategy.

This combination of two normalised objective responses which correspond to an individual ($\vec{x}_i$) is known as an object ($\vec{y}_i$), so accordingly, an original set of objects (O) which correspond to the population (P) can be determined, as depicted in Eq. (5.16). As a result, an ideal object which consists of the two minimal normalised objective responses in this generation can then be identified. The ideal optimal solution in the current generation has the coordinates of (0, 0) in the normalised objective space in the generation, so then an ideal object set (Γ) is generated by duplicating the ideal object to a certain number (n_{io}), which is then incorporated into the original set of the objects (O) to form an augmented object set (O').

$$O = \{\vec{y}_i | \vec{y}_i = (y_{i,1}, y_{i,2}), i = 1,2, \dots, n_P\} \quad (5.16)$$

where $\vec{y}_i$ is the i^{th} object corresponding to the i^{th} individual.

In the next step, the augmented object set (O') is partitioned into several clusters using a fuzzy clustering algorithm, so based on the clustering results, a termination criterion is then applied to determine whether the optimisation process is completed or not. If it is not complete, an intergeneration selection involving a cluster-based election, and inverse mapping and mutation will then be used to generate a new generation of population for the next iteration. Otherwise, the optimisation process is terminated and the objects in the last generation of the population will be compared and the optimal individuals can be identified as the optimal solutions. The fuzzy clustering algorithm used in this study is presented in Section 5.2.6.1. Details of the intergeneration selection are specified in Section 5.2.6.2.

5.2.6.1 Fuzzy clustering algorithm

Cluster analysis, as an unsupervised classification algorithm, is an important technique in data mining because it can be used to partition a given data set into several groups. These groups are called clusters which means that objects in the same cluster tend to be similar, while those in different groups are as dissimilar as possible (Kaufman *et al.* 1990). Similarities and dissimilarities between objects are usually described by metrics such as the Manhattan distance, the Euclidean distance, and cosine similarity. Compared to hard clustering such as K-mean clustering, fuzzy clustering allows for some ambiguity in the data by giving the membership coefficients to each object that represent the extent to which it belongs to different clusters, rather than assigning one object to only one cluster. The range of the membership coefficients of an object to different clusters is from 0 to 1, and the sum of them should equal to 1.

A L_1-norm based fuzzy clustering algorithm (Jajuga 1991) is used here, and it can minimise the objective function L, as shown in Eq. (5.17) (Tan *et al.* 2006), where the distance function *dist* and the membership coefficient (u_{ik}) are defined in Eqs. (5.18) and (5.19), respectively (Tan *et al.* 2006).

$$L = \sum_{k=1}^{n_k} \sum_{i=1}^{n_P} u_{ik}^r dist(\vec{y}_i, \vec{c}_k) \quad (5.17)$$

$$dist(\vec{y}_i, \vec{c}_k) = w_1|y_{i,1} - c_{k,1}| + w_2|y_{i,2} - c_{k,2}| \tag{5.18}$$

$$u_{ik} = \frac{1/dist(\vec{y}_i, \vec{c}_k)}{\sum_{k=1}^{n_k} 1/dist(\vec{y}_i, \vec{c}_k)} \tag{5.19}$$

where $\vec{c}_k$ is the centre coordinate of the k^{th} cluster, n_k is the number of the clusters, u_{ik} is the membership coefficient of the object $\vec{y}_i$ to cluster $\vec{c}_k$, n_k is the number of clusters, w_1 and w_2 are the weighting factors of the two normalised optimisation objectives, and r is the membership exponent which determines the level of fuzziness. Note that r approaching 1 gives crisper clustering, whereas approaching infinity leads to complete fuzziness. Previous studies revealed that assigning r equal to 2 is a reasonable choice (Kaufman *et al.* 1990; Bezdek *et al.* 1984) so r was therefore set as 2 in this study.

To facilitate bi-objective optimisation, the fuzzy clustering is implemented onto the augmented object set (O'). Accordingly, a number of clusters are partitioned, in which a small amount of the original objects and the ideal object set are partitioned into the same cluster (called a target cluster hereafter), as shown in Fig. 5.8. As mentioned, the ideal object set contains a number of identical objects whose coordinates are at (0, 0) in the normalised object space; the objects close to the ideal object set can be identified as part of the target cluster (see the green points in Fig. 5.8).

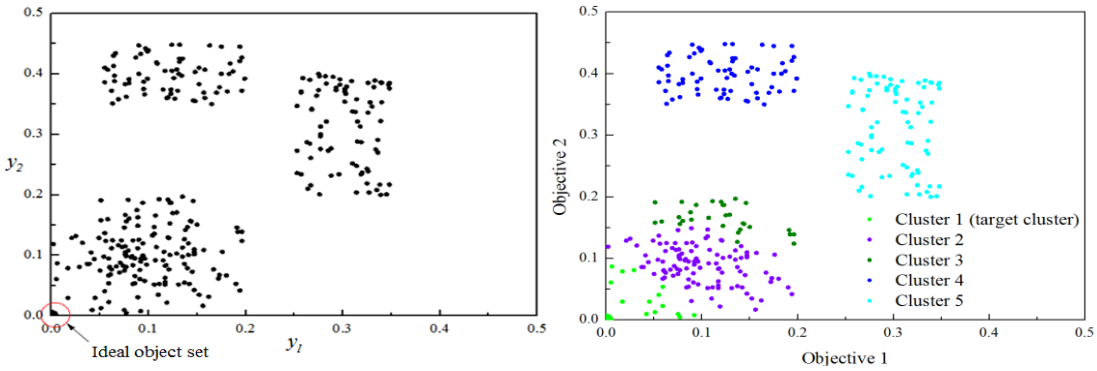

a) Before clustering b) After clustering

Fig. 5.8 Schematic of the clustering result based on the augmented object set (O').

5.2.6.2. Intergeneration selection

Intergeneration selection serves to generate a population for the next generation so that the characteristics of the objects identified near the ideal object set can be transmitted

to the next generation to facilitate the convergence of the optimisation problem, while keeping the diversity of the objects from different clusters.

1) Cluster-based election

Based on the clustering results, an elite set (Λ) which consists of the objects selected under two criteria is identified, so the objects that satisfy either *Criterion I* or *Criterion II*, or both, will be selected into the elite set. The two selection criteria are shown in Fig. 5.9. Under *Criterion I*, the objects partitioned into the target cluster, excluding those in the ideal object set (Γ), are considered to be the elites and are directly selected into the elite set (Λ). The objects selected into the elite set (Λ) under *Criterion I* are shown in the yellow shaded area in Fig. 5.9. In *Criterion II*, two ranking operations were used to identify the qualified objects. The first ranking is called the global ranking because the objects ranked as the top ϕ per cent of the current generation (*i.e.* ranked as the top $\phi \times n_P$ in the current generation) were identified and are displayed by the red shaded area in Fig. 5.9; here ϕ is the elite rate, a user-defined parameter to determine the number of elites during the optimisation process. The second ranking is the local ranking because the objects ranked as top ϕ percentage in the corresponding clusters (*i.e.* ranked as the top $\phi \times n_{P,k}$ in the corresponding clusters) were identified and are shown in the blue shaded area in Fig. 5.9. Accordingly, the objects identified simultaneously by the global ranking and local ranking were considered to satisfy *Criterion II* and are thus selected into the elite set (Λ), which is shown by the overlapping shaded areas in red and blue in Fig. 5.9.

To rank the objects in the current generation and in their corresponding clusters, a global ranking indicator (GRI) and a local ranking indicator (LRI) were developed. The GRI is used to identify the top $\phi \times n_P$ of the objects in the generation and is calculated by Eq. (5.20), while the LRI is used to identify the top $\phi \times n_{P,k}$ of the objects in each cluster; this is defined by the membership of the objects to the target cluster (*i.e.* u_{ik} in Eq. (5.19)).

$$\mathrm{GRI}_i = w_1\left(1 - y_{i,1}\right) + w_2\left(1 - y_{i,2}\right) \tag{5.20}$$

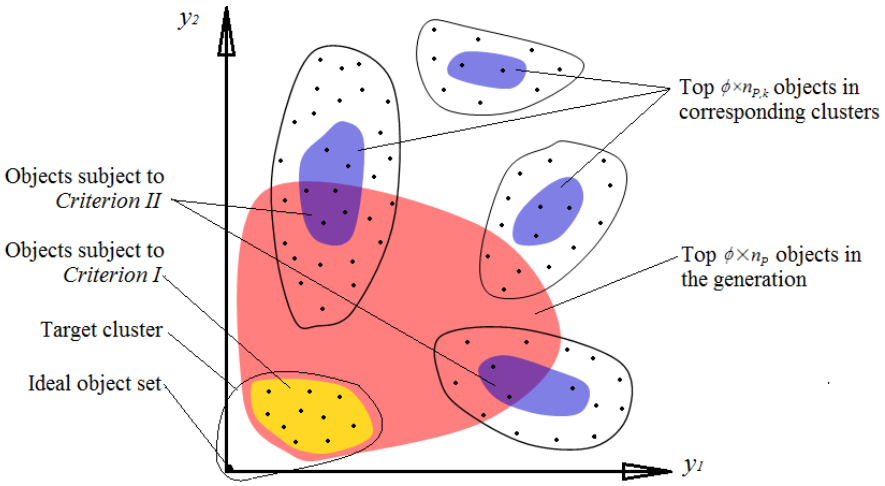

Fig. 5.9 Cluster-based election.

2) Inverse mapping and mutation

To generate a new population for the next generation, objects in the elite set (known as elites) of the current generation must be mapped inversely to identify the variable space for the next generation. Meanwhile, a mutation of the individuals which correspond to the elites is introduced to avoid the local optimal solutions. In the next generation, as shown in Fig. 5.10, (1-ς) per cent of the total population (*i.e.* (1-ς)×n_P) is generated directly by inverse mapping, while the remainder (*i.e.* $\varsigma \times n_P$) are generated from the mutation, as described in Eq. (5.21), In inverse mapping (see Fig. 5.10a), the maximal and the minimal values of the variables which correspond to the elites are adopted as the upper and lower bounds of the variable space for the next generation, so (1-ς)×n_P number of individuals are generated randomly within the space identified, as described in Eq.(5.22).

$$P^g = P_{im}^g \cup P_{mu}^g \tag{5.21}$$

$$P_{im}^g = \left\{ \vec{x}_i^g \middle| \vec{x}_i^g = \left(x_{i,1}^g, x_{i,2}^g, \dots, x_{i,v}^g \dots x_{i,n_v}^g \right), i = 1,2, \dots, n_{im} \right\},$$
$$\left(x_{i,v}^g \in \left[min\left(x_{e,v}^{g-1} \middle| \vec{x}_e^{g-1} \sim \vec{y}_e^{g-1}, \vec{y}_e^{g-1} \in \Lambda \right), max\left(x_{e,v}^{g-1} \middle| \vec{x}_e^{g-1} \sim \vec{y}_e^{g-1}, \vec{y}_e^{g-1} \in \Lambda \right) \right] \right) \tag{5.22}$$

where Λ is the elite set, superscript g indicates the g^{th} generation (*i.e.* the next generation), $\vec{x}_{e,v}^{g-1}$ is the variable vector corresponding to the e^{th} elite $\left(\vec{y}_e^{g-1}\right)$ in the elite set at the current generation where it is defined as $\vec{x}_e^{g-1} = \left(x_{e,1}^{g-1}, x_{e,2}^{g-1}, \dots, x_{i,v}^g \dots x_{e,n_v}^{g-1} \right), e = 1,2, \dots, n_e$, ς is the mutation rate, n_e is the number

of elites in the elite set, n_{im} is the number of individuals mapped inversely to the next generation; here it is equal to $(1-\varsigma)\times n_P$, and the subscripts *im* and *mu* indicate inverse mapping and mutation, respectively.

In the mutation, a sub-variable space with a rate of variance (μ) is assigned to each individual that corresponds to the elites, as shown in Fig. 5.10b, after which $\varsigma \times n_P$ number of individuals for the next generation are then distributed to the sub-variable spaces which correspond to the elites. Specifically, the number of individuals distributed to each sub-variable space is based on the weight of the GRI of the corresponding elites, as described in Eqs. (5.23) - (5.25), whereas the individual distribution of sub-variable spaces is random.

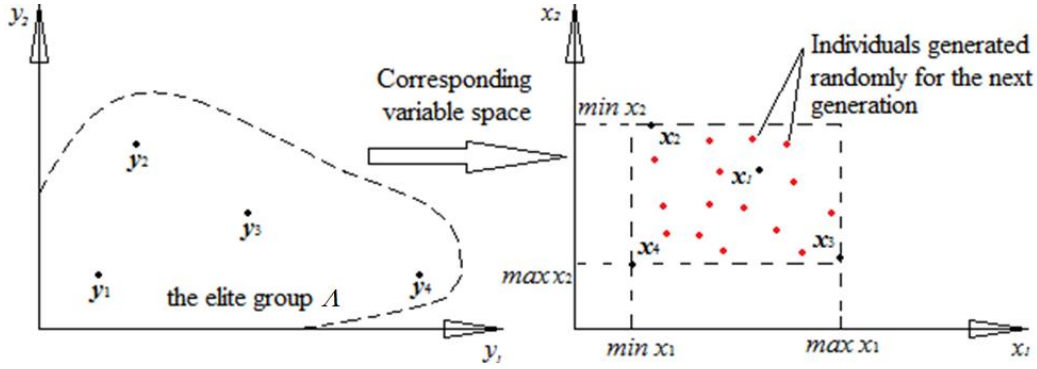

a) Inverse mapping process

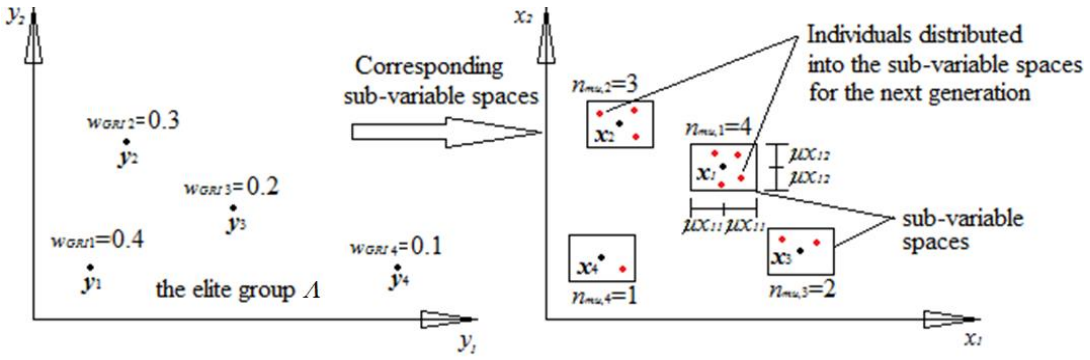

b) Mutation process

Fig. 5.10 Inverse mapping and mutation (assuming n_p=25, n_v=2, n_e=4, ς =0.4, accordingly, $n_{im,1}$=15, $n_{mu,1}$=4, $n_{mu,2}$=3, $n_{mu,3}$=2, $n_{mu,4}$=1).

$$P_{mu}^{g} = \sum_{e=1}^{n_e} P_{mu,e}^{g} \tag{5.23}$$

$$P_{mu,e}^{g} = \left\{ \vec{x}_i^{\,g} \middle| \vec{x}_i^{\,g} = \left(x_{i,1}^{g}, x_{i,2}^{g}, \dots, x_{i,v}^{g}, \dots x_{i,n_v}^{g} \right), i = 1,2,\dots,n_{mu,e} \right\},$$
$$\left(x_{i,v}^{g} \in \left[(1-\mu) x_{e,v}^{g-1}, (1+\mu) x_{e,v}^{g-1} \right] \right) \tag{5.24}$$

$$n_{mu,e} = n_P \cdot \varsigma \cdot w_{GRI_e} = n_P \cdot \varsigma \cdot \frac{GRI_e^{g-1}}{\sum_{e=1}^{n_e} GRI_e^{g-1}} \tag{5.25}$$

where w_{GRI} is the weight of *GRI*, GRI_e corresponds to the e^{th} elite in the elite set, and $n_{mu,e}$ is the number of individuals distributed in the e^{th} sub-variable space at the next generation.

5.3 Characterisation and evaluation of the PCM TES system

5.3.1 Differential Scanning Calorimetry (DSC) test

A DSC test was first carried out to determine the phase change melting range and enthalpy-temperature (*h*-*T*) relationship of PCM S21 in order to facilitate the design of charging and discharging inlet air temperatures. Fig. 5.11a) illustrates the DSC test results with a sampling mass of 1,030 mg under a scanning rate of 0.05 K/min (Gschwander 2014). The heat of fusion in the heating and cooling processes is 162.3 kJ/kg and 162.1 kJ/kg respectively. The onset temperatures for the heating and cooling are 22.27ºC and 22.06ºC, respectively, while the peak temperatures for the heating and cooling are 26.21ºC and 20.68ºC, respectively. Fig. 5.11b) shows the *h*-*T* relationship of PCM S21.

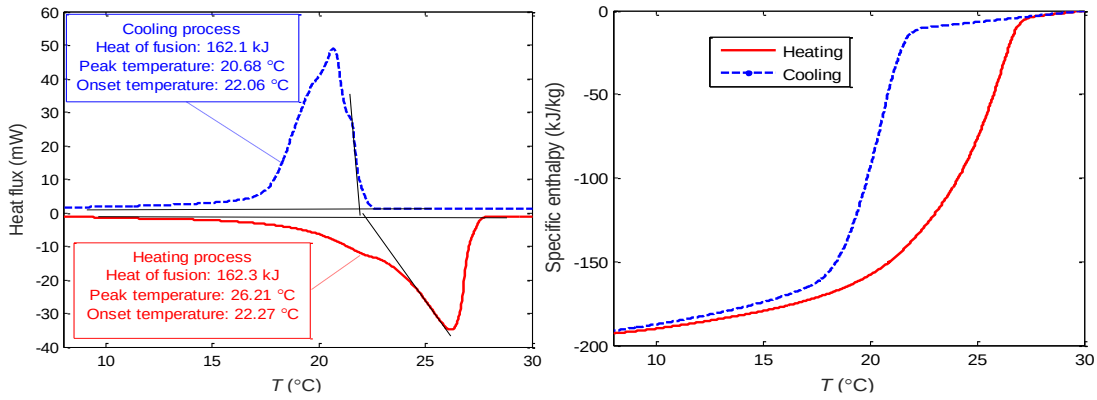

a) DSC curves b) *h*-*T* relationship

Fig. 5.11 DSC curves at the scanning rate of 0.05K/min and the *h*-*T* relationship of PCM S21.

5.3.2 PCM charging and discharging processes

To understand the heat transfer characteristics of the PCM TES unit during a phase change process, an experiment was carried out based on the test condition specified

for Trial test 1 in the Taguchi experimental plan (see Table 5.3). Before the experiment, the PCM bricks in the TES unit were cooled by the chiller and heat exchanger to around 14^{o}C, and then heated air from the PVT emulator was directed into the PCM TES unit for thermal heat charging once the temperature of the heated air from the PVT emulator reached the desired temperature. The PCM charging mode continued until the temperature of the outlet air from the PCM TES unit was close to the inlet air temperature, after which the system was switched to the PCM discharging mode *option A* (see Fig. 5.4); the thermal discharging process was complete when the temperature of the PCM bricks decreased to around 14^{o}C. Note that during the PCM charging process, temperature sensors #2 and #5 measured the air temperature at the inlet and outlet of the PCM TES unit respectively, whereas during the PCM discharging process, their measurements were opposite due to a reverse air flow direction.

The outlet air temperature from the PVT emulator, and the inlet and outlet air temperatures of the PCM TES unit are shown in Fig. 5.12; note that when charging began the air temperature at the inlet and outlet of the PCM TES unit increased rapidly. Then, the outlet air temperature (measured by temperature sensor #5) experienced a relatively small variation in the temperature gradient, which indicates that the heat was continuously charged into the PCM TES unit mainly as latent heat. Afterward, the outlet air temperature gradually increased until it was close to the 42^{o}C inlet air temperature at the end of the charging process. During the discharging process, the outlet air temperature (measured by temperature #2) from the PCM TES unit decreased and then increased slightly as the PCM supercooled, and then it decreased continuously to around 14^{o}C at the end of the discharging process.

The PCM temperatures in the two PCM bricks at both ends of the TES unit during the charging and discharging processes are shown in Fig. 5.13; note that the temperature of the PCM brick close to the outlet of the PCM TES unit (measured by temperature sensor #4) increased rapidly at the beginning of the charging process, and then increased slowly until around the 5th hour. Afterwards, the temperature increased quickly and then gradually approached the inlet air temperature (measured by temperature sensor #2) until the end of the charging process.

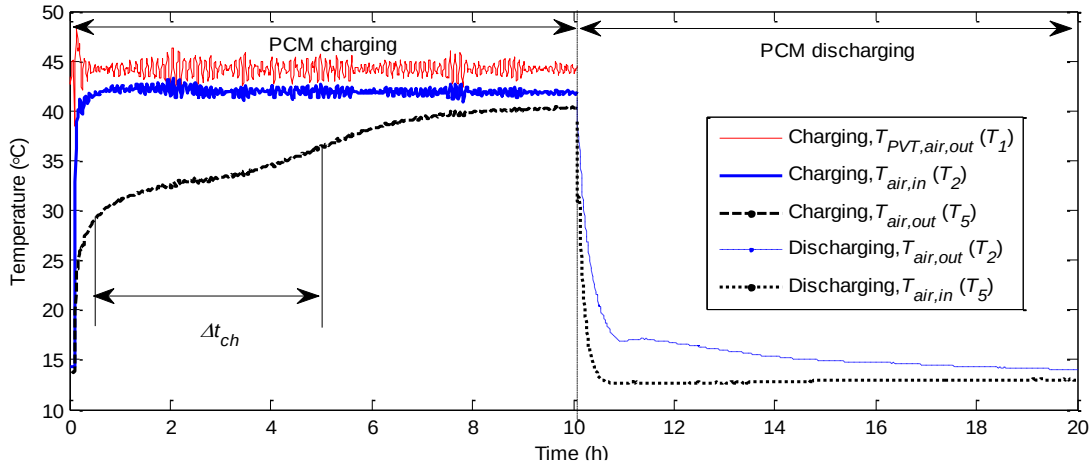

Fig. 5.12 Air temperatures at the outlet of PVT emulator (T_1), and at the inlet and outlet of the PCM TES unit (T_2 and T_5 depending on whether charging or discharging).

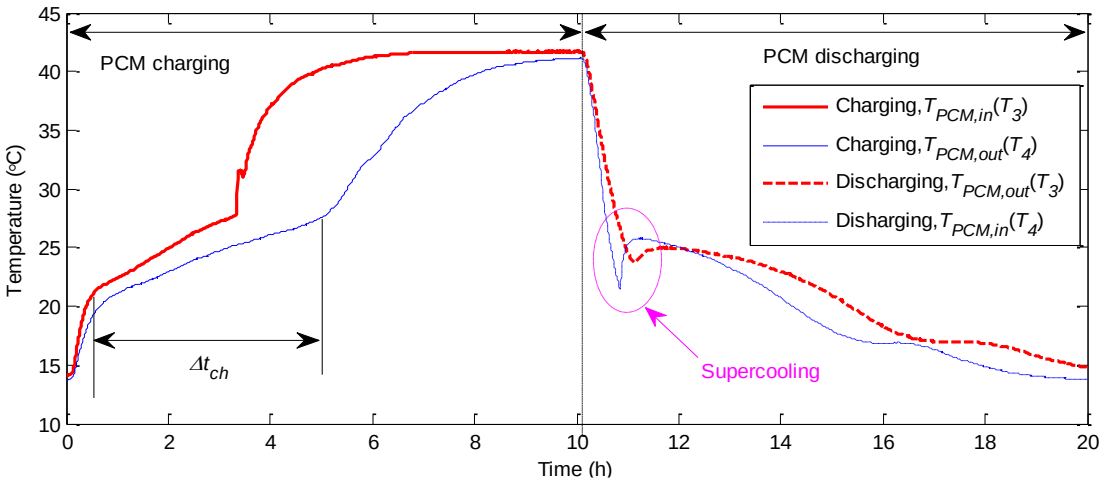

Fig. 5.13 Temperature of the PCM bricks near the inlet and outlet of the TES unit.

This data indicates that the thermal energy stored in the PCM was mainly latent heat until most of the PCM mass melted at around the 5th hour, after which the heat was stored as sensible heat in a liquid-state in the PCM. A similar phenomenon occurred in the PCM brick close to the inlet of the PCM TES unit (measured by temperature #3) during the charging process.

To provide an insight into the performance characteristics during the PCM charging, the heat transfer effectiveness of the PCM TES unit is shown in Fig. 5.14. Note that the heat transfer effectiveness decreased continuously during the charging process, and due to the phase change of the PCMs, there was a relatively small variation in the heat transfer effectiveness within the effective PCM charging time period. A relatively

small variation in the heat transfer effectiveness after the effective PCM charging time period also occurred due to the small difference in temperature between the PCM bricks and the air passing through the air channels. Since the initial PCM temperature is lower than the low limit of the PCM phase change range, the heat transfer effectiveness at the beginning of the charging process is greater than 100% due to the sensible coolness stored in the solid PCM. This phenomenon has been discussed by Tay *et al.* (2012a) and Amin *et al.* (2012).

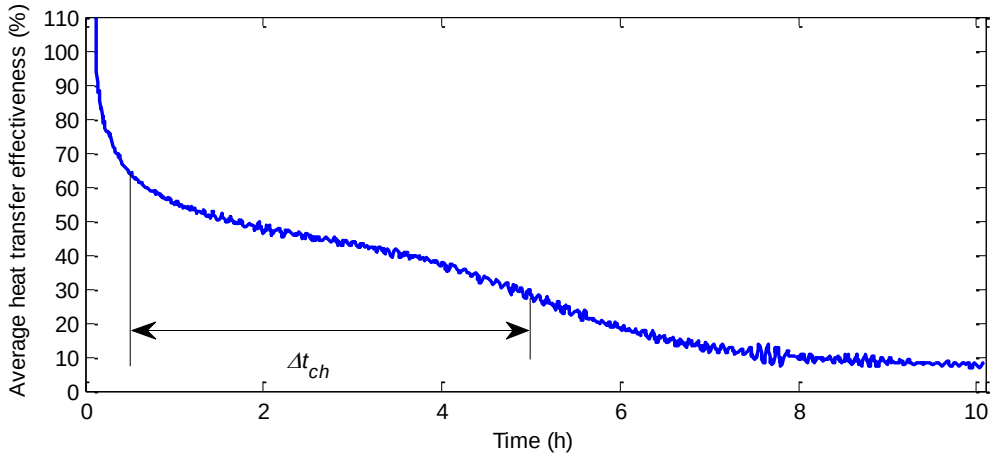

Fig. 5.14 Heat transfer effectiveness and the effective PCM charging time period.

A similar experimental process was also used for the other trial tests specified in the Taguchi experimental plan. The similar experimental process was also used for the other trial tests specified in the Taguchi experimental plan, and the detailed experimental results are provided in Fig. 5.15.

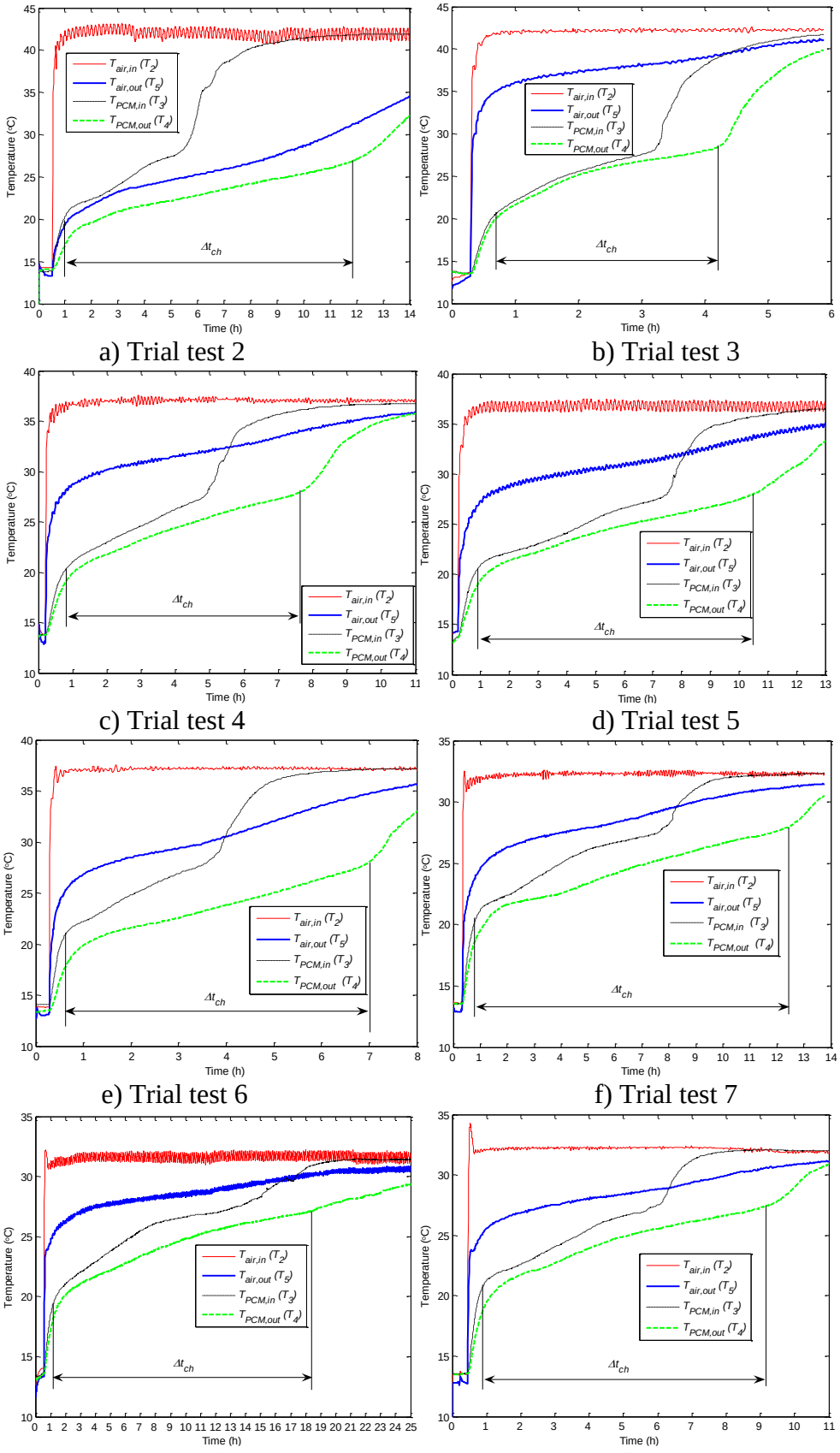

a) Trial test 2 b) Trial test 3

c) Trial test 4 d) Trial test 5

e) Trial test 6 f) Trial test 7

g) Trial test 8 h) Trial test 9

Fig. 5.15 Temperatures of the inlet and outlet air and temperatures of the PCM bricks near the inlet and outlet of the TES unit for Trial tests 2-9.

5.3.3 Taguchi experimental results and data analysis

5.3.3.1 Average heat transfer effectiveness

The average heat transfer effectiveness and corresponding *S/N* ratio of each Taguchi experiment are summarised in Table 5.4; here the average heat transfer effectiveness and *S/N* ratios of all experiments varied from 22.74% to 81.68% and from -12.87 to -1.76, respectively.

The mean average heat transfer effectiveness and *S/N* ratios for every level of the control factors are presented in Table 5.5; here the optimal combination of control factor levels can be identified by selecting the levels with the highest *S/N* ratios. The optimal values identified in terms of average heat transfer effectiveness were 42.0°C for the inlet air temperature of the PCM TES unit ($T_{a,in}$), 50.0 l/s for the air flow rate ($\dot{Q}_v$), 5 for the number of the PCM bricks in the direction of the air flow (*M*), and 5 for the number of air channels (*N*). Note that the maximum differences in the *S/N* ratio among the three different levels (*i.e.* S/N_{max}- S/N_{min}) of the air flow rate, the number of PCM bricks along the direction of air flow, and the number of air channels were much higher than that of the inlet air temperature; this indicates that the inlet air temperature had less impact on the average heat transfer effectiveness.

Table 5.4 Taguchi experimental results.

No.	$\bar{\varepsilon}_{ch}$ (%)		Δt_{ch} (h)	
	Value	*S/N*	Value	*S/N*
1	44.25	-7.08	4.53	-13.11
2	81.68	-1.76	10.84	-20.70
3	22.74	-12.87	3.51	-10.90
4	36.71	-8.70	6.86	-16.72
5	40.50	-7.85	9.58	-19.62
6	43.74	-7.18	6.39	-16.11
7	35.74	-8.94	11.67	-21.34
8	33.05	-9.62	17.20	-24.71
9	37.38	-8.55	8.30	-18.38

5.3.3.2 Effective PCM charging time

The effective PCM charging time and corresponding *S/N* ratio of each Taguchi experiment are also summarised in Table 5.4. Note that the effective PCM charging time and *S/N* ratios of all experiments ranged from 3.51 h to 17.20 h, and from -24.71

to -10.90, respectively. Table 5.6 shows the response of the effective PCM charging time, including the mean effective PCM charging time and *S/N* ratios for each level of the control factors. The number of PCM bricks in the direction of air flow was considered to be the least significant control factor in this study (*i.e. a* maximum difference in the *S/N* ratio among the three different levels of 1.315). The optimal design for the effective PCM charging time is 42.0°C for the inlet air temperature of the PCM TES unit ($T_{air,in}$), 150.0 l/s for the air flow rate ($\dot{Q}_v$), 3 for the number of PCM bricks in the direction of the air flow (*M*), and 4 for the number of air channels (*N*), respectively.

Table 5.5 Response table for the average heat transfer effectiveness.

Level	$T_{air,in}$		$\dot{Q}_v$		M		N	
	$\bar{\varepsilon}_{ch}$	*S/N*	$\bar{\varepsilon}_{ch}$	*S/N*	$\bar{\varepsilon}_{ch}$	*S/N*	$\bar{\varepsilon}_{ch}$	*S/N*
1	49.56%	-7.235	38.90%	-8.241	40.35%	-7.960	40.71%	-7.826
2	40.32%	-7.912	51.74%	-6.409	51.92%	-6.336	53.72%	-5.959
3	35.39%	-9.034	34.62%	-9.532	32.99%	-9.885	30.83%	-10.395
Optimal	Level 1		Level 2		Level 2		Level 2	
S/N_{max}-S/N_{min}	1.799		3.123		3.548		4.436	
Rank	4		3		2		1	

Table 5.6 Response table for the effective PCM charging time.

Level	$T_{air,in}$		$\dot{Q}_v$		M		N	
	Δt_{ch}(h)	*S/N*	Δt_{ch}(h)	*S/N*	Δt_{ch}(h)	*S/N*	Δt_{ch}(h)	*S/N*
1	6.29	-14.905	7.68	-17.059	9.37	-17.978	7.47	-17.039
2	7.61	-17.487	12.54	-21.678	8.67	-18.603	9.63	-19.384
3	12.39	-21.477	6.07	-15.132	8.25	-17.288	9.19	-17.446
Optimal	Level 1		Level 3		Level 3		Level 1	
S/N_{max}-S/N_{min}	6.572		6.546		1.315		2.345	
Rank	1		2		4		3	

5.4 Optimising the PCM TES unit using the bi-objective optimisation strategy with controlled elitist GA – MCDM process

The two performance models were first trained through regressions based on the results of the experiments. The coefficients of a_0-a_3 identified in Eq. (5.3) are -35.425, 8.2838, -0.37 and 0.0052 while those of b_0-b_2 in Eq. (5.7) are 20.1218, -8.3341, 1.1504, and -0.695×10^{-3}, respectively. The resulting coefficients of determination (R^2) for Eq. (5.3) and Eq. (5.7) are 0.937 and 0.9889, respectively.

5.4.1 Identifying the optimal Pareto front

In order to handle the discrete variables (*i.e.* the number of PCM bricks in the direction of air flow and the number of air channels), the bi-objective optimisation problem was carried out for each combination of the number of PCM bricks in the direction of air flow and the number of air channels (*i.e.* $M\times N$ combinations) individually. As a result, the Pareto fronts for each combination of M and N can be identified, and are presented in Fig. 5.16.

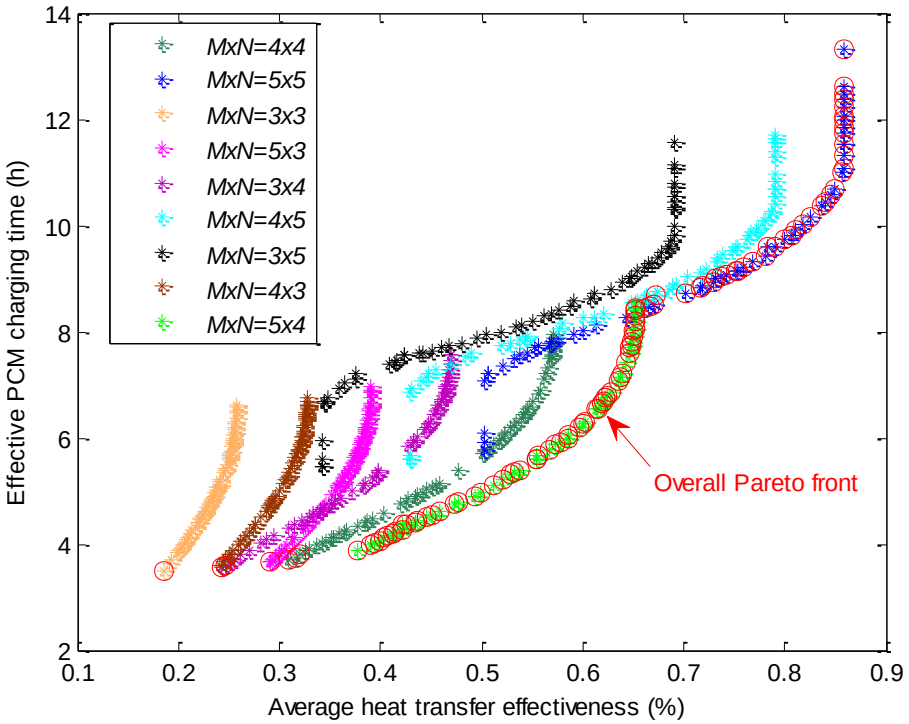

Fig. 5.16 Pareto front of the average heat transfer effectiveness and the effective PCM charging time.

The initial population of the multi-objective controlled elitist GA was set as 200 with a crossover fraction of 0.8, a uniform mutation rate of 0.01, and a Pareto fraction of 0.3. An overall Pareto front (marked as a red circle in Fig. 5.16) can be further identified among the Pareto fronts with different $M \times N$ combinations using the non-dominated sorting algorithm. The resulting overall Pareto front is mainly on the Pareto fronts of the $M \times N$ combinations of 5×5 and 5×4, although small parts of the Pareto fronts of the $M \times N$ combinations of 3×4, 4×5,4×4, 3×3 and 5×3 are also included. The overall Pareto front can facilitate the design of the PCM TES unit. For instance, an optimal design at the bottom left part of Fig. 5.16, which has a small effective PCM charging time, could be more suitable for weather conditions with short solar radiation periods, while an optimal design at the top right side of the figure with large average heat transfer effectiveness could be preferred when a high amount of solar radiation is regularly available during the daytime.

5.4.2 Multi-criteria decision-making process

The overall Pareto front indicates all the candidates for optimal designs of the PCM TES unit. Multi-criteria decision-making using the compromise ranking method (VIKOR) was then used to select the globally optimal solution(s).

5.4.2.1 Parametric study of weight (v)

The influence of the weight (v) in Eq. (5.12) on the result of MCDM was first investigated through a parametric study by varying the weight (v) from 0.0 to 1.0 with a step change of 0.1. In the parametric study, the weighting factor (w_1/w_2) of each KPI was fixed at 0.5. The corresponding ranking results using VIKOR are shown in Table 5.7. Note that the number of the PCM bricks in the direction of air flow, the number of air channels, and the inlet air temperature of the compromise solutions were around 5, 4 and 42^{o}C, respectively, under different values for the weight (v). However, the air flow rate of the compromise solutions was around 84 l/s, when the v values are high and range from 0.7 - 1.0, whereas it was around 73 l/s, respectively, under low v values from 0 - 0.4. The weight (v) of 0.5 and 0.6 act like a critical value, under which the compromise solutions include two types of air flow rates: around 84 l/s and 73 l/s, respectively. Accordingly, where $v \geq 0.7$ or $v \leq 0.4$, there are a number of compromise solutions which are close to each other, so the MCDM with two typical weight (v) of 0.8 and 0.2 were further studied.

Table 5.7 Influence of different weight (v) on the results of MCDM.

$T_{air,in}$ (°C)	$\dot{Q}_v$ (l/s)	M	N	$\bar{\varepsilon}_{ch}$ (%)	Δt_{ch} (h)	Rank of Q_j under different weight (v) values										
						0	0.1	0.2	0.3	0.4	0.5	0.6	0.7	0.8	0.9	1.0
41.78	72.66	5	4	62.46	6.80	2	2	2	2	5	9	11	15	17	20	22
41.91	82.39	5	4	59.72	6.20	13	12	11	10	10	10	2	2	3	3	4
41.87	74.17	5	4	62.07	6.68	4	4	4	4	2	1	6	9	12	16	19
41.86	91.38	5	4	56.81	5.77	21	19	19	18	17	15	15	12	7	5	3
41.95	86.31	5	4	58.48	5.99	16	14	14	13	11	11	8	3	2	1	1
41.95	81.19	5	4	60.08	6.25	12	11	10	8	8	4	1	1	1	2	5
41.80	76.93	5	4	61.32	6.53	7	7	7	7	7	5	5	6	9	12	14
41.83	74.88	5	4	61.88	6.65	5	5	5	5	4	2	7	8	14	14	18
41.85	80.89	5	4	60.17	6.29	11	10	9	9	9	8	3	4	4	6	10
41.88	88.06	5	4	57.91	5.92	17	17	16	15	14	13	12	5	5	4	2
41.83	73.35	5	4	62.28	6.75	3	3	3	3	3	6	9	11	15	18	21
41.91	71.37	5	4	62.78	6.86	1	1	1	1	1	7	10	14	18	21	24
41.82	76.35	5	4	61.48	6.56	6	6	6	6	6	3	4	7	10	13	15

* The designs with underline '_' were idntified as compromise designs with individual weight (v) based on Eq. (5.13) in VIKOR.

5.4.2.2 Results of MCDM under a weight (v) of 0.8.

A weight (v) of 0.8 was assumed to give more priority to the global performance of these alternatives in respect to the whole of the criteria. A MCDM was carried out for three cases with different weighting factors (w_1/w_2) for the average heat transfer effectiveness and effective PCM charging time. In *Case* 1, the same weighting factor (w_1/w_2) of 0.5/0.5 was assigned for the average heat transfer effectiveness and the effective PCM charging time, while different weighting factors (w_1/w_2) of 0.1/0.9 and 0.9/0.1 were assigned for the two KPIs under *Case* 2 and *Case* 3, respectively. By implementing VIKOR analysis, 5, 9, and 8 compromise solutions were identified for *Case*s 1, 2, and 3 respectively, as summarised in Table 5.8.

Table 5.8 Results of MCDM (under weigh (v) of 0.8) based on overall Pareto front

Case	Rank of Q_j	$T_{air,in}$ (°C)	$\dot{Q}_v$ (l/s)	M	N	$\bar{\varepsilon}_{ch}$ (%)	Δt_{ch} (h)
Case 1 (w_1/w_2=0.5/0.5)	1	41.95	81.19	5.00	4.00	60.08	6.25
	2	41.95	86.31	5.00	4.00	58.48	5.99
	3	41.91	82.39	5.00	4.00	59.72	6.20
	4	41.85	80.89	5.00	4.00	60.17	6.29
	5	41.88	88.06	5.00	4.00	57.91	5.92
Case 2 (w_1/w_2=0.1/0.9)	1	42.00	150.00	4.00	4.00	31.01	3.68
	2	42.00	150.00	5.00	3.00	29.03	3.65
	3	42.00	149.99	3.00	4.00	24.30	3.56
	4	41.95	149.40	5.00	3.00	29.14	3.68
	5	42.00	148.34	3.00	4.00	24.64	3.60
	6	42.00	147.94	5.00	4.00	37.70	3.87
	7	42.00	147.71	4.00	4.00	31.58	3.74
	8	41.99	149.47	3.00	3.00	18.66	3.51
	9	41.99	145.88	4.00	4.00	32.04	3.79
Case 3 (w_1/w_2=0.9/0.1)	1	41.50	50.04	5.00	5.00	85.80	11.09
	2	41.57	50.70	5.00	5.00	85.58	10.99
	3	40.74	50.00	5.00	5.00	85.81	11.33
	4	40.13	50.00	5.00	5.00	85.81	11.54
	5	41.99	52.55	5.00	5.00	84.93	10.67
	6	39.58	50.00	5.00	5.00	85.81	11.74
	7	39.27	50.00	5.00	5.00	85.81	11.86
	8	41.99	53.48	5.00	5.00	84.59	10.57

Note that the compromise solutions for each case were very close to each other, so any of them could be considered as a 'globally' optimal solution for individual cases. However, the optimal solutions identified for the resulting average heat transfer effectiveness and the effective PCM charging time for the three different cases was

almost completely different. The highest average heat transfer effectiveness of the PCM TES unit occurred in *Case* 3, followed by *Case* 1, and *Case* 2, while the lowest effective PCM charging time of the PCM TES unit occurred in *Case* 2, followed by *Case* 1, and *Case* 3. This shows the importance of selecting appropriate weighting factors (w_1/w_2) for the optimisation problem. Weighting factors (w_1/w_2) close to those used in *Case* 3 can be considered for a long solar radiation period during the daytime, while weighting factors (w_1/w_2) such as those used in *Case* 2, which can reduce the effective PCM charging time by sacrificing the average heat transfer effectiveness, can be used for a short solar radiation period during the daytime.

5.4.2.3 Comparison between different designs under a weight (v) of 0.8

An optimal design was obtained by averaging the values of the optimisation variables of the five compromise designs which resulted from the bi-objective optimisation using the controlled elitist GA - MCDM for *Case* 1. To present the benefits of the optimal design (with a weighting factor (w_1/w_2) of 0.5), it was further compared to the baseline case (*i.e.* Taguchi trial test 1) and two near-optimal designs identified in Section 5.3.3 using the Taguchi method for individual KPIs. The two near-optimal designs that were achieved through *S/N* ratio analysis can only be 'near optimal' for the average heat transfer effectiveness and the effective PCM charging time, respectively. These four design options were ranked further by using the scalar quantity L_{com}-*metric* in VIKOR under a weight (v) of 0.8, as presented in Table 5.9.

Table 5.9 Ranking results for different designs (under weight (v) of 0.8).

Design	Rank of Q_j	$T_{air,in}$ (°C)	$\dot{Q}_v$ (l/s)	M	N	$\bar{\varepsilon}_{ch}$ (%)	Δt_{ch} (h)
Baseline case	2	42.0	102.3	4	4	44.25	4.53
Taguchi design identified based on the average heat transfer effectiveness	3	42.0	50.0	5	5	85.81	10.94
Taguchi design identified based on the effective PCM charging time	4	42.0	150.0	3	4	24.30	3.56
Optimal design under *Case* 1	1	42.0	83.8	5	4	59.29	6.11

Note here that the optimal design identified by the bi-objective optimisation strategy with the controlled elitist GA - MCDM was the best one with an average heat transfer effectiveness of 59.29% and an effective PCM charging time of 6.11 h, followed by the baseline design. Moreover, the optimal design determined using bi-objective optimisation outperformed those identified using the Taguchi method.

5.4.2.4 Results and discussions of MCDM under weight (v) of 0.2

An MCDM under a weight (v) of 0.2 was also performed for three cases with the following different weighting factors (w_1/w_2): 0.5/0.5 (*Case* 4), 0.1/0.9 (*Case* 5) and 0.9/0.1 (*Case* 6). A total of 4, 12, and 12 compromise solutions were identified for *Case*s 4, 5, and 6 respectively, as summarised in Table 5.10.

Table 5.10 Results of MCDM (under weight (v) of 0.2) based on overall Pareto front.

Case	Rank of Q_j	$T_{air,in}$ (°C)	$\dot{Q}_v$ (l/s)	M	N	$\bar{\varepsilon}_{ch}$ (%)	Δt_{ch} (h)
Case 4 (w_1/w_2=0.5/0.5)	1	41.91	71.37	5	4	62.78	6.86
	2	41.78	72.66	5	4	62.46	6.80
	3	41.83	73.35	5	4	62.28	6.75
	4	41.87	74.17	5	4	62.07	6.68
Case 5 (w_1/w_2=0.1/0.9)	1	42.00	147.94	5	4	37.70	3.87
	2	42.00	140.42	5	4	39.94	4.07
	3	41.95	143.54	5	4	38.99	4.00
	4	41.94	142.38	5	4	39.34	4.03
	5	42.00	136.42	5	4	41.19	4.18
	6	41.97	138.02	5	4	40.69	4.14
	7	41.93	135.65	5	4	41.44	4.22
	8	41.88	139.06	5	4	40.36	4.14
	9	41.93	133.53	5	4	42.13	4.28
	10	42.00	150.00	5	4	31.01	3.68
	11	42.00	147.71	5	4	31.58	3.74
	12	41.99	145.88	5	4	32.04	3.79
Case 6 (w_1/w_2=0.9/0.1)	1	41.99	53.48	5	5	84.59	10.57
	2	41.99	52.55	5	5	84.93	10.67
	3	41.98	54.85	5	5	84.06	10.44
	4	41.96	55.86	5	5	83.65	10.35
	5	41.82	58.36	5	5	82.61	10.17
	6	41.57	50.70	5	5	85.58	10.99
	7	41.92	60.14	5	5	81.82	10.00
	8	41.50	50.04	5	5	85.80	11.09
	9	41.78	61.74	5	5	81.09	9.91
	10	40.74	50.00	5	5	85.81	11.33
	11	41.90	62.57	5	5	80.69	9.82
	12	40.13	50.00	5	5	85.81	11.54

Note that the compromise solutions for *Case*s 4, 5 and 6 are very close, respectively. Corresponding to different values of the weighting factors (w_1/w_2), the highest average heat transfer effectiveness of the PCM TES unit occurred in *Case* 6, followed by *Case* 4 and *Case* 5, while the shortest effective PCM charging time of the PCM TES unit occurred in *Case* 5, followed by *Case* 4, and *Case* 6.

An optimal design was derived by averaging the optimisation variables of the four compromise designs identified in *Case* 4. To present the benefit of optimal design (with a weighting factor (w_1/w_2) of 0.5), it was also compared to the baseline case and two near-optimal designs identified using the Taguchi method. A further ranking of these four design options using scalar quantity L_{com}-*metric* in VIKOR under a weight (v) of 0.2 are presented in Table 5.11. Note here that the optimal design identified by the bi-objective optimisation strategy with the controlled elitist GA -MCDM is the best one with an average heat transfer effectiveness of 62.40% and an effective PCM charging time of 6.73 h.

Table 5.11 Ranking results for different designs (under weight (v) of 0.2).

Design	Rank of Q_i	$T_{air,in}$ (°C)	$\dot{Q}_v$ (l/s)	M	N	$\bar{\varepsilon}_{ch}$ (%)	Δt_{ch} (h)
Baseline design	2	42.0	100.0	4.0	4.0	44.25	4.53
Taguchi design identified based on average heat transfer effectiveness	3	42.0	50.0	5.0	5.0	85.81	10.94
Taguchi design identified based on effective PCM charging time	4	42.0	150.0	3.0	4.0	24.30	3.56
Optimal design under *Case* 4	1	42.0	72.9	5.0	4.0	62.40	6.73

The results in Section 5.4.2.3 and Section 5.4.2.5 show that the optimal design determined using the bi-objective optimisation strategy with the controlled elitist GA - MCDM outperformed the 'near optimal' ones identified using the Taguchi method, even though the weights (v) are different.

5.4.2.5 Confirmation experiment for the optimal design

To validate the performance of the PCM TES unit by using the compromise optimal design identified, a confirmation experiment was carried out and the results were compared with the optimal designs identified by the bi-objective optimisation strategy

with controlled elitist GA – MCDM process (under the weights (v) of 0.8 and 0.2, respectively). The validation result showed that the resulting average heat transfer effectiveness and the effective PCM charging time from the confirmation test were 52.76% and 6.68 h, respectively. It is close to that the average heat transfer effectiveness of 59.29% and the effective PCM charging time of 6.11 h identified by using the optimal design identified by the multi-objective optimisation strategy with controlled elitist GA – MCDM process under the weight (v) of 0.8, as well as that of 62.4% and 6.73 h under the weight (v) of 0.2

Based on the above discussion, it can be concluded that the multi-objective optimisation strategy using the controlled elitist GA and a multi-criteria decision-making process can be used to identify the optimal design of the bi-objective optimisation problem for the PCM TES unit for solar air systems.

5.5 Optimising the PCM TES unit using the fuzzy clustering-based bi-objective optimisation strategy

5.5.1 Optimisation process and results

The bi-objective optimisation problem described in Section 5.2.4 was also solved using the proposed fuzzy clustering-based bi-objective optimisation strategy where $\bar{\varepsilon}_{ch}$ and Δt_{ch} are used as the optimisation objectives $f_1(\vec{x})$ and $f_2(\vec{x})$, respectively. The parameters used in this optimisation are summarised in Table 5.12. These parameters were obtained through trial tests which were able to achieve decent optimisation results, in which, the trial test for the number of cluster numbers (n_k) in the fuzzy clustering-based bi-objective optimisation was shown in Fig. 5.17.

Table 5.12 Parameters used to implement the fuzzy clustering-based strategy.

Parameter	Value
Generation	100
Elite rate (ϕ)	0.1
Mutation rate (ς)	0.05
Population size (n_P)	200
Duplicated number of ideal objects (n_{io})	100
Number of cluster (n_k)	5
Rate of variance (μ)	0.05

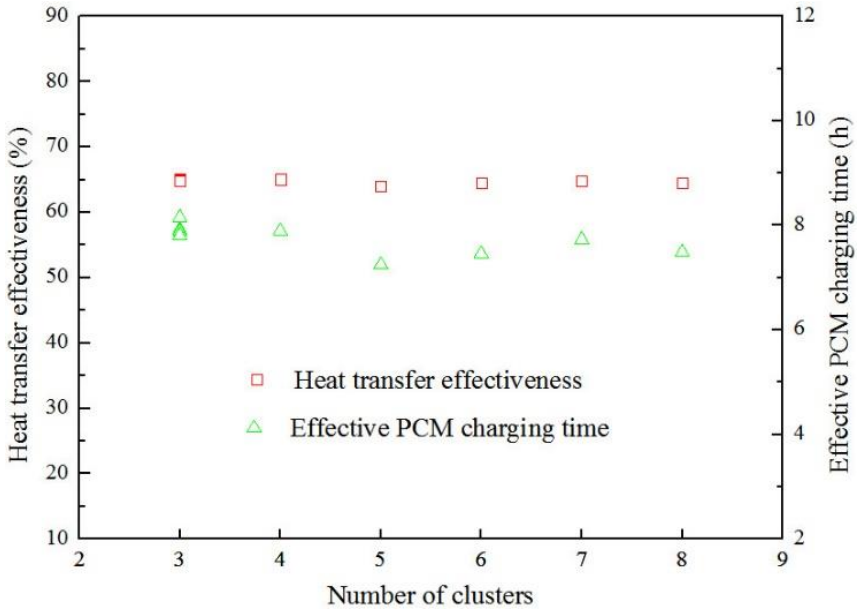

Fig. 5.17 The resulting top 5 optimal solutions under different cluster numbers (n_k).

The optimisation process with the same weighting factor (w_1/w_2) of 0.5 for the two objectives is shown in Fig. 5.18, where combinations of the objective responses were dispersed widely over the object space and partitioned into 5 clusters in Generation 1. In Generation 3, the combination of objective responses clearly narrowed, while the corresponding objects formed a special configuration in which five clusters can clearly be identified. For instance, Cluster 2 contained a combination of objective responses with a high value of the objective 1 $f_1(\vec{x})$ (*i.e.* the average heat transfer effectiveness) and low value of objective 2 $f_2(\vec{x})$ (*i.e.* the effective PCM charging time), while Cluster 5 contained a combination of objective responses with a high value for objective 2 and a low value for objective 1. In Generation 10, the combination of objective responses further narrowed. Generally, from Generation 1 to Generation 100, the dispersion of the combination of objective responses gradually narrowed, however, there is no significant variation in the ranges of a combination of objective responses after Generation 50, which indicates the optimisation process has converged. The same optimisation process was also carried out under weighting factors (w_1/w_2) of 0.9/0.1 and 0.1/0.9, respectively.

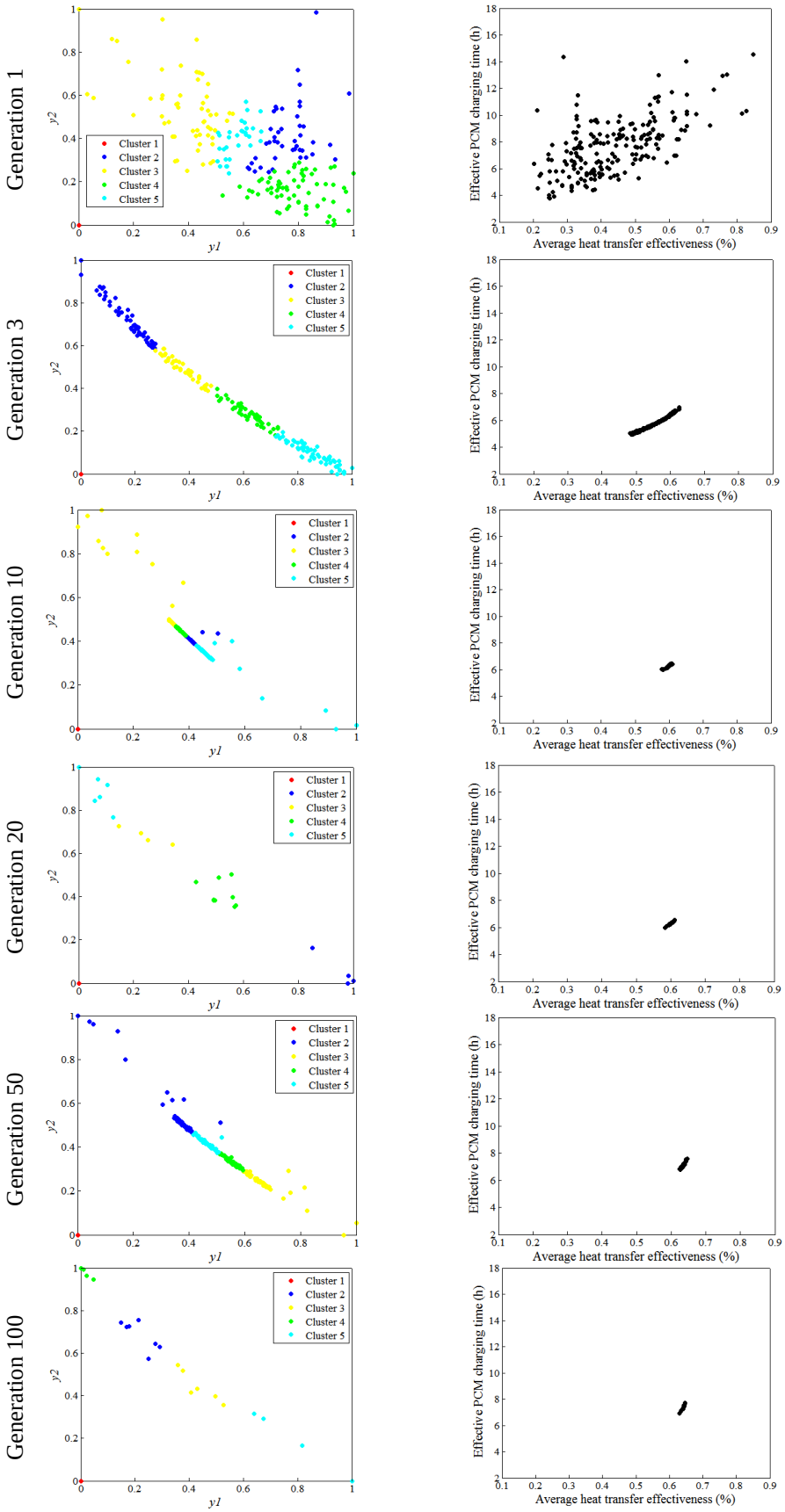

Fig. 5.18 Optimistion process under weighting factors *(w_1/w_2)* of 0.5/0.5.

The best five solutions with different weighting factors (w_1/w_2) are given in Table 5.13; note that when using the fuzzy clustering-based optimisation strategy the top five solutions are so close that they seem identical. According to the optimisation results, an optimal design can be identified for each combination of weighting factors (w_1/w_2): 64.02% and 7.25 h under the weighting factors (w_1/w_2) of 0.5/0.5, 18.6% and 3.49 h under the weighting factors (w_1/w_2) of 0.1/0.9, and 85.81% and 10.94 h under the weighting factors (w_1/w_2) of 0.9/0.1, respectively.

Table 5.13 The optimisation results with different weighting factors (w_1/w_2).

w_1/w_2	Optimal designs identified by using the FCBO algorithm					
	$T_{air,in}$ (°C)	$\dot{Q}_v$ (l/s)	M	N	$\bar{\varepsilon}_{ch}$ (%)	Δt_{ch} (h)
0.5/0.5	42.00	65.61	5	4	64.02	7.25
	42.00	65.61	5	4	64.02	7.25
	42.00	65.61	5	4	64.02	7.25
	42.00	65.61	5	4	64.02	7.25
	42.00	65.61	5	4	64.02	7.25
0.1/0.9	42.00	149.97	3	3	18.60	3.49
	42.00	149.97	3	3	18.60	3.49
	42.00	149.97	3	3	18.60	3.49
	42.00	149.97	3	3	18.60	3.49
	42.00	149.97	3	3	18.60	3.49
0.9/0.1	41.99	50.01	5	5	85.81	10.94
	41.99	50.01	5	5	85.81	10.94
	41.99	50.01	5	5	85.81	10.94
	41.99	50.01	5	5	85.81	10.94
	41.99	50.01	5	5	85.81	10.94

5.5.2. Comparison of the optimal results between the two optimisation strategies

The results from the optimisation using the fuzzy clustering-based strategy were compared to the bi-objective optimisation strategy using the controlled elitist GA – MCDM process. Unlike the bi-objective optimisation strategy using the controlled elitist GA – MCDM process, the weighting factors for each optimisation objective are embodied into the optimisation process when implementing the fuzzy clustering-based bi-objective optimisation strategy. As a consequence, the fuzzy clustering-based bi-objective optimisation process could identify an optimal solution directly, rather than identifying an optimal Pareto front before identifying the compromise optimal solutions.

Fig. 5.19 presents the three optimal solutions identified under different combinations of weighting factors (w_1/w_2) of 0.5/0.5, 0.1/0.9 and 0.9/0.1 using the fuzzy clustering-based bi-objective optimisation strategy and the controlled elitist GA – MCDM strategy with different weight (v), together with the optimal Pareto front identified by the controlled elitist GA.

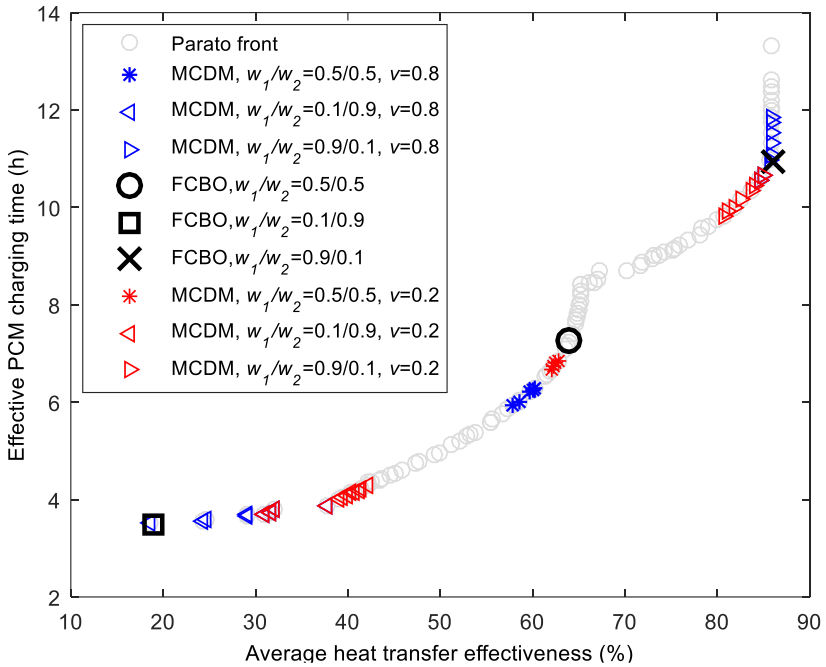

Fig. 5.19 Comparison between the optimisation results using the fuzzy clustering-based bi-objective optimisation strategy and using the controlled elitist GA – MCDM strategy.

It can be seen from Fig. 5.19 that the optimal solutions identified using the fuzzy clustering-based bi-objective optimisation strategy located on the Pareto front. Furthermore, the optimal solutions with three weighting factors (*i.e.* 0.9/0.1, 0.5/0.5 and 0.1/0.9) identified by the fuzzy clustering-based bi-objective optimisation strategy were close to the optimal solutions identified by identified using the bi-objective optimisation strategy using the control elitist GA – MCDM strategy. This process demonstrated that both strategies can identify optimal solutions to the optimisation problem under the given weighting factors (w_1/w_2).

It is noteworthy to mention that deviation existed between the optimal solutions identified by the two optimisation strategies. This is due to the fact that the measures which represent the distances between potential optimal solutions and ideal optimums,

are different in the two methods. In the control elitist GA and the MCDM process, three scalar quantities (*i.e.* S_j, R_j and Q_j, known as L_1-*metric*, L_∞-*metric* and L_{com}-*metric*, respectively) with the weighting factor (v) were used, while the global ranking indicator (GRI) was employed in the fuzzy clustering-based bi-objective optimisation strategy. It is also worthwhile to mention that the optimal solutions identified by the fuzzy clustering-based bi-objective optimisation could still be near optimal solutions. The parameters of the fuzzy clustering-based bi-objective optimisation strategy could be different in different studies, but they could be identified through trial tests.

5.6 Summary

This chapter presented an experimental study and a bi-objective optimisation of a centralised PCM TES system with integrated air-based solar PVT collectors. The performance of the PCM TES unit during the charging process was evaluated by developing and using two key performance indicators (KPIs), the average heat transfer effectiveness and the effective PCM charging time. The effects of the following four design variables were investigated through a range of Taguchi experiments: the inlet air temperature of the PCM TES unit; the air flow rate; the number of PCM bricks in the direction of air flow, and the number of air channels. Two single-objective near-optimal designs were then identified using signal-to-noise (*S/N*) ratio analysis for each KPI. Two bi-objective optimisation strategies, one using the controlled elitist Genetic Algorithm (GA) – multi-criteria decision-making (MCDM) process and the other using fuzzy clustering, were used to identify the optimal designs of the PCM TES system. The optimisation results of the two bi-objective optimisation strategies were then compared to each other.

The experimental results showed that the performance of the PCM TES system varied with variations in the design parameters. Through *S/N* ratio analysis of Taguchi experimental data, when using the near-optimal design that was identified based on the KPI of the average heat transfer effectiveness, the average heat transfer effectiveness and the effective PCM charging time were 85.30% and 9.17 hours, respectively, as opposed to 23.30% and 4.52 hours respectively, when using the KPI of the effective PCM charging time as the objective. This difference shows the importance of considering the trade-off between contradictory KPIs to achieve the overall performance enhancement of PCM TES systems. Under the weight (v) of 0.8,

the average heat transfer effectiveness and effective PCM charging time using the optimal design identified by the bi-objective optimisation strategy using the controlled elitist GA – MCDM process with weighting factor (w_1/w_2) of 0.5/0.5 were 59.29% and 6.11 hours, respectively; while that under the weight (v) of 0.2 were 62.4% and 6.73 hours, respectively. Both of optimal designs under different weight (v) outperformed a baseline case and the two near-optimal designs in terms of scalar quantity L_{com}-*metric* in the compromise ranking method VIKOR. These results showed that a bi-objective optimisation which considered two different objectives can achieve a more reasonable solution than the single-objective optimisation using the Taguchi method. The optimisation results identified by the fuzzy clustering-based bi-objective optimisation strategy were close to the compromise optimal solutions identified by the bi-optimisation strategy using the controlled elitist GA - MCDM process. The average heat transfer effectiveness and the effective PCM charging time using the optimal design identified by the fuzzy clustering-based bi-objective optimisation strategy with weighting factors (w_1/w_2) of 0.5/0.5 were 64.02% and 7.25 hours respectively (close to the optimisation results using the controlled elitist GA - MCDM process under the weight (v) of 0.2). These results indicated that the proposed fuzzy clustering-based bi-objective optimisation strategy can also identify the optimal solution of bi-objective optimisation problems. It also provided an innovative bi-objective optimisation which can identify optimal designs directly rather than identifying the optimal Pareto front followed by a MCDM process.

.

Chapter 6 Development and Design Optimisation of a Heat Pump System with Integrated PVT Collectors and PCM layers Laminated into the Building Ceiling

The literature review carried out in Chapter 2 showed that integrating the phase change materials (PCMs) with photovoltaic thermal (PVT) collectors appears to be a promising solution to reduce the energy consumption of heating, ventilation and air conditioning (HVAC) systems while maintaining an acceptable indoor thermal comfort. Chapters 3 and 4 also showed that integrating PCMs and PVT collectors into building envelopes for space heating could significantly enhance the building thermal performance, however, since the performance of PVT collectors and PCMs rely on the weather conditions, integrating them with traditional air conditioning systems (*e.g.* air source heat pump) is a better and more reliable way to maintain stable indoor thermal comfort.

Moreover, the passive and active utilisations of PCMs in Chapters 3 and 5 revealed different characteristics because the charging and discharging processes of passive PCM systems are highly dependent on the temperature difference between indoor and outdoor conditions, whereas that of active PCM systems can be controlled via heat transfer fluids to enable the PCM TES units to respond rapidly to the load variation. A combination of these two characteristics can lead to a new concept of thermal energy storage using PCMs.

This chapter presents the development, evaluation and design optimisation of an air source heat pump system with integrated PVT collectors and PCM layers laminated into the building ceiling for space air conditioning. The system was named as "PVT-PCM enhanced heat pump (HP) system" hereafter. These PVT collectors produce electricity and low grade thermal energy simultaneously, whereas two PCM layers with an air channel between them are integrated into the ceiling to increase the local thermal mass and also acts as a centralised thermal energy storage (TES) unit. This system was evaluated through computer simulations based on an Australian house, and the design optimisation was developed to maximise the net generation of electricity using a hybrid Particle Swarm Optimisation and Hooke-Jeeves pattern search (PSO-HJ) technique.

This chapter is as follows: Section 6.1 introduces the development of the building integrated PVT-PCM enhanced HP system. Section 6.2 presents the research methodology used in this chapter. Section 6.3 shows how the key system components were modelled. The results of the evaluation and design optimisation of this system are presented in Sections 6.4 and 6.5 respectively, and the key findings are summarised in Section 6.6.

6.1 Development of the building integrated PVT-PCM enhanced HP system

Fig. 6.1 is a schematic of the proposed building integrated PVT-PCM enhanced HP system for space air conditioning. This system consists of PVT collectors, two layers of PCM in ceiling, a fan for the PVT air channel (called a PVT fan hereafter), a fan for the ceiling duct in which the PCMs are installed (called a PCM fan hereafter), and an air source heat pump. The two layers of PCM with an air channel between them were integrated into the ceiling to increase the local thermal mass and serve as a centralised TES unit that temporarily stores the thermal energy collected from the PVT collectors for later use in indoor space heating in winter.

This system can operate with different modes depending on the weather conditions, the thermal energy stored in the PCM and the indoor heating demand is via ON/OFF control of the dampers of D1-D8, the PVT fan, the PCM fan and the air source heat pump system. As summarised in Table 6.1, this system can operate with five modes: the PCM charging mode, the PVT exhausting mode, the PCM discharging mode, the PVT direct heating mode, and the normal air conditioning mode.

During the daytime, hot air heated by the PVT collectors can be directed into the PCM TES unit for thermal energy charging by switching on the PVT fan and opening dampers D2 and D3, or it can be exhausted directly by switching on the PVT fan and opening damper D1. The thermal energy stored in the PCMs can be used to facilitate the space heating through pre-heating the return air for the indoor unit of the air source heat pump by switching on the PCM fan and opening dampers D4, D6, and D8, or it could be used directly for space heating by switching on the PCM fan and opening dampers D4, D6, and D7. In the normal air conditioning mode, only the air source heat pump will be used to maintain indoor thermal comfort by opening dampers D5 and D8. Note that the PVT direct heating mode was not considered in this study and is not

shown in Fig 6.1 because the direct use of hot air from the PVT collectors for space heating may cause overheating, however, the direct heating mode could be considered under some cold weather conditions. Moreover, the system was investigated under winter heating conditions because the main benefit of using low grade thermal energy derived from the PVT collectors is for space heating, even though the night time radiative cooling effect of PVT collectors in summer could also improve the energy performance of the proposed system.

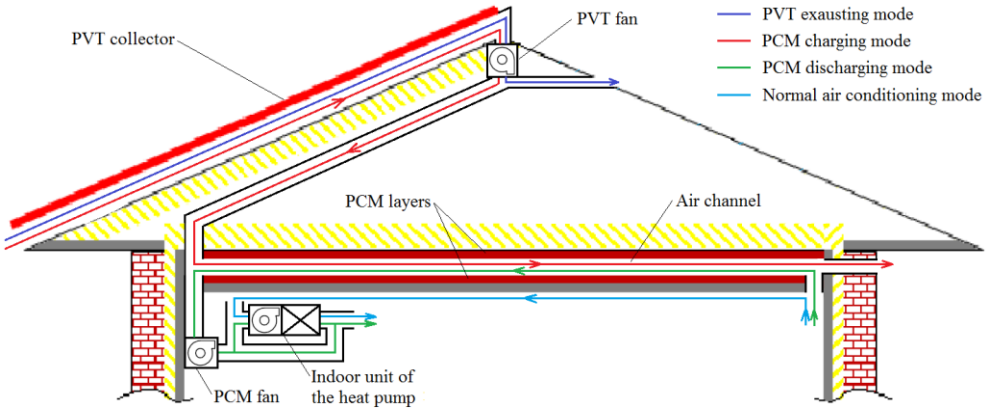

a) Schematic of the proposed system

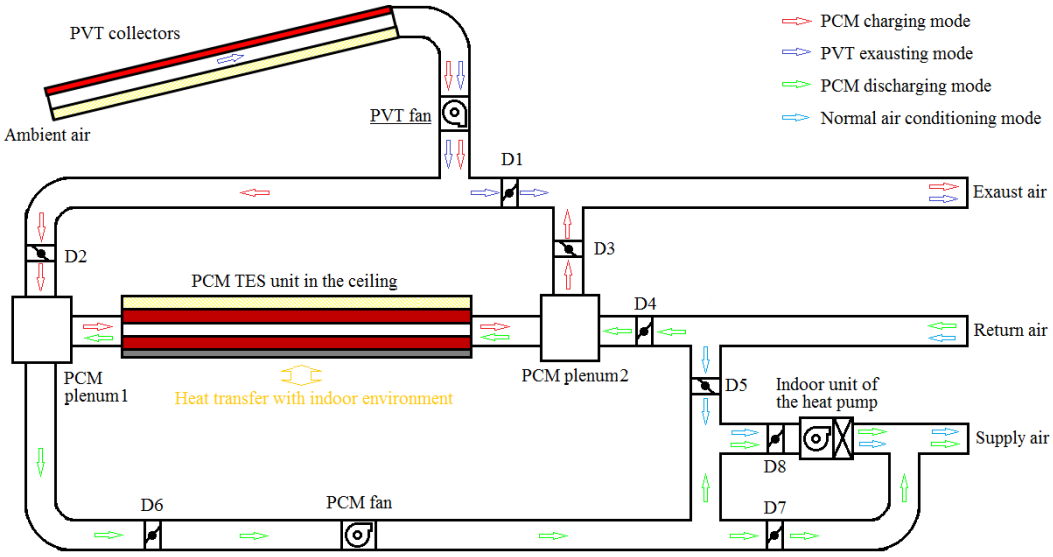

b) System operation modes

Fig. 6.1 Schematic of the building integrated PVT-PCM enhanced HP system.

Table 6.1 Summary of the system operation modes.

Operation mode	ON/OFF status of dampers, fans and heat pump										
	D1	D2	D3	D4	D5	D6	D7	D8	PCM fan	PVT fan	Heat pump
PCM charging	OFF	ON	ON	OFF	-*	OFF	-	-	OFF	ON	-
PVT exhausting	ON	OFF	OFF	-	-	-	-	-	-	ON	-
PCM discharging	-	OFF	OFF	ON	OFF	ON	ON/OFF**	OFF/ON**	ON	-	OFF/ON**
PVT direct heating	OFF	ON	OFF	OFF	OFF	ON	ON	OFF	ON	ON	OFF
Normal air conditioning	-	-	-	OFF	ON	OFF	OFF	ON	OFF	-	ON

* Symbol '-' indicates that the ON/OFF status is not related to the operation mode;

** If the PCM discharging mode can maintain the indoor air temperature above the thermostat setting, the heat pump is switched off, damper D8 is OFF and damper D7 is ON; otherwise, the heat pump will be used, damper D8 is ON and damper D7 is OFF.

The performance of this system was simulated based on one of the 'typical' Australian dwellings considered as representing Australian residential building stock since 5 and 6 star regulations were introduced (Wong 2013; Australian Government Department of Industry 2013). This house is a single storey dwelling with three bedrooms, as shown in Fig. 6.2.

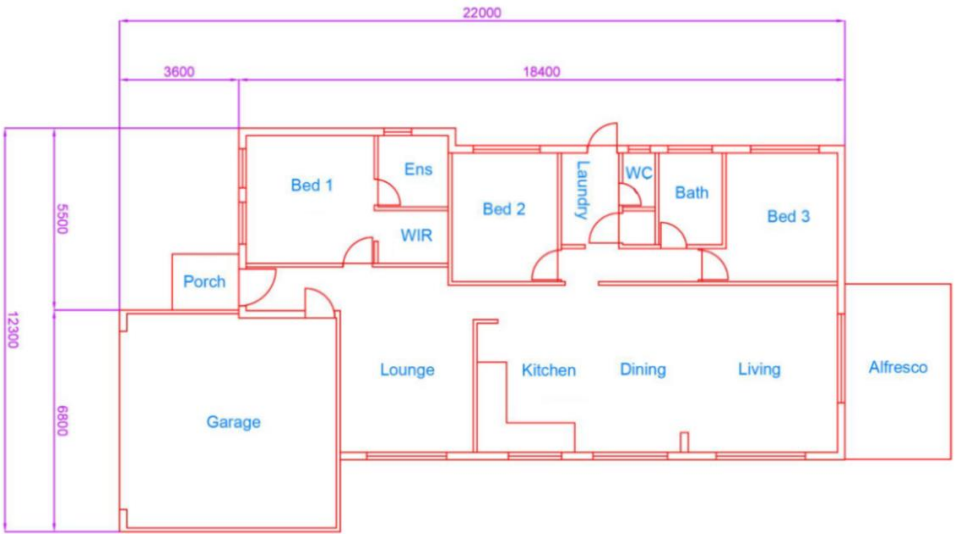

Fig. 6.2 Floor plan of the house of concern (Wong 2013).

The specifications of the major house envelopes are summarised in Table 6.2. The total air-conditioned area is 150 m^2 excluding the garage, bathroom, washroom, and laundry. The air-conditioned area can be divided into the living space (including kitchen, dining room, living room and lounge) with a total area of 92.9 m^2 and the sleeping spaces (*i.e.* the three bedrooms) with the areas of 26.88 m^2, 14.28 m^2, and 15.94 m^2 for bedroom 1, bedroom 2 and bedroom 3, respectively. The living space of the house is assumed to face north, while the bedrooms face south. The angle of the roof is 22.5°.

Table 6.2 Specification of building envelopes.

Envelope	Materials used
External wall	12 mm plasterboard
	Glass wool insulation with a *R*-value of 1.35 m^2K/W
	30 mm air gap
	110 mm brick
Normal ceiling	12 mm plasterboard
	Glass wool insulation with a *R*-value of 3.0 m^2K/W
Floor	Slab-on-ground: 100 mm concrete slab

6.2 Methodology

6.2.1 Outline of the methodology

The overall research methodology is shown in Fig. 6.3. The performance of the building integrated PVT-PCM enhanced HP system but without optimisation (called a *PVT-PCM baseline* case hereafter) was evaluated first and then compared to the house using a conventional air source heat pump system only (called a *baseline case* hereafter). Afterwards, a series of trial tests were designed using Taguchi method, based on which the the influence of the design variables and their interactions to the performance of the system was further analysed via *S/N* ratio analysis and analysis of variance (ANOVA). The optimal value of discrete variable(s) (*i.e.* PCM type) was directly determined based on results from the Taguchi analysis. Meanwhile, the objective function was developed and the continuous optimisation variables and their constraints (*i.e.* search ranges) were identified to formulate the optimisation problem. The hybrid PSO-HJ algorithm was then used as an optimisation tool to solve the optimisation problem. Lastly, the optimal design (called an *optimal PVT-PCM* case hereafter) was assessed by comparing it to the *baseline* case and the *PVT-PCM baseline* case without optimisation.

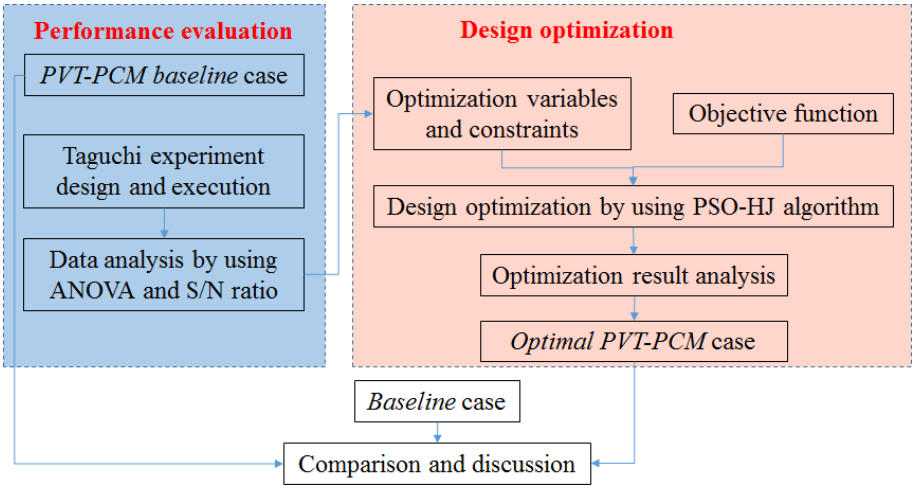

Fig. 6.3 The overall research methodology used in this study.

6.2.2 Hybrid Particle Swarm Optimisation and Hooke-Jeeves pattern search algorithm

In this study, the hybrid Particle Swarm Optimisation and Hooke-Jeeves pattern search algorithm implemented in GenOpt (Wetter 2011) was used to identify the optimal solution of the optimisation problem. GenOpt is an optimisation program to minimise a cost function that is evaluated by an external simulation program (for instance TRNSYS) (Wetter 2011), and contains various optimisation algorithms. In the hybrid PSO-HJ algorithm implemented in GenOpt, the Particle Swarm Optimization (PSO) was first used to identify a near optimal region, and then the Hooke-Jeeves (HJ) pattern search was initialised and used to search for optimal solutions within the near optimal region identified by the PSO.

Particle Swarm Optimisation is a primary population-based search approach that is commonly used in building optimisation studies (Wetter 2011). In the PSO, the velocity of every particle (*i.e.* individuals in the swarm) is updated by its current position relative to the positions of its personal best and neighbourhood best solutions, such that the individual accelerates towards both potential optimal positions from generation to generation (Futrell *et al.* 2015). Detailed steps for implementing the PSO are reported in Kennedy *et al.* (2001) and Clerc and Kennedy (2002).

The Hooke-Jeeves pattern search algorithm is one of the generalised pattern search methods, and in the HJ method there are two types of searches: exploratory search and pattern search (Rios-Coelho *et al.* 2010). Exploratory search is used to identify the direction of the objective optimisation, while pattern search uses the optimisation direction identified to accelerate the search process (Somasundaram and Trabia 2011). The step size of the exploratory search is slowly reduced until the predefined minimal step size is reached when a better solution cannot be found during the optimisation process. The general steps of using the HJ algorithm to determine the optimal solutions can be found in Hooke and Jeeves (1961).

Through the combination of the population based PSO algorithm which boasts its reliability, and the HJ pattern search algorithm which boasts its local optimum search efficiency, the hybrid PSO-HJ algorithm can identify a more reliable optimal solution with a reasonable computational cost.

6.3 System modelling

System modelling includes the modelling of the building, the PVT collectors, the PCM TES unit and the heat pump, and the coupling among these models. The logic connections of these main components in TRNSYS are shown in Fig. 6.4.

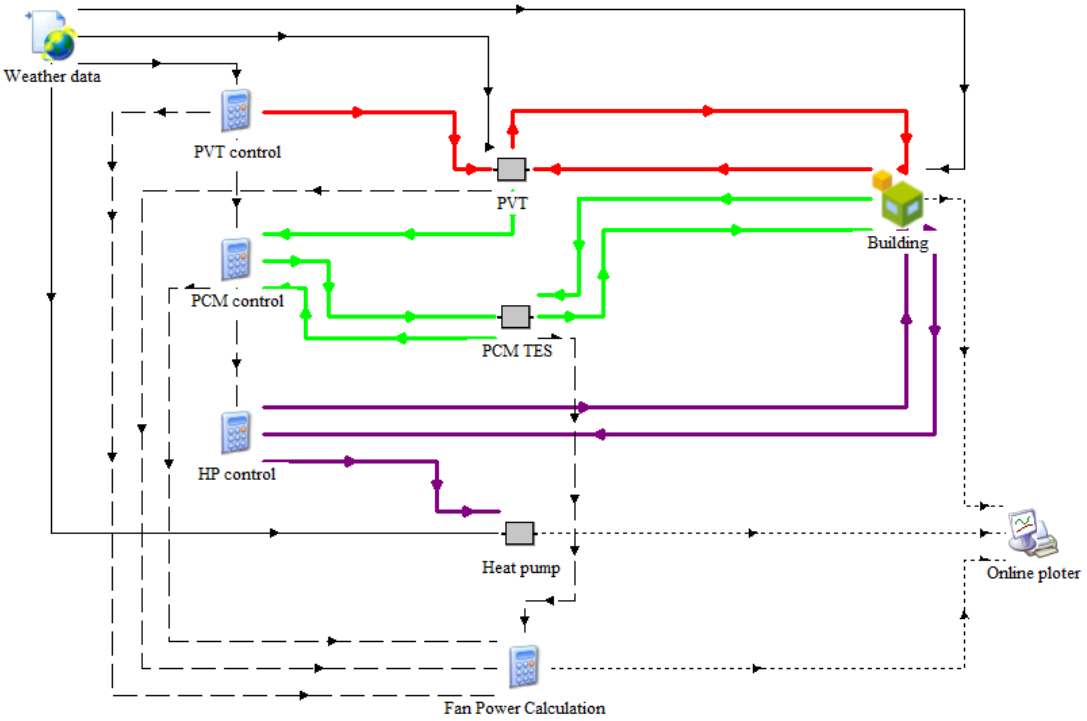

Fig. 6.4 The simplified connection of the key components in the modelling system.

6.3.1 Building model

The house model was developed using Google SketchUp and TRNBuild, and then imported into TRNSYS Type 56 Multi-zone building component model (Beckman 2001). In the house model, the living space (*i.e.* kitchen, dining room, living room and lounge) was modelled as one air node, while the three bedrooms were considered as three air nodes. The heating thermostat settings in winter for the living and sleeping spaces are shown in Fig. 6.5 (NatHERS 2016). It is worthwhile to mention that the heating thermostat setting represented the lower limit of the indoor air temperature range, while the issue of overheating was not considered in this winter heaing condition

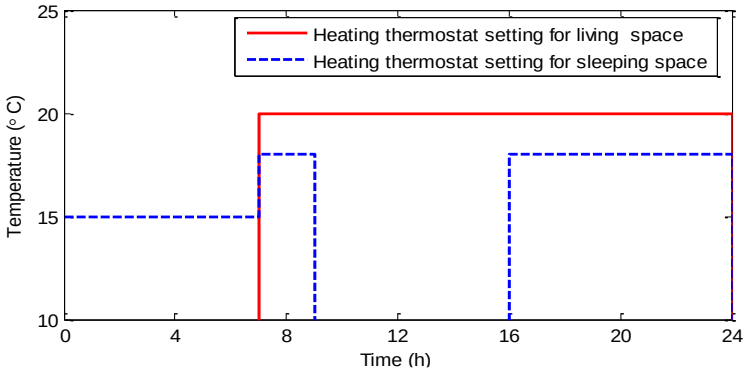

Fig. 6.5 Heating thermostat settings for living and sleeping spaces in winter (NatHERS 2016).

6.3.2 PVT model

In this chapter, a model of the PVT collectors with a glass cover and a number of fins, as shown in Fig. 6.6, was used (Fan *et al.* 2017). This PVT model was updated based on the model used in the previous chapters. In this model, the PVT collector is divided into a number of control elements along the flow direction, and each element is further divided into 6 nodes that are perpendicular to the flow direction to represent the following PVT components: top glazing, PV plate, solar absorber plate, fins, fluid air, and bottom plate layer. The energy balance equations for the glass cover and the fins are described in Eqs. (6.1) and (6.2), and the energy balance equations for the PV plate, the solar absorber plate, and the bottom plate can be described in the same way. The energy balance equation for the air flowing through the air channel is given by Eq. (6.3). By using this model, the outlet air temperature of the PVT collectors, the temperature of the bottom plate, electrical power generation, and collected thermal energy can easily be determined.

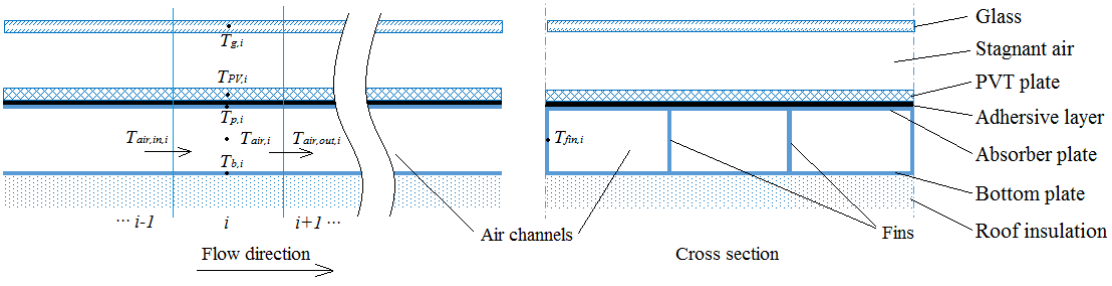

Fig. 6.6 Schematic of the PVT model.

$$c_{p,g} m_g \frac{\partial T_{g,i}}{\partial t} = A_{air}\left(\alpha_g I_t + \dot{q}_{nc,PV-g,i} + \dot{q}_{rad,PV-g,i} - \dot{q}_{wind} - \dot{q}_{sky}\right) \quad (6.1)$$

$$c_{p,fin} m_{fin} \frac{\partial T_{fin,i}}{\partial t} = A_{fin,cs} \left(\dot{q}_{cond,p-fin,i} - \dot{q}_{cond,fin-b,i} \right) - 2A_{fin} \dot{q}_{conv,fin-air,i} \quad (6.2)$$

$$c_{p,air} \rho_{air} A_{air} \delta_{air} \frac{\partial T_{air,i}}{\partial t} = c_{p,air} \dot{Q}_m \left(T_{air,in,i} - T_{air,out,i} \right) + A_{air} \left(\dot{q}_{conv,p-air,i} + \dot{q}_{conv,b-air,i} \right) + 2A_{fin} \dot{q}_{conv,fin-air,i} \quad (6.3)$$

where T is the temperature, $\dot{q}$ is the heat flux, c_p is the specific heat capacity, ρ is the density, $\dot{Q}_m$ is the mass air flow rate, m is the mass, A is the heat transfer area, α_g is the absorptivity of glass cover, i is the PVT elements index, the subscript *cs* indicates the cross-section areas of fins, the subscripts *g* and *fin* represent the glass and fins, respectively, the subscripts *cond*, *conv*, *rad*, *nc*, *wind* and *sky* indicate the conductive heat transfer, convective heat transfer, radiative heat transfer, natural convective heat transfer, wind-driven force convective heat transfer and sky radiative heat transfer, respectively, and the subscripts *PV-g*, *p-fin*, *p-air*, *fin-air*, *fin-b* and *b-air* indicate the heat transfer direction from the PV plate to the glass, from the absorber plate to the fin, from the absorber plate to the air, from the fin to the air, from the fin to the bottom plate and from the bottom plate to the air, respectively. Details of the PVT model and validation can be found in Fan *et al.* (2017).

6.3.3 PCM TES unit model

A physical model for the TES unit which contains two PCM layers on the opposite side of an air channel was developed, and the enhanced enthalpy method was used to model the phase change process of the PCM by considering the hysteresis phenomenon. The key assumptions used to develop this model are as follows.

- Convection heat transfer within the liquid PCM is omitted and conduction heat transfer within the PCM bricks is one-dimensional;
- The specific heat capacities of liquid PCM and solid PCM out of the phase change region are assumed to be constants, respectively;
- The air temperature gradient only exists in the direction of the air flow;
- The air flow distribution to the air channel is uniform, and;

- The shrinkage cavity caused by the change in density during the phase change process is considered to be evenly distributed within each PCM element (Shamsundar and Sparrow 1976).

A schematic of the nodes in modelling the PCM TES unit is shown in Fig. 6.7. The PCM TES unit is divided into multiple elements containing both air nodes and PCM control volumes in the direction of air flow. The governing equation for the air node is shown in Eq. (6.4), which can easily be discretised by using the first order upwind difference scheme.

$$\frac{\partial T_{air}}{\partial t} = u_{air}\frac{\partial T_{air}}{\partial x} + \frac{1}{\rho_{air} c_{p,air} \delta_{air}}\left(\dot{q}_{PCM1-air} - \dot{q}_{air-PCM2}\right) \tag{6.4}$$

where u is the air velocity, δ_{air} is the size of the air gap, x is the coordinate in the direction of air flow, and the subscripts *PCM1-air* and *air-PCM2* indicate the heat transfer direction from PCM layer 1 to air and from air to PCM layer 2, respectively.

The same governing equation for the PCM layer shown in Chapter 3 is used for the PCM layers in the PCM layers in the PCM TES model, but the boundary conditions are different, as shown in Eq. (6.5).

$$\begin{cases} k_{PCM}\left.\dfrac{\partial T_{PCM}}{\partial y}\right|_{y=2\delta_{PCM}+\delta_{air}} = \dot{q}_{top} \\ k_{PCM}\left.\dfrac{\partial T_{PCM}}{\partial y}\right|_{y=\delta_{PCM}+\delta_{air}} = -\dot{q}_{PCM1-air} - \dot{q}_{rad,PCM1-PCM2} \\ k_{PCM}\left.\dfrac{\partial T_{PCM}}{\partial y}\right|_{y=\delta_{PCM}} = \dot{q}_{rad,PCM1-PCM2} + \dot{q}_{air-PCM2} \\ k_{PCM}\left.\dfrac{\partial T_{PCM}}{\partial y}\right|_{y=0} = -\dot{q}_{bottom} \end{cases} \tag{6.5}$$

where δ_{PCM} is the thickness of each PCM layer, y is the coordinate in the direction perpendicular to the air flow, and the subscripts *PCM1-PCM2*, *top* and *bottom* indicate the directions of the heat flux from PCM layer 1 to PCM layer 2, from the ceiling insulation to PCM layer 1, and from PCM layer 2 to the ceiling plasterboard, respectively. Accordingly, the discretised energy balance can easily be obtained by using the first-order central difference scheme.

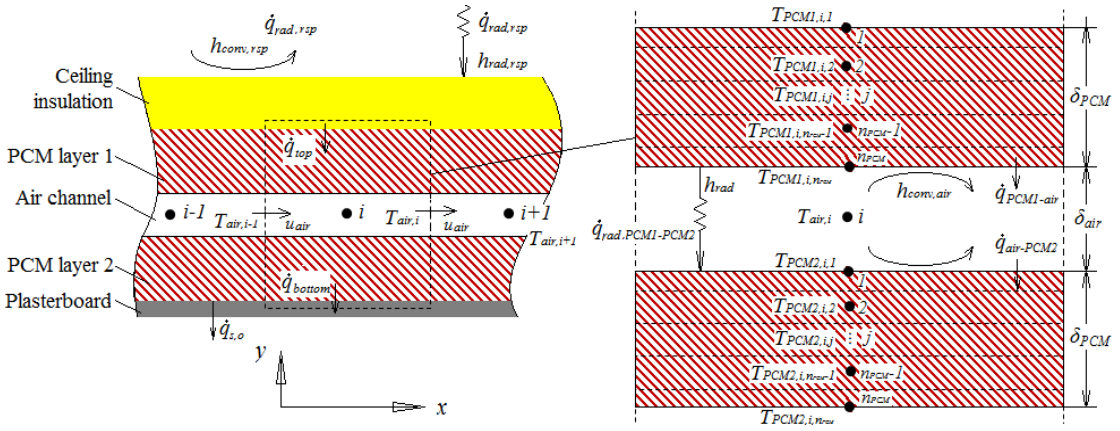

Fig. 6.7 Schematic of the nodes in modelling the PCM thermal energy storage unit.

Heat fluxes from the ceiling insulation to the PCM and ceiling plasterboard (*i.e.* $\dot{q}_{top}$ and $\dot{q}_{bottom}$) are provided by the building model which is coupled at a TRNSYS time step level to the PCM model. The forced convective heat transfer and radiative heat transfer among the air and PCM layers are calculated using Eqs. (6.6) and (6.7).

$$\dot{q}^{k}_{PCM1-air,i} = h_{conv,air}\left(T^{k}_{PCM1,i,n_{PCM}} - T^{k}_{air,i}\right) \tag{6.6}$$

$$\dot{q}^{k}_{air-PCM2,i} = h_{conv,air}\left(T^{k}_{air,i} - T^{k}_{PCM2,i,1}\right) \tag{6.7}$$

where the superscript k indicates the k^{th} time step, the subscript i presents the i^{th} air element, the subscripts n_{PCM}, *PCM1* and *PCM2* indicate the number of PCM element in each PCM layer, PCM layers 1 and 2, respectively, $h_{conv,air}$ is the convective heat transfer coefficient between the air and PCM layers, which can be calculated from the Nusselt (*Nu*) number. Gnielinski equation (Gnielinski 1976) was used to calculate the Nusselt number of the turbulent flow, while the Nusselt number is set as a constant relating the length to the width of the air channel (Bergman 2011) under laminar flow, as shown in Eq. (6.8).

$$Nu = \begin{cases} 7.54, \text{ for } Re < 2300 \\ \dfrac{(\xi/8)(Re-1000)Pr}{1+12.7\sqrt{\xi/8}\left(Pr^{2/3}-1\right)}\left[1+\left(\dfrac{d_h}{L}\right)^{2/3}\right]c_t, \text{ for } Re = 2300\sim 10^6, Pr = 0.6\sim 10^5 \end{cases} \tag{6.8}$$

where *Re* is the Reynolds number, *Pr* is the Prandtl number, *L* is the length of the air channel, d_h is the hydrate diameter of the air channel, ξ is the Darcy coefficient, and c_t is the correction factor.

Radiative heat transfer between the two PCM layers is calculated as:

$$\dot{q}^{k}_{PCM1-PCM2,i} = h_{rad}\left(T^{k}_{PCM1,i,n_{PCM}} - T^{k}_{PCM2,i,1}\right) \tag{6.9}$$

where h_{rad} is the radiative heat transfer coefficient between the two PCM layers, which is determined by Eq. (6.10).

$$h_{rad} = \sigma \frac{\varepsilon_{b,PCM}}{2-\varepsilon_{b,PCM}}\left(T^{k}_{PCM1,n_{PCM}} + T^{k}_{PCM2,1} + 273.15\times 2\right)\left[\left(T^{k}_{PCM1,n_{PCM}} + 273.15\right)^2 + \left(T^{k}_{PCM2,1} + 273.15\right)^2\right] \tag{6.10}$$

where σ is the Stefan-Boltzmann constant, and $\varepsilon_{b,PCM}$ is the emissivity of the surface of the PCM layer.

When there is no forced air flow, the free convective heat transfer across the air channel between the two PCM layers is considered, which is determined by the Nusselt number calculated by Eq. (6.11) (Hollands *et al.* 1976):

$$Nu_{\delta_{air}} = 1+1.11\left[1-\frac{1708}{Ra\cos\theta}\right]^{*}\left(1-\frac{(\sin 1.8\theta)^{1.6}1708}{Ra\cos\theta}\right)+\left[\left(\frac{Ra\cos\theta}{5830}\right)^{1/3}-1\right]^{*}, \text{for } \theta < 60^{o} \tag{6.11}$$

where θ is the inclined angle of the air channel, which was 0^{o} in this study, []* is defined by $[X]^{*} = (|X| + X)/2$, $Ra_{\delta_{air}}$ is the Rayleigh number in which the size of the air channel (δ_{air}) was used as the characteristic length.

The percentage of thermal energy stored and the equivalent PCM TES temperature were defined to indicate the status of the PCM TES unit. As described in Eq.(6.12), the percentage of thermal energy stored was the ratio of the average specific enthalpy of the PCM TES unit to the specific enthalpy difference between the upper and lower limits of the hysteresis region of the PCM used. The equivalent PCM TES temperature can be calculated according to the PCM *h*-*T* relationship. If several PCM TES units are connected in series or in parallel to form an overall PCM TES system, a weighted mean value of individual equivalent PCM TES temperatures can be calculated and treated as the equivalent temperature of the overall PCM TES system.

$$\psi = \frac{\bar{h}_{PCM\ TES}}{(h_l - h_s)} \tag{6.12}$$

where ψ is the percentage of thermal energy stored in the PCM TES unit, $\bar{h}_{PCM\ TES}$ is the average specific enthalpy of the PCM TES unit, and h_l and h_s are the specific PCM enthalpies at the upper and lower boundary temperatures of the hysteresis region, respectively. Note that the percentage of thermal energy stored is negative if the

average specific enthalpy of the PCM TES unit is less than the specific enthalpy of the PCM used at the lower limit temperature of the hysteresis region.

The governing questions were solved based on the PCM enthalpy-temperature relationship (see Eq. (3.7) in Chapter 3). By using this PCM TES model, the top surface temperature of PCM layer 1, the bottom surface temperature of PCM layer 2, the outlet air temperature, and the thermal energy storage status can be derived and coupled with the building model. As the finite difference method was used in this chapter to develop the PCM TES unit model, it is therefore more accurate and informative than the two prediction models regressed from the experimental data in Chapter 5. The validation of the PCM TES model is specified in Section 6.4.1.

6.3.4 Heat pump model

The heat pump used in this study is assumed to be a split-type air conditioner. The power consumption of this air source heat pump can be calculated according to the heating/cooling demand to match the actual heating load based on the part load factor and heat pump performance map, as described in Eq. (6.13).

$$P_{HP} = \frac{\dot{Q}_{load}}{\mathrm{COP}} = \frac{\dot{Q}_{load}}{\mathrm{PLF} \cdot F_{COP} \cdot \mathrm{COP}_{norminal}} \tag{6.13}$$

where P_{HP} is the heat pump power consumption, $\dot{Q}_{load}$ is the actual load, F_{COP} is the COP modifier which can be determined according to the heat pump performance map, PLF is the partial load factor which is assumed to be a function of the partial load ratio (PLR) (Blervaque *et al.* 2016; Henderson *et al.* 1999), as shown in Fig. 6.8. The nominal performance of the heat pump can be calculated based on the catalogue data provided by the manufacturers.

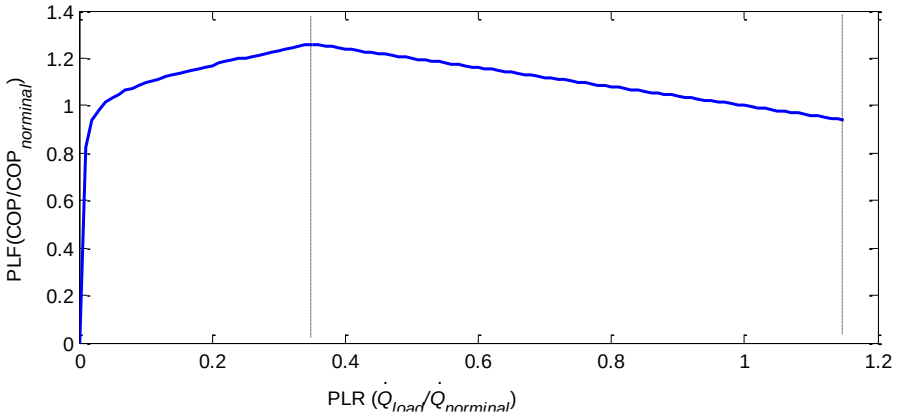

Fig. 6.8 Partial load factor as a function of partial load ratio.

6.3.5 Fan power calculation

The PCM fan was used to overcome the friction pressure drop over the PCM TES unit (see Eq. (6.14) (ASHARE 2009)) and the pressure drop through the corresponding ducting system. PCM fan power consumption can then be calculated using Eq. (6.15).

$$\Delta p_{f,PCM} = \frac{\xi L}{d_h} \frac{\rho_{air} u_{air}^2}{2} \tag{6.14}$$

$$P_{PCM\ fan} = \frac{1}{\rho_{air} \eta_{fan}} \Delta p_{total} \dot{Q}_m = \frac{1}{\rho_{air} \eta_{fan}} \left(\Delta p_{f,PCM} + \Delta p_{other,PCM} \right) \dot{Q}_m \tag{6.15}$$

where $\Delta p_{f,PCM}$ is the friction pressure drop over the PCM TES unit, $P_{PCM.fan}$ is the PCM fan power consumption, η_{fan} is the fan efficiency, Δp_{total} is the total pressure drop to be covered by the PCM fan. The power consumption of the PVT fan can be calculated using Eq. (6.15) as used in this section.

6.4 Performance test and evaluation

6.4.1 Validation of PCM TES unit model

The model of the two-layer PCM TES unit was validated using the experimental data reported by Lopez *et al.* (2013), in which a series of charging and discharging experiments were carried out based on a lab-scale test rig, as shown in Fig. 6.9. The PCM-to-air heat exchanger tested by Lopez *et al.* (2013), consisted of three PCM slabs, where the middle slab was twice as thick as the other two slabs, thus creating two symmetric air channels. The PCM-to-air heat exchanger was well insulated and the PCM slabs tested were ENERGAIN slabs, a commercial product from the Dupont de Nemours Society. The inlet and outlet air temperatures of the PCM-to-air heat exchanger were measured by T-type thermocouples with an accuracy of ±0.4°C. Two sets of experiments were carried out, as summarised in Table 6.3.

Numerical modellings which corresponded to the two sets of experiments were carried out under the same conditions and the results are shown in Fig. 6.10. Note that the simulated outlet air temperatures of the PCM-to-air heat exchanger generally agreed well with the experimental data and therefore it is expected that the model can provide relatively reliable estimates under different working conditions.

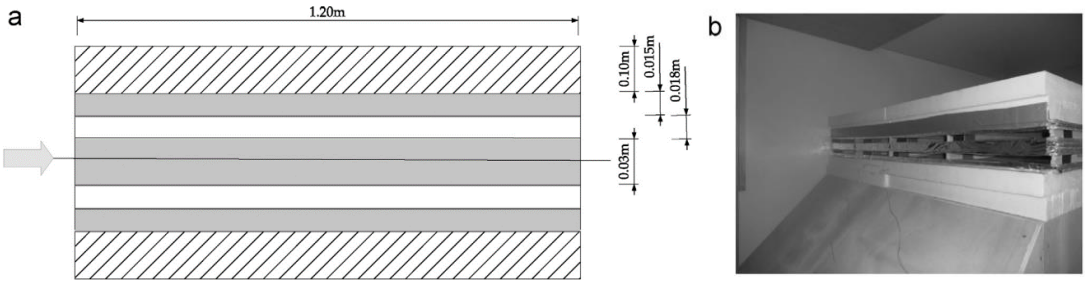

Fig. 6.9 The lab-scale PCM-to-air heat exchanger test rig (Lopez *et al.* 2013).

Table 6.3 Two sets of experiments (Lopez *et al.* 2013).

Experiment set	Initial PCM temperature (°C)		Air flow rate (m^3/h)
	charging	discharging	
Set 1	5	35	240
Set 2	5	30	330

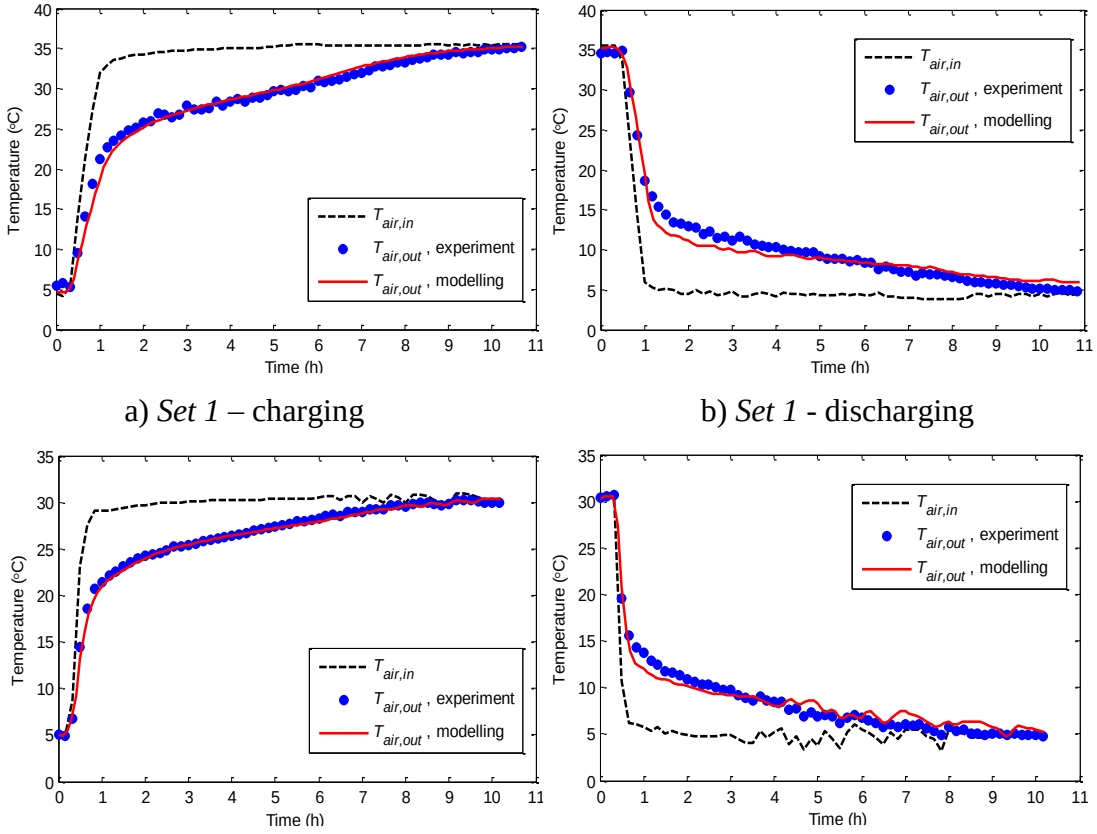

a) *Set 1* – charging

b) *Set 1* - discharging

c) *Set 2* – charging

d) *Set 2* - discharging

Fig. 6.10 Comparison between modelling and the experimental results from Lopez *et al.* (2013).

6.4.2 Setup of the performance test and evaluation

In this study, it was assumed that the PVT collectors were installed onto the north part of the roof with an installation area of 101 m^2. Four PCM TES units were integrated into the ceilings of the living space and three bedrooms respectively, as shown in Fig. 6.11. The PCM TES units in the bedroom ceilings were connected in parallel and then connected to the PCM TES unit in the living space ceiling in series to serve as an overall PCM TES system; this is because that the living space and sleeping space are located in the north and south respectively and have different heating schedules and demands.

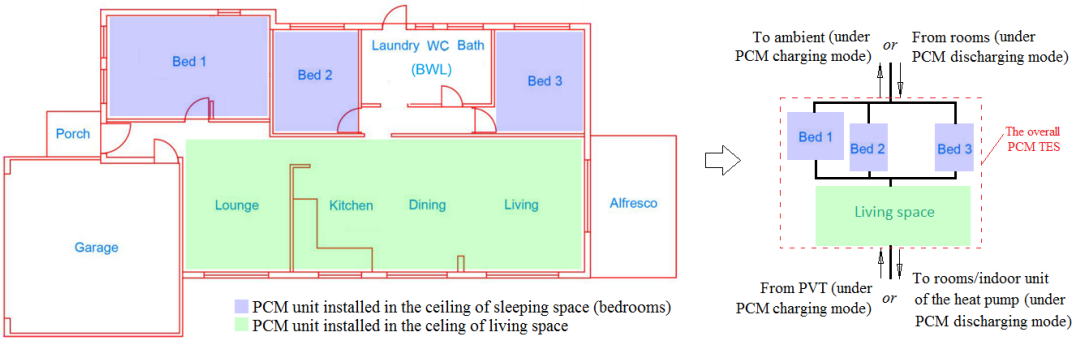

Fig. 6.11 Locations of the PCM TES units.

The operating modes of the proposed system can be determined according to the equivalent temperature of the overall PCM TES system, the PVT outlet air temperature, the percentage of thermal energy stored in the overall PCM TES system, and the indoor air temperature. Fig. 6.12 summarises the logic for the operating mode. During the daytime, the PCM charging mode can be activated if the PVT outlet air temperature is higher than the equivalent temperature of the overall PCM TES system; otherwise the PVT exhausting mode is activated. In the PCM discharging mode, the return air from the indoor space can be directed to the PCM TES units for PCM discharging if the percentage of thermal energy stored in the overall PCM TES system is above zero; otherwise the normal air conditioning mode can be activated.

The air flow distributed to each room is assumed to be proportional to the maximal heating demand of each individual room under design condition, but under the PCM discharging mode, the warm air supplied to an individual room will be turned off if the air temperature in the room is 2^{o}C higher than the thermostat settings, and the air

supply will then be recovered until the air temperature falls back to the thermostat settings. The 2^{o}C dead-band setting is used to conserve the thermal energy stored in the PCM TES units when the indoor air temperature is warm enough, while avoiding a high fluctuation of indoor air temperature. Under the PCM discharging mode, if a room temperature cannot be maintained above the corresponding thermostat settings with the heated air passing through the PCM TES units for space heating, the extra heating demand will be covered by the air source heat pump to keep the room temperature at the thermostat setting, and a perfect control was assumed for the heat pump to control the indoor air temperature right at the thermostat settings.

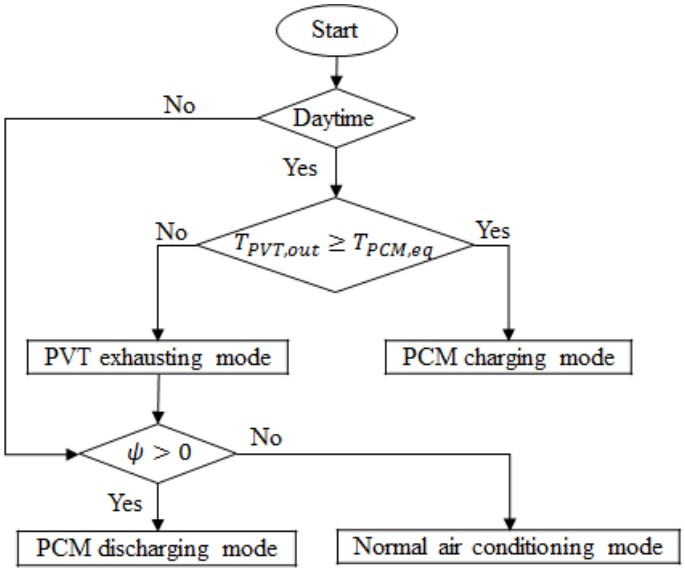

Fig. 6.12 Illustration of the selection of the operation modes.

This proposed system was evaluated for a week under winter weather conditions in Melbourne. Fig. 6.13 shows the weather data over the selected week. The air source heat pump for winter weather conditions was sized based on the maximal heating demand of the house at the design condition for Melbourne and the results are presented in Table 6.4.

Two cases were designed and compared to evaluate the performance of the building integrated PVT-PCM enhanced HP system. In the first case, the house only used the air source heat pump for indoor space heating (*i.e.* the *baseline* case). In the second case, the building integrated PVT-PCM enhanced HP system is used for indoor space heating (*i.e.* the *PVT-PCM baseline* case), where the design values of the system are the PCM charging air flow rate of 2500 kg/h, air channel size of 50 mm, the thickness

of each PCM layer of 10 mm, and the PCM type of SP24E. The PCM charging air flow rate of 2500 kg/h in the *PVT-PCM baseline* case corresponds to the design air flow rate of the heat pump, while the PCM SP24E showed decent performance based on some trial tests.

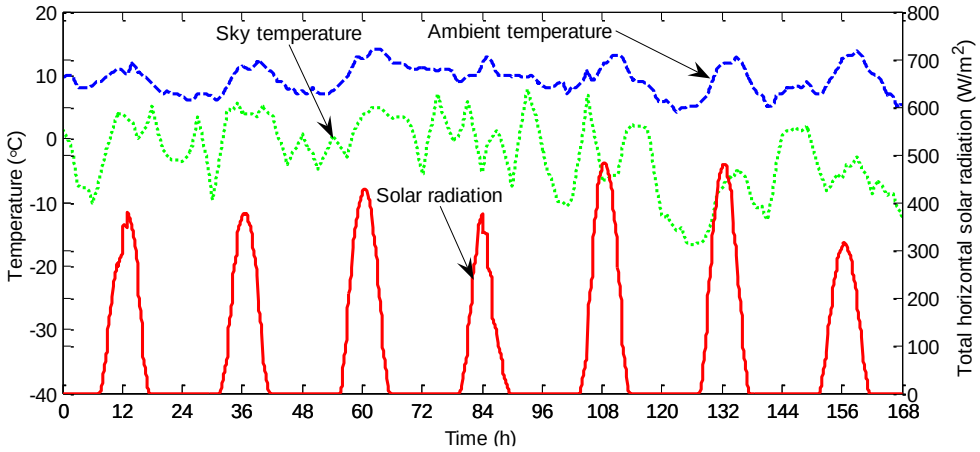

Fig. 6.13 Weather data for the winter week.

Table 6.4 Sizing the air source heat pumps and design air flow rate of the air conditioning systems under Melbourne weather conditions.

Heat pump sizing	Value
Design air flow rate (kg/h)	2500
Heating capacity (kW)*	14
Total input (kW)*	3.5

* Rated at indoor dry-bulb temperature of 20°C, outdoor wet-bulb temperature of 6°C.

6.4.3 Results from performance test and evaluation

6.4.3.1 Comparison between the *baseline* case and the *PVT-PCM baseline* case

The performance of the *PVT-PCM baseline* case was simulated and compared to the *baseline* case in terms of the indoor air temperature, generation and consumption of electricity, and the thermal energy stored in the overall PCM TES system.

Fig. 6.14 shows the indoor air temperatures of the house with the *PVT-PCM baseline* case and the *baseline* case under the selected winter week. Unlike the *baseline* case, the indoor air temperatures of the living and sleeping spaces for the *PVT-PCM baseline* case were higher, while the time period with the heat pump in operation had decreased. It is worthwhile to mention that slight overheating occurred during daytime of the 5th

and 6th days over the winter week in the PVT-PCM baseline case, however, as mentioned, it was not considered as the analysis of indoor space heating performance by using the proposed system was focused on. Fig. 6.15 compares the ON/OFF status of the heat pump over the selected winter week under the *PVT-PCM baseline* case and the *Baseline* case. It shows that under the *baseline* case, the air source heat pump was switched on for most of the week (*i.e.* 121.8 hours out of 168 hours) to maintain the indoor air temperatures at the required settings, while the working period of heat pump was decreased to only 61 hours over the week due to integrating the PVT collectors and PCM TES under the *PVT-PCM baseline* case.

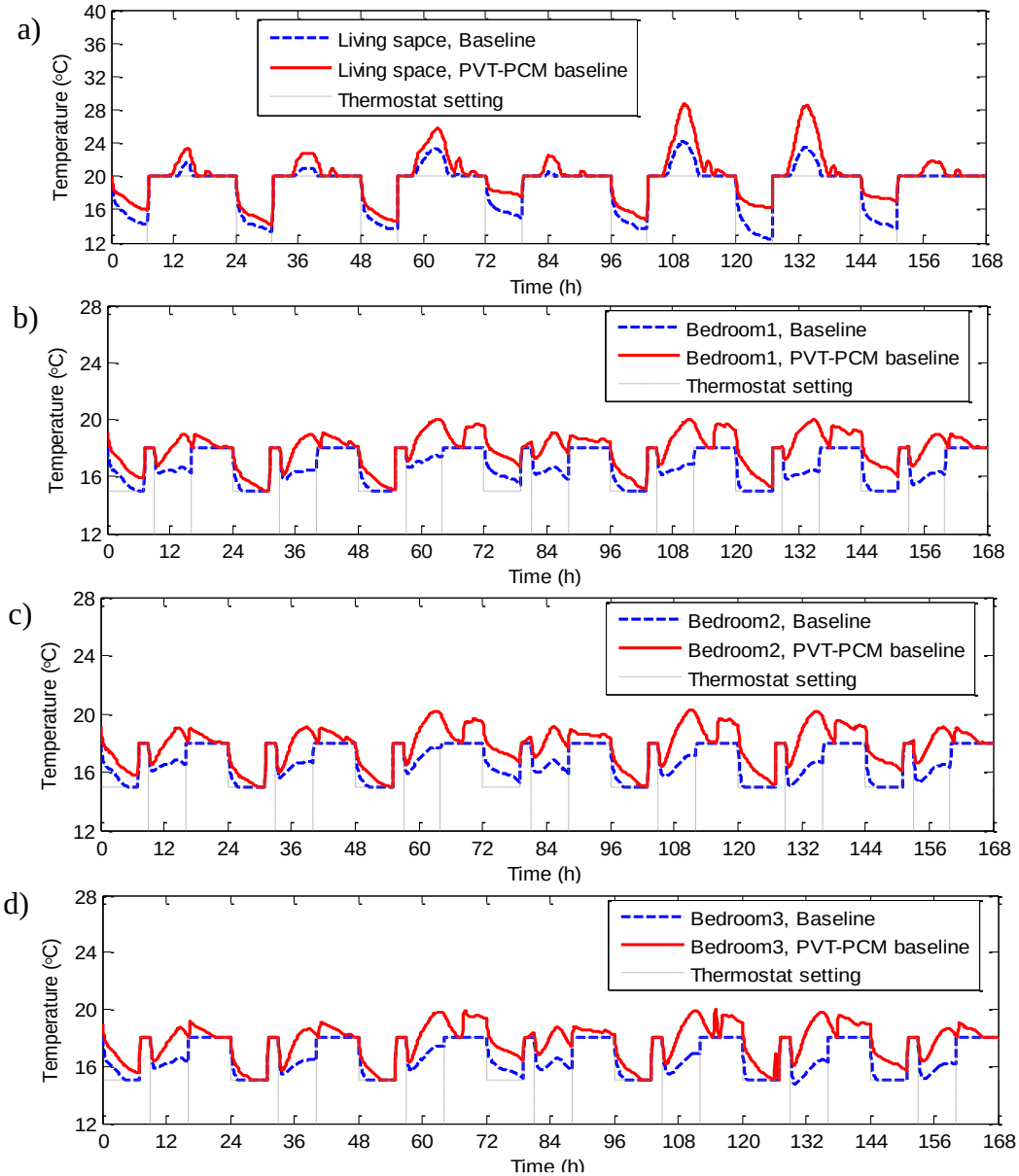

Fig. 6.14 Indoor air temperatures of the *PVT-PCM baseline* case and the *baseline* case.

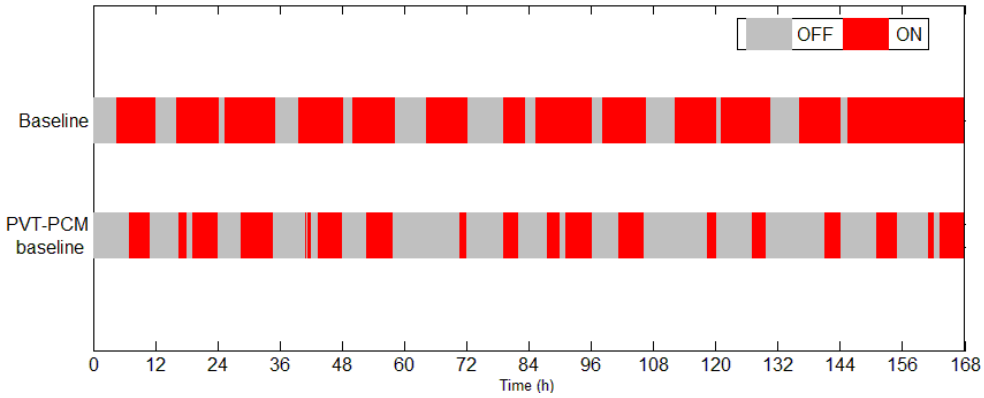

Fig. 6.15 ON/OFF state of the heat pump under the *PVT-PCM baseline* and the *baseline* case.

Fig. 6.16 shows the accumulated generation and the total consumption of electricity under the *PVT-PCM baseline* case, and the accumulated consumption of electricity under the *baseline* case over the selected winter week. Details of the generation and consumption of electricity are compared further in Table 6.5. It shows that the electricity consumed in the *PVT-PCM baseline* case kept increasing and eventually reached 42.3 kWh, which is much lower than the 72 kWh of the *baseline* case. In the *PVT-PCM baseline* case, most of the electricity consumed was due to the air source heat pump (23.7 kWh) while the PCM fan required 8.9 kWh and the PVT fan required 9.7 kWh of electricity. Compared to the *baseline* case, 41.3% of electricity was saved. The electricity generated by the PV panels was 156.5 kWh under the *PVT-PCM baseline* case, so the net generation of electricity reached 114.2 kWh.

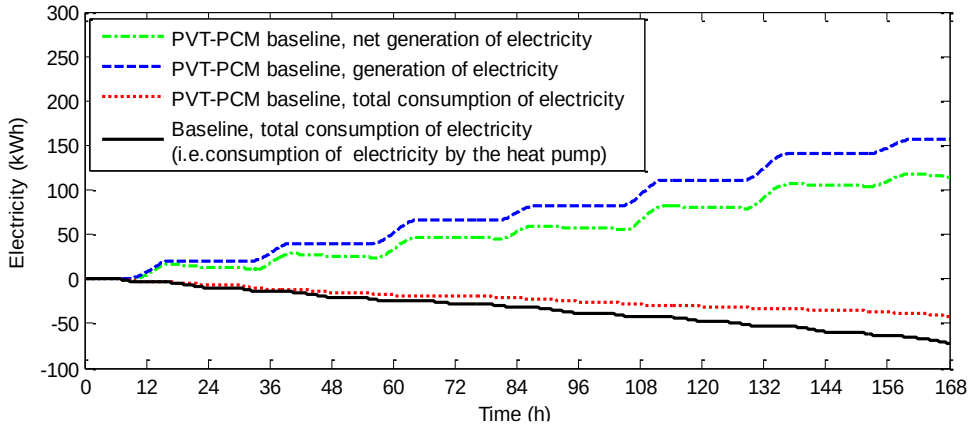

Fig. 6.16 Accumulated generation and consumption of electricity under the *PVT-PCM baseline* case and the *baseline case*.

The average COP of the building integrated PVT-PCM enhanced HP system for space heating during the selected week was 5.21, which is much higher than the 3.06 of the air source heat pump system in the *baseline* case. These results indicate that integrating the PCM TES units into the ceiling and PVT collectors with the air source heat pump system substantially reduced the electricity consumed for indoor space heating during winter.

Table 6.5 Generation and consumption of electricity under the *PVT-PCM baseline* case and the *baseline* case during a Melbourne week in winter.

Generation or consumption of electricity (kWh)		*Baseline*	*PVT-PCM baseline*
Net generation of electricity(E_{net})		-	114.2
Generation of electricity from the PVT collectors (E_{PV})		-	156.5
Total consumption of electricity (E_{con})	Consumption of electricity by the heat pump (E_{HP})	72.0	23.7
	Consumption of electricity by the PCM fan ($E_{PCM,fan}$)	-	8.9
	Consumption of electricity by the PVT fan ($E_{PVT,fan}$)	-	9.7

Fig. 6.17 presents the inlet and outlet air temperatures of the overall PCM TES system during PCM charging and discharging processes. During PCM charging, the maximum PCM inlet air temperature supplied by the PVT collectors to the PCM TES units was 45.2°C. Due to the exchange of heat between the PCM layers and the air, the heat stored in the PCM and the air temperature decreased significantly at the outlet of the PCM TES. Whereas during PCM discharging, the maximum difference in temperature between the inlet and outlet of the overall PCM TES was 5.9°C, which was much lower than that under the PCM charging mode.

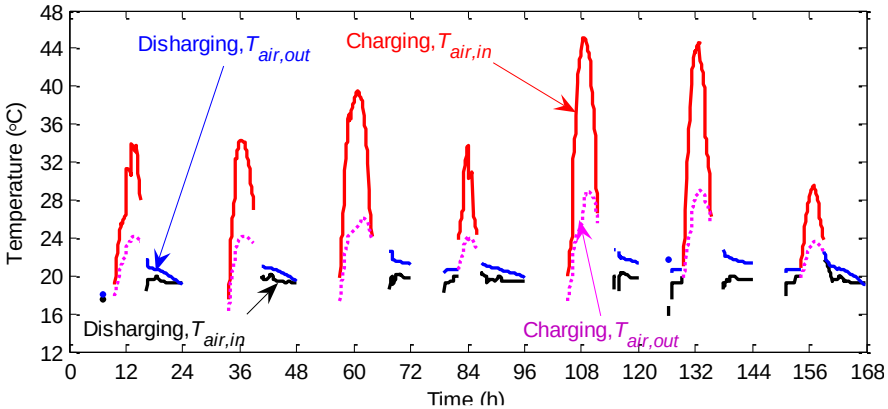

Fig. 6.17 Inlet and outlet air temperature of the overall PCM TES.

The percentage of thermal energy stored in the overall PCM TES system under the *PVT-PCM baseline* case is shown in Fig. 6.18, where the percentage of thermal energy stored fluctuated greatly between daytime and night time, from a minimum of -5.57% to a maximum of 88.46% over the winter week. This shows that a large amount of thermal energy was being stored rapidly in the PCM TES during the PCM charging process and then used slowly during the PCM discharging process, taking the period of 96^{th} - 120^{th} hours as an example. The release rate of thermal energy was much slower than the storage rate because the temperature difference between the PCM and the return air was much lower than the temperature difference between the PCM and the heated air from the PVT collectors, as shown in Fig. 6.17. It also indicates that the primary design in the *PVT-PCM baseline* case was reasonable because most of the PCM thermal storage capacity has been used.

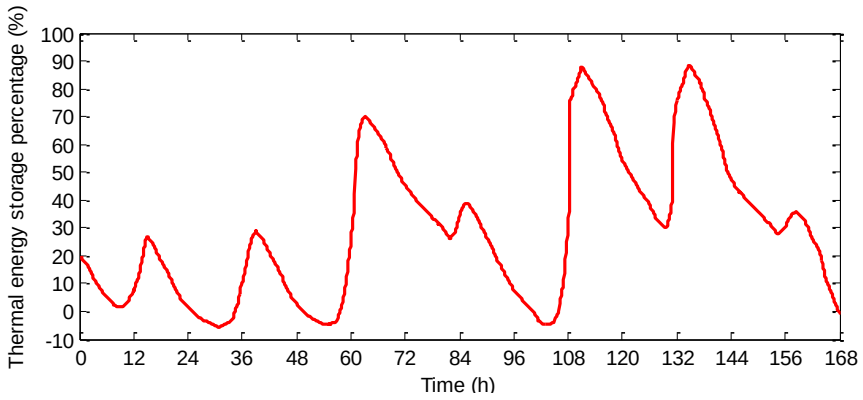

Fig. 6.18 Percentage of the thermal energy stored in the overall PCM TES under the *PVT-PCM baseline* case.

6.4.3.2 Influence of design variables on system performance

1) Design of Taguchi experimental plan

The design variables (*i.e.* control factors) considered for the proposed system in the Taguchi experiment are the type of PCM, the PCM charging air flow rate, the size of the air channel, and the thickness of the PCM layers. These four variables have been found to have the most influence on the performance of air-based PCM TES units (Waqas and Kumar 2013; Saman *et al.* 2006; Lazaro *et al.* 2009a and 2009b; Summers *et al.* 2012; Chen C. *et al.* 2014; Dolado *et al.* 2011). Note that the thickness of the PCM layers for the living and sleeping spaces were two different factors due to the

different internal heating demands, orientations, and heating schedule between the living and sleeping spaces.

Two levels were considered for each control factor so that the influence of both the control factors and their interactions on system performance can be considered in Taguchi analysis. The Taguchi experimental plan based on L_{16} (2^{15}) orthogonal array is presented in Table 6.6. Two PCMs from Rubitherm (Rubitherm 2015), *i.e.* SP24E and SP26E, were the two factor levels for the PCM type, whose thermo-physical properties can be found in Table 4.1 in Chapter 4. Since the PCM type is a discrete variable involving the enthalpy-temperature relationship, the density and thermal conductivity, the PCM type which can perform better for the proposed system was identified directly from the Taguchi analysis. The two factor levels for the PCM charging air flow rate were 500 and 2500 kg/h; the higher factor level is limited by the designated air flow rate of the heat pump, while a lower limit of 500 kg/h was used as the air flow rate should not be too low otherwise the thermal efficiency of PVT collectors will be unacceptable. The two factor levels used for the size of air channel were 22 and 78 mm, to avoid high power consumption by the fan and noise by the high air velocity, whilst still enabling an acceptable heat transfer performance between the air and the PCM layers. The PCM layers were 5 mm and 25 mm thick (*i.e.* the total thickness of the two-layer PCM TES unit was 10mm and 50 mm); these two factor levels gave consideration to manufacturing the encapsulation of PCMs and weight load bearing by the building ceiling. The net generation of electricity was the objective response in the Taguchi analysis, and it was considered to be the-higher-the-better. The resulting net generation of electricity for each trial test and the corresponding *S/N* ratio are also presented in Table 6.6, and the response table of the Taguchi experiment is shown in Table 6.7.

Based on the *S/N* ratio analysis, the *S/N* ratio of PCM SP26E was higher than SP24E so it was used in the system design. The charging air flow rate was ranked as the most significant factor with a maximal *S/N* ratio difference between the two factor levels of 0.76, followed by the size of the air channel with a maximal *S/N* ratio difference of 0.56, however the maximal *S/N* ratio difference of the interactions of $\dot{Q}_{m,charging}\times\delta_{PCM,Bed}$ and $\delta_{PCM,KDLL}\times\delta_{PCM,Bed}$ were lower than 0.01.

Table 6.6 Taguchi experiment plan and corresponding results (A, B, C, D and E are used to represent the PCM type, the PCM charging air flow rate ($\dot{Q}_{m,charing}$), the size of air channel (δ_{air}), the PCM layer thickness in the living space ($\delta_{PCM,KDLL}$) and the PCM layer thickness in the sleeping space ($\delta_{PCM,Bed}$) to save the space in the table.).

No.	PCM	$\dot{Q}_{m,charing}$	A×B	δ_{air}	A×C	B×C	D×E	$\delta_{PCM,KDLL}$	A×D	B×D	C×E	C×D	B×E	A×E	$\delta_{PCM,Bed}$	E_{net} (kWh)	*S/N*
	A	B		C				D							E		
1	SP24E	500	1	22	1	1	1	5	1	1	1	1	1	1	5	102.22	40.19
2	SP24E	500	1	22	1	1	1	25	2	2	2	2	2	2	25	102.11	40.18
3	SP24E	500	1	78	2	2	2	5	1	1	1	2	2	2	25	101.48	40.13
4	SP24E	500	1	78	2	2	2	25	2	2	2	1	1	1	5	93.04	39.37
5	SP24E	2500	2	22	1	2	2	5	1	2	2	1	1	2	25	112.77	41.04
6	SP24E	2500	2	22	1	2	2	25	2	1	1	2	2	1	5	115.65	41.26
7	SP24E	2500	2	78	2	1	1	5	1	2	2	2	2	1	5	103.30	40.28
8	SP24E	2500	2	78	2	1	1	25	2	1	1	1	1	2	25	104.98	40.42
9	SP26E	500	2	22	2	1	2	5	2	1	2	1	2	1	25	102.52	40.22
10	SP26E	500	2	22	2	1	2	25	1	2	1	2	1	2	5	102.68	40.23
11	SP26E	500	2	78	1	2	1	5	2	1	2	2	1	2	5	98.35	39.86
12	SP26E	500	2	78	1	2	1	25	1	2	1	1	2	1	25	99.45	39.95
13	SP26E	2500	1	22	2	2	1	5	2	2	1	1	2	2	5	109.03	40.75
14	SP26E	2500	1	22	2	2	1	25	1	1	2	2	1	1	25	119.32	41.53
15	SP26E	2500	1	78	1	1	2	5	2	2	1	2	1	1	25	106.16	40.52
16	SP26E	2500	1	78	1	1	2	25	1	1	2	1	2	2	5	104.63	40.39

Table 6.7 Response table of the Taguchi experiment.

Level	PCM		$\dot{Q}_{m,charing}$		A×B		δ_{air}		A×C	
	E_{net}	*S/N*	E_{net}	*S/N*	E_{net}	*S/N*	E_{net}	*S/N*	E_{net}	*S/N*
Level 1	104.44	40.36	100.23	40.02	104.75	40.38	108.29	40.68	105.17	40.42
Level 2	105.27	40.43	109.48	40.78	104.96	40.41	101.42	40.12	104.54	40.37
S/N_{max}-S/N_{min}	0.0708		0.7603		0.0243		0.5606		0.0578	
Rank	9		1		13		2		10	

(*Continue*)

Level	B×C		D×E		$\delta_{PCM,KDLL}$		A×D		B×D	
	E_{net}	*S/N*	E_{net}	*S/N*	E_{net}	*S/N*	E_{net}	*S/N*	E_{net}	*S/N*
Level 1	103.58	40.30	104.85	40.40	104.48	40.37	105.73	40.47	106.14	40.50
Level 2	106.14	40.49	104.87	40.40	105.23	40.42	103.98	40.32	103.57	40.29
S/N_{max}-S/N_{min}	0.1831		0.0005		0.0453		0.1468		0.2088	
Rank	6		15		11		7		3	

(*Continue*)

Level	C×E		C×D		B×E		A×E		$\delta_{PCM,Bed}$	
	E_{net}	*S/N*	E_{net}	*S/N*	E_{net}	*S/N*	E_{net}	*S/N*	E_{net}	*S/N*
Level 1	105.21	40.43	103.58	40.29	104.94	40.40	105.21	40.42	103.61	40.29
Level 2	104.51	40.36	106.13	40.50	104.77	40.40	104.50	40.38	106.10	40.50
S/N_{max}-S/N_{min}	0.0719		0.2060		0.0002		0.0410		0.2074	
Rank	8		5		14		12		4	

Table 6.8 presents the ANOVA results of the Taguchi experiment. Note that the charging air flow rate had the highest percentage contribution to the net generation of electricity (51.86%), followed by the size of the air channel with a percentage contribution of 28.46%. The thickness of the PCM layers for the sleeping space had a percentage contribution of 3.56% while that for the living space was pulled out. However, the percentage contributions from the interactions $\dot{Q}_{m,charing} \times \delta_{PCM,KDLL}$ and $\delta_{air} \times \delta_{PCM,KDLL}$ were 3.84% and 3.75%, respectively, thus indicating that the thickness of the PCM layers for the living space cannot be omitted. The PCM type was pulled out because it only had a minor influence on the objective response.

Table 6.8 Analysis of variance of the Taguchi experiment results.

Source	*DOF*	*SS*	*Var*	Variance ratio	*SS'*	%C
PCM (A)	(1)	2.71	-	-	-	-
$\dot{Q}_{m,charing}$ (B)	1	342.23	342.23	253.90	340.88	51.86%
A×B	(1)	0.18	-	-	-	-
δ_{air} (C)	1	188.42	188.42	139.79	187.07	28.46%
A×C	(1)	1.56	-	-	-	-
B×C	1	26.21	26.21	19.44	24.86	3.78%
D×E	(1)	0.00	-	-	-	-
$\delta_{PCM,KDLL}$ (D)	(1)	2.27	-	-	-	-
A×D	1	12.32	12.32	9.14	10.97	1.67%
B×D	1	26.56	26.56	19.71	25.22	3.84%
C×E	(1)	1.96	-	-	-	-
C×D	1	25.98	25.98	19.27	24.63	3.75%
B×E	(1)	0.11	-	-	-	-
A×E	(1)	1.99	-	-	-	-
$\delta_{PCM,Bed}$ (E)	1	24.75	24.75	18.36	23.41	3.56%
Error	8	10.78	1.35	1.00	20.22	3.08%
Total	15	657.25	43.82	-	-	100.00%

The contribution percentages made by the design variables can be used to further determine the search step sizes for continuous design variables during system optimisation. The higher contribution percentages generally correspond to a smaller search size because a small variation in the variable may cause obvious changes in the objective response.

6.5 Design optimisation of the building integrated PVT-PCM enhanced HP system

6.5.1 Formulation of the optimisation problem

The objective of the optimisation problem is to maximise the net generation of electricity (E_{net}) of the building integrated PVT-PCM enhanced HP system, as described in Eq. (6.16). The generation of electricity (E_{PV}) was derived from the PVT collectors.

$$\max E_{net} = \max\left[E_{PV} - E_{con}\right] = \max\left[E_{PV} - \left(E_{HP} + E_{PVT\ fan} + E_{PCM\ fan}\right)\right] \quad (6.16)$$

where E is the electrical energy generated or consumed. The total consumption of electricity (E_{con}) is the aggregated consumption of electricity by the air source heat pump (E_{HP}), the PVT fan ($E_{PVT\ fan}$) and the PCM fan ($E_{PCM\ fan}$).

Note also that these optimisation variables focus mainly on the PCM TES in this design optimisation because thermal energy storage using PCMs is the key to rationalising the management of thermal energy and reducing the consumption of electricity for indoor space heating in this study. Since the discrete variable of the PCM type was optimised through Taguchi analysis, the continuous design variables, including the PCM charging air flow rate, the size of the air channel, and the thicknesses of the PCM layers for the living and sleeping spaces were considered to be the optimisation variables in the following optimisation using the hybrid PSO-HJ algorithm. The constraints of these continuous design variables are summarised in Table 6.9, where the two factor levels used in the Taguchi experiment were used as the upper and lower search boundaries.

Table 6.9 Design variables and corresponding constraints used in the optimisation.

Item	Design variables	Constraint
$\dot{Q}_{m,charing}$	The mass air flow rate for PCM charging, (kg/h)	500-2500
δ_{air}	The size of air channel, (mm)	22-78
$\delta_{PCM,KDLL}$	The PCM layer thickness for the living space, (mm)	5-25
$\delta_{PCM,Bed}$	The PCM layer thickness for the bedrooms, (mm)	5-25

6.5.2 Optimisation process using the hybrid PSO-HJ algorithm

The parameter settings for the hybrid PSO-HJ algorithm used to optimise the proposed system are summarised in Table 6.10. The neighbourhood topology used was von Neumann topology because it performs better than the other topologies (Kennedy and Mendes 2002). The size of the population was 20 because the PSO algorithm is not sensitive to population size (Shi and Eberhart 1999). The cognitive and social accelerations were set as 2.8 and 1.3, as recommended by Carlisle and Dozier (2001). The maximum velocity gain was set as 0.5, which is a common value recommended in GenOpt (Wetter 2011). The other parameter settings were the same as in Futrell *et al.* (2015), as they were reported to be better able to balance the quality of optimisation result and simulation time (Futrell *et al.* 2015).

Table 6.10 Settings of the hybrid PSO-HJ algorithm in the design optimisation.

Settings for PSO-HJ	Parameter	Value
PSO	Neighbourhood topology	Von Neumann
	Number of particles	20
	Number of generations	20
	Cognitive acceleration	2.8
	Social acceleration	1.3
	Maximum velocity gain	0.5
	Constriction gain	0.5
	Mesh size divider	2
	Initial mesh size exponent	0
HJ	Mesh size divider	2
	Initial mesh size exponent	0
	Mesh size exponent increment	1
	Number of step reductions	3

The optimisation process is illustrated in Fig. 6.19, which consists of two parts, *i.e.* PSO process and HJ pattern search. During the PSO process, the maximal net electricity generation fluctuated significantly (see Fig. 6.19a)), while the average value of the net electricity generation in each generation increased and was finally stabilised at the end of the PSO process (see Fig. 6.19 b)). Based on the optimal solution with the maximal net electricity generation identified by the PSO, the HJ pattern search was initialised and implemented. Eventually, the HJ pattern converged and the optimisation process terminated. The corresponding optimal design that was identified was as follows: a PCM charging air flow rate of 1965 kg/h, an air channel size of 22

mm, and PCM layer thicknesses of the PCM TES units installed in the living and sleeping spaces of 12 mm and 23 mm, respectively. The optimal net electricity generation of 129.8 kWh can be achieved, if the optimal design was used.

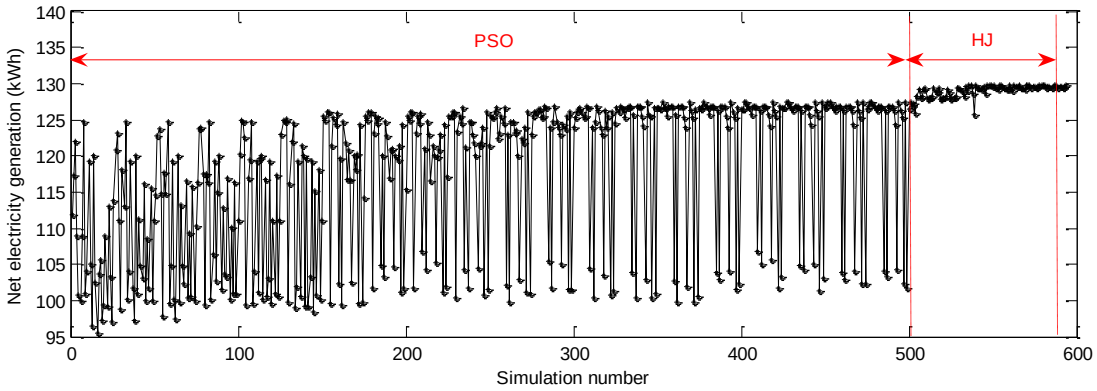

a) Net generation of electricity

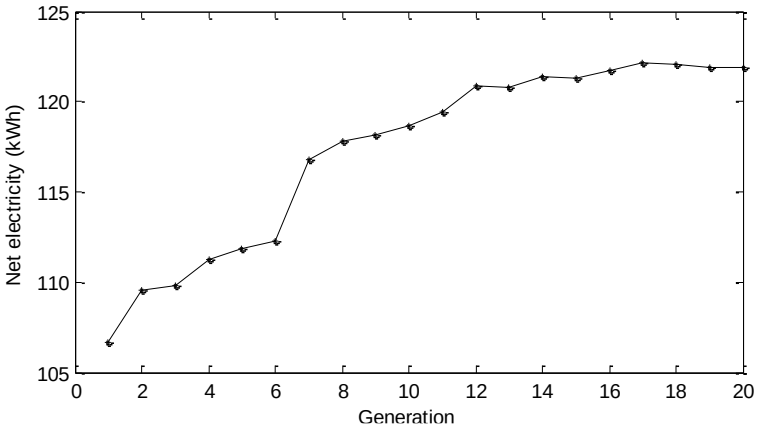

b) Average net generation of electricity in each generation of PSO

Fig. 6.19 Illustration of the optimisation process using the hybrid PSO-HJ search techniques.

6.5.3 Optimisation results and discussion

To investigate the benefits of the design optimisation, the *Optimal PVT-PCM* case was compared to the *PVT-PCM baseline* case. Fig. 6.20 compares the indoor air temperatures in the *Optimal PVT-PCM* case and the *PVT-PCM baseline* case. Note that the air temperature of the living space during both daytime and night time in the *Optimal PVT-PCM* case was slightly higher than the *PVT-PCM baseline* case (Fig. 6.20a). The fluctuations in temperature between 7:00 am - 9:00 am and 4:00 pm - 12:00 pm were mainly due to the on/off operation of the air flow supply (see Fig. 6.20b, c and d).

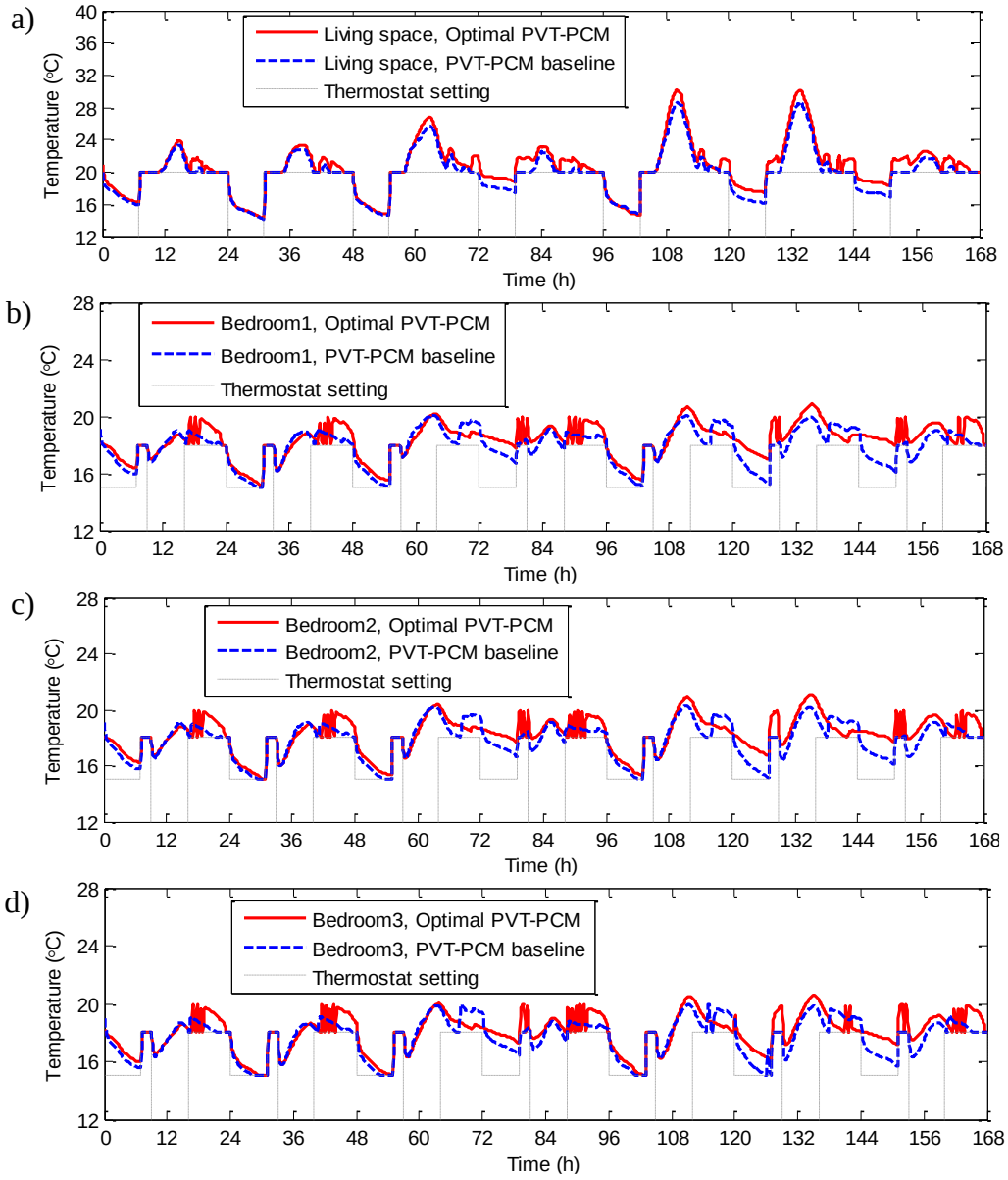

Fig. 6.20 Indoor air temperatures under the *Optimal PVT-PCM* case.

The percentage of thermal energy stored varied from -5.84 % to 79.9% under the *Optimal PVT-PCM* case, which was slightly lower than the *PVT-PCM baseline* case of -5.57% - 88.46% (see Fig. 6.18) because the storage capacity for thermal energy in the *Optimal PVT-PCM* case was much higher than the *PVT-PCM baseline* case, although the optimal design stored more thermal energy. This means the capacity for storing thermal energy in the *Optimal PVT-PCM* case was 1.65 times as the one in the *PVT-PCM baseline* case because the PCM layers were 46 mm and 24 mm thick in the sleeping and living spaces, rather than 20 mm thick for both spaces in the *PVT-PCM baseline* case. The amount of thermal energy stored in the overall PCM TES system under the *Optimal PVT-PCM* case can reach a maximum of 2.04×10^5 kJ, which was

higher than the 1.38×10^5 kJ in the *PVT-PCM baseline* case, as shown in Fig. 6.21. This indicates that much more thermal energy can be stored and then used to facilitate indoor space heating when the optimal design was used, compared to the *PVT-PCM baseline* case.

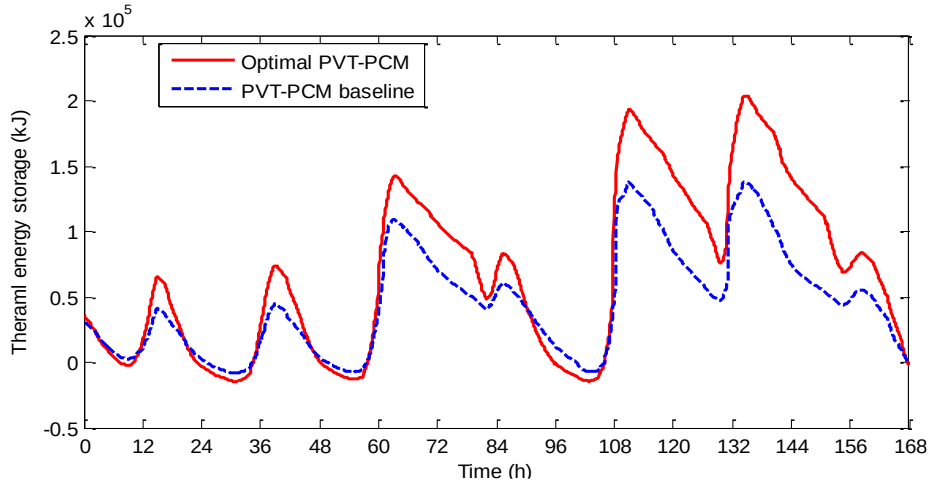

Fig. 6.21 Comparison of the thermal energy stored in the overall PCM TES for the *Optimal PVT-PCM* case and the *PVT-PCM baseline* case.

Fig. 6.22 presents the accumulated generation of electricity and total consumption of electricity in the *Optimal PVT-PCM case*. A comparison of electricity generation and consumption between the *Optimal PVT-PCM* case, the *PVT-PCM baseline*, and the *baseline* case is presented in Table 6.11.

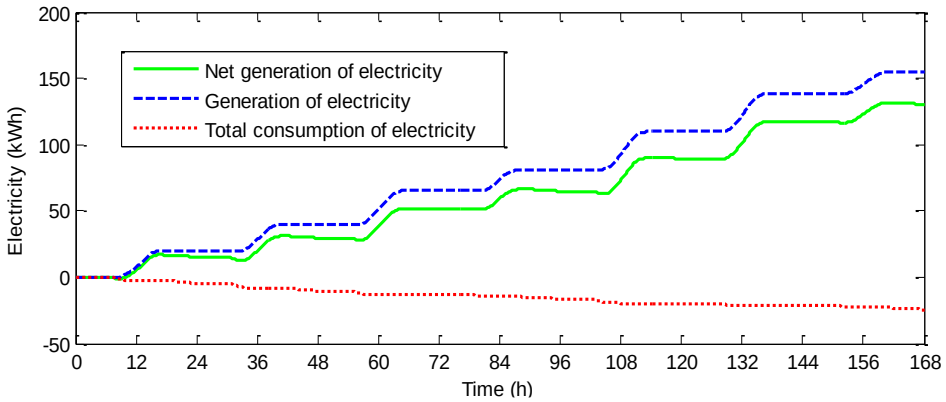

Fig. 6.22 Accumulated generation of electricity and total consumption of electricity under the *Optimal PVT-PCM* case.

Table 6.11 Comparison between the *Optimal PVT-PCM* case, the *PVT-PCM baseline* case and *baseline* case.

Generation or consumption of electricity (kWh)		*Optimal PVT-PCM*	*Baseline*	Relative difference	*PVT-PCM baseline*	Relative difference
Generation of electricity from the PVT collectors (E_{PV})		154.5	-	-	156.5	1.3%
Total consumption of electricity (E_{con})	Consumption of electricity by the heat pump (E_{HP})	13.0	72.0	65.7%	23.7	41.6%
	Consumption of electricity by the PCM fan ($E_{PCM,fan}$)	6.7			8.9	
	Consumption of electricity by the PVT fan ($E_{PVT,fan}$)	5.0			9.7	
Net generation of electricity (E_{net})		129.8	-	-	114.2	13.7%

The electricity generated by the PVT collectors under the *Optimal PVT-PCM* case was 154.5 kWh, which was less by 1.3% compared to the *PVT-PCM baseline* case. This is because the PVT air flow rate was lower than the *PVT-PCM baseline* case, resulting in a higher PV temperature. However, the net generation of electricity under the *Optimal PVT-PCM* case reached 129.8 kWh, which was improved by 13.7%, compared to net generation from the *PVT-PCM baseline* case. This was mainly due to a reduction in the consumption of electricity by the heat pump and the fans.

In the *Optimal PVT-PCM* case, the heat pump was the main consumer of electricity (13.0 kWh), followed by the PCM fan (6.7 kWh), and the PVT fan (5.0 kWh). This reduction in electricity required by the fans and the heat pump helped to improve the average COP to 8.92, which was much higher than the 5.21 of the *PVT-PCM baseline*.

6.6 Summary

A building integrated PVT-PCM enhanced HP system for space heating was developed, evaluated and then optimised. In this system, PVT collectors were used to generate electricity and low grade thermal energy, while a new concept of PCM utilisation was proposed by laminating PCM layers with an air channel between them in the building ceiling to enhance the local thermal mass and also serve as an overall TES system to temporally store the low grade thermal energy collected from the PVT collectors for space heating. This system was evaluated numerically based on an Australian house in terms of the indoor air temperature, the consumption of electricity, the electricity generated by PV panels, and the thermal energy stored in the PCM TES. This evaluation showed that the PCM TES units can store a large amount of thermal energy which could facilitate indoor space heating. The weekly winter analysis revealed that the total consumption of electricity by the air conditioning system can be reduced from 72.0 kWh to 42.3 kWh by using the building integrated PVT-PCM enhanced HP system, unlike the baseline house that only used the air source heat pump.

An optimal design of this system was achieved through optimisation using the hybrid PSO-HJ technique. The optimal design identified that a PCM type of PCM SP26E, a 22 mm air channel, a PVT air flow rate of 1965 kg/h, and 12 mm and 23 mm thick PCM layers for living space and sleeping were ideal. By adopting this optimal design, the optimal net generation of electricity during the Melbourne winter week was 129.8

kWh, which had an improvement of 13.7% in comparison to the *PVT-PCM baseline case* without optimisation, even though the electricity generated from the PVT collectors was lower by 1.3%. This improvement in the net generation of electricity was mainly due to a decrease in the electricity consumed by the fans and the heat pump from 42.3 kWh to 24.7 kWh, compared to the *PVT-PCM baseline* case. This means that optimisation can enhance the energy performance of the building integrated PVT-PCM enhanced HP system.

Chapter 7 Conclusions and Recommendations

This thesis presented the development, evaluation and optimisation of phase change materials (PCMs) and photovoltaic thermal (PVT) systems integrated into buildings and building heating, ventilation and air conditioning (HVAC) systems for building thermal management and energy efficiency enhancement. Three systems were developed and evaluated, and then their performance was optimised in order to improve their thermal performance and energy efficiency. These systems are:

i. Buildings with envelopes enhanced by PCMs and PVT collectors for space heating. In this system, the thermal performance of the PCM enhanced building using the heated air collected from PVT collectors for space heating was investigated numerically, and an optimisation strategy was developed to facilitate the design optimisation.

ii. A centralised PCM thermal energy storage (TES) system with integrated PVT collectors for solar heat storage. In this system, the charging performance of the PCM TES was investigated using a lab-scale test rig, and the charging performance of the PCM TES system was further optimised through bi-objective optimisations.

iii. An air source heat pump system with integrated PVT collectors and PCM layers laminated into building ceiling for space conditioning. The system evaluation and optimisation were carried out numerically.

The key findings from this study and recommendations for further work are summarised and presented in the following sections.

7.1 Summary of main findings

7.1.1 Evaluation and optimisation of the thermal performance of PCM enhanced buildings with integrated PVT collectors for space heating

The performance of PCM enhanced buildings with integrated PVT collectors for indoor space heating was evaluated and the design was optimised based on system modelling. A model of building envelope component integrated with PCMs with considering the hysteresis phenomenon during the phase change process was

developed and then validated. The performance of this system was then modelled and evaluated through a parametric study while the further analysis was carried out using the Taguchi method. The system was then optimised to maximise the building thermal performance enhanced by the PCMs and PVT collectors used for space heating. A design optimisation strategy called the Taguchi-Fibonacci search method, was developed and used as a tool for the optimisation, because it could optimise both continuous variables and discrete variables, and also identify the optimal solution with a limited number of iterations. The key findings achieved are as follows:

- The building envelope-integrated PCM model which considered the hysteresis phenomenon during phase change process can provide reliable estimates of phase change process for PCMs integrated in building envelopes;

- The simultaneous use of PCMs in building envelopes and PVT collectors for space heating can significantly enhance the thermal performance of buildings. The corresponding Coefficient of Thermal Performance Enhancement (CTPE) during a winter heating season reached over 40% unlike the baseline house without using the PVT ventilation and PCMs (*i.e.* CTPE of 0 as the baseline case);

- The thermal resistance of the wall insulation layer of the house was a critical factor affecting the thermal performance of the PCM enhanced buildings with the PVT ventilation, but it cannot replace the function of the PCM layers in terms of reducing fluctuations in the indoor temperature;

- The proposed Taguchi-Fibonacci search method can identify the near optimal values of the optimisation variables with a limited number of iterations. The CTPE of the PCM enhanced house with the PVT ventilation could reach 72.2% over two winter weeks, compared to a non-optimal case of 45.5%, if the optimal design identified by the proposed optimisation strategy is adopted.

7.1.2 Experimental investigation and optimisation of a centralised PCM TES system with integrated PVT collectors

An experimental investigation and bi-objective optimisation of a centralised PCM TES system was carried out based on a lab-scale test rig. A range of experiments was

designed using the Taguchi method, and the following two key performance indicators (KPIs) were developed to evaluate the charging performance of the PCM TES unit: the average heat transfer effectiveness and the effective PCM charging time. Two performance models were then developed based on the experimental data to facilitate the formulation of a bi-objective optimisation problem, which was then solved using the controlled elitist genetic algorithm (GA) - multi-criteria decision-making (MCDM) process. To increase confidence in the optimal solutions identified, as well as simplifying the bi-objective optimisation process, another optimisation strategy using fuzzy clustering was also used to determine the optimal solutions of the optimisation problem. The main conclusions achieved are as follows:

- The two KPIs were contradictory based on an analysis of the experimental result; this means that a high average heat transfer effectiveness comes with a long effective PCM charging time, and vice versa, so it is therefore important to consider the trade-off between the contradictory KPIs;

- Through the single-objective optimisation using Taguchi method, the average heat transfer effectiveness could be optimised to 85.3% when this KPI was considered as the optimisation objective, however, the KPI of the effective PCM charging time was low (*i.e.* as long as 9.17 hours). In contrast, the average heat transfer effectiveness and effective PCM charging time were 23.3% and 4.52 hours, respectively, when the KPI of the effective PCM charging time was used as the optimisation objective. These findings indicated that a bi-objective optimisation of the PCM TES unit is needed to consider the two contradictory performance indicators;

- Compared to single-objective optimisation, a more reasonable solution emerged when a bi-objective optimisation strategy with the controlled elitist GA - MCDM process was used. The average heat transfer effectiveness and the effective PCM charging time using the optimal design were 59.29% and 6.11 hours respectively; this optimal design was ranked as the best among the comparison with the single-objective optimal designs; and

- The fuzzy clustering-based bi-objective optimisation strategy, which simplified the optimisation process, can directly identify an optimal design for

the PCM TES unit, rather than undergoing a two-step process by identifying the optimal Pareto front first followed by an MCDM process. By using the optimal design identified using the fuzzy clustering-based bi-objective optimisation strategy, the average heat transfer effectiveness and the effective PCM charging time can reach 64.02% and 7.25 hours, respectively.

- The optimal designs identified by the bi-objective optimisation strategy using the controlled elitist GA - MCDM process, and the fuzzy clustering-based bi-objective optimisation strategy were very close, indicating that both strategies can identify the optimal solutions of the optimisation problem.

7.1.3 Performance evaluation and optimisation of the heat pump system with integrated PVT collectors and PCM layers laminated in the building ceiling

The heat pump system with PVT collectors and laminated PCM layers in the building ceiling was developed, in which the two PCM layers with an air channel between them were laminated into the ceiling to simultaneously enhance the local thermal mass and serve as a centralised TES to temporally store the low grade thermal energy generated from the PVT collectors. A mathematical model for the PCM TES unit which considered the hysteresis phenomenon was developed and validated. A study using the Taguchi method was then carried out to investigate the influence of the design variables on the energy performance of the integrated system. Lastly, a design optimisation strategy using the hybrid Particle Swarm Optimisation and Hooke-Jeeves pattern search (PSO-HJ) technique was developed to maximise the net generation of electricity of the proposed system. The main findings obtained are as follows:

- The proposed building integrated PVT-PCM enhanced HP system reduced the electricity required for space heating in an Australian house (with an air conditioned area of 150 m^2) during a winter week under Melbourne weather conditions) from 72 kWh to 42.3 kWh, however, the electricity consumed by the fans (8.9 kWh for the PCM fan and 9.7 kWh for the PVT fan) accounted for a substantial part of the total consumption of electricity;

- A large amount of net generation of electricity of 114.2 kWh was obtained by using the proposed system during a Melbourne winter week because the PVT collectors can generate 156.5 kWh of electricity;

- The optimisation strategy using the hybrid PSO-HJ algorithm was able to identify the optimal design of the proposed system. Unlike the baseline design case without optimisation, the net generation of electricity increased by 13.7%, when the optimal design was used. This is due to that the optimal design could reduce the consumption of electricity used for space heating by 41.6%, even though the electricity generated from the PVT collectors was lower by 1.3%; and

- With using the optimal design identified, much more thermal energy can be stored in the PCM TES and used to facilitate the indoor space heating, and the indoor thermal performance can be better than the case without optimisation.

7.1.4 Guideline of using PVT collectors and PCM TES in buildings

The three systems with integrated PCMs and PVT collectors in buildings and building HVAC systems employed different integration strategies and their application guideline is discussed in accordance with specific circumstances and climates.

In the first system, there is no direct interaction between the PVT collectors and the PCMs in the building envelope, and the PCMs were used passively. The results showed a thick PCM layer can provide a better indoor thermal performance, and the suitable wall insulation is important to ensure the performance of the PCM layer. Optimisation is necessary to ensure reasonable designs in terms of building thermal performance enhancement. This system can be used under a mild winter conditions with large temperature fluctuations between daytime and night time.

In the second system, the PCM TES unit is used to temporially store the heat generated by the PVT collectors. The system can therefore be used for building load shifting and peak demand control, assisting in reducing building operational cost. The PCM TES unit served as an active component and can be coupled with various building systems to enhance the flexibilities of thermal energy storage and utilisation. For this active solar thermal storage system, the balance of charging efficiency and charging time need to be considered according to specific weather conditions.

The third system combines the advantage of the above two systems by integrating two PCM layers on the building ceiling as active centralised TES units, in addition to which,

an air source heat pump is integrated as a backup. Apart from using the thermal energy stored in the PCM for space heating directly, the thermal energy can be fully used to further enhance the efficiency of the heat pump. These advantages extend the application capability in cold winter weather conditions while providing better indoor thermal performance. However, due to the complexity of the system, it tends to be more expensive and a complicated control system is necessary in practice. Optimisation is also recommended to better couple the different components when using the system.

The thermal performance analysis of these systems mainly focused on winter heating conditions in this study, due to the fact that the main benefit of using the low grade thermal energy derived from PVT collectors is for space heating. It is worthwhile to mention that the cool air generated by the PVT collectors in summer by night time radiative cooling effect can also be used for indoor space cooling and/or used as pre-cooled air to improve the efficiency of HVAC systems. However, only a small among of cool energy can be collected by PVT collectors, compared to the potential solar thermal energy can be collected.

7.2 Recommendations for future work

The use of PVT collectors and PCMs to enhance building performance and energy efficiency was investigated in this study. The economic benefit of using the proposed systems was not studied, so it would be better if a life cycle cost analysis could be implemented.

The design optimisation of these PCMs and PVT systems could lead to the design of high performance systems. It will be more practical if the design optimisation process can be summarised as road maps for the optimal design of these types of systems based on a wide range of studies for different applications.

The design optimisation carried out in this study focused mainly on the PCM system because thermal energy storage using PCMs is the key to achieving thermal management and enhanced energy efficiency of buildings. It would be worthwhile developing appropriate optimisation strategies for the optimal design of the whole HVAC system with integrated PVT collectors and PCMs.

Furthermore, since a design optimisation was carried out in this study, it would also be beneficial to develop advanced control strategies to optimise system operation to maximise the overall benefits from using PCM and PVT collectors in buildings.

The performance of the developed systems under Sydney and Melbourne winter weather conditions were analysed and discussed. It will be beneficial if the application of these systems can be further evaluated and discussed under different climates.

References

Abhatlow A. 1983. Temperature latent heat thermal energy storage: heat storage materials. *Solar Energy*, vol.30, no.4, pp.313-332.

Agyenim F., Hewitt N., Eames P. and Smyth M. 2010a. A review of materials, heat transfer and phase change problem formulation for latent heat thermal energy storage systems (LHTESS). *Renewable and Sustainable Energy Reviews*, vol.14, no.2, pp.615-628.

Agyenim F., Hewitt N., Eames P.C. and Smyth M. 2010b. Heat transfer enhancement in medium temperature thermal energy storage system using a multi-tube heat transfer array. *Renewable and Sustainable Energy Reviews*, vol.14, no.2, pp.615-628.

Ahmad M., Bontemps A., Sallee H. and Quenard D. 2006. Experimental investigation and computer simulation of thermal behaviour of wallboards containing a phase change material. *Energy and Buildings*, vol.38, no.4, pp.357-366.

Alawadhi E.M. 2008. Thermal analysis of a building brick containing phase change material. *Energy and Buildings*, vol.40, no.3, pp. 351–357.

Alawadhi E.M. and Alqallaf H.J. 2011. Building roof with conical holes containing PCM to reduce the cooling load: numerical study. *Energy Conversion and Management*, vol.52, no.8-9, pp.2958–2964.

Alawadhi E.M. 2012. Using phase change materials in window shutter to reduce the solar heat gain. *Energy and Buildings*, vol.47, pp.421-429.

Aldoss T.K. and Rahman M.M. 2014. Comparison between the single-PCM and multi-PCM thermal energy storage design. *Energy Conversion and Management*, vol.83, pp.79-87.

Al-Imam M.F.I, Beg R.A., Rahman M.S. and Khan M.Z. 2016. Performance of PVT solar collector with compound parabolic concentrator and phase change materials. *Energy and Buildings*, vol.113, pp.139-144.

Al-Shannaq R., Kurdi J., Al-Muhtaseb S， Dickinson M. and Farid M., 2015. Supercooling elimination of phase change materials (PCMs) microcapsules. *Energy*, vol.87, pp., 654–662.

Amin N.A.M., Belusko M. and Bruno F. 2009. Optimization of a phase change thermal storage system. *World Academy of Science, Engineering and Technology*, vol.3, no.1, pp.708-712.

Amin N.A.M , Belusko M., Bruno F. and Liu M. 2012. Optimizing PCM thermal storage systems for maximum energy storage effectiveness. *Solar Energy*, vol.86, no.9, pp.2263–2272.

Antonion A. and Lu W.S. 2007. Practical optimisation algorithms and engineering applications. Springer Science+Business Media. New York, USA.

Ascione F. *et al.* 2014. Energy refurbishment of existing buildings through the use of phase change materials: energy saving and indoor comfort in the cooling season. *Applied Energy*, vol.113, pp.990–1007.

American Society of Heating, Refrigerating and Air-Conditioning Engineers 2009, 2009 ASHRAE Handbook – Fundamentals.

Assoa Y.B., Menezo C., Fraisse G., Yezou R. and Brau J. 2007. Study of a new concept of photovoltaic-thermal hybrid collector. *Solar Energy*, vol.81, pp.1132-1143.

Aste N., Chiesa G. and Verri F. 2008. Design, development and performance monitoring of a photovoltaic-thermal air collector. *Renewable Energy*, vol.32, pp.914-927.

Athienitis A.K., Liu C., Hawes D., Banu D. and Feldman D. 1997. Investigation of the thermal performance of a passive solar test room with wall latent heat storage. *Building and Environment*, vol.32, no.5, pp.405-410.

Australian Government Department of Industry 2013. Representative dwelling models: industry consultation summary paper for survey participants.

Baetens R., Jelle B.P. and Gustavsen A. 2010. Phase change materials for building applications: a state-of-the-art review. *Energy and Buildings*, vol.42, no.9, pp.1361-1368.

Bambrook S.M. and Sproul A.B. 2012. Maximizing the energy output of a PVT air system. *Solar Energy*, vol.86, pp.1857-1871.

Bastani A., Haghighat F. and Kozinski J. 2014. Design building envelope with PCM wallboards: design tool development. *Renewable and Sustainable Energy Reviews*, vol.31, pp.554-562.

Bathelt A.G. and Viskanta R. and Leidenfrost W. 1979. An experimental investigation of natural convection in the melted region around a heated horizontal cylinder. *Journal of Fluid Mechanics*, vol.90, no.2, pp.227-239.

Bazilian M.D., Leenders F., Van Der Ree B.G.C. and Prasad D. 2001. Photovoltaic cogeneration in the built environment. Solar Energy, vol.71, no.1, pp.57-69.

Beatens R., Jelle B.P. and Gustavsen A. 2010. Phase change materials for building applications: a state-of-the-art review. Energy and Buildings, vol.42, no.9, pp.1361-13689.

Belusko M and Bruno F. 2008. Design methodology of PCM thermal storage systems with parallel plates. *EuroSun 2008 Congress*, Lisbon, Portugal, October 7-10 2008.

Beek J. 1962. Design of packed catalytic reactors. *Advances in Chemical Engineering*, vol.3, pp.203-271.

Bergman T.L., Lavine A.S., Incropera F.P. and Dewitt D.P. 2011. Fundamentals of Heat and Mass Transfer. 7th edition, *John Wiley & Sons*, Hoboken, New Jersey, USA.

Beckman W.A. 2001. TRNSYS reference manual. vol.2. Solar Energy Laboratory.

Biswas K. and Abhari R. 2014. Low-cost phase change material as an energy storage medium in building envelopes: experimental and numerical analyses. *Energy Conversion and Management*, vol.88, pp.1020-1031.

Blervaque Hl, Stabat P., Filfli S., Chumann M. and Marchio D. 2016. Variable-speed air-to-air heat pump modelling approaches for building energy simulation and comparison with experimental data. *Journal of Building Performance Simulation*, vol.9, no.22, pp.210-225.

Bony J. and Citherlet S. 2007. Numerical model and experimental validation of heat storage with phase change materials. *Energy and Buildings*, vol.39, no.10, pp.1065-1072.

Bontempsa A., Ahmadb M., Johannesc K. and Salleec H. 2011. Experimental and modelling study of twin cells with latent heat storage walls. *Energy and Buildings*, vol.43, no.9, pp.2456-2461.

Borderon J., Virgone J. and Cantin R. 2015. Modelling and simulation of a phase change material system for improving summer comfort in domestic residence. *Applied Energy*, vol.140, pp.288-296.

Browne M, Norton B. and McCormack S.J. 2015. Phase change materials for photovoltaic thermal management. *Renewable & Sustainable Energy Reviews*, vol. 47, pp.762-782.

Butala V. and Stritih U. 2009. Experimental investigation of PCM cold storage. *Energy and Buildings*, vol.41, no.3, pp.354-359.

Butler D. 2008. Architecture: architects of low-energy future. *NATURE*, vol.452, no.7187, pp.520-523.

Cabeza L.F., Castellon C., Nogues M., Medrano M., Leppers R. and Zubillaga O. 2007. Use of microencapsulated PCM in concrete walls for energy savings. *Energy and Buildings*, vol.39, no.2, pp.113-119.

Cabeza L.F., Castell A., Barrenechea C., De Graciaa A. and Fernándezb A.I. 2011. Materials used as PCM in thermal energy storage in buildings: A review. *Renewable and Sustainable Energy Review*s, vol.15, no.3, pp.1675-1695.

Calise F., d'Accadia M.D., Figaj R.D. and Vanoli L. 2016. A novel solar-assisted heat pump driven by photovoltaic/thermal collectors: dynamic simulation and thermoeconomic optimization. *Energy, vol.95*, pp.346-366.

Castell A., Martorell I., Medrano M., Perez G. and Cabeza L.F. 2010. Experimental study of using PCM in brick constructive solutions for passive cooling. *Energy and Buildings*, vol.42, no.4, pp.534-540.

Castellani B., Morini E., Filipponi M., Nicolini A. Palombo M. 2014. Clathrate hydrates for thermal energy storage in buildings: overview of proper hydrate-forming compounds. *Sustainability*, vol.6, no.6, pp.6815-6829.

Caterino N. 2009. Comparative analysis of multi-criteria decision-making methods for seismic structural retrofitting. *Computer-Aided Civil and Infrastructure Engineering*, vol.24, pp.432-445.

Carlisle A. and Dozier G. 2001. An off-the-shelf PSO. *Proceedings of the Workshop on Particle Swarm Optimisation*. Indianapolis, Purdue School of Engineering and Technology, IUPUI, Indianapolis, IN, USA, 2001.

Cerona I., Neilaa J. and Khayet M. 2011. Experimental tile with phase change materials (PCM) for building use. *Energy and Buildings*, vol.43, no.8, pp.869–1874.

Chandrasekharan R., Lee S.E., Fisher D.E. and Deokar P.S. 2013. An enhanced simulation model for building envelopes with phase change materials. 2013 *ASHRAE Annual Conference*, Denver, Colorado, USA, June 22-26, 2013.

Charvat P., Klimes L. and Ostry M. 2014. Numerical modelling and experimental investigation of a PCM-based thermal storage unit for solar air systems. *Energy and Buildings*, vol.68, part A., pp.488-497.

Chaiyat N. 2015. Energy and economic analysis of a building air conditioner with a phase change material. *Energy Conversion and Management*, vol.94, pp.150–158.

Charalambous P.G., Maidment G.G., Kalogirou S.A. and Yiakoumetti K. 2007. Photovoltaic thermal (PV/T) collectors: a review. *Applied Thermal Engineering*, vol.27, pp.275-286.

Chen C., Liang L., Zhang Y., Chen Z. and Xie G.Y. 2014. Heat transfer performance and structural optimization design method of vertical phase change thermal energy storage device. *Energy and Buildings*, vol.68, Part B, pp.679–685.

Chen X.J., Worall M., Omer S., Su Y.H. and Riffat S. 2014. Experimental investigation on PCM cold storage integrated with ejector cooling system. *Applied Thermal Engineering*, vol.63, no.1, pp.419–427.

Chen Y.X., Galal K. and Athienitis A.K. 2010. Modelling, design and thermal performance of a BIPVT system thermally coupled with a ventilated concrete slab in a low energy solar house: part 2, ventilated concrete slab. *Solar Energy*, vol.84, pp.1908-1919.

Cho K. and Choi S.H. 2000. Thermal characteristics of paraffin in a spherical capsule during freezing and melting processes. *International Journal of Heat and Mass Transfer*, vol.43, no.17, pp.3183-3196.

Chow T.T. 2010. A review on photovoltaic/thermal hybrid solar technology. *Applied Energy*, vol.87, pp.365-379.

Clerc M. and Kennedy J. 2002. The particle swarm – explosion, stability and convergence in a multidimensional complex space. *IEEE Transactions on Evolutionary Computation*, vol.6, pp. 58-73.

Cui Y.B., Liu C.H., Hu S. and Yu X. 2011. The experimental exploration of carbon nanofiber and carbon nanotube additives on thermal behaviour of phase change materials. *Solar Energy Materials & Solar Cells*, vol.95, no.4, pp.1208-1212.

De Falco M., Capocelli M. and Giannattasio A. 2016. Performance analysis for an innovative PCM-based device for cold storage in the civil air conditioning. *Energy and Buildings*, vol.122, pp.1 -10.

De Gracia A. and Cabeza L.F. 2016. Numerical simulation of a PCM packed bed system: A review. *Renewable and Sustainable Energy Reviews*, vol.69, pp.1055–1063.

Deb K., Agrawal S, Pratap A. and Meyarivan T. 2000. A fast elitist non-dominated sorting genetic algorithm: NSGA-II. *Lecture Notes in Computer Science* 1917, pp. 849-858.

Drake J.B. 1987. A study of the optimal transition temperature of PCM wallboard for solar energy storage. Oak Ridge National Laboratory.

Delcroix B., Kummert M. and Daoud A. 2015. Thermal behaviour mapping of a phase change material between heating and cooling enthalpy-temperature curves. *Energy Procedia*, vol.78, pp.225-230.

Dolado P., Lazaro A., Zalba B. and Marin J.M. 2006. Numerical simulation of the thermal behaviour of an energy storage unit with phase change materials for air conditioning application between 17ºC and 40ºC. *ECOSTOCK 10th international conference on thermal energy storage*, Stockton, California, USA, May 31 - June 2, 2006.

Dolado P., Lazaro A., Marin J.M. and Zalba B. 2011a. Characterization of melting and solidification in a real scale PCM-air heat exchanger: experimental results and empirical model. *Renewable Energy*, vol.36, no.11, pp.2906-2917.

Dolado P., Lazaro A., Marin J.M. and Zalba B. 2011b. Characterization of melting and solidification in a real scale PCM-air heat exchanger: Numerical model and experimental validation. *Energy Conversion and Management*, vol.52, pp.1890-1907.

Dolado P., Lazaro A., Delgado M., Penalosa C., Mazo J., Marin J.M. and Zalba B. 2012a. Thermal energy storage by PCM-air heat exchanger: temperature maintenance in a room. *Energy Porcedia*, vol.30, pp.225-234.

Dolado P., Mazo J., Lazaro A., Marin J.M. and Zalba B. 2012b. Experimental validation of a theoretical model: uncertainty propagation analysis to a PCM-air thermal energy storage unit. *Energy and Buildings*, vol.45, pp.124–131.

Diana U.V., Luisa F.c., Susana S., Camila B. and Ksenia P. 2015. Heating and cooling energy trends and drivers in buildings. *Renewable and Sustainable Energy Reviews*, vol.41, pp.85–98.

Dieckman J.H. 2008 (cited 10 Feburary. 2017). Latent heat storage in concrete. Available at http://www.eurosolar.org.

Dutil Y., Rousse D.R., Salah N.B.,Lassue S. and Zalewski L. 2011. A reviews on phase change materials: mathematical modelling and simulations. *Renewable and Sustainable Energy Reviews*, vol.15, no.1, pp.112-130.

Edwards D.P. and Jensen M.K. 1994. Pressure Drop and Heat Transfer Predictions of Turbulent Flow in Longitudinal Finned Tubes. *Advances in Enhanced Heat Transfer*, vol.287, pp.17-23.

Eicker U. and Dalibard A. 2011. Photovoltaic-thermal collectors for nigh radiative cooling of buildings. *Solar Energy*, vol.85, pp.1322-1335.

Esen M., Durmus A. and Durmus A. 1998. Geometric design of solar-aided latent store depending on various parameters and phase change materials. *Solar Energy*, vol.62, no.1, vol.19-28.

Evers A.C. Medina M.A., and Fang Y. 2010. Evaluation of the thermal performance of frame walls enhanced with paraffin and hydrated salt phase change materials using a dynamic wall simulator. *Building and Environment*, vol.45, no.8, pp.1762-1768.

Evins R. 2015. Multi-level optimization of building design, energy system sizing and operation. *Energy*, vol.90, part 2, pp.1775-1789.

Faghri A., Zhang Y.W. and Howell J.R. 2010. Advanced Heat and Mass Transfer. *Global Digital Press*, Columbia, MO, USA.

Fan W.K., Kokogiannakis G., Ma Z.J. and Cooper P. 2017. Development of a dynamic model for a hybrid photovoltaic thermal collector - solar air heater with fins. *Renewable Energy*, vol.101, pp.816-834.

Farid M.M. and Husian R.M. 1990. An electrical storage heater using the phase-change method of heat storage. *Energy Conversion and Management*, vol.30, no.3, pp.219-230.

Farid M.M. and Chen X.D. 1999. Domestic electrical space heating with heat storage. *Proceedings of the Institution of Mechanical Engineers*, vol.213, part A, pp.83-92.

Farid M.M., Khudhair A.M., Siddique A.K.R. and Said A.H. 2004. A review on phase change energy storage and applications. *Energy Conversion and Management*, vol.45, no.9, pp.1597-1615.

Feldman D. and Banu D. 1991. Obtaining an energy storing building material by direct incorporation of an organic phase change material in gypsum wallboard. *Solar Energy Materials*, vol.22, no.2-3, pp.231-242.

Fiorentini M., Cooper P. and Ma Z.J. 2015. Development and optimization of an innovative HVAC system with integrated PVT and PCM thermal storage for a net-zero energy retrofitted house. *Energy and Buildings*, vol.94, pp.21-32.

Futrell B.J., Ozelkan E.C. and Brentrup D. 2015. Bi-objective optimisation of building enclosure design for thermal and lighting performance. *Building and Environment*, vol.92, pp.591-602.

Furzerland R.M. 1980. A comparative study of numerical methods for moving boundary problems. *Journal of the Institute of Mathematics and its Applications*, vol.26, pp.411-429.

Gnielinski V. 1976. New equations for heat and mass-transfer in turbulent pipe and channel flow. *International chemical engineering*, vol.16, no.2, pp.359-368.

Gowreesunker B.L., Tassou S.A. and Kolokotroni K. 2013. Coupled TRNSYS-CFD simulations evaluating the performance of PCM plate heat exchangers in an airport terminal building displacement conditioning system. *Building and Environment*, vol.65, pp.132–145.

Gschwander S. Comparision of TA-instrument's MC-DSC and Setaram's uDSC-III',

Fraunhofer Institute of Solar Energy System (ISE).

Guichard S., Miranville F., Bigot D., Malet-Damour B. and Boyer H. 2015. Experimental investigation on a complex roof incorporating phase-change material. *Energy and Buildings*, vol.108, pp.36-43.

Hasnain S.M. 1998. Review on sustainable thermal energy storage technologies, part I: heat storage materials and techniques. *Energy Conversion and Management*, vol.39, no.11, pp.1127-1138.

Hasan A., McCormack S.J., Huang M.J. and Norton B. 2010. Evaluation of phase change materials for thermal regulation enhancement of building integrated photovoltaics. *Solar Energy*, vol.84, no.9, pp.1601-1612.

Hasan A., McCormack S.J., Huang M.J. and Norton B. 2014. Energy and Cost Saving of a Photovoltaic-Phase Change Materials (PV-PCM) System through Temperature Regulations and Performance Enhancement of Photovoltaics. *Energies*, vol.7, pp.1318-1331.

Hadjieva M., Stoykova R., Filipova T. 2000. Composite salt-hydrate concrete system for building energy storage. *Renewable Energy*, vol.19, no.1-2, pp.111-115.

Hamada Y., Ohtsu W. and Fukai J. 2003. Thermal response in thermal energy storage material around heat transfer tubes - effect of additives on heat transfer rates. *Solar Energy*, vol.75, no.4, pp.317–328.

Halford C.K. and Boehm R.F. 2007. Modelling of phase change material peak load shifting. *Energy and Buildings*, vol.39, no.3, pp.298-305.

Hed G. and Bellander G. 2006. Mathematical modelling of PCM air heat exchanger. *Energy and Buildings*, vol.38, no.2, pp.82-89.

Hendra R., Hamdani, Mahlia T.M.I. and Masjuki H.H. 2005. Thermal and melting heat transfer characteristics in a latent heat storage system using mikro. *Applied Thermal Engineering*, vol.25, no.10, pp.1503–1515.

Henderson H., Huang J.Y. and Parker D. 1999. Residential equipment part load curves for use in DOE-2, LBNL-42175

Helm M., Keil C., Hiebler S., Mehling H. and Schweigler C. 2009. Solar heating and cooling system with absorption chiller and low temperature latent heat storage energetic performance and operational experience. *International Journal of Refrigeration*, vol.32, no.4, pp.596–606.

Ho C.J., Tanuwijava A.O. and Lai C.M. 2012. Thermal and electrical performance of a BIPV integrated with a microencapsulated phase change material layer. *Energy and Buildings*, vol.50, pp.331-338.

Hollands K.G.T., Unny T.E., Raithby G.D. and Konicek L. 1976. Free convective heat transfer across inclined air layers. *Journal of Heat Transfer*, ASME Transactions, vol.98, pp.189-193.

Holman J.P. 1997. Heat transfer. 8th edition, *McGraw Hill*, New York, USA.

Hooke R. and Jeeves T.A. 1961. Direct search solution of numerical and statistical problems, *Journal of the Association for Computing Machinery*, vol.8, pp.212-229.

Hirata T. and Nishida K. 1989. An analysis of heat transfer using equivalent thermal conductivity of liquid phase during melting inside an isothermally heated horizontal cylinder. *International Journal of Heat and Mass Transfer*, vol. 32, no. 9, pp. 1663-1670.

Huang M.J., Eames P.C. and Hewitt N.J. 2006. The application of a validated numerical model to predict the energy conversion potential of using phase change material in the fabric of a building. *Solar Energy Materials and Solar Cells*, vol.90, no.13, pp.1951-1960.

Huang K.L., Feng G.H and Zhang J.S. 2014. Experimental and numerical study on phase change material floor in solar water heating system with a new design. *Solar Energy*, vol.105, pp.126–138.

Huang M.J. 2011. The effect of using two PCMs on the thermal regulation performance of BIPV systems. *Solar Energy Mater Solar Cells*, vol.95, no.3, pp.957-963.

Hunter L.W. and Kuttler J.R. 1989. The enthalpy method for heat conduction problems with moving boundaries. *Journal of Heat Transfer*, Transactions of ASME, vol.111, pp.239-242.

International Renewable Energy Agency 2011, Technology Roadmap Energy-efficient Buildings: Heating and Cooling Equipment. Available at http://www.iea.org/.

Ismail K.A.R. and De Jesus A.B. 1999. Modelling and solution of the solidification problem of PCM around a cold cylinder. Numerical Heat Transfer, vol. 36, no.1, pp. 95-114.

Ismail K.A.R. and Stuginsky R.J. 1999. A parametric study on possible fixed bed models for PCM and sensible heat storage. *Applied Thermal Engineering*, vol.19, no.7, pp.757-788.

Ismail K.A.R. and Henríquez J.R. 2000. Solidification of PCM inside a spherical capsule. *Energy Conversion and Management*, vol.41, no.2, pp.173–187.

Ismail K.A.R., Henríquez J.R., da Silva T.M. 2003. A parametric sturdy on ice formation inside a spherical capsule. *International Journal of Thermal Sciences*, vol.42, no.9, pp.881-887.

Iten M. and Liu S. 2014. A working procedure of utilizing PCMs as thermal storage systems based on air –TES systems. *Energy Conversion and Management*, vol.77, pp.608–627.

Iten M., Liu S.L. and Shukla A. 2016. A review on the air-PCM-TES application for free cooling and heating in the buildings. *Renewable and Sustainable Energy Review*, vol.61, pp.175-186.

Jajuga K. 1991. L1-norm based fuzzy clustering. *Fuzzy Sets and Systems*, vol.39, no.1, pp.43-50.

Jayalath A., Nicolas R.S., Sofi M., Shanks R., Ngo T., Aye L. and Mendisa P. 2016b. Properties of cementitious mortar and concrete containing micro-encapsulated phase change materials. *Construction and Building Materials*, vol.120, pp.408-417.

Jayalath A., Aye L., Mendis P. and Ngo T. 2016a. Effects of phase change material roof layers on thermal performance of a residential building in Melbourne and Sydney. *Energy and Buildings*, vol.121, pp.152-158.

Ji J., Han J., Chow T.T., Yi H., Lu J.P., He W. and Sun W. 2006. Effect of fluid flow and packing factor on energy performance of a wall-mounted hybrid photovoltaic/water-heating collector system. *Energy and Buildings*, vol.38, pp.1380-1387.

Jin X. and Zhang X.S. 2011. Thermal analysis of a double layer phase change material floor. *Applied Thermal Engineering*, vol.31, no.10, pp.1576–1581.

Kang Y.B., Jiang Y. and Zhang Y.P. 2003. Modelling and experimental study on an innovative passive cooling system – NVP system. *Energy and Buildings*, vol.35, no.4, pp.417–425.

Kang Y.B., Zhang Y.B., Jiang Y. Zhu Y.X. 1999. A general model for analysing the thermal characteristics of a class of latent heat thermal energy storage systems. *Journal of Solar Energy Engineering*, vol.121, no.4, pp.185-193.

Kaufman L. and Rousseeuw P.J. 1990. Finding Groups in Data: An Introduction to Cluster Analysis. John Wiley & Sons, New Jersey, USA.

Kennedy J. and Mendes R. 2002. Population structure and particle swarm performance *Proceedings of the 2002 Congress on Evolutionary Computation*, 2002.5.12-17, Washington, USA.

Kissock K. and Limas S., 2006. Diurnal load reduction through phase change building components. *ASHRAE Transactions*, vol.112, pp.509-517.

Ko J.M., Kim Y.S., Chung M.H. and Jeon H.C. 2015. Multi-objective optimisation design for a hybrid energy system using the genetic algorithm. *Energies*, vol.8, pp.2924-2949.

Kondo T. and Ibamoto T. 2006. Research on thermal storage using rock wool phase change material ceiling board. *ASHARE Transactions*, vol.112, pp.526-531.

Koschenz M. and Lehmann B. 2004. Development of a thermally activated ceiling panel with PCM for application in lightweight and retrofitted buildings. *Energy and Buildings*, vol.36, no.6, pp.567–578.

Kumar R. and Rosen M.A. 2011. A critical review of photovoltaic-thermal solar collectors for air heating. *Applied Energy*, vol.88, pp.3603-3614.

Kuznik F., Virgone J. and Noel J. 2008a. Optimization of a phase change material wallboard for building use. *Applied Thermal Engineering*, vol.28, no.11-12, pp.1291-1298.

Kuznik F., Virgone J. and Roux J.J. 2008b. Energetic efficiency of room wall containing PCM wallboard: a full-scale experimental investigation. *Energy and Buildings*, vol.40, no.2, pp.148-156.

Kuznik F. and Virgone J. 2009a. Experimental investigation of wallboard containing phase change material: data for validation of numerical modelling. *Energy and Buildings*, vol.41, no.5, pp.561-570.

Kuznik F. and Virgone J. 2009b. Experimental assessment of a phase change material for wall building use. *Applied Energy*, vol.86, no.10, pp.2038-2046.

Kuznik F., Virgone J. and Johannes K. 2010. Development and validation of a new TRNSYS type for the simulation of external building walls containing PCM. *Energy and Building*, vol.42, no.7, pp.1004-1009.

Kuznik F., David D., Johannes K. and Roux J.J. 2011. A review on phase change materials integrated in building walls. *Renewable and Sustainable Energy Review*s, vol.15, no.1, pp.379-391.

Kuznik F., Juan Pablo Arzamendia Lopez J.P.A., Baillis D. and Johannes K. 2015. Design of a PCM to air heat exchanger using dimensionless analysis: application to electricity peak shaving in buildings. *Energy and Buildings,* Vol.106, pp.65–73.

Labat M., Virgone J., David D. and Kuznik F. 2014. Experimental assessment of a PCM to air heat exchanger storage system for building ventilation application. *Applied thermal engineering*, vol.66, no.1-2, pp.375-382.

Lamberg P. 2004. Approximate analytical model for two-phase solidification problem in a finned phase-change. *Applied Energy*, vol.77, no.2, pp. 131–152.

Laia C.M., Chenb R.H. and Lin C.Y. 2010. Heat transfer and thermal storage behaviour of gypsum boards incorporating micro-encapsulated PCM. *Energy and Buildings*, vol.42, no.8, pp. 1259–1266.

Lazaro A., Dolado P., Marin J.M. and Zalba B. 2009a. PCM-air heat exchangers for free cooling applications in buildings: experimental results of two real-scale prototypes. *Energy Conversion and Management*, vol.50, no.3, pp.439-443.

Lazaro A., Dolado P., Marin J.M. and Zalba b. 2009b. PCM-air heat exchangers for free-cooling applications in buildings: empirical mental and application to design. *Energy Conversion and Management*, vol.50, pp.444-449.

Lee T., Hawes D.W., Banu D., Feldman D. 2000. Control aspects of latent heat storage and recovery in concrete. *Solar Energy Materials and Solar Cells*, vol.62, no.3, pp.217-237.

Li H., Liu X. and Fang G.Y. 2010. Preparation and characteristics of n-nonadecane/cement composites as thermal energy storage materials in buildings. *Energy and Buildings*, vol.44, no.10, pp.1661-1665.

Li X.Q., Wei H.T., Lin X.S. and Xie X.Z. 2016. Preparation of stearic acid/modified expanded vermiculite composite phase change material with simultaneously enhanced thermal conductivity and latent heat. *Solar Energy Materials and Solar Cells*, vol.155, pp.9–13.

Lin K.P., Zhang Y.P., Xu X., Di H.F., Yang R. and Qin P.H 2005. Experimental study of under-floor electric heating system with shape-stabilized PCM plates. *Energy and Buildings*, vol.37, no.3, pp.215–220.

Liu M., Saman W. and Bruno F. 2011. Validation of a mathematical model for encapsulated phase change material flat slabs for cooling applications. Applied Thermal Engineering, vol.31, no.14–15, pp.2340–2347.

Lopez J.P.A., Kuznik F., Baillis D. and Virgone J. 2013. Numerical modelling and experimental validation of a PCM to air heat exchanger. *Energy and Buildings*, vol.64, pp.415-422.

Lu S.L., Liu S.B., Huang J.Y. and Kong X.F. 2014. Establishment and experimental verification of PCM room's TRNSYS heat transfer model based on latent heat utilization ratio. Energy and Buildings, vol.84, pp.287–298.

Malvi C.S., Dixon-Hardy D.W. and Crook R. 2011. Energy balance model of combined photovoltaic solar-thermal system incorporating phase change material. *Solar Energy*, vol.85, no.7, pp.1440–1446.

Mathworks (cited in 23 March 2016), Available at http://au.mathworks.com/help/gads/examples/multiobjective-genetic-algorithm-options.html.

Matrawy K.K. 1998. Theoretical analysis for an air heater with a box-type absorber. *Solar Energy*, vol.63, no.3, pp.191-198

Medina M.A., King J.B. and Zhang M. 2008. On the heat transfer rate reduction of structural of structural insulated panels (SIPs) outfitted with phase change materials (PCMs). *Energy*, vol.33, no.4, pp.667-678.

Mehling H. and Cabeza L.F. 2008. Heat and cold storage with PCM: An up to date introduction into basics and applications. Springer-Verlag, Berlin Heidelberg.

Michael J.J., Iniyan S., Goic R. 2015, 'Flat plate solar photovoltaic–thermal (PV/T) systems: A reference guide', Renewable and Sustainable Energy Reviews, vol.51, pp.62-88.

Milos M. and Miroslav R. 2013. Application of the Taguchi method for optimisation of laser cutting: a review. *Nonconventional Technologies Review*, Romania, December, pp.50-57.

National House Energy Rating Scheme, Australia (cited 15 January 2014), Available at www.nathers.gov.au.

Nedjar B. 2002. An enthalpy-based finite element method for nonlinear heat problems involving phase change. *Computers and Structures*, vol.80, no.1, pp.9-21.

Novais R.M., Ascensao G., Seabra M.P. and Labrincha J.A. 2015. Lightweight dense/porous PCM-ceramic tiles for indoor temperature control. *Energy and Buildings*, vol.108, pp.205-214.

Nualboonrueng T., Tuenpusa P., Ueda Y. and Akisawa A. 2012. Field experiments of PV-thermal collectors for residential application in Bangkok. *Energies*, vol.5, pp.1229-1244.

Osterman E., Tyagi V.V., Butala V., Rahim N.A. and Stritih U. 2012. Review of PCM based cooling technologies for buildings. *Energy and Buildings*, vol.49, pp.37-49.

Opricovic S. 1998. Multi-criteria optimisation of civil engineering systems. Faculty of Civil Engineering, Balgrade.

Opricovic S. and Tzeng G.H. 2004. Compromise solution by MCDM methods: a comparative analysis of VIKOR and TOPSIS. *European Journal of Operational Research*, vol.156, pp.445-455.

Padovan R. and Manzan M. 2014. Genetic optimization of a PCM enhanced storage tank for solar domestic hot water systems. Solar Energy, vol. 1.3, pp. 563-573.

Pasupathy A. and Velraj R. 2008. Effect of double layer phase change material in building roof for year round thermal management. *Energy and Buildings*, vol.40, no.3, pp.193-203.

Parameshwaran R., Kalaiselvam S., Harikrishnan S. and Elayaperumal A. 2012. Sustainable thermal energy storage technologies for buildings: A review. *Renewable and Sustainable Energy Reviews*, vol.16, no.5, pp.2394-2433.

PCM. Phase Change Material products Limited (cited 23 March 2016), Available at http://pcmproducts.net/home.htm.

Peippo K., Kauranen P. and Lund P.D. 1991. A multicomponent PCM wall optimized for passive solar heating. *Energy and Buildings*, vol.17, no.4, pp.259-270.

Perez-Lombard L., Ortiz J. and Pout C. 2008. A review on buildings energy consumption information. *Energy and Buildings*, vol.40, pp.394-398.

Py X., Olives R. and Mauran S. 2001. Paraffin-porous graphite matrix composite as a high and constant power thermal storage material. *International Journal of Heat and Mass Transfer*, vol.44, pp. 2727-2737.

Rakesh K. and Marc A.R. 2011. A critical review of photovoltaic-thermal solar collectors for air heating. *Applied Energy*, vol.88, pp.3603-3614.

Rohsenow W. M., Hartnett J. P. and Ganic E. N. 1985. Handbook of Heat Transfer Fundamentals. 3rd edition, *McGraw-Hill*, New York, USA.

Roy K.R. 2010. A primer of the Taguchi method, 2nd edition, Society of Manufacturing Engineers, Michigan, USA.

Rios-Coelho A.C., Sacco W.F. and Henderson N. 2010. A metropolis algorithm combined with Hooke-Jeeves local search method applied to global optimisation. *Applied Mathematics and Computation*, vol.217, pp.843-853.

Rubitherm PCMs 2014 (cited 07 June 2014). Available at www.rubitherm.com.

Saitoh H., Hamada Y., Kubota H., Nakamura M., Ochifuji K., Yokoyama S. and Nagano K. 2003. Field experiments and analyses on hybrid solar collector. *Applied Thermal Engineering*, vol.23, pp.2089-2105.

Salunkhe P.B. and Shembekar P.S. A review on effect of phase change material encapsulation on the thermal performance of a system. *Renewable and Sustainable Energy Reviews*, vol.18, no.8, pp.5603-5616.

Saman W., Bruno F. and Halawa E. 2005. Thermal performance of PCM thermal storage unit for a roof integrated solar heating system. *Solar Energy*, vol.78, no.2, pp.341–349.

Saxena S., Subrahmaniyam S. and Sarka M.K. 1982. Preliminary model for phase change thermal energy storage in a shell and tube heat exchanger. *Solar Energy*, vol.29, no.3, pp.257-263.

Scalat S. Banu D., Hawes D. Paris J., Haghighata F. and Feldman D. 1996. Full scale thermal testing of latent heat storage in wallboard. *Solar Energy Materials and Solar Cells*, vol.44, no.1, pp.49-61.

Schneider Electric (cited 23 March 2016), Available at http://www.schneider-electric.com.au.

Shah R.K. and London A.L. 1978. Laminar flow forced convection in ducts. 1st edition, *Academic Press*, New York, USA.

Shahsavar A. and Ameri M. 2010. Experimental investigation and modelling of a direct-couple PV/T air collector. *Solar Energy*, vol.84, pp.1938-1958.

Shahsavar A., Salmanzadeh M., Ameri M. and Talebizadeh P. 2011. Energy saving in buildings by using the exhaust and ventilation air for cooling of photovoltaic panels. *Energy and Buildings*, vol.43, pp.221-2226.

Shamsundar N. and Sparrow E.M. 1976. Effect of density change on multidimensional conduction phase change. *Journal of Heat Transfer*, vol.98, no.4, pp.550-557.

Sharma A., Tyagi V.V., Chen C.R. and Buddhi D 2009. Review on thermal energy storage with phase change materials and applications. *Renewable and Sustainable Energy Review*s, vol.13, no.2, pp.318-345.

Sharma S.D. and Sagara K. 2005. Latent heat storage materials and systems: a review. *Internal Journal of Green Energy*, vol.2, no.1, pp.1-56.

Shi Y.H. and Eberhart R.C. 1999. Empirical study of particle swarm optimisation. *Proceedings of the 1999 Congress on Evolutionary Computation*, vol. 3, pp.1945-1949.

Silva T., Vicente R., Amaral C. and Figueiredo A. 2016. Thermal performance of a window shutter containing PCM: Numerical validation and experimental analysis. *Applied Energy*, vol.179, pp.64-84.

Soares N., Costa J.J., Caspar A.R. and Santos P. 2013. Review of passive PCM latent heat thermal energy storage systems towards building's energy efficiency. *Energy and Buildings*, vol.59, pp.82-103.

Sohel M.l., Ma Z.J., Cooper P., Adams J. and Scott R.A. 2014. A dynamic model for air-based photovoltaic thermal systems working under real operation conditions. *Applied Energy*, vol.123, pp.216-225.

Somasundaram D.S. and Trabia M.B. 2011. A fuzzy-controlled Hooke-Jeeves optimisation algorithm. *Engineering Optimisation*, vol.43, pp.1043-1062.

Sparrow E.M. Schmidt R.R. and Ramsey J.W. 1978. Experiments on the roles of natural convection in the melting of solid. *Journal of Heat Transfer*, vol.100, no.1, pp.11-16.

Stefan J. 1889. Uber einige problem der theorie der warmeleitung. *Sber Akad Wiss Wien*, vol.98, pp.473-484.

Summers E.K., Antar M.A. and Lienhard V J.H. 2012. Design and optimization of an air heating solar collector with integrated phase change material energy storage for use

in humidification-dehuimidification desalination. *Solar Energy*, vol.86, no. 11, pp. 3417–3429.

Sukhorukov G., Fery A., Mohwald H. 2005. Intelligent micro- and nano-capsules. *Progress in Ploymer Science*, vol.30, no.8-9, pp.885-897.

Taguchi G., Chowdhury S. and Wu Y. 2004. Taguchi's quality engineering handbook. Wiley, New Jersey, USA.

Tan P.N., Steinbach M. and Kumar V. 2005. Introduction to data mining. 1st edition, Addison-Wesley Longman, Boston, USA.

Tay N.H.S., Bruno F. and Belusko M. 2010. Design methodology for coils in a phase change thermal energy storage system using effectiveness-NTU method. 48th annual conference of the Australian Solar Energy Society, Canberra, December1 - 3, 2010.

Tay N.H.S., Belusko M. and Bruno, F. 2012a. An effectiveness-NTU technique for characterising tube-in-tank phase change thermal energy storage systems. *Applied Energy*, vol.91, no.1, pp.309-319.

Tay N.H.S., Belusko M. and Bruno F. 2012b. Experimental investigation of tubes in a phase change thermal energy storage system. *Applied Energy*, vol.90, no.1, pp.288-297.

Tonui J.K. and Tripanagnostopoulos Y. 2007. Air-cooled PV/T solar collectors with low cost performance improvement. *Solar Energy*, vol.81, pp.498-511.

Toppi T. and Mazzarella L. 2013. Gypsum based composite materials with micro-encapsulated PCM: Experimental correlations for thermal properties estimation on the basis of the composition. *Energy and Buildings*, vol.57, pp. 227–236.

Tyagi V.V. and Buddhi D. 2007. PCM thermal storage in buildings: a state of art. *Renewable and Sustainable Energy Reviews*, vol.11, no.6, pp.1146-1166.

Vakilaltojjar S.M. and Saman W. 2001. Analysis and modelling of a phase change storage system for air conditioning application. *Applied Thermal Engineering*, vol.21, pp.249-263.

Velibor M. and Miloš M. 2011. Optimisation of surface roughness in turning alloy steel by using Taguchi method. *Scientific Research and Essays*, vol.6, no.16, pp.3473-3483.

Verma P., Varun, and Singal V.S.K 2008. Review of mathematical modelling on latent heat thermal energy storage systems using phase change material. *Renewable and Sustainable Energy Reviews*, vol.12, no.4, pp.999-1031.

Voller V.R. 1990. Fast implicit finite differential method for the analysis of phase change problem. *Numerical Heat Transfer*, vol.17, no.2, pp.155-169.

Wang S., Ma Z. and Gao D.C. 2010. Performance enhancement of a complex chilled water system using a check valve: experimental validation. *Applied Thermal Engineering*, vol. 30, pp. 2827-2832.

Wang W.L., Yang X.X., Fang Y.T. and Ding J. 2009. Preparation and performance of form-stable polyethylene glycol/silicon dioxide composites as solid–liquid phase change materials. *Applied Energy*, vol.86, no.2, pp.170-174.

Waqas A. and Kumar A. 2013. Phase change material based solar air heating system for residential spacing heating in winter. *International Journal of Green Energy*, vol.10, pp.402-426.

Wen S.Y., Fleming E., Shi L., and da Silva A.K. 2014. Numerical optimization and power output control of a hot thermal battery with phase change material. *Numerical Heat Transfer*, vol.65, part A., pp.825-843.

Weinlader H., Beck A. and Fricke J. 2005. PCM facade panel for daylighting and room heating. Solar Energy, vol.78, no.2, pp.177-186.

Weinstein R.D., Kopec T.C., Fleischer A.S., D'Addio E. and Bessel C.A. 2008. The experimental exploration of embedding phase change materials with graphite nanofibers for the thermal management of electronics. *Journal of Heat Transfer*, vol.130, no.4, pp.42405.1-42405.8.

Wetter M. 2011. Generic optimization program user manual. Lawrence Berkeley National Laboratory, version 3.1.0.

Wong J.P.C. 2013. Development of representative dwelling designs for technical and policy purposes. Sustainable Building Innovation Laboratory, Royal Melbourne Institute of Technology University, version 6.

Wong J.Y.Q., Sharma S. and Rangaiah G.P. 2016. Design of shell-and-tube heat exchangers for multiple objectives using elitist non-dominated sorting genetic algorithm with termination criteria. *Applied Thermal Engineering*, vol.93, pp.888-899.

Xiao M., Feng B. and Gong K.C. 2001. Thermal performance of a high conductive shape-stabilized thermal storage material. *Solar Energy Materials and Solar Cells*, vol.69, no.3, pp.293-296.

Xiao M., Feng B. and Gong K.C. 2002. Preparation and performance of shape stabilized phase change thermal storage materials with high thermal conductivity. *Energy Conversion and Management*, vol.43, no.1, pp.103-108.

Yamaha M. and Misaki S. 2011. The evaluation of peak shaving by a thermal storage system using phase change materials in air conditioning systems. *HVAC&R Research*, vol.12, no.S3, pp.861-869.

Zalba B. and Marin J.M. 2003. Review on thermal energy storage with phase change: materials, heat transfer analysis and applications. *Applied Thermal Engineering*, vol.23, pp.251-283.

Zhang X.X., Fan Y.F., Tao X.M. and Yick K.L. 2005. Crystallization and prevention of supercooling of microencapsulation n-alkanes. *Journal of Colloids and Interface Science*, vol.281, no.2, pp.299-306.

Zhang Y., Du K., Medina M.A., and He J.P. 2014. An experimental method for validating transient heat transfer mathematical models used for phase change materials (PCMs) calculations. *Phase Transitions*, vol.87, no.6, vol.541-558.

Zhang Y. and Faghri A. 1996. Heat transfer enhancement in latent heat thermal energy storage system by using the internally finned tube. *International Journal of Heat and Mass Transfer*, vol.139, no.15, pp.3165-3173.

Zhang Y.P., Lin K.P., Yang B., Di H.F. and Jiang Y. 2006. Preparation, thermal performance and application of shape-stabilized PCM in energy efficient buildings. *Energy and Building*, vol.38, no.10, pp.1262-1269.

Zhai X.Q., Cheng X.W., Wang C. and Wang R.Z. 2015. Experimental investigation and performance analysis of a fin tube phase change cold storage unit for high temperature cooling application. *Energy and Buildings*, vol.89, pp.9-17.

Zhai X.Q., Wang X.L., Wang C. and Wang R.Z. 2014. Experimental investigation of a novel phase change cold storage used for a solar air conditioning system. *HVAC Research*, vol.20, no.3, pp.302-310.

Zhao C.Y. and Zhang G.H., 2011. Review on microencapsulated phase change materials (MEPCMs): Fabrication, characterization and applications. *Renewable and Sustainable Energy Reviews*, vol.15, no.8, pp.3813-3832.

Zhou D., Zhao C.Y. and Tian Y. 2012. Review on thermal energy storage with phase change materials in building applications. *Applied Energy*, vol.92, pp.593-605.

Zhou G.B. and He J. 2015. Thermal performance of a radiant floor heating system with different heat storage materials and heating pipes. *Applied Energy*, vol.138, pp.648–660.

Zhu N., Ma Z.J. and Wang S.W. 2009. Dynamic characteristics and energy performance of buildings using phase change materials: a review. *Energy Conversion and Management*, vol.50, pp.3169-3181.

Zondag H.A., De Vries D.W., Van Helden W.G.j., Van Zolingen R.JU.C. and Van Stenhoven A.A. 2002. The thermal and electrical yield of a PV-thermal collector. *Solar Energy*, vol.72, no.2, pp.113-128.

Zondag H.A. 2008. Flat-plate PV-thermal collectors and systems: a review. *Renewable Sustainable Energy Review*, vol.12, pp.891-959.